1-P

NASA TECHNICAL MEMORANDUM

NASA TM X-64735

HEAT FLOW AND CONVECTION DEMONSTRATION (APOLLO 14)

By Tommy C. Bannister
Space Sciences Laboratory

March 29, 1973

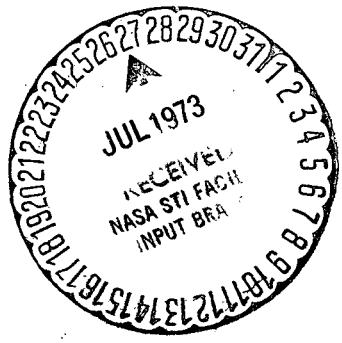

NASA

George C. Marshall Space Flight Center
Marshall Space Flight Center, Alabama

MSFC - Form 3190 (Rev June 1971)

138

TECHNICAL REPORT STANDARD TITLE PAGE

1. REPORT NO.	2. GOVERNMENT ACCESSION NO.	3. RECIPIENT'S CATALOG NO.
NASA TM X-64735		

4. TITLE AND SUBTITLE	5. REPORT DATE
Heat Flow and Convection Demonstration (Apollo 14)	March 29, 1973
	6. PERFORMING ORGANIZATION CODE
7. AUTHOR(S)	8. PERFORMING ORGANIZATION REPORT #
Tommy C. Bannister	
9. PERFORMING ORGANIZATION NAME AND ADDRESS	10. WORK UNIT NO.
George C. Marshall Space Flight Center Marshall Space Flight Center, Alabama 35812	11. CONTRACT OR GRANT NO.
	13. TYPE OF REPORT & PERIOD COVERED
12. SPONSORING AGENCY NAME AND ADDRESS	Technical Memorandum
National Aeronautics and Space Administration Washington, D. C. 20546	14. SPONSORING AGENCY CODE

15. SUPPLEMENTARY NOTES

Prepared by Space Sciences Laboratory, Science and Engineering

16. ABSTRACT

Apollo 14 Astronaut Stuart A. Roosa conducted a group of experiments during the lunar flyback on February 7, 1971, to obtain information on heat flow and convection in gases and liquids in an environment of less than 10^{-6} g. Flow observations and thermal data have shown that (1) as expected, there are convective motions caused by surface tension gradients in a plane liquid layer with a free upper surface; (2) heat flow in enclosed liquids and gases occurs mainly by diffusive heat conduction; and (3) some convective processes, whose characteristics are not fully known, add to the heat transfer. The raw data are presented in this report, and the analysis approach is given.

EDITOR'S NOTE

Use of trade names or names of manufacturers in this report does not constitute an official endorsement of such products or manufacturers, either expressed or implied, by the National Aeronautics and Space Administration or any other agency of the United States Government.

17. KEY WORDS	18. DISTRIBUTION STATEMENT
	Unclassified - Unlimited Tommy C Bannister

19. SECURITY CLASSIF. (of this report)	20. SECURITY CLASSIF. (of this page)	21. NO. OF PAGES	22. PRICE
Unclassified	Unclassified	138	9.00

For sale by National Technical Information Service, Springfield, Virginia 22151

ACKNOWLEDGMENTS

The success of the Heat Flow and Convection Demonstration performed during the Apollo 14 flight by Maj. Stuart A. Roosa was due in large measure to the many dedicated personnel of the Marshall Space Flight Center (MSFC), Manned Spacecraft Center (MSC), Kennedy Space Center (KSC), NASA Headquarters, and various contractors. All displayed an attitude of cooperation and responsibility which enabled deliverance of the flight hardware to KSC within 100 days of the "go-ahead" date.

Although it is not possible to acknowledge all of the persons involved, this author would like to extend a personal thanks to Dr. Philomena Grodzka, of the Lockheed Missiles and Space Company, who originally proposed the flow pattern cell and who has worked hard in evaluating the data.

As principal investigator, the author wishes to convey special appreciation to the following members of the investigator team: B. Facemire, L. Russell, R. Holland, and B. Jones, of the Space Sciences Laboratory; F. Rodrigue, Computation Laboratory; and J. Beal, Quality and Reliability Assurance Laboratory, all of MSFC; Dr. C. Fan and R. Heddon, Lockheed Missiles and Space Company, and S. Brown, U. S. Army Missile Command.

TABLE OF CONTENTS

LIST OF ILLUSTRATIONS

LIST OF ILLUSTRATIONS (Continued)

LIST OF ILLUSTRATIONS (Continued)

LIST OF ILLUSTRATIONS (Continued)

LIST OF ILLUSTRATIONS (Continued)

LIST OF ILLUSTRATIONS (Concluded)

LIST OF TABLES

TECHNICAL MEMORANDUM X-64735

HEAT FLOW AND CONVECTION DEMONSTRATION (APOLLO 14)

SUMMARY

The final results of the Heat Flow and Convection (HFC) Demonstration experiments conducted aboard the Apollo 14 spacecraft on February 7, 1971, during the lunar flyback indicate significant convection as the result of heating fluids in nominally zero-g environments. In the case of a liquid having a free, unbound surface, a cellular convection was observed. The cause of this convection was conclusively established as surface tension gradients, as predicted by existing theory. Completely contained liquids and gases exhibited a small, though significant, amount of first-and second-order convection. The cause of these convections is being investigated.

INTRODUCTION

The HFC Demonstration experiments conducted aboard the Apollo 14 spacecraft were designed to evaluate the effects the spacecraft environment would have on the mechanism of thermal convection. The basic objective of the demonstration was to demonstrate the combined effect of various forces on the kind and magnitude of fluid flows that occur in actual flight. Although normal convection is suppressed at near weightlessness, some fluid flow will occur because of acceleration impulses, surface effects, and expansion. Predicting flows from these effects is like predicting the weather. NASA had received many industry proposals involving fluid flow in a near weightless environment. The information obtained from this demonstration will provide some of the data required to evaluate these proposals for future space applications, as well as practical knowledge for designing future approved flight experiment and logical follow-on fluid physics experiments.

The thermal behavior of fluids is a vital part of manufacturing processes involving liquid separation, precipitation, solidification, etc. The HFC Demonstration was carried on the Apollo 14 flight as part of the NASA Material

Science and Manufacturing in Space (MS/MS) Program to obtain data on heat transfer and convection in fluids in a low gravitational environment. The apparatus consisted of a box 23 cm by 23 cm by 9.6 cm (9 in. by 9 in. by 3.8 in.), to which an onboard 16-mm Data Acquisition Camera (DAC) was attached (Fig. 1). Four test configurations, each of a particular geometry and each containing a specially chosen fluid, were mounted in the apparatus. The required information was recorded in color by the DAC. The astronauts were Comdr. Alan B. Shepard, Jr., and Comdr. Edgar D. Mitchell, U. S. Navy, and Maj. Stuart A. Roosa, U. S. Air Force. Major Roosa performed the demonstration on February 7, 1971 during the lunar flyback coast period. Astronauts Shepard and Mitchell also participated in the demonstration. The g level was typically 10^{-6}g at the location of the HFC Demonstration during this period, which was at the lower equipment bay. In this position the small acceleration force vector was in the same direction as if the box were lying on a table in 1-g environment.

The unit is a small 3.2-kg (7-lb) box containing three different types of test cells: the radial cell, the flow pattern cell, and the zone cell. Each cell contains a small electric heater to heat the fluid being tested (Table 1). Power for heating is obtained from the 28-Vdc spacecraft system. Seven tests were made, each requiring 10 to 15 min. The data were recorded by the 16-mm DAC attached to the unit and operating at a rate of one frame per second. No recorded data were taken.

TABLE 1. HEATER POWER LEVELS

Flow Pattern Cell	
Run 1	7.4 W
Zone Heating Cell	
Run 1	9.8 W
Run 2	14.4 W
Radial Heating Unit	
Run 1	5.5 W
Run 2	8.7 W

The radial cell is a circular cell filled with carbon dioxide gas used to test radial heat flow. The cell, a cylindrical dish with a small electric heater mounted in its center, is covered by a plastic film coated with a liquid crystal

material that changes color as it is heated. This film is divided into quarters, and the different sectors are sensitive in different temperature ranges. The changing color patterns map the temperature distribution as it develops and are recorded by the camera.

The flow pattern cell is designed to test the convective flow pattern induced in an oil layer by thermal changes in surface tension. The cell consists essentially of a shallow aluminum dish which is uniformly heated from the bottom. Thin layers of a heavy oil, called Krytox, were introduced from a reservoir. This oil contains a suspension of aluminum flakes which enables the oil flow patterns to be viewed. The window to this cell was opened during the tests to establish a thermal gradient across the Krytox. Therefore, the heat from the oil was dissipated into the spacecraft atmosphere.

The zone cells are composed of two transparent cylinders with electric heating elements located in the center of each cylinder. The left tube contains water and the right, a sugar solution. Strips coated with liquid crystal materials are located along the central axis of each cylinder and also on the surface. The presence or absence of convection is based on the temperature color maps observed on the strips as heat flows in both directions from the center heated zone.

SECTION 1. THE DATA

Data Reduction Process

The 16-mm DAC film was received, and the reduction of data into quantitative values has been completed. Since the temperature data were obtained from liquid crystal colors recorded on ordinary color indoor film, a lengthy color calibration procedure was used to establish a matrix for conversion to temperature.

To reduce the data, however, the first step was to read the positions of the color bands on the various strips (identified in Fig. 2), using a computational telereader. The telereader magnified the image by a factor of 100 and has sensitive cross hairs which are tied into an electronic counter and cardpunch. Once a frame was read, the cards plus the calibration were read into the computer, where conversion into isotherms was made. In addition to the regular output, each isotherm was filtered for output according to a Bessel

function routine recommended by the MSFC Computation Laboratory. This essentially filters out the frequency close to the reader frequency (random error of reading). The filter function is presented in Figure 3. A study was made to determine the optimum frames to read, i.e., precision versus workload. It was found by a least-squares method that one reading every fifth frame was nominally sufficient. The standard deviations in reader color determination were also calculated (Table 2).

TABLE 2. STANDARD DEVIATIONS IN READINGS

Point	Standard Deviations		
	First	Second	Third
Center	0.022	0.019	0.019
Amber	0.040	0.052	0.057
Yellow	0.021	0.021	0.030
Green	0.025	0.029	0.036
Blue	0.035	0.031	0.034

Perhaps the most significant test run was the comparison of "blue" and "red" processed film. The differences here were within the above standard deviation.

Figure 2 shows the face of the Apollo 14 HFC unit and identifies the temperature strips. The data are given in the Appendix (Figs. A-1 through A-89).

The g Levels

The g levels were obtained from the spacecraft orbital coordinate data through the calculation of the acceleration for given motion as well as gravity gradients. Figures 4 and 5 show the X, Y, Z accelerations for the HFC unit [1]. These curves do not include movement of the unit relative to the spacecraft. The unit was accidentally bumped during flight. The time, but not the magnitude, of these impulses can be determined from the film. Time data were obtained from film frames showing Major Roosa's wristwatches (Table 3).

TABLE 3. THE RUN TIMES

Run	Time (Start)		Frame Number (First Frame)
	Central Standard Time	Apollo Elapsed Time	
Radial Run No. 1	5:22	170 hr, 19 min	0
Zone Run No. 1	5:34	170 hr, 31 min	740
Zone Run No. 2	5:53	170 hr, 50 min	1875
Radial Run No. 2	6:01	170 hr, 57 min	2323
Flow Pattern	11:01	175 hr, 57 min	3705

Liquid Crystal Calibrations

The liquid crystal strips used in this demonstration require a calibration matrix for conversion of color to temperature. These strips were fabricated from the basic pigment purchased from Hoffman - La Roche, Inc.; therefore, ground-based calibrations were required. The calibrations used in the data reduction presented in this report were static, i.e., using controlled heating to constant temperature levels. A copper-constantan thermocouple was placed in the center of a liquid crystal strip that was mounted on an aluminum diffusion plate. A duplicate of the strip that was located near the unit on/off switch was used in these calibrations. Several runs were made, care being taken to prevent extraneous heat flow. Table 4 shows the results.

Although liquid crystals have been used frequently in recent years, no data were found in the literature or through personal contacts in which an application similar to this one was found. Because of well-known problems in color matching during photography and the relative newness of using liquid crystals quantitatively, additional work has been done and is continuing. No apparent effect caused by film processing was seen. All calibrations were made under flight-simulated lighting conditions.

Liquid crystals exhibit a change in color with viewing angle. A typical example of this effect (from Hoffman - La Roche, Inc.) is shown in Figure 6. The equivalent uncertainty caused by this effect is estimated to be 0.25°C. Work was done on two other possible effects — transient effects and aging effects. A change of about 1° C every 3 months has been seen in the calibration crystals. This effect has been shown to be a function of time and light exposure.

TABLE 4. TEMPERATURE CALIBRATIONS[a]

Color of Liquid Crystals[b]	Range Number			
	1	2	3	4
	Temperature Range (°C)			
	24 - 31.0	30 - 37	37 - 43.5	43 - 49.5
	Temperature[c] [°C(°F)]			
Brown	25.4 (77.7)	30.9 (87.6)	37.2 (99.0)	42.9 (109.3)
Yellow-Brown[d]	27.5 (81.3)	32.5 (90.5)	38.6 (101.5)	44.4 (112.0)
Light Green	28.0 (82.4)	33.6 (92.5)	39.2 (102.5)	45.8 (114.5)
Dark Green	28.9 (84.0)	34.7 (94.5)	40.0 (104.0)	46.4 (115.5)
Blue-Green	29.4 (84.9)	35.3 (96.5)	40.9 (105.6)	47.0 (116.6)
Light Blue	30.0 (86.0)	36.3 (97.4)	42.0 (107.6)	47.8 (118.0)
Blue	30.5 (86.9)	36.9 (98.4)	42.9 (109.3)	48.7 (119.6)

a. Although color references are not included, the interpretation is relatively clear after the color ranges of the crystals are once viewed.

b. Black-dark brown -- below sensing range; royal blue (dark) — above sensing range.

c. The calibrations appear to be readily repeatable within ± 0.25° C (or 0.45°F).

d. Or light brown.

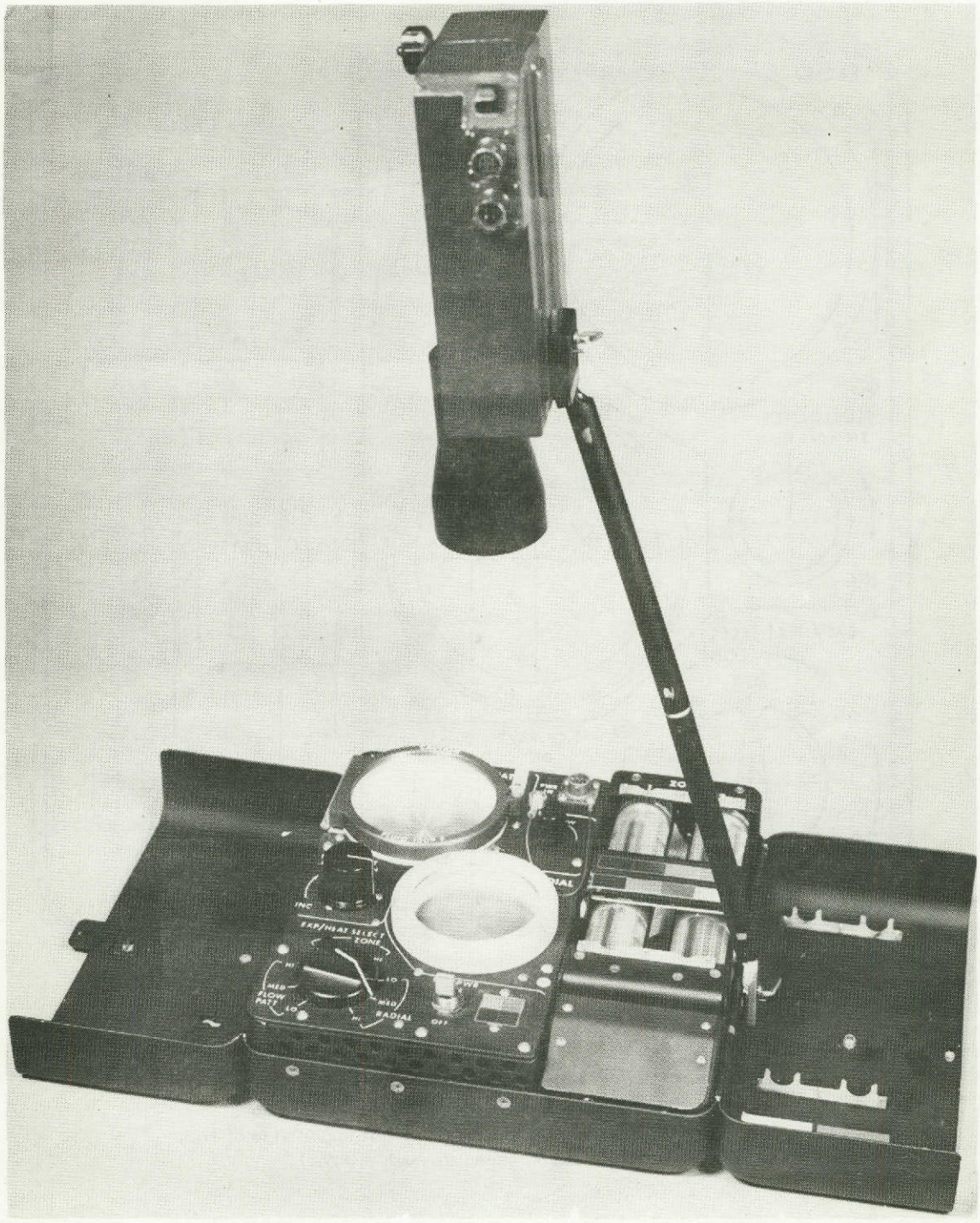

Figure 1. The apparatus.

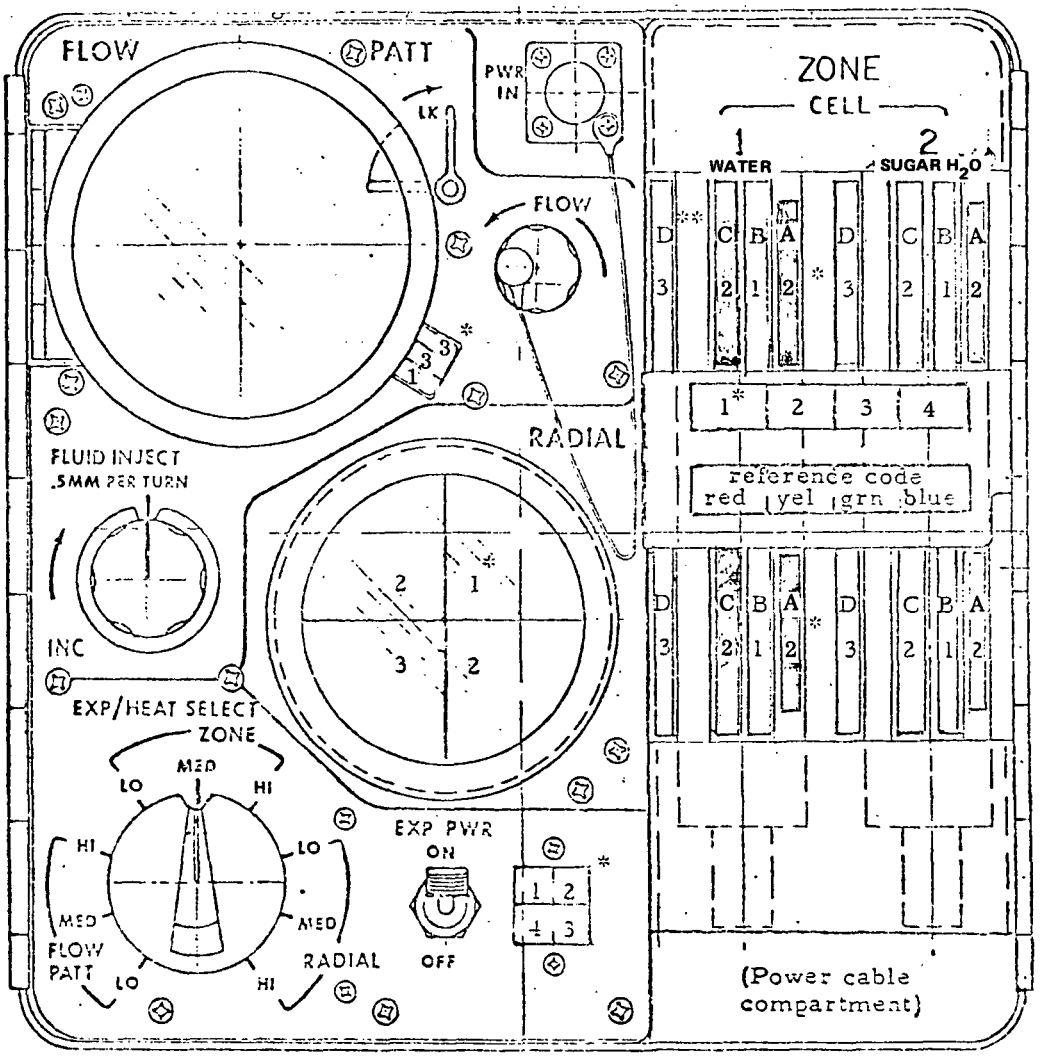

NOTES*: Typed numbers indicate the liquid crystal temperature ranges.

1. 24 to 31.0° C
2. 30 to 37.0° C
3. 37 to 43.5° C
4. 43 to 49.5° C

** Liquid crystal locations for zone units: A, glass tubes; B, right upper side of center rod; C, left upper side of rod; D, left lower side of rod (seen through mirror).

Figure 2. Panel face of heat flow and convection unit (flight unit). (Primary data on zone cells are from shaded strips.)

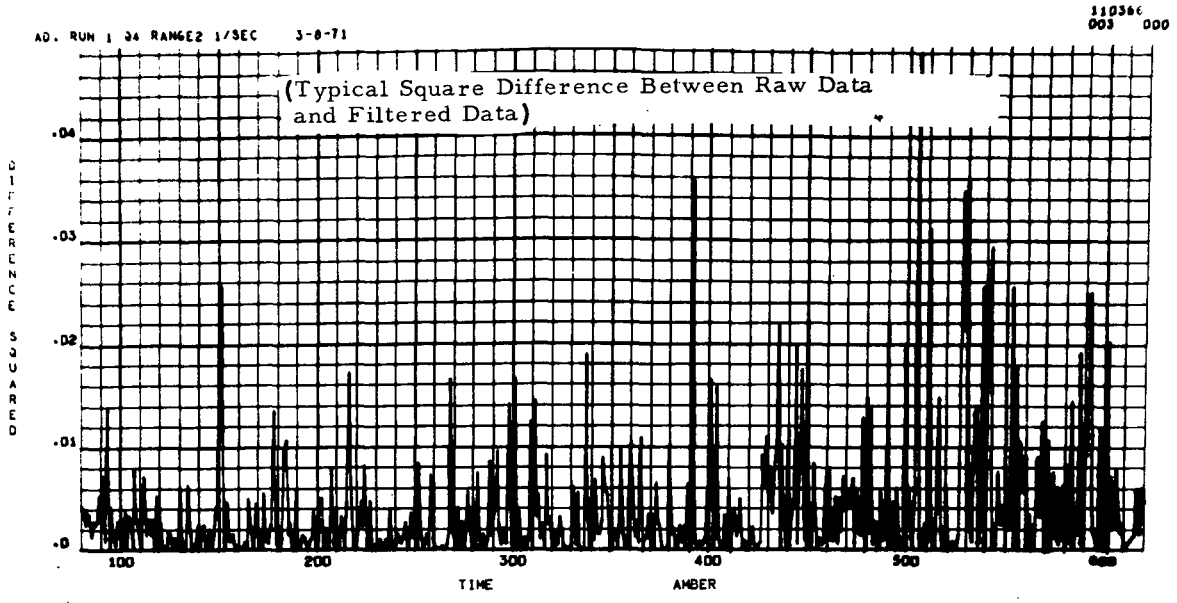

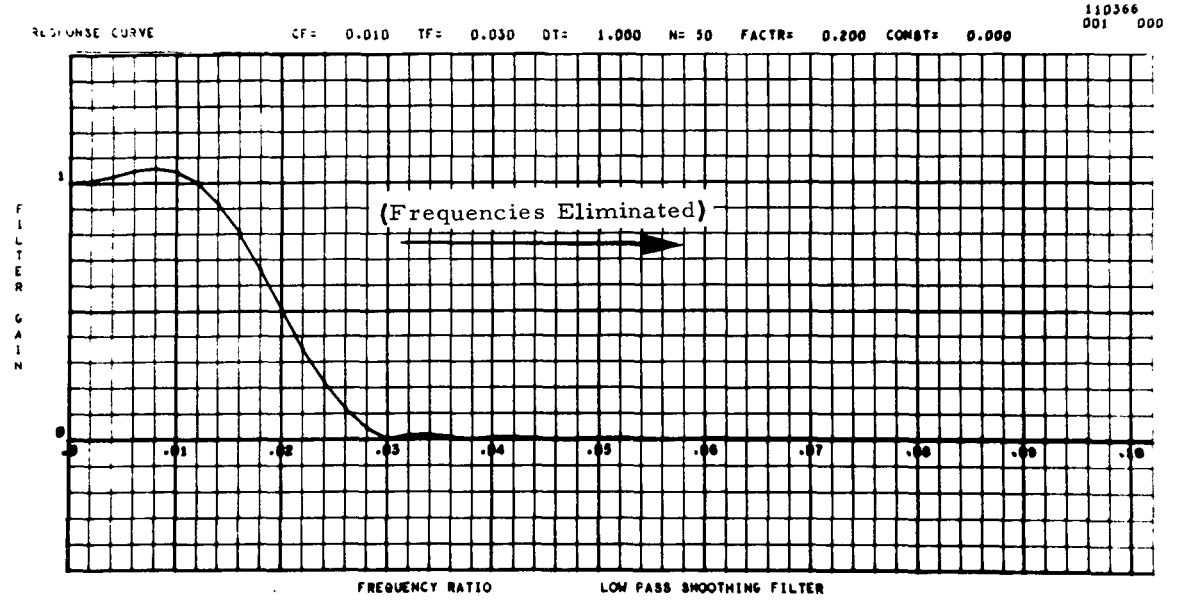

Fig. 3 THE FILTER FUNCTION

Figure 3. The filter function.

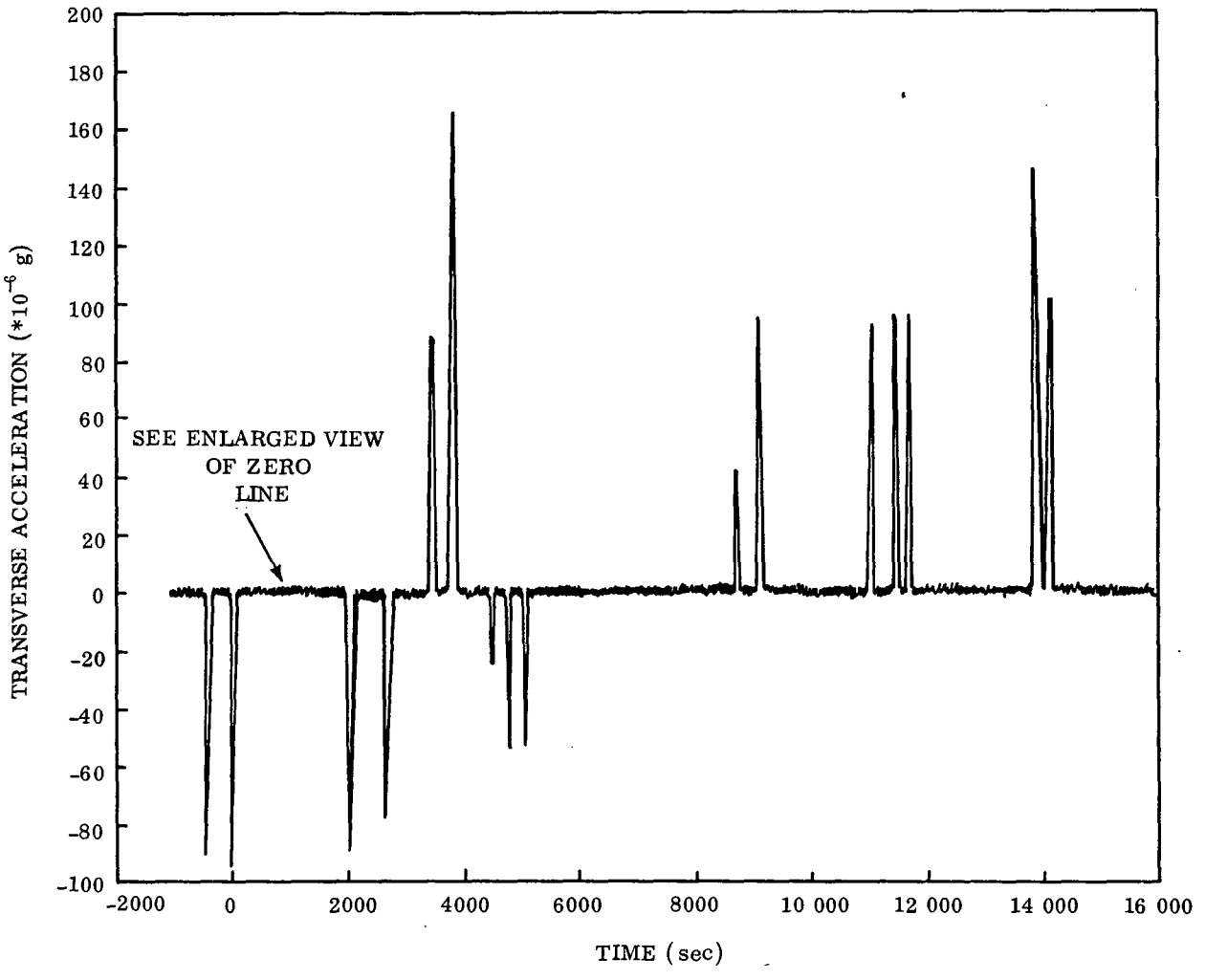

Fig. 5: Apollo 14 Gravitational Curve

Figure 4. Apollo 14 gravitational curve (large scale).

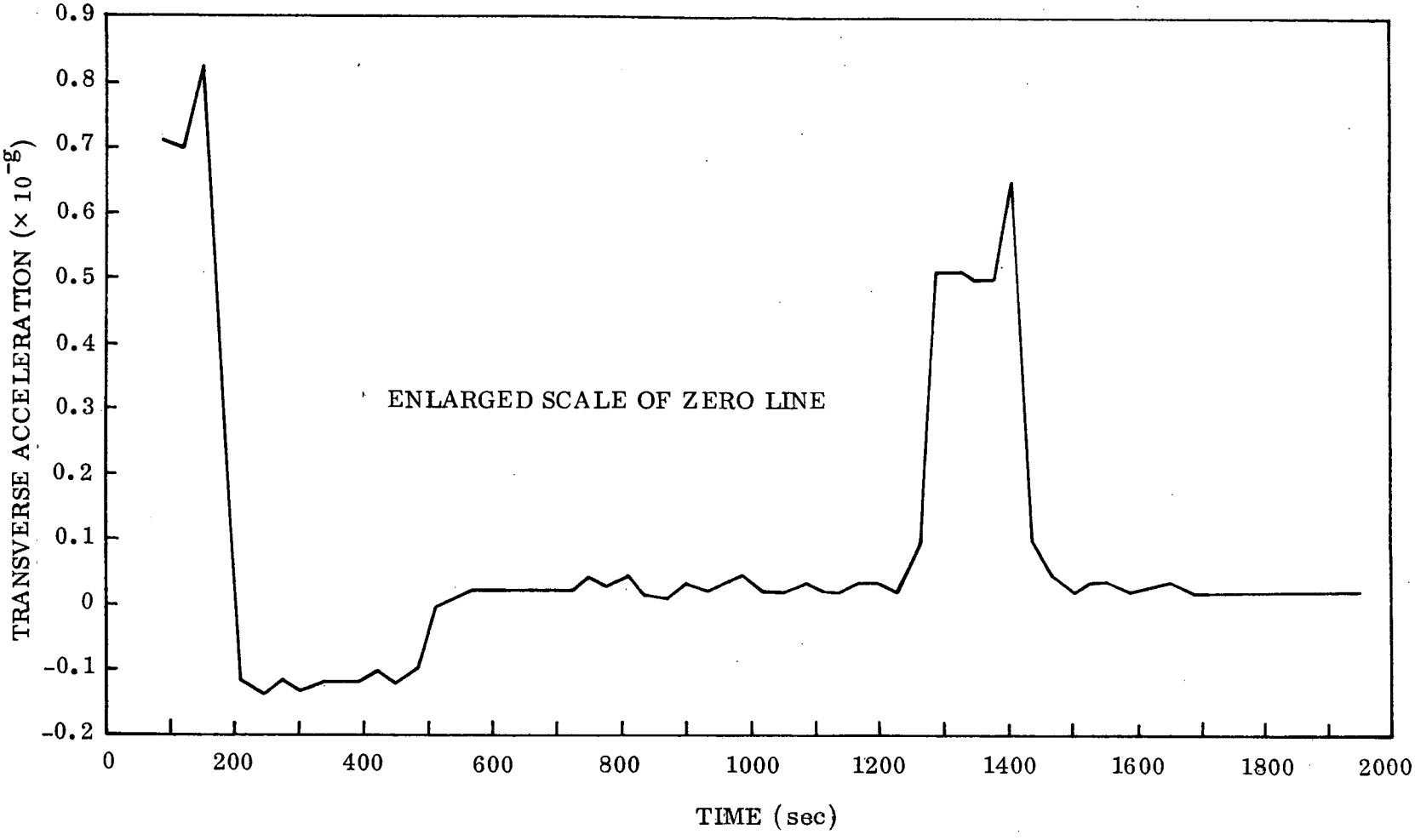

Figure 5. Apollo 14 gravitational curve (small scale).

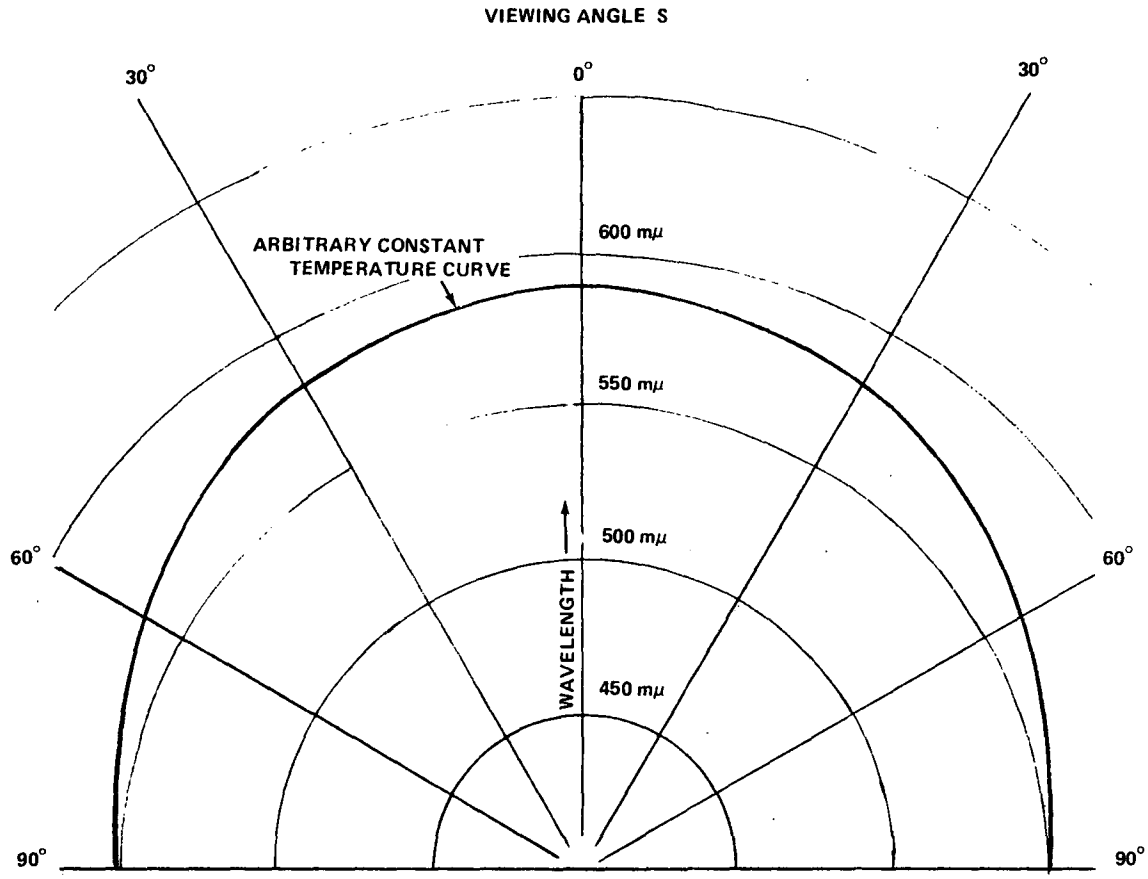

Figure 6. Liquid crystal viewing angle.

SECTION 2. ANALYSIS AND RESULTS

The Data Analysis

The primary data (the 16-mm film) were received on February 18, 1971. The films were examined and found to be of excellent quality, both in focus and color, although they had a slight yellow tint. Two radial tests and two zone tests were performed and the data quality appears, for the most part, to be excellent. The unit was accidentally jarred on occasion, particularly during the zone runs. During flight, 4987 frames were taken (out of 5000 available). This means that about 200 000 data points were recorded. Because of this, the complete set of data curves is presented in the Appendix.

Flow Pattern Experiment. The flow pattern cell is designed to test the convective flow pattern induced in an oil layer by thermal changes in surface tension. The cell consists essentially of a shallow aluminum dish which is uniformly heated from the bottom. Thin layers of a heavy oil, called Krytox, were introduced from a reservoir. The oil contains a suspension of aluminum flakes which enables the oil flow patterns to be viewed. The window to this cell was opened during the tests to establish a thermal gradient across the Krytox. Therefore, the heat from the oil was dissipated into the spacecraft atmosphere.

The flow pattern experiment consists of generating a cellular convective motion in an open, heated pan of oil. The primary objective of this experiment was to demonstrate that surface tension alone can generate considerable cellular convection. A secondary objective was to obtain data on the pattern of convection that is uncoupled from gravity. An explanation of these objectives is as follows. A relatively thin (less than 10 mm) uncovered layer of oil, when heated from below in a 1-g environment, will exhibit a cellular form of convection. The flow pattern is made visible by means of fine, flaky aluminum powder which is dispersed throughout the oil. Liquid upflows or downflows appear dark, and flows parallel to the surface appear light because of light reflection off of the flaky, aluminum particles. A hexagonal, cellular pattern is called Bénard cells after Henri Bénard, who first studied the phenomenon in 1901 [2]. Liquid upflows occur at the center of the hexagonal cells and liquid downflows at the cell peripheries. Very frequently the flow pattern is not hexagonal but assumes a roll or "wormy" appearance.

Lord Rayleigh's subsequent classic theory of Bénard cells assumed that gravity is the only motive force [3]. The general features of the phenomenon are adequately described by Rayleigh's theory if the fluid layers thicker

than about 5 mm are considered. In thinner layers of fluids, however, Block [4] shows that surface tension gradients — as the result of temperature gradients — are the predominant cause of cellular convection. However, the experiments were, of necessity, run under 1-g conditions. The possibility, therefore, remained that gravity somehow is an indispensable ingredient in all cellular convection, particularly as some second-order effect. The generation of cellular convection in the very low-g environment of the Apollo 14 spacecraft would thus provide conclusive confirmation of previous ground-based experiments.

The results of the flow pattern experiment are shown in Figure 7. A square-shaped pattern is seen in the oil fillets. In the thin center layer a pattern of undetermined form is seen. The resolution of the DAC was not sufficient to resolve the exact pattern in the center region.

It was conclusively demonstrated that surface tension alone can generate cellular convection. The secondary objective was partially achieved. The pattern of the convection in near zero-g was partially defined but not in the desired constant depth configuration. The walls of the flow pattern cell were designed to be nonwetting by the application of a special silicone grease to a special liner molded of RTV material (Fig. 8). The Apollo 14 film shows that the Krytox wetted the liner so that a fillet having a cross section somewhat similar to a wedge was obtained in flight. Figure 9 shows ground-based cells for a flat layer of Krytox. Ground experiments on the generation of Bénard cells in a wedge-shaped container of dimensions similar to the flight cell have shown that approximately square-shaped cells occur only when the heat is turned off and the oil is cooling. Upon heating, one long convective cell is obtained. If the gravity and surface tension force vectors acted in the same direction as assumed by Nield [5], it would be obtained both on cooling and heating. The fact that square-shaped cells were observed upon heating in flight substantiates the conclusion that gravity and surface tension act in opposite directions in cellular convection.

The previous mathematical analyses of surface tension-driven cellular convection dealt only with those cases in which a thin layer of fluid of large extent was involved [2-9]. Neither theoretical nor experimental studies have been available in the literature regarding the edge effects on cellular motion induced by surface tension forces. To analyze the cellular motion observed in the flow pattern experiments, an attempt was made to mathematically formulate the problem of hydrodynamics stability for a corner flow. An inclined fluid layer with variable thickness was considered. The fluid was sustained by adhesion force in a two-dimensional corner in a small acceleration

field. The boundary conditions were such that one side of the corner received a uniform heat flux whereas the other side was thermally insulated. The free surface lost heat to the surrounding atmosphere by convection. Surface tension force was considered to be the primary driving force. This closely simulated the geometry and boundary conditions of the flow pattern experimental configuration. A mathematical formulation for the considered stability problem has been completed, and the result is a set of coupled nonlinear perturbation equations with complicated boundary conditions. Although a rigorous analytic solution to the derived perturbation equations was not obtained, the formulation yielded valuable insight into and a further understanding of the problem. The analytical analysis used in the computer program was performed by the Lockheed Missiles and Space Company [10], which supported the Marshall Space Flight Center in the overall analysis and particularly in the computer analysis.

Radial Heating Experiment. The radial cell is a circular cell filled with carbon dioxide gas used to test radial heat flow. The cell, a cylindrical dish with a small electric heater mounted in its center, is covered by a plastic film coated with a liquid crystal material that changes color as it is heated. This film is divided into quarters, and different sectors are sensitive in different temperature ranges. The changing color patterns indicate the temperature distribution as it develops and is recorded by the camera.

The objective of the radial heating experiment was to obtain information on thermal flow in a gas in a low-g environment. In this experiment the rate of temperature propagation in carbon dioxide gas, as the result of heating with a small heat source, was measured in near zero-g. The radial heating unit (Fig. 10) consists of a shallow aluminum cup with a stud heater in the center. Most aluminum parts were anodized; the aluminum surface can be assumed anodized unless otherwise stated. A glass window covers the cup, maintaining a gas-tight seal. Just below the window is a temperature-sensitive membrane, which is divided into four quadrants, each coated with a liquid crystal layer. The liquid crystal quadrants respond to temperature changes by changing colors: Each quadrant changes colors upon heating through the spectrum of red, yellow, green, and blue in different temperature ranges. The stud heater is turned on, and the rate of propagation of the resulting spectra of color bands, or isotherms, is recorded by the DAC. Temperature versus time curves are obtained from the film record by measuring the displacement of the color bands as a function of time.

The data and identifications of the various strips on these cells, as well as for the entire unit, are given in Section 1. The analytical curve was obtained with, and data were calculated on, the assumption that conduction and

radiation were the only modes of heat transfer. All graphs of the measured isotherms show similar convective trends (see Appendix).

Comparisons between flight data and analytical predictions are shown in Figures 11a, 11b, and 11c based upon a radiative and conductive heat transfer model. The analytical predictions presented in Figure 11b assume an initial temperature of 23.9°C (cabin temperature). Nominal effective thermal conductivity of the liquid crystal membrane (diaphragm) was assumed. Figure 11c is for a somewhat higher initial temperature (27.4°C) because the first data frames show that the 24 to 31°C temperature range was yellow. In Figure 11c a higher tolerance value for the effective thermal conductivity of the diaphragm is also assumed. The latter temperature run gave the better correlation, however, although neither of the cases satisfactorily explains the fact that the flight data lead the analytical data during the initial minutes.

It is concluded that convection occurred in the radial cell, causing faster changes in the temperature than can be attributed to thermal conduction and radiation. This convection was caused either by low-g gravity forces or some other unidentified nongravity influence. To distinguish this convection from the oscillatory kind which is discussed next, the term first-order is applied. Oscillatory convection exhibiting small-amplitude temperature oscillations is here called second-order. It was concluded that second-order convection was the cause of the small temperature cycles observed on both the heating and cooling of the radial heating unit. These cycles have a period of approximately 70 sec and an amplitude of about 1 mm. Figure 12 shows a typical manifestation of these low-frequency temperature oscillations. In that figure oscillations of a frequency greater than 0.03 per second have been eliminated. Frequencies between 0.01 and 0.03 have been linearly damped (see Section 1). These oscillations were completely unexpected and are definitely larger than the standard deviations (see Section 1).

The literature on theoretical and experimental studies of thermal instability (due to gravitation) for completely confined fluids was reviewed. It was found that the convection heat transfer system investigated by Eckert and Carlson [11] most resembles the radial heating experiment. Eckert and Carlson have conducted (ground) experiments for a layer of fluid confined in a rectangular container having two isothermal vertical walls (at different temperatures) and insulated plates at the top and bottom. The container has

a height H, a width L, and a depth which is much larger than H and L. Eckert and Carlson determined that for air, the region of pure conduction ended at $Ra \geq 500\ (H/L)$, where Ra is the Rayleigh number based on L. This experimentally determined stability criterion was used to predict for the possibility of convective motion in the radial heating unit. It was estimated that for a maximum temperature difference of 275°C between the heating post and the cell wall, convection is possible when the magnitude of acceleration reaches 5.8×10^{-4} g, where g = 980 cm/sec^2. Since the calculated g value (see Section 1) during the Apollo 14 flight test was of the order of 10^{-6} g and only occasionally reached 2×10^{-4} g, it was concluded that sustained convection in the radial heating unit caused by gravity is unlikely.

Zone Cell Experiment. The zone cells are composed of two transparent cylinders with electric heating elements located in the center of each cylinder. The left tube contains water and the right, a sugar solution. Strips coated with liquid crystal materials are located along the central axis of each cylinder and also on the surface. The presence or absence of convection is based on the temperature change rates as shown by the color pattern observed in the strips when heat flows from the center heated zone toward each end.

In the zone heating unit, temperature changes, as sensed by liquid crystals, at the centers and walls of the liquid-filled glass cylinders were monitored as the cylinders were heated by a hollow cylindrical heater located at the center of the cell. Figure 13 shows a schematic of the zone heating units. The heat transfer in configurations of the geometry of the zone heating units is of interest because this geometry is basic for many projected space manufacturing processes. The objective of the zone heating experiment was to obtain data on the mode and magnitude of heat transfer in liquids subjected to zone heating in low-g environments. In this experiment, one cell contained distilled water and the other a 20-percent sugar solution. The purpose of the sugar water solution was to vary the liquid viscosity. The viscosity of a 20-percent sugar solution is approximately twice that of pure water (Table 5). The thermal gradients were small because the wattage level of the zone cells was limited by the fact that water changes phase at 100°C. Consequently, possible convection effects were sought by using two cells for comparison. The curves were calculated on the assumption that heat conduction is the only mode of heat transfer. The zone heating unit run under 1-g conditions showed extensive convection, which was manifested by temperature changes occurring first at the upward end of the cell, rather than from the center heater outward. The raw data from the zone heating experiments showed the same type of oscillations as were observed in the radial heating runs. The amplitudes of the oscillations in the case of the zone heating experiments, however, were not quite as large as those observed in the radial heating runs; average

amplitudes of about 0.5 mm were observed. Faster rates of propagation were observed in the 20-percent sugar water solution.

TABLE 5. FLUID PROPERTIES

	CO_2	Water	20-Percent Sugar Water	Krytox 143A2
Fluid Viscosities (cP)	1.48×10^{-2} (20°C)	1.002 (20°C)	1.945 (20°C)	32.4 (24°C)
Thermal Conductivity (W/m°C)	7.00×10^{-2} (30°C)	6.24×10^{-1} (41°C)	5.18×10^{-1}	8.38×10^{-2} (38°C)
Surface Tension (dyne/cm)				15.4 (210°C) 12.2 (55°C)

On occasion, the liquid crystal strips on the sugared water cell (which was located on the extreme edge of the unit) were not clearly visible; this resulted in having isotherms which covered shorter periods of time. Also, the HFC unit was accidentally bumped during both zone runs. Interestingly, the spacecraft experienced an acceleration impulse during the second zone run. A typical isotherm showed a corresponding change (Fig. 14). The heat flow rates in the zone cells were generally low, and the future experiments, if possible, should be run at somewhat higher heating rates.

A comparison between flight data and analytical predictions is shown in Figures 15a, 15b, and 15c. The analytical predictions presented in Figure 15b were based on an initial temperature of 23.9°C (cabin temperature), which was the expected temperature of the entire unit before the flight data acquisition began. Figure 15c is based on an observation of the radial heating unit diaphragm, which showed that the 24 to 31°C temperature range was yellow, corresponding to an initial temperature of 27.4°C. As can be seen from the figures, the elevated temperature case gave an excellent correlation with the flight data when the tolerances of the analytical predictions and flight data are taken into consideration. Because of the construction of the zone cells, no data were obtained corresponding to the early radial data.

From past experience, thermal models similar to those used for the analytical predictions have proved to be accurate within ± 10 percent of the temperature rise or, for the case under investigation, ± 1 to 2° C. (The 100° C limit on water prevented higher wattage values to increase the rise rate.) This deviation, in addition to the variation in calibration, could account for the approximately ± 2° C tolerance in the analytical predictions.

When applied to the analytical predictions, the tolerance accounts for a - 0.1-cm deviation in the curves for a +2° C tolerance or a + 0.2-cm deviation in the curves for a -2° C tolerance. If the latter were applied to the elevated temperature case, then the data are within the tolerance of the analytical predictions.

A comparison of the flight data for the distilled water and sugar water units is shown in Figure 15d. It is evident that a small variation exists between the two cases. The primary difference in these two cells is the viscosity of the two fluids (Table 5). Viscosity does not play a role in conduction or radiation.

As a point of interest, the color change along the Teflon rod inside the zone unit containing distilled water lagged the color change along the glass in the same cell tube wall by approximately 8° C during the heating process. During cooling, the liquid crystal strip along the glass tube wall cooled more rapidly than the other modes. The temperature along the rod continued to increase, causing the curves to cross. For further evidence of this phenomenon, refer to Section 1.

A simple stability analysis was also made regarding gravity-driven convective motion in the zone heating units during flight test. This analysis was based on the experimental results of Liu, et al. [12], who performed ground experiments of natural convection in water and other fluids confined in horizontal cylindrical annuli. One of the major findings in Reference 12 was that convective motion occurs when $Ra \geq 1000\ (1 + 1.36/Pr)$, where Pr is the Prandtl number of the fluid and Ra is the Rayleigh number based on the gap width between the inner and outer cylinders. Using this result, it was estimated that for the zone heating system with pure water under a maximum temperature difference of 80° C, gravity-driven convection would not occur unless the acceleration level exceeded 9.4×10^{-4} g.

Conclusions

A number of promising hypotheses concerning the nature of low-g convection observed in the radial and zone heating experiments are being investigated. One tentative hypothesis is that the observed first-order convections are caused by a nongravity driving force. The two nongravity forces being considered are the force caused by fluid volume expansion on heating and an interfacial tension force generated by some sort of a fluid boundary layer. Sizable increases in heat and mass transfer have been predicted for

gases in zero-g as the result of volume expansion on heating [13]. The motion is, however, acoustical in nature. The hypothesis that a fluid boundary layer can cause fluid flow by means of an interfacial tension mechanism is, for the moment, a speculation requiring theoretical and experimental substantiation. The possibility appears remote that average gravity levels on the order of 10^{-4} g caused the observed first-order convection.

A number of explanations for the observed second-order convection are being considered concurrently. A motion of acoustical nature caused by volume expansions does not appear likely because the period of acoustical temperature oscillations is estimated to be a fraction of a millisecond for the boundary conditions of the experiments. The observed temperature oscillations are about a minute. The possibility that random vibrations on the spacecraft transmitted shear and pressure impulse to the experimental fluids also appears unlikely. A "bump" should be apparent as a temperature oscillation at the same time on all of the different temperature isotherms during a given run, and no such coincident bumps were noted.

The flow pattern experiment confirmed conclusively the theoretical prediction that surface tension alone can cause cellular convection. However, the confirmation of theory details, such as cell shape and size, depends on the results of a mathematical analysis of cellular convection in a corner geometry which is currently underway and future flight experiments in which a more uniform liquid layer is maintained.

The preliminary results have the following implications for projected space manufacturing processes. Contained fluids under nominally zero-g environments can sustain significantly steeper temperature gradients than they can under 1-g conditions. Therefore, manufacturing processes which depend on carefully controlled thermal environments could be more easily accomplished in space orbits. The small, though significant, amount of observed first- and second-order convection, however, indicates that ultra-temperature control previously envisioned [14, 15] cannot be routinely assumed. In any contemplated process where a free or uncontained liquid is subjected to a temperature or concentration gradient, sizable convection can be assumed under Apollo 14 environmental conditions.

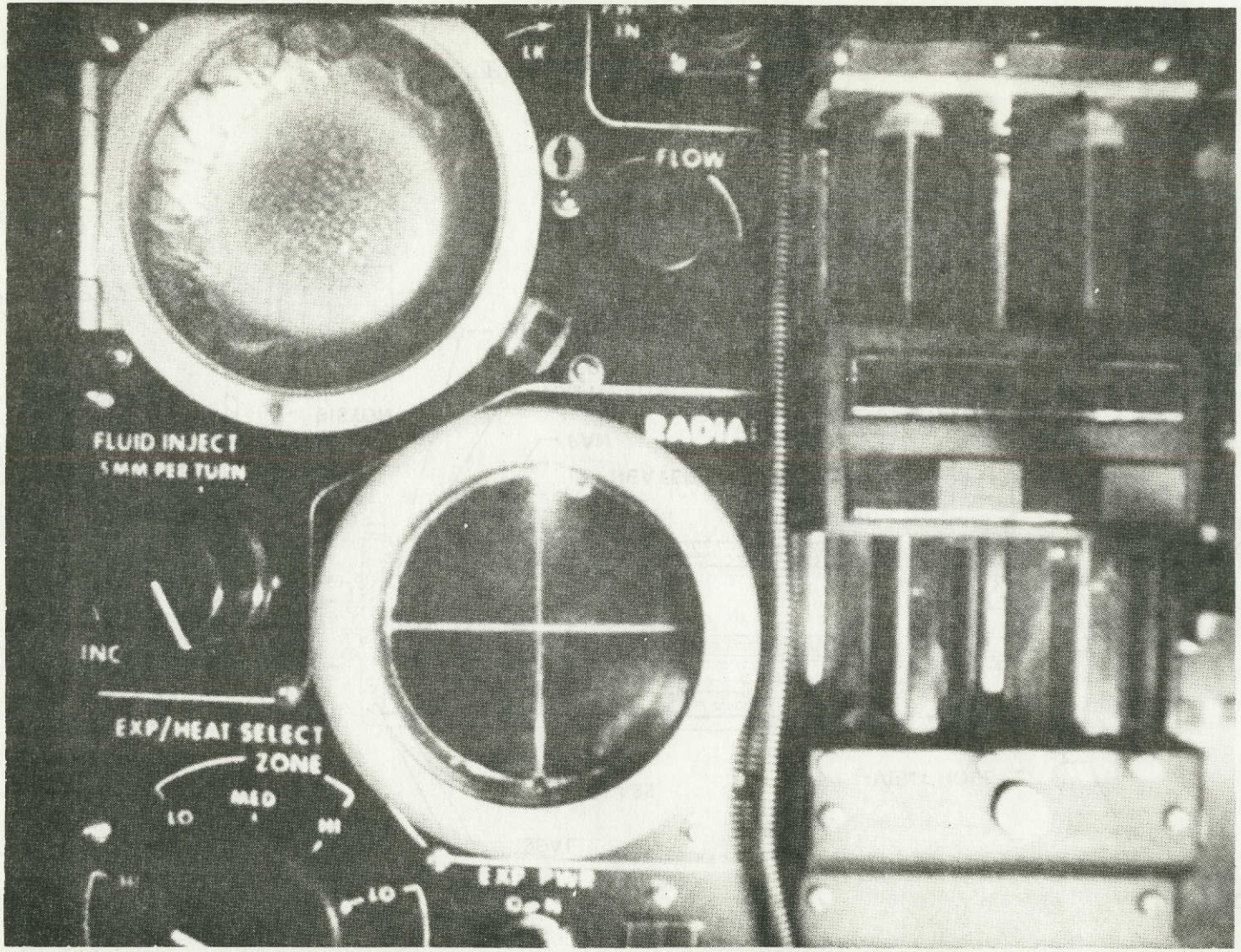

Figure 7. Flight Bénard cells (circumferential pattern — upper left-hand corner of photograph).

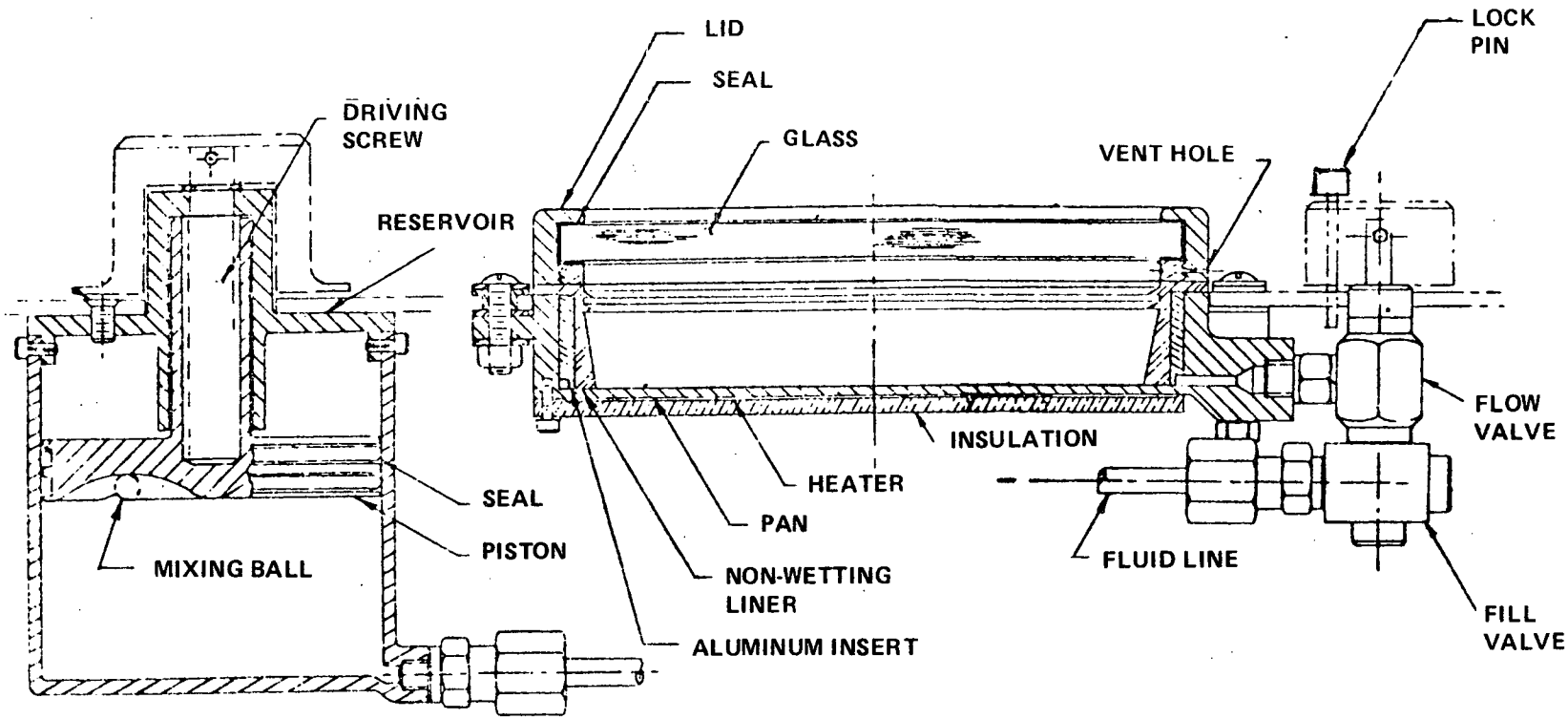

Figure 8. Flow pattern cell diagram.

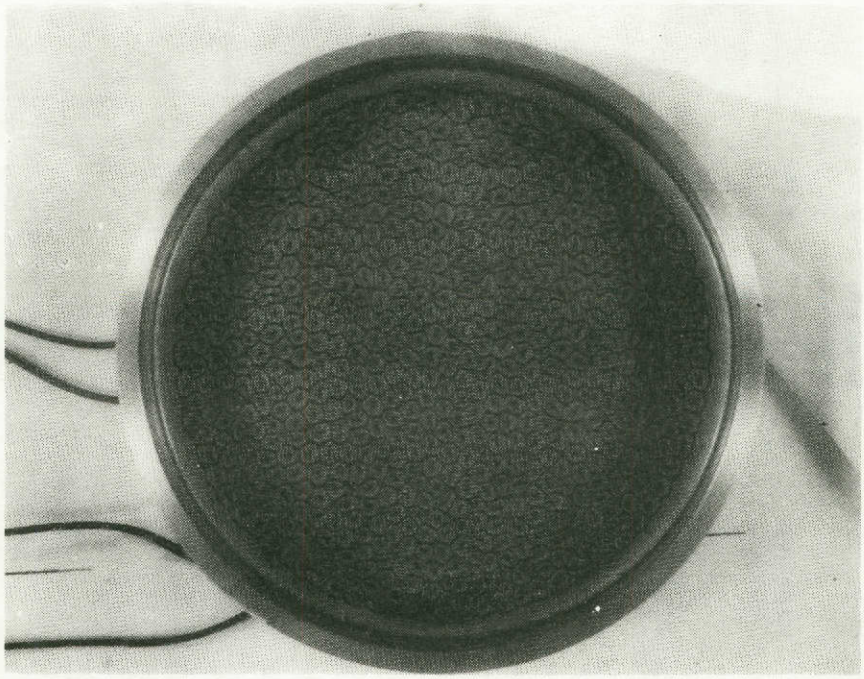

Figure 9. Ground-based Bénard cells
(1 mm depth; shown 1.6 actual size; 7.4W).

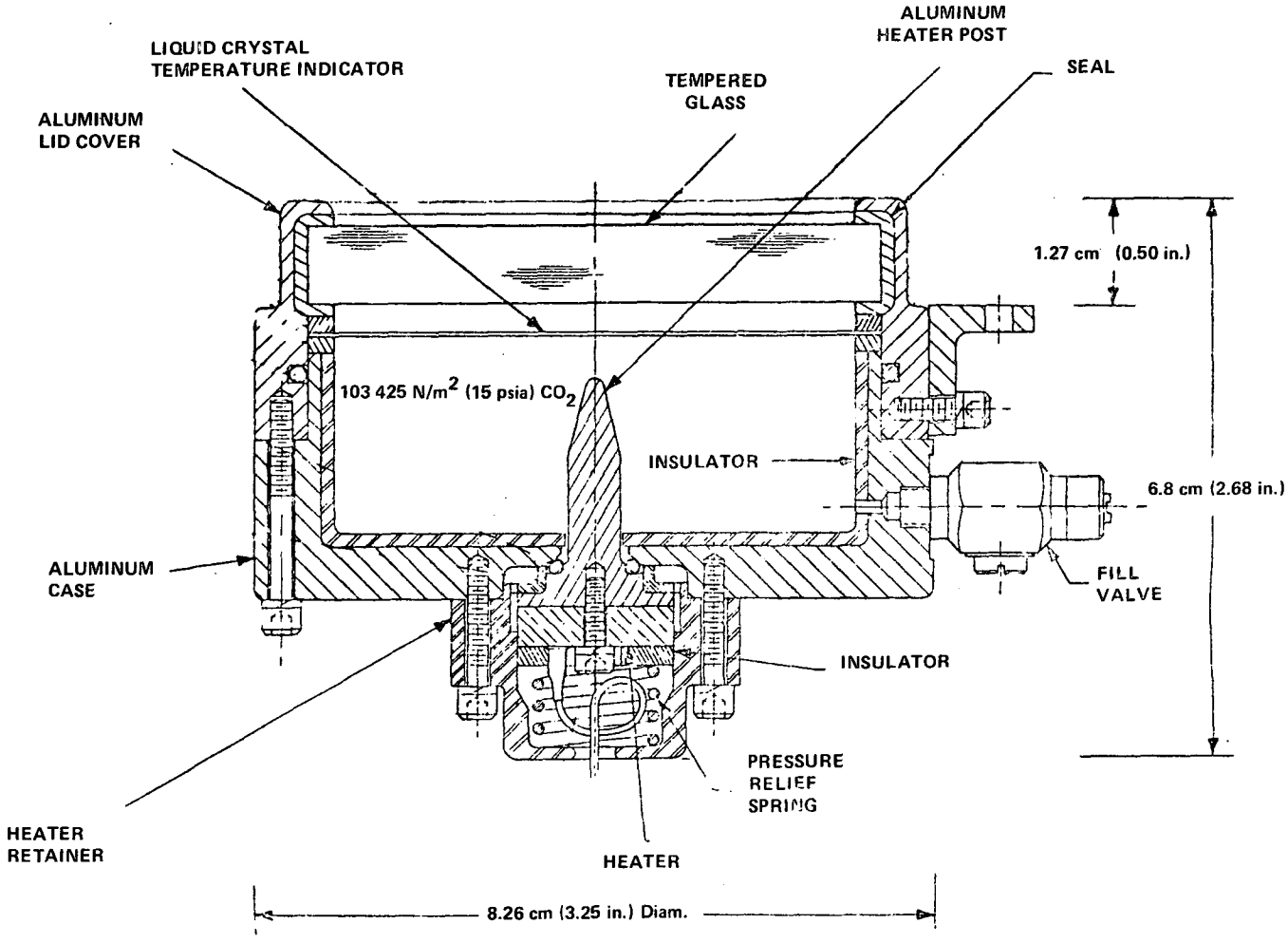

Figure 10. Radial heating cell diagram.

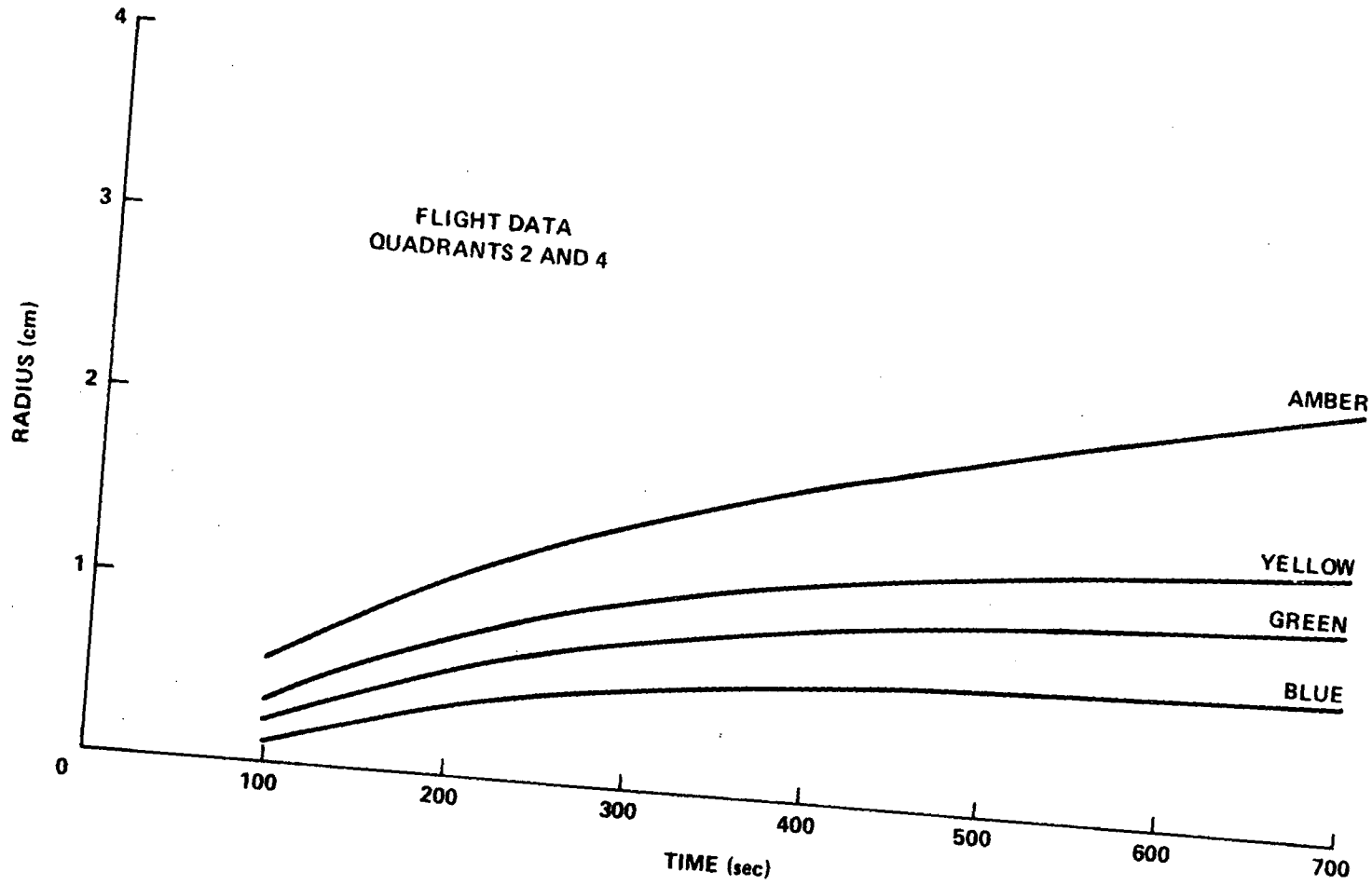

a. 30.8° C isotherm (flight).

Figure 11. Radial heating unit temperature distribution.

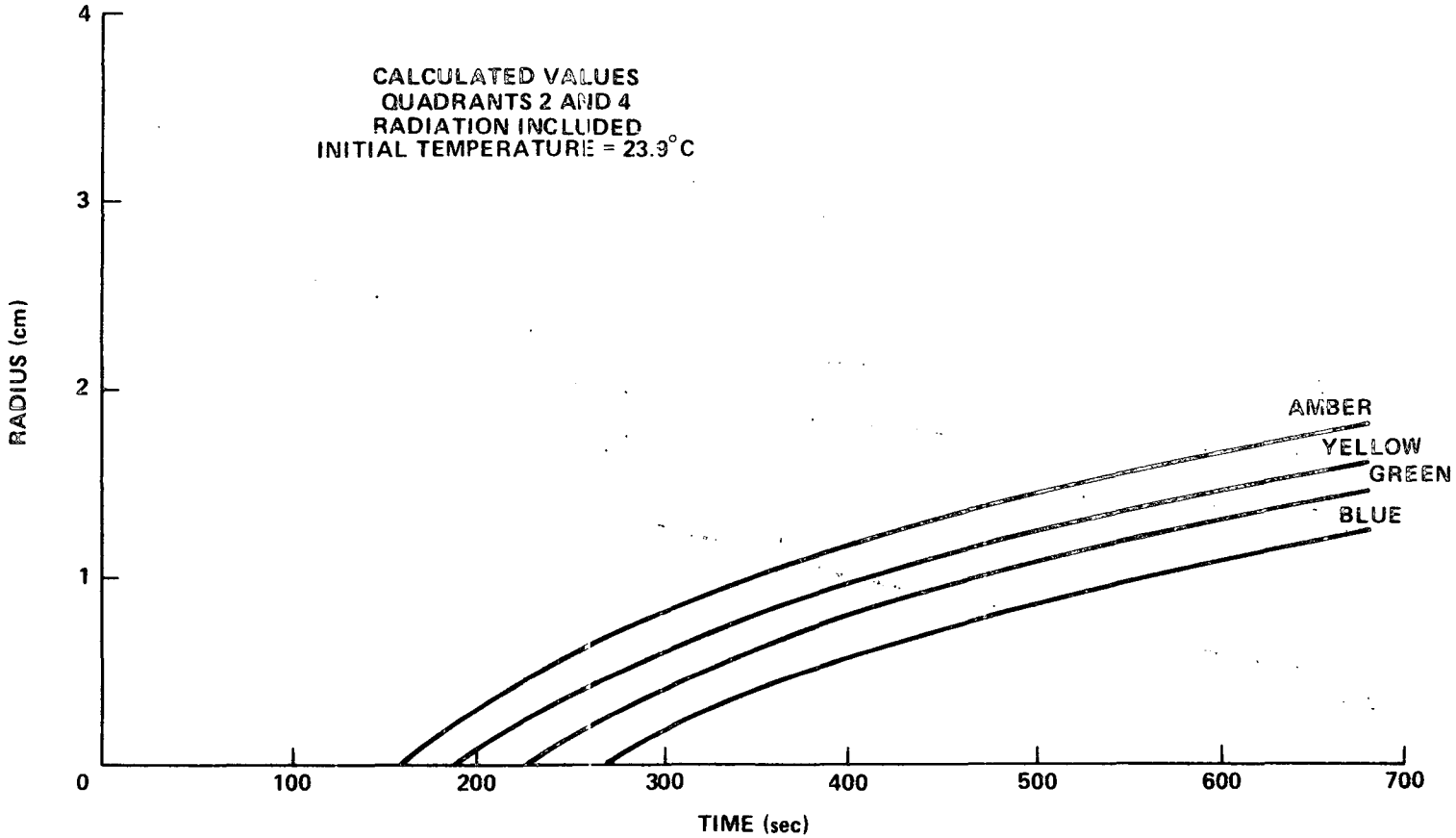

b. 30.8°C isotherm (calculated, Case 1).

Figure 11. (Continued)

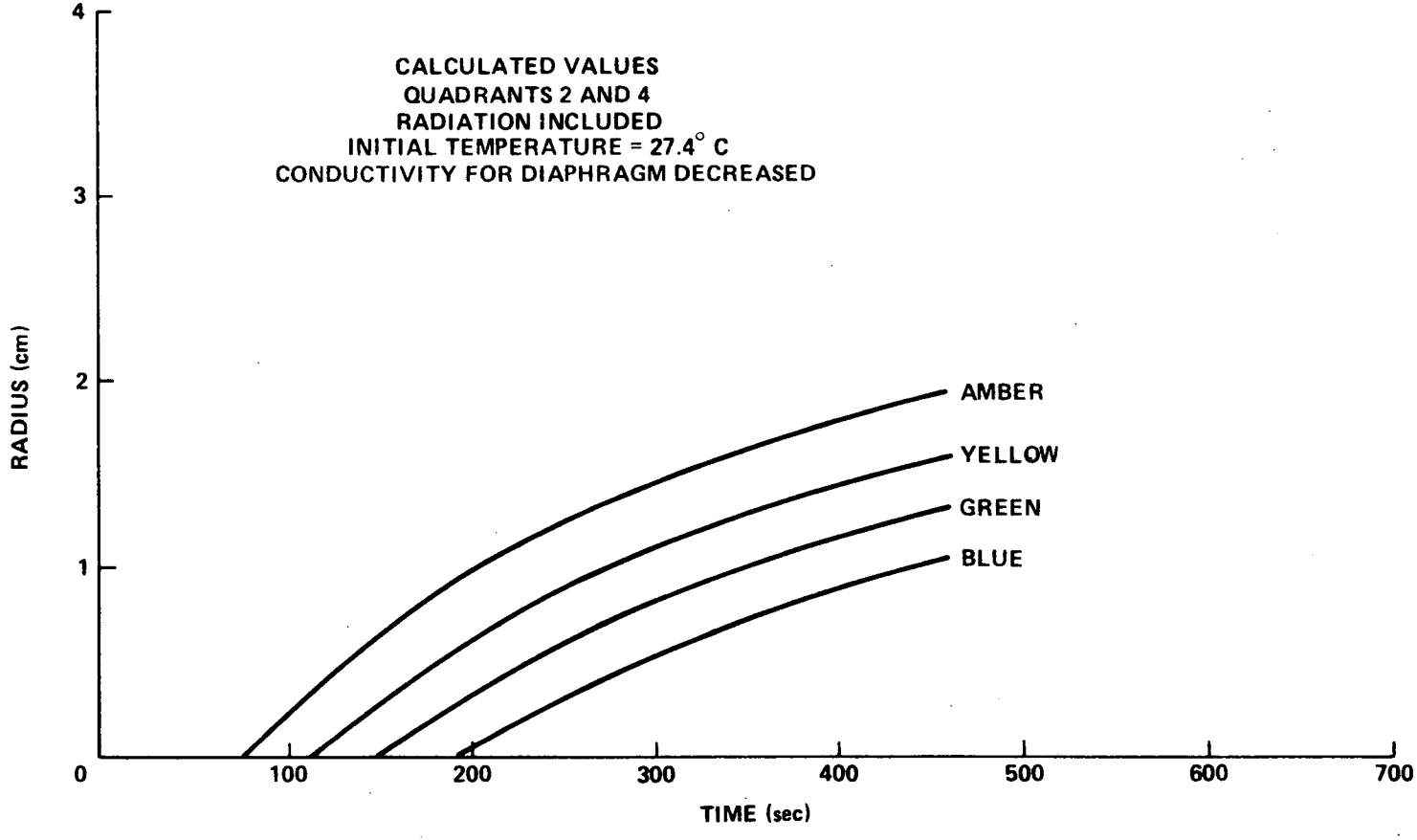

c. 30.8°C isotherm (calculated, Case 2).

Figure 11. (Concluded)

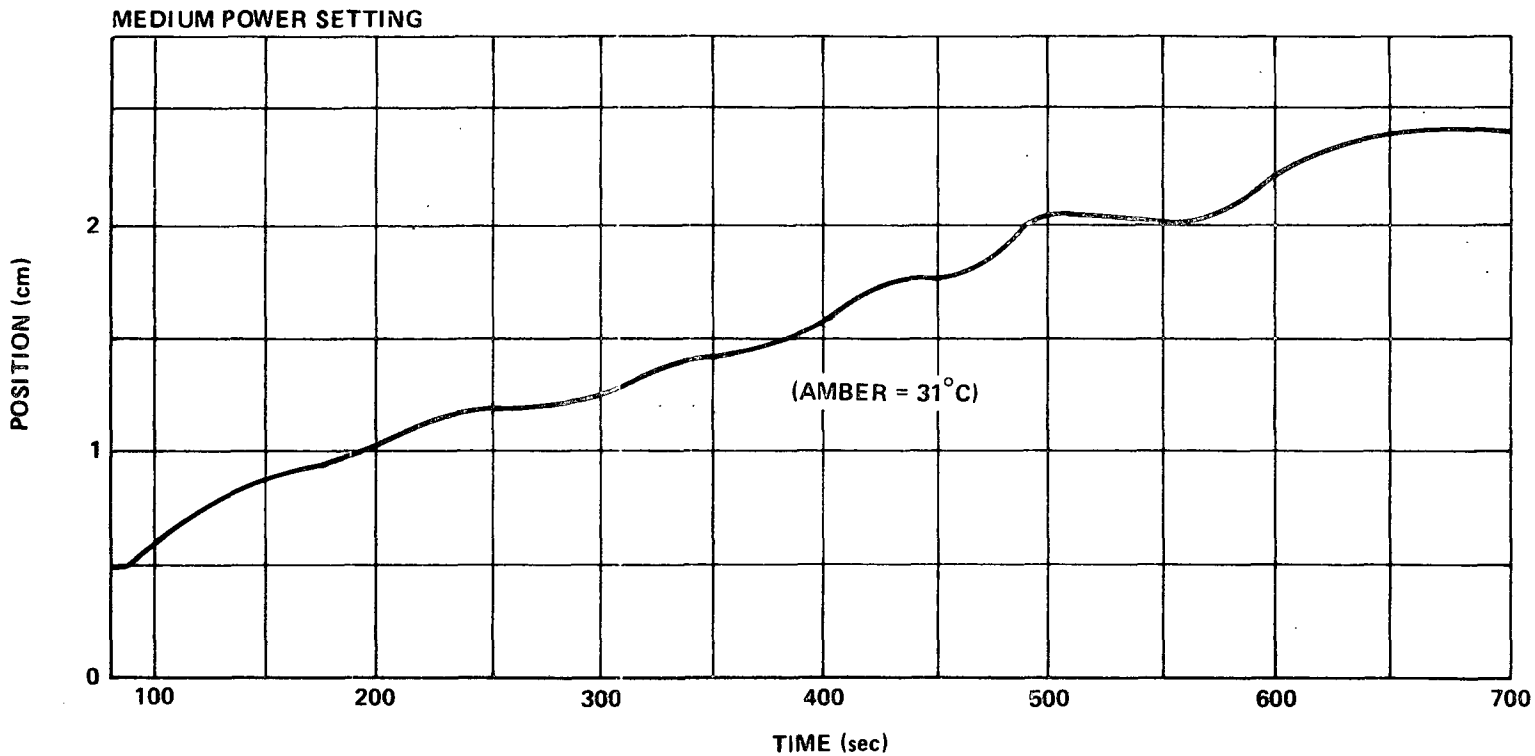

Figure 12. Temperature oscillations.

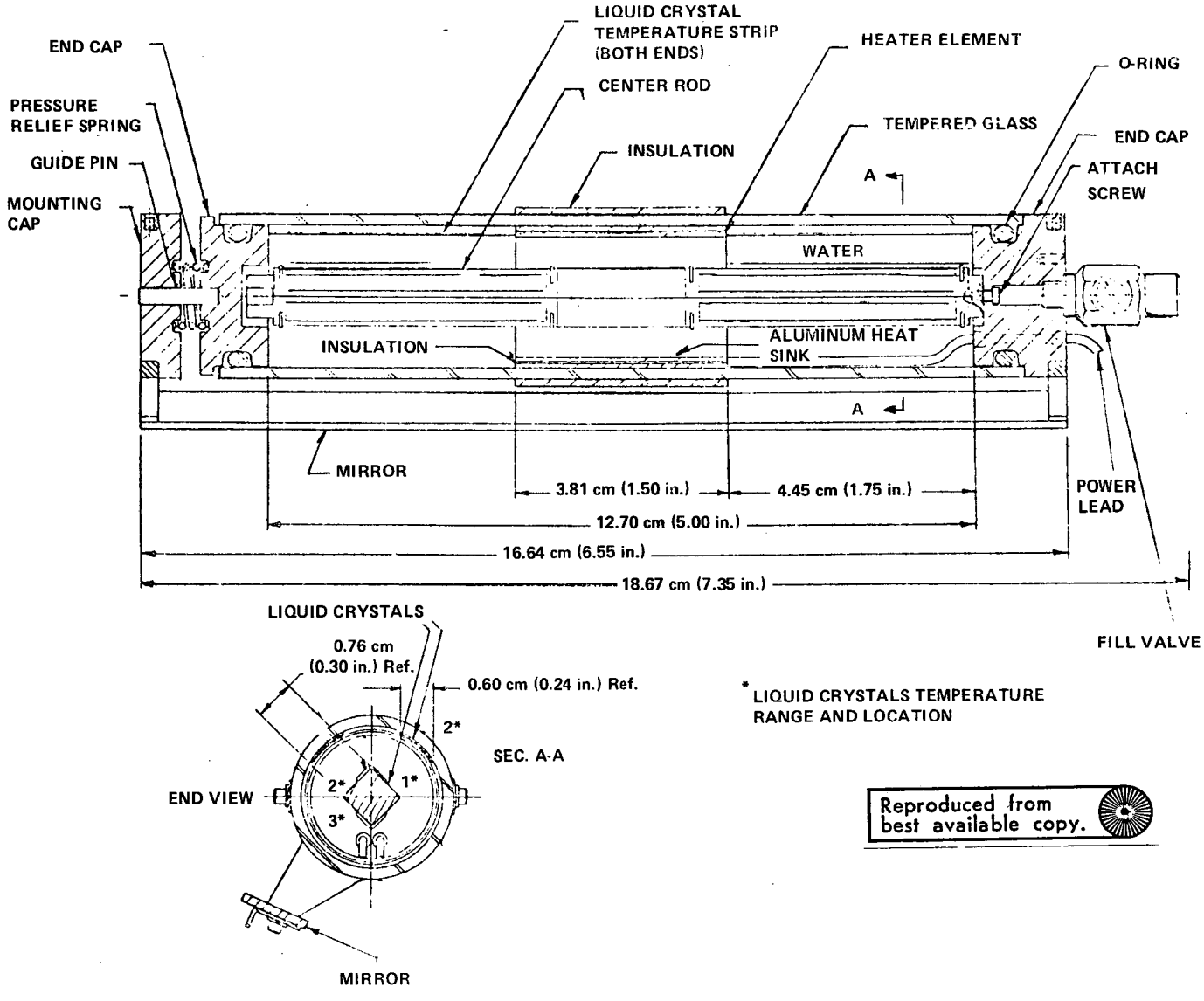

Figure 13. Zone heating diagram.

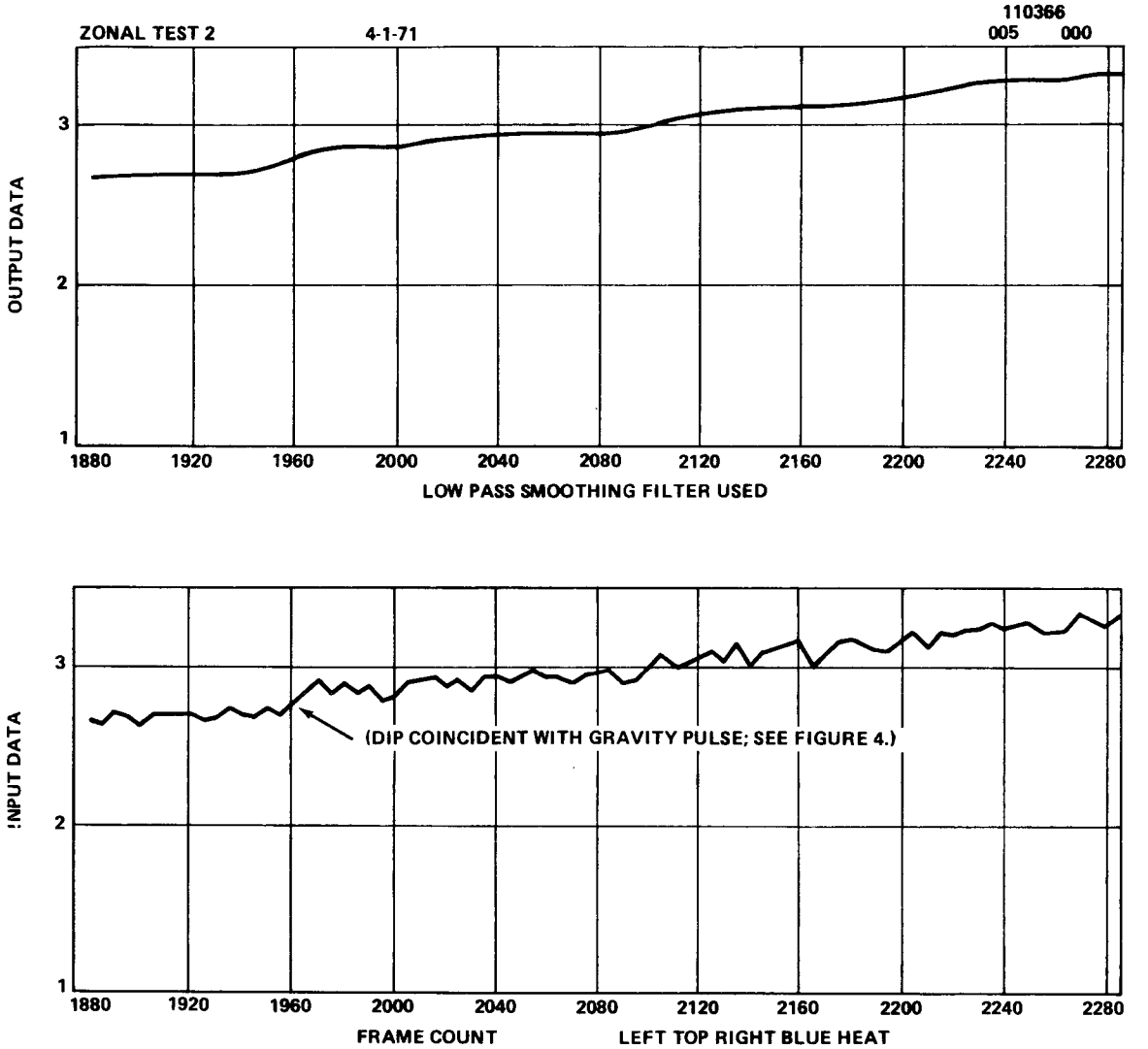

Figure 14. Temperature change at 1960 sec.

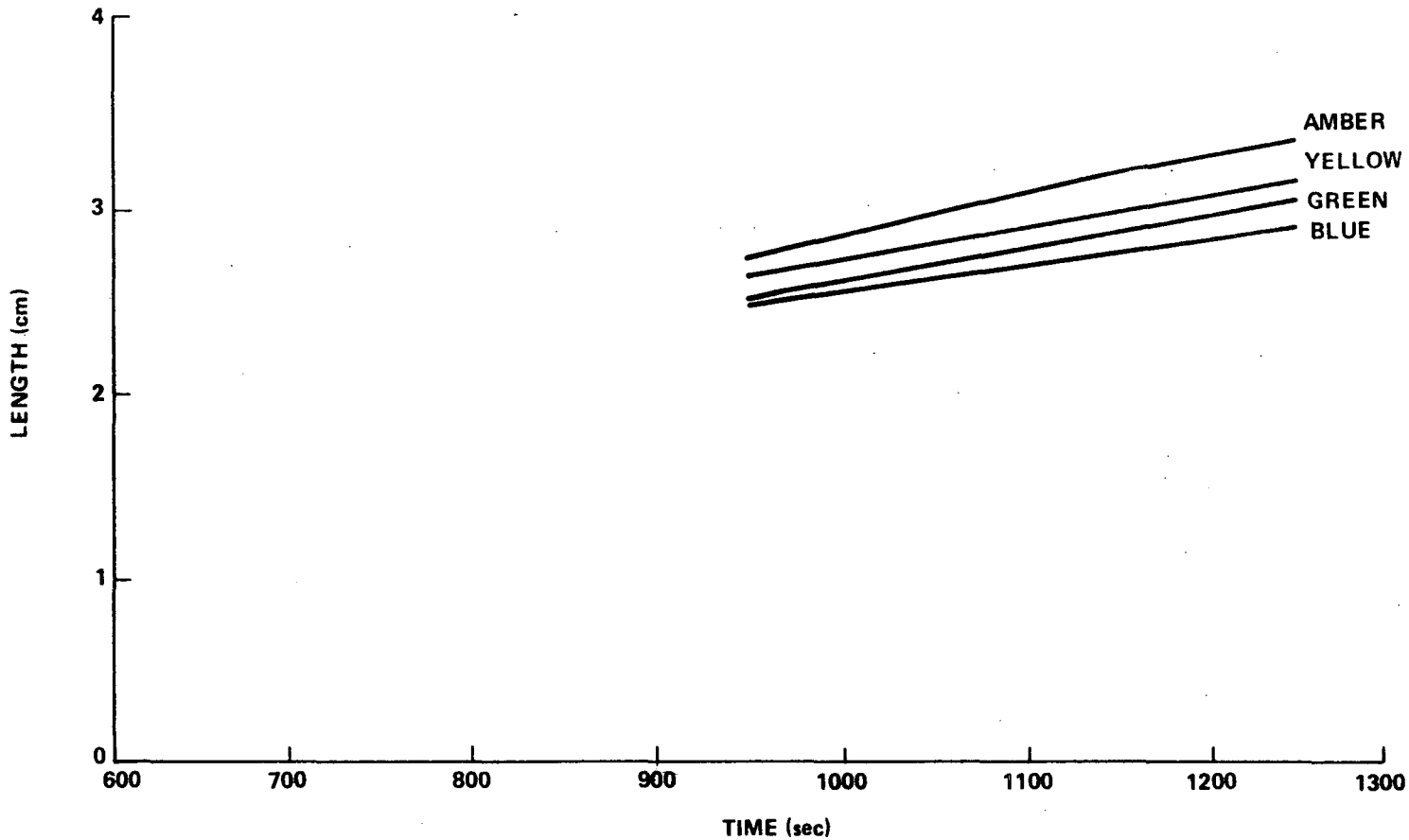

a. Flight data.

Figure 15. Zone heating unit temperature distribution.

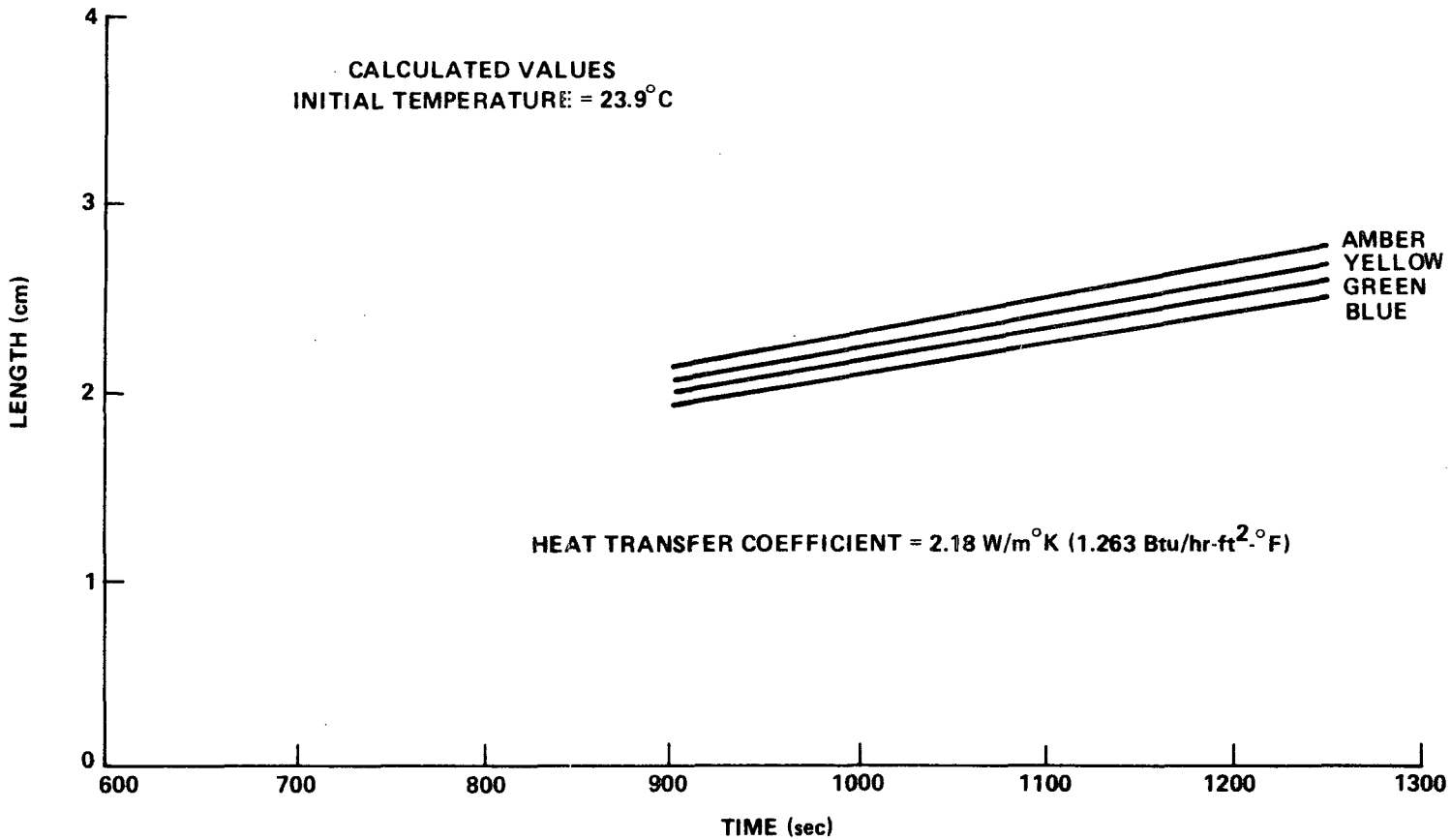

b. Calculated, Case 1.

Figure 15. (Continued)

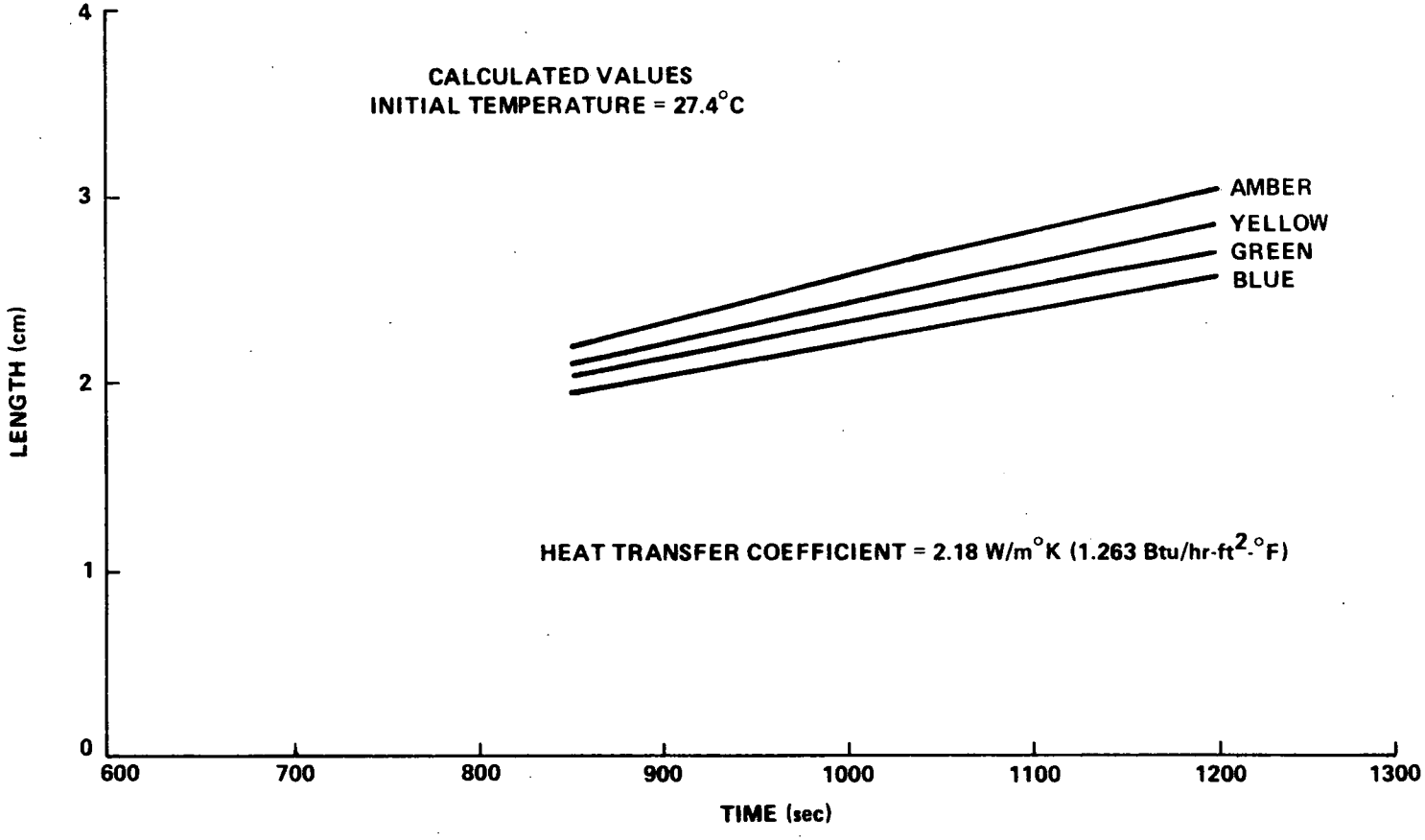

c. Calculated, Case 2.

Figure 15. (Continued)

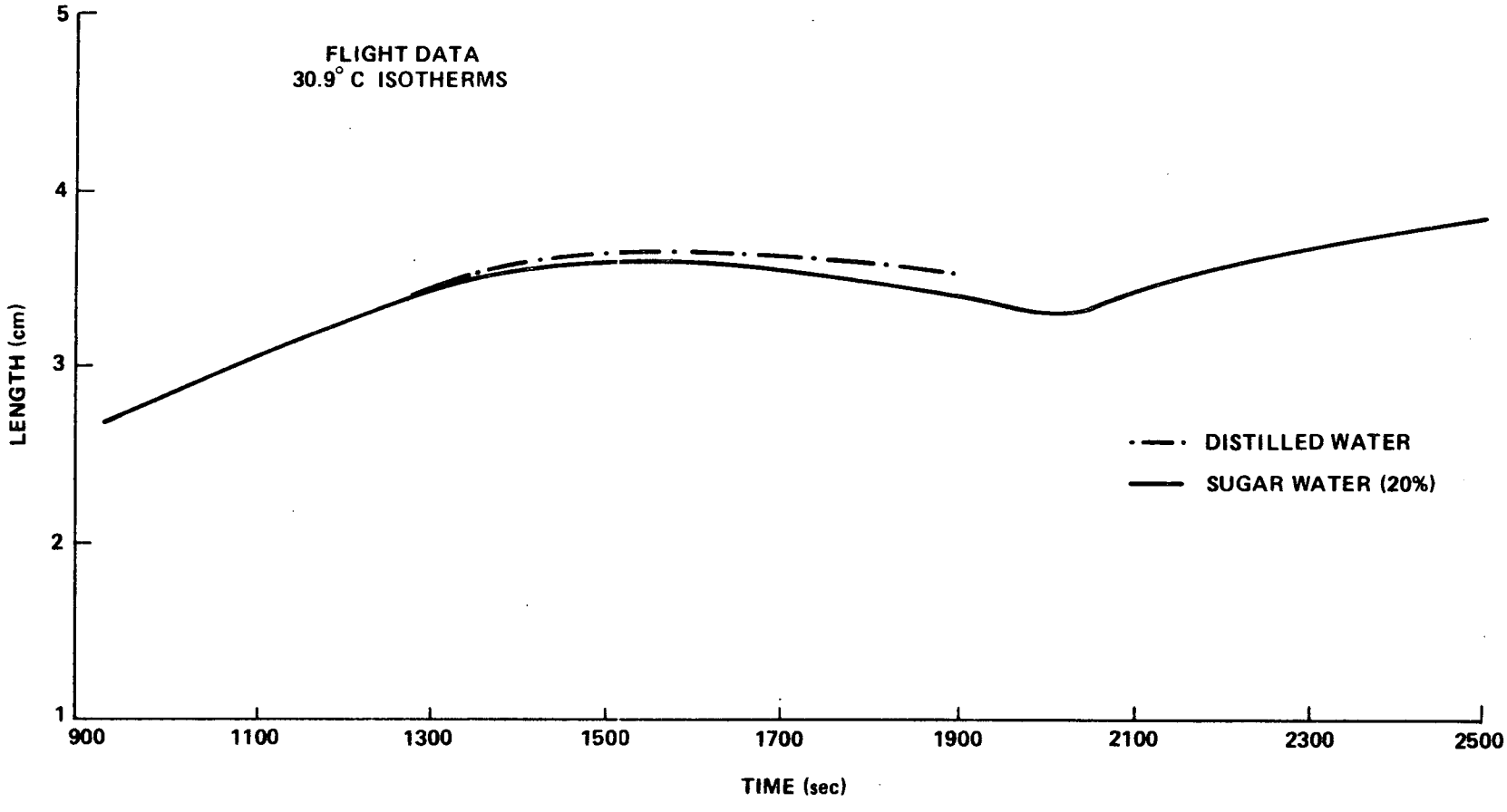

d. Comparison of the two zone cells.

Figure 15. (Concluded)

APPENDIX

DATA CURVES

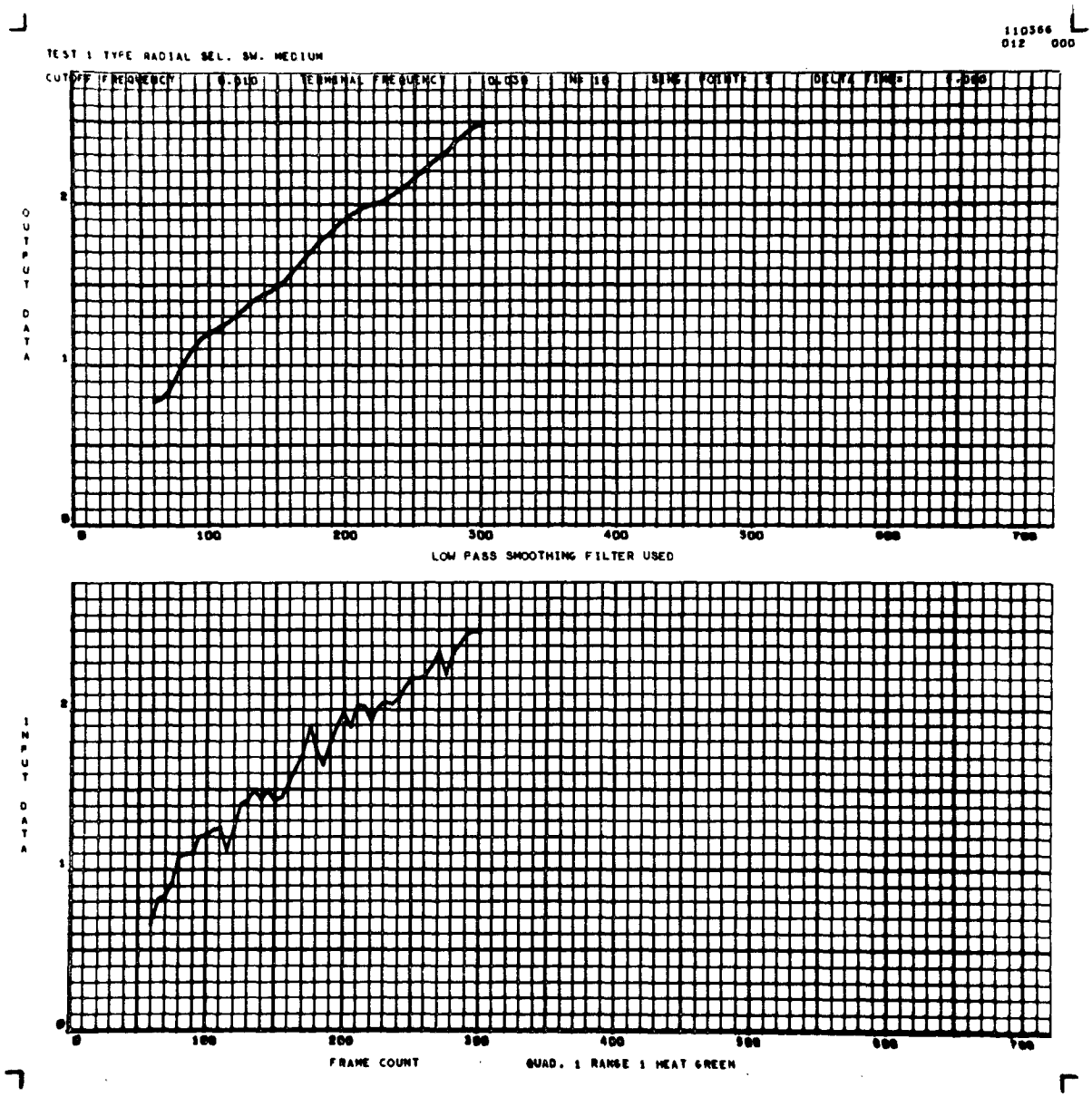

Figure A-1. Radial cell, run 1, quadrant 1, range 1, green, power on.

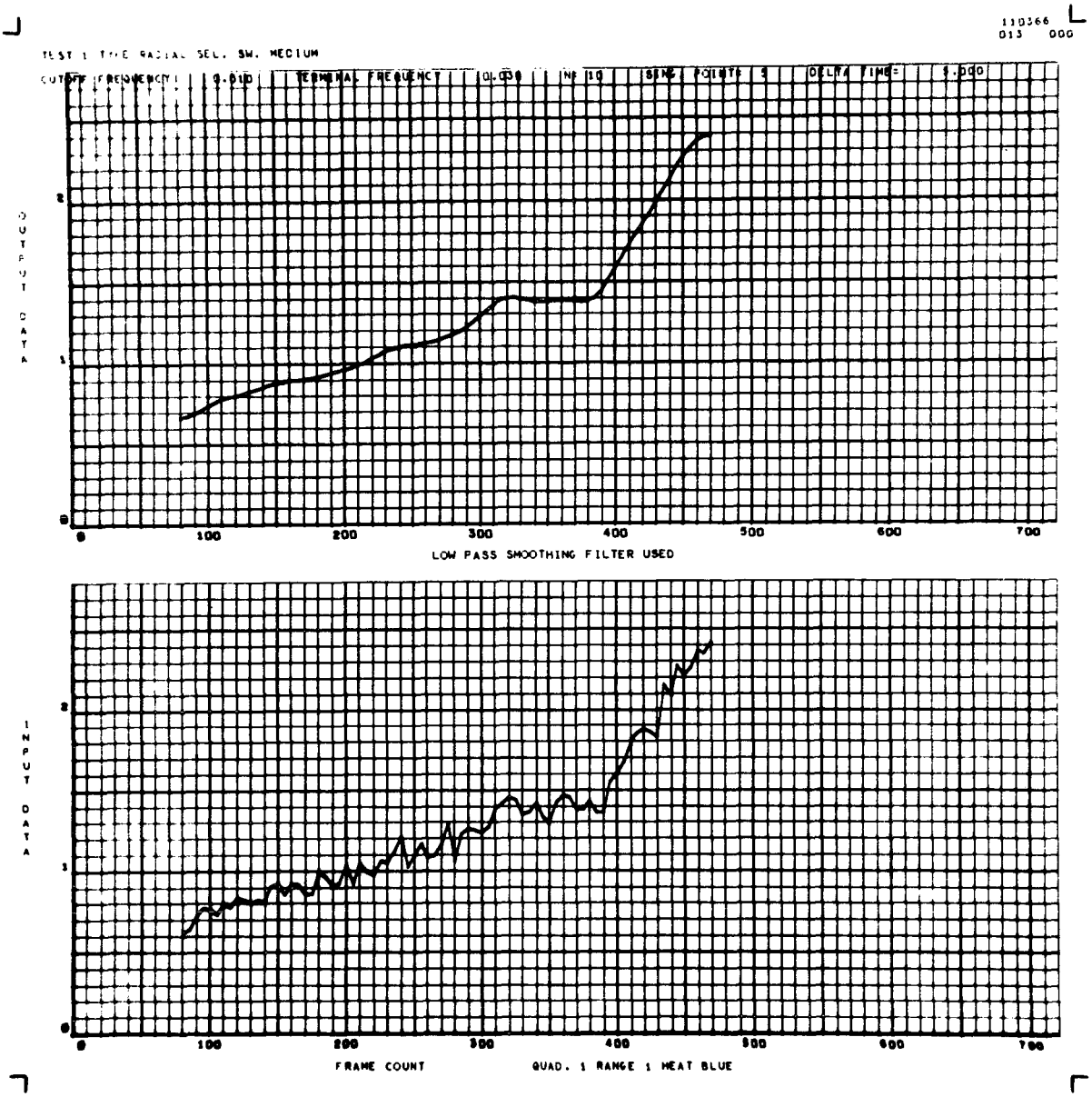

Figure A-2. Radial cell, run 1, quadrant 1, range 1, blue, power on.

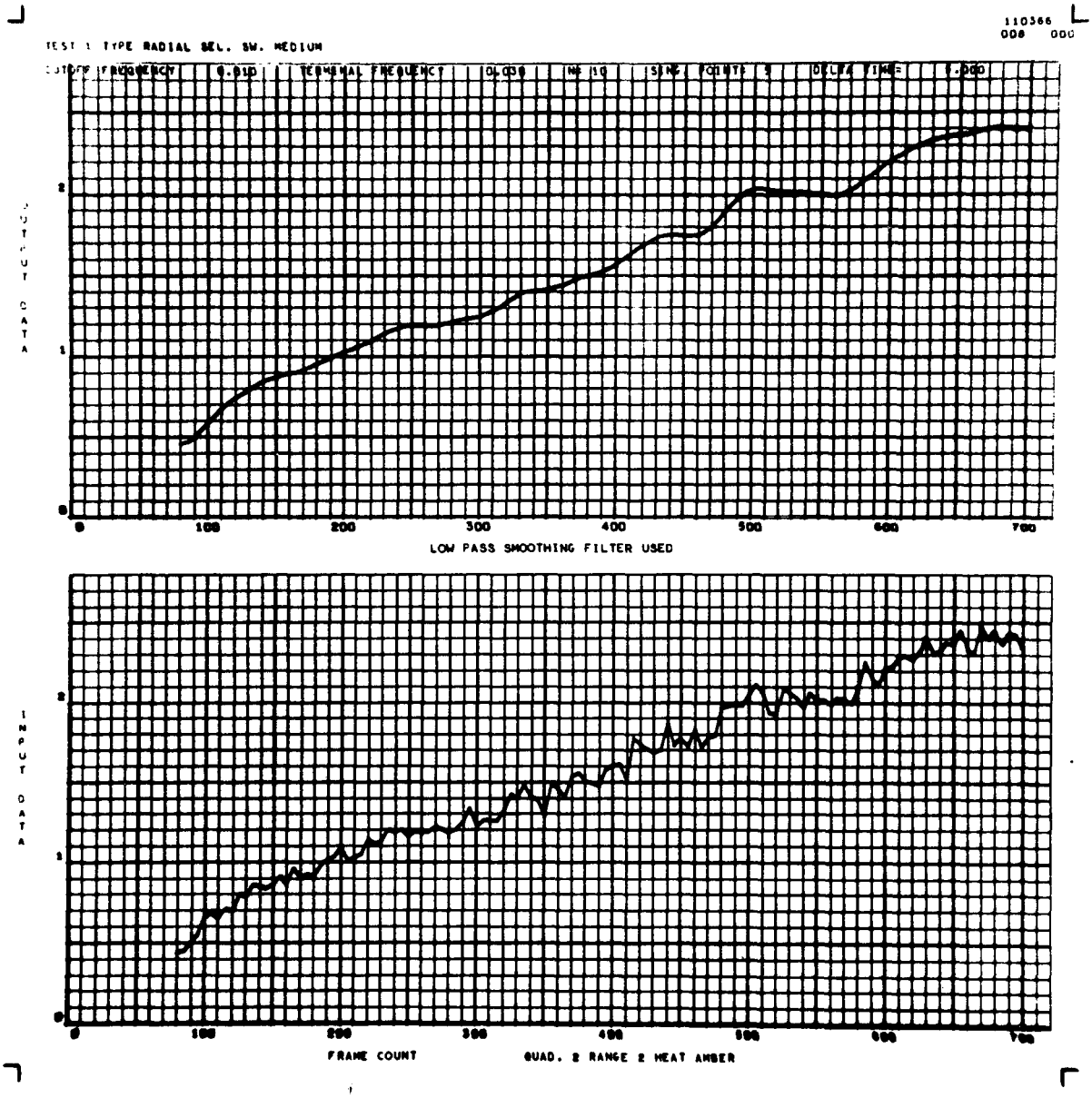

Figure A-3. Radial cell, run 1, quadrant 2, range 2, amber, power on.

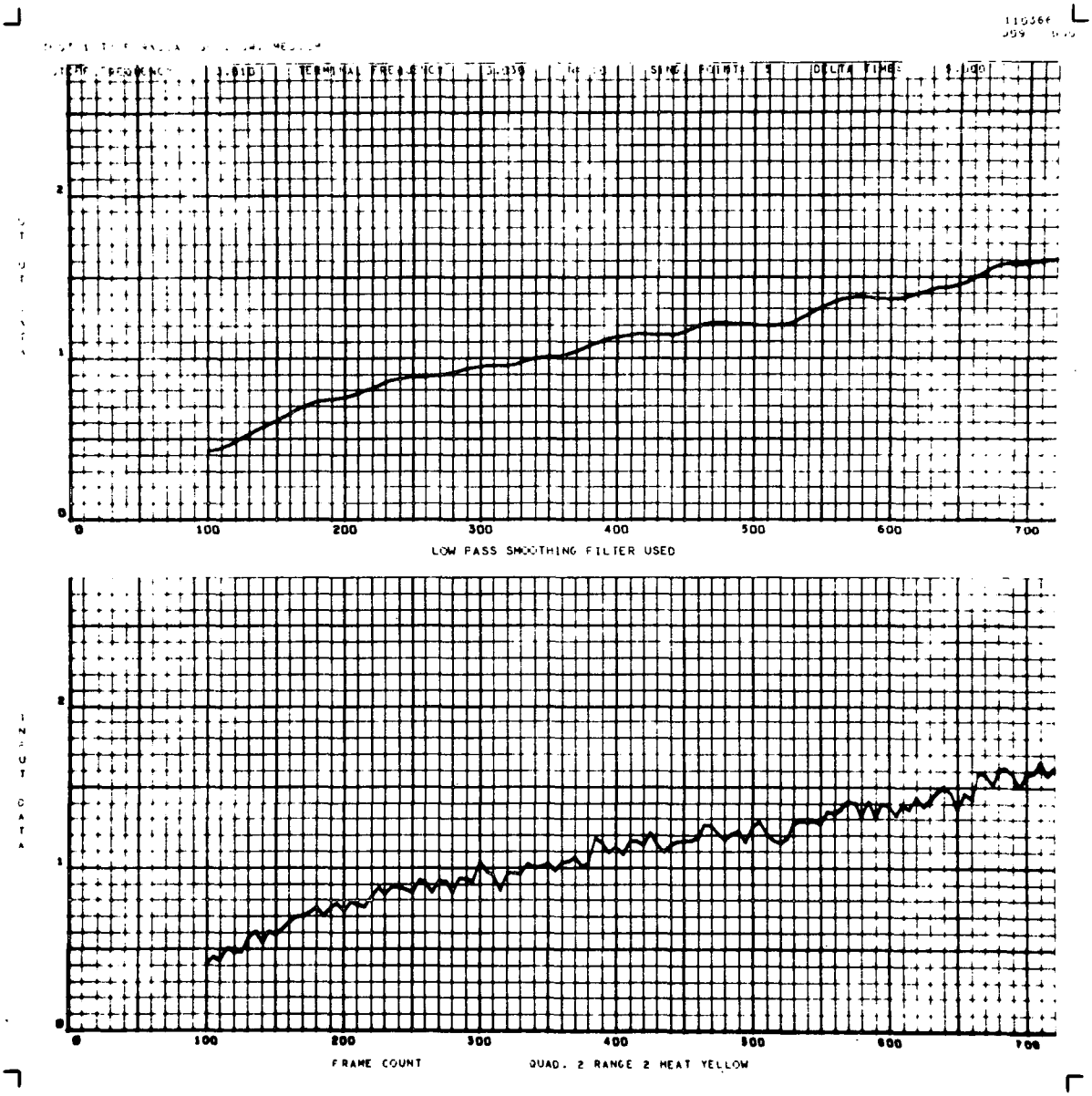

Figure A-4. Radial cell, run 1, quadrant 2, range 2, yellow, power on.

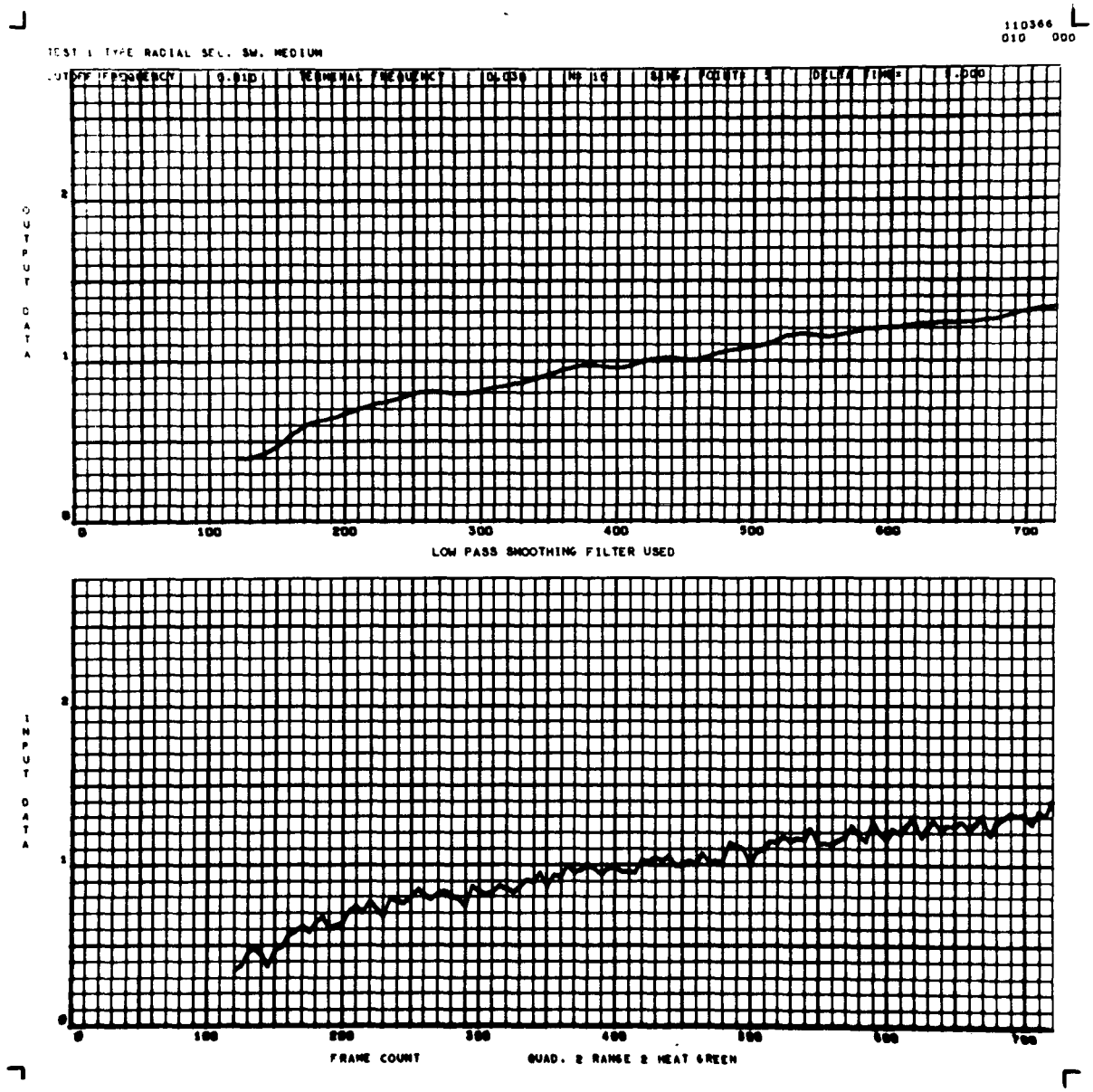

Figure A-5. Radial cell, run 1, quadrant 2, range 2, green, power on.

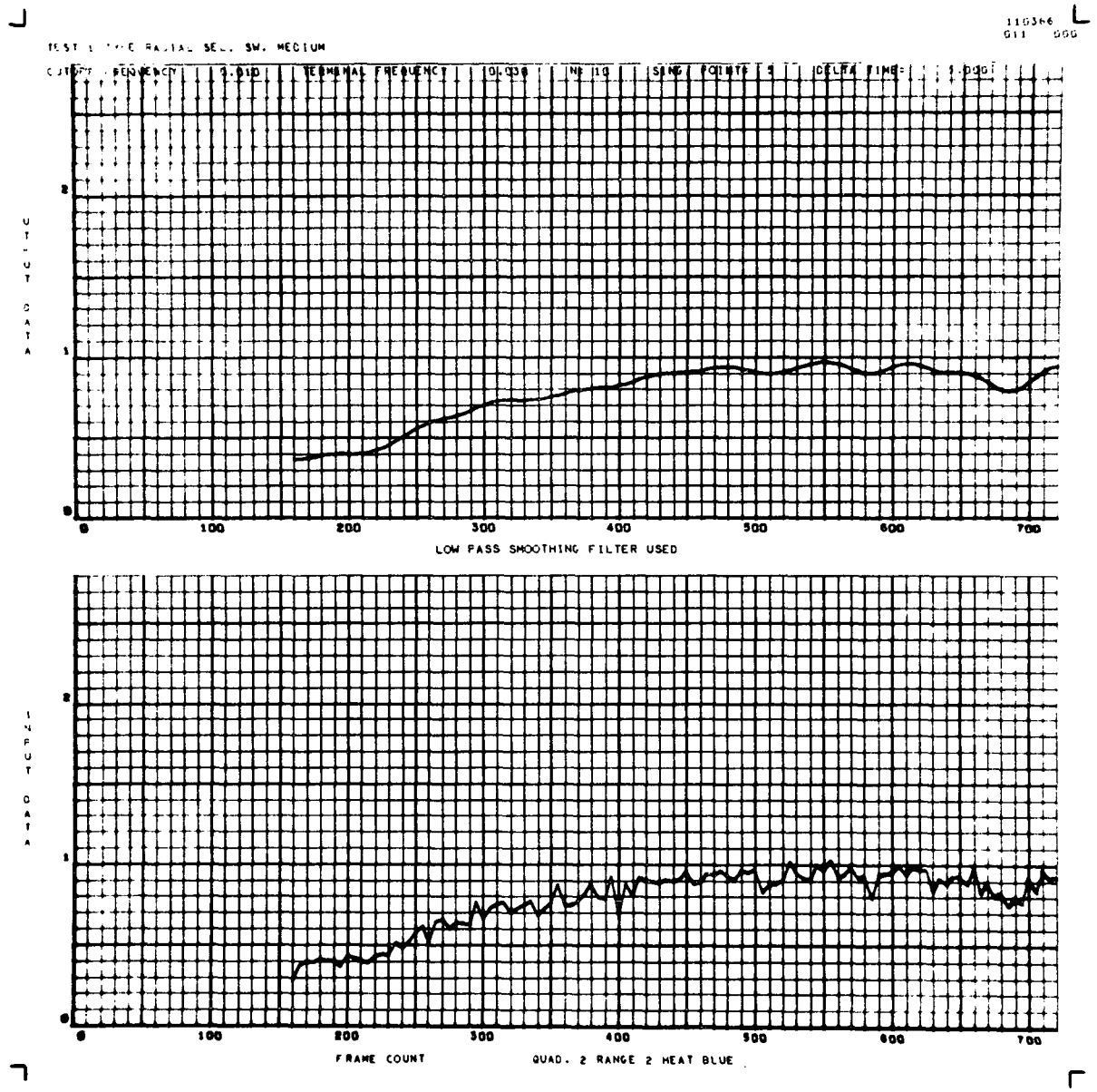

Figure A-6. Radial cell, run 1, quadrant 2, range 2, blue, power on.

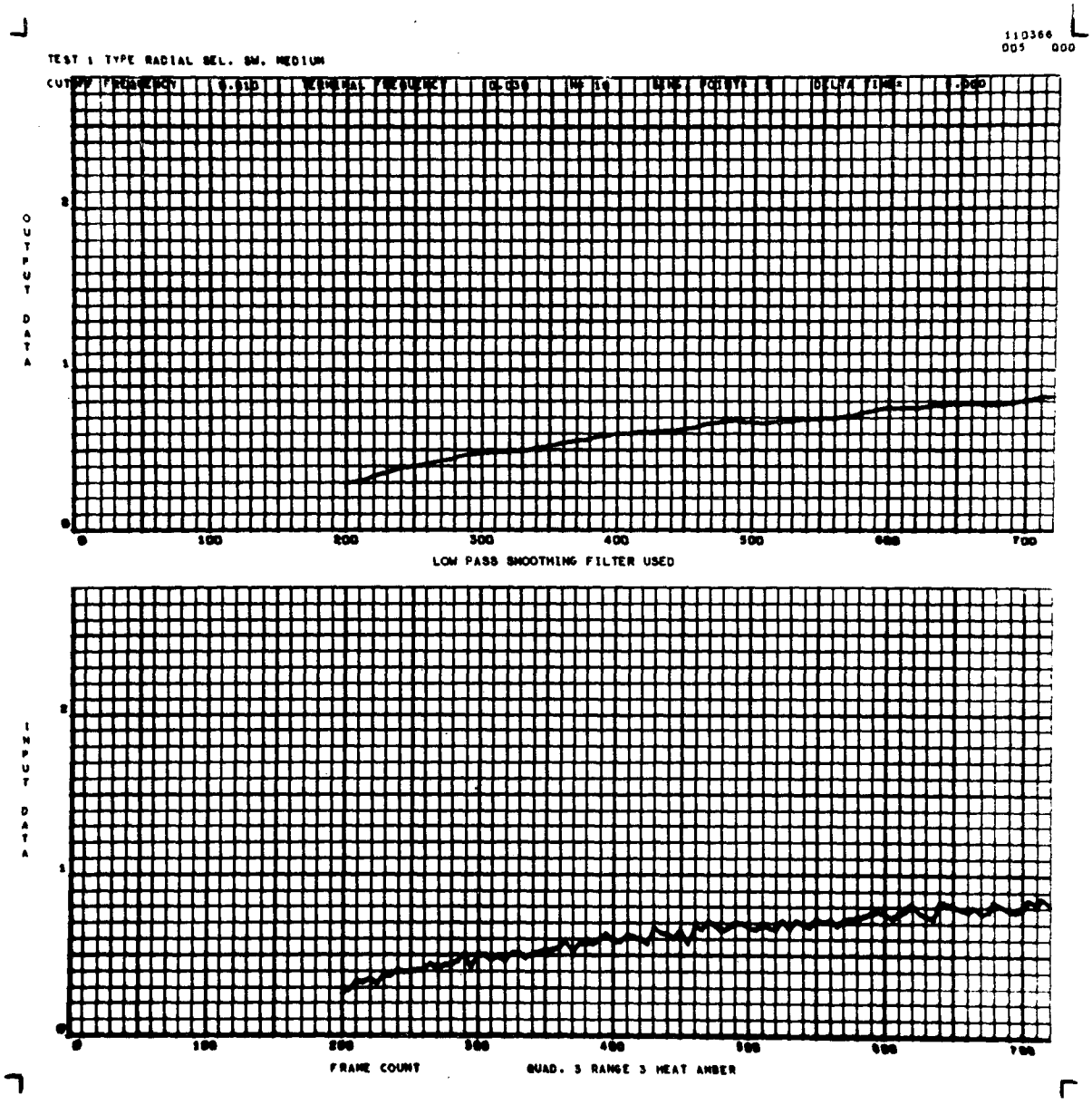

Figure A-7. Radial cell, run 1, quadrant 3, range 3, amber, power on.

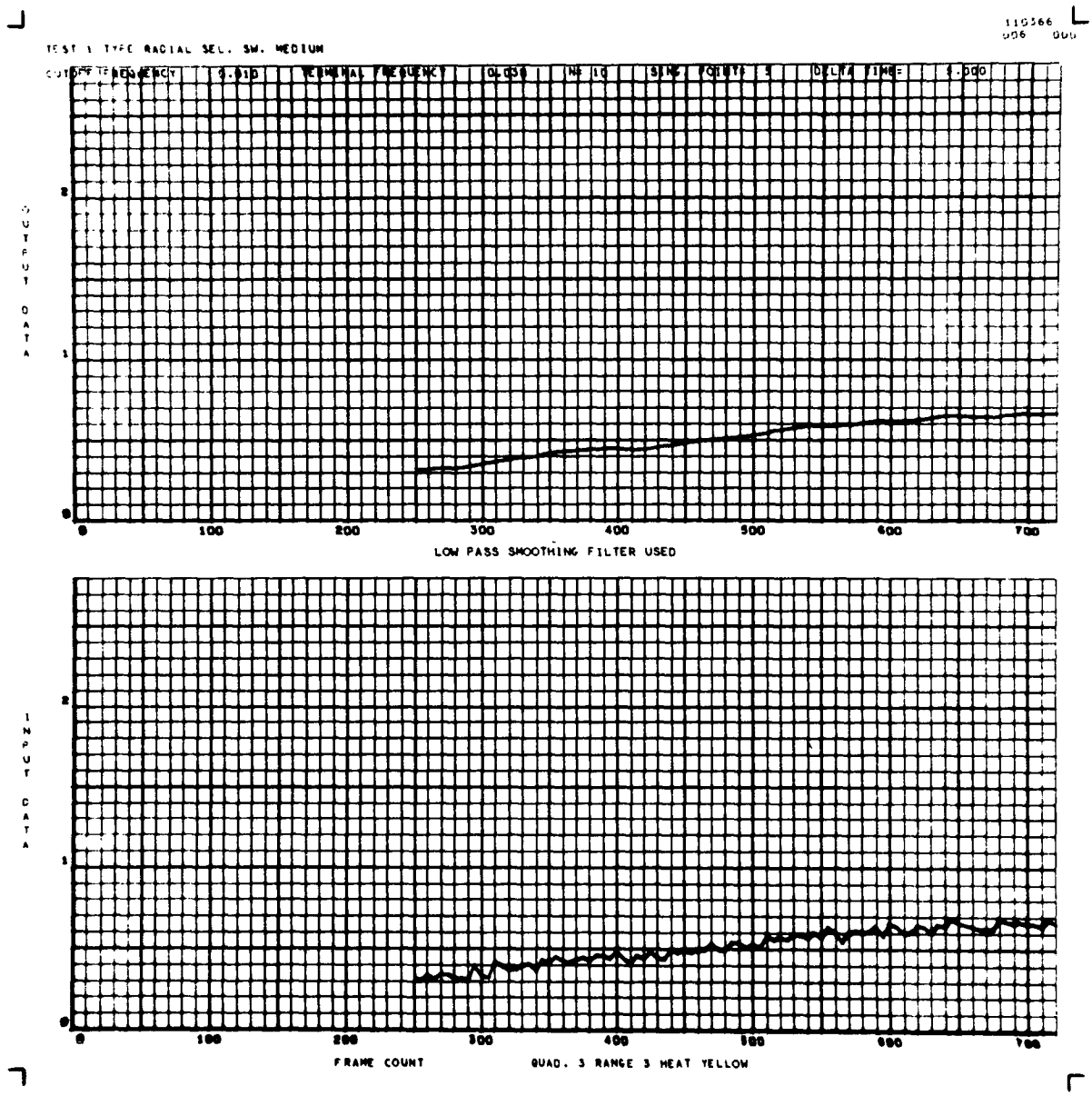

Figure A-8. Radial cell, run 1, quadrant 3, range 3, yellow, power on.

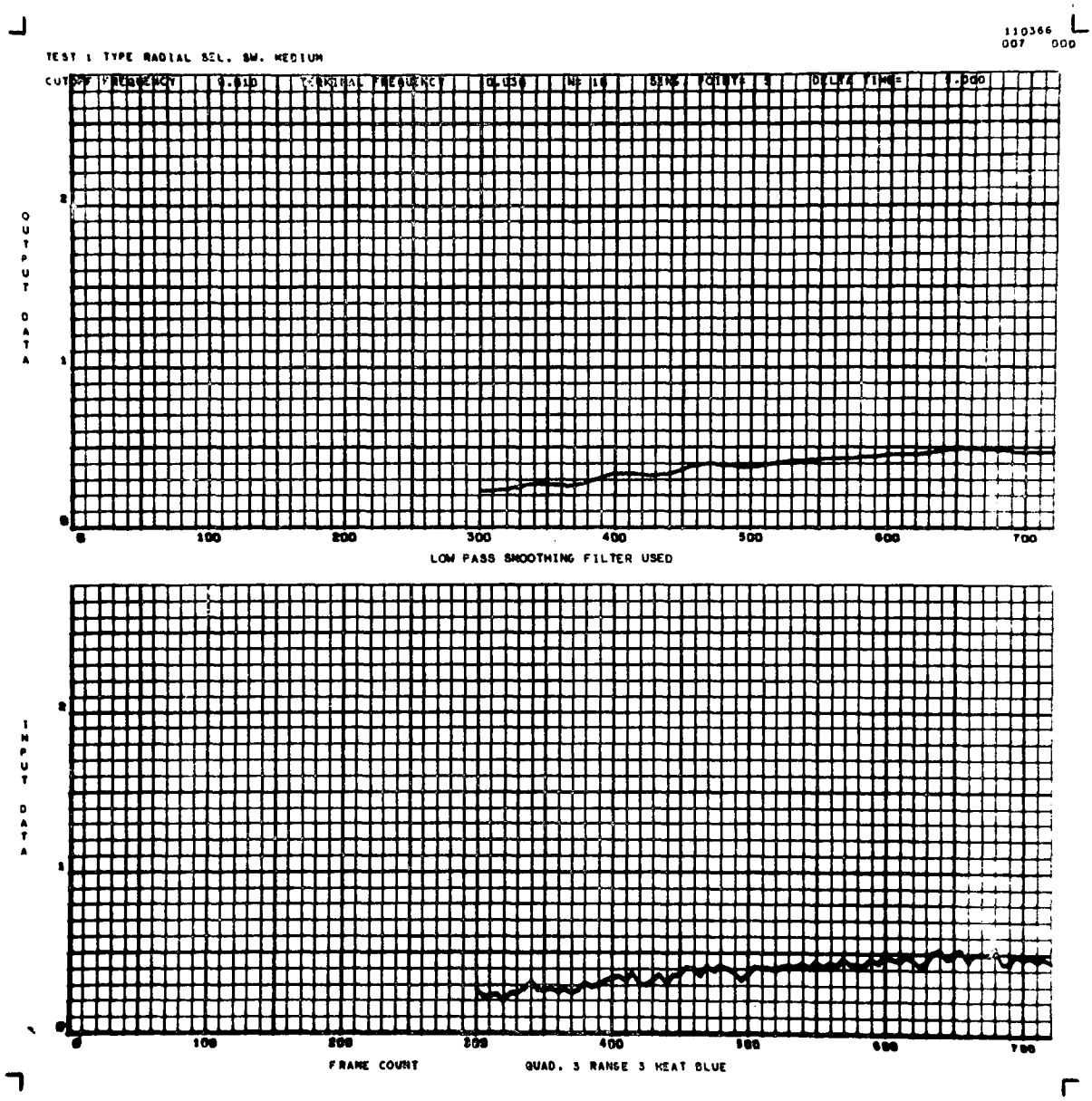

Figure A-9. Radial cell, run 1, quadrant 3, range 3, blue, power on.

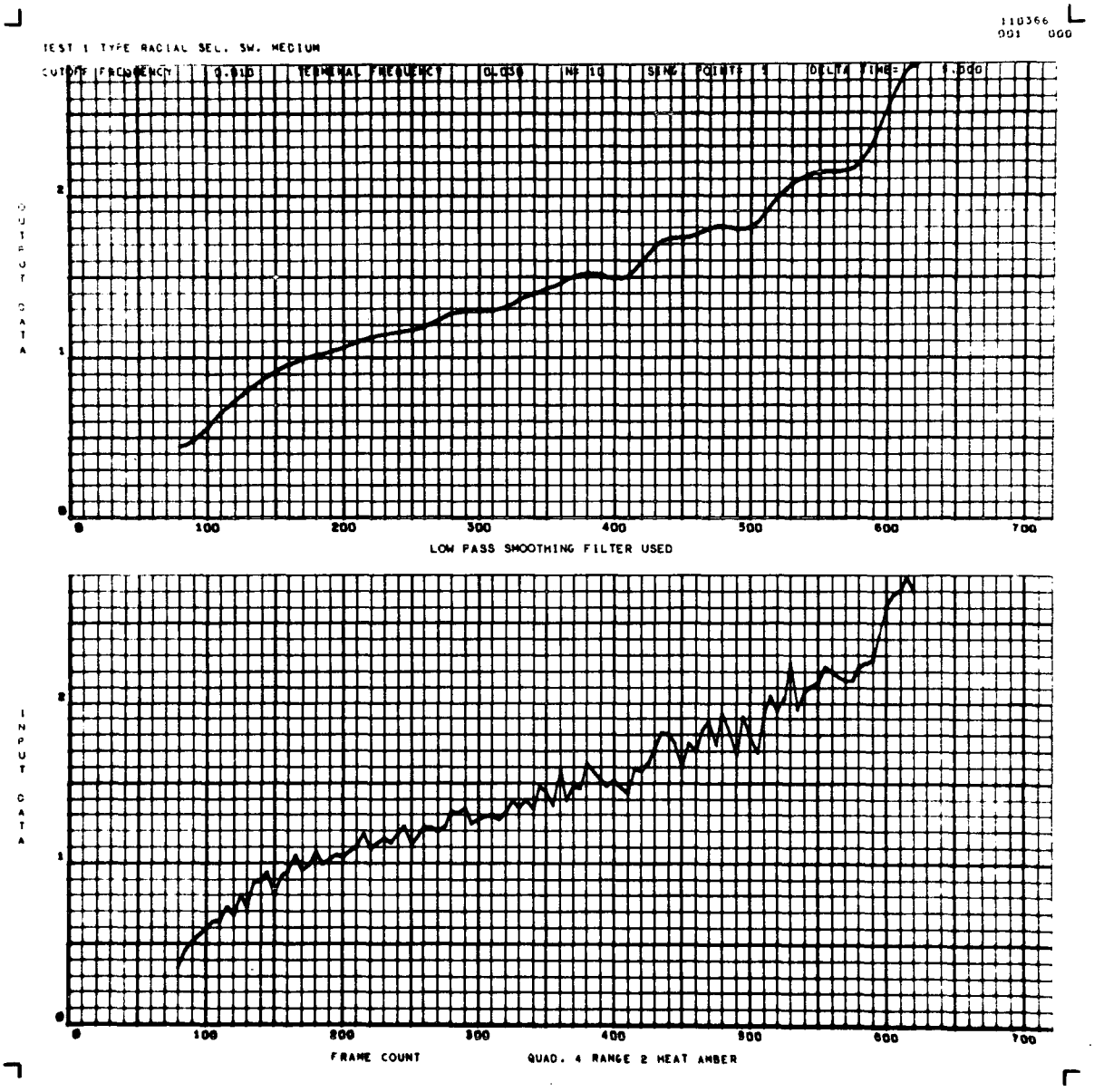

Figure A-10. Radial cell, run 1, quadrant 4, range 2, amber, power on.

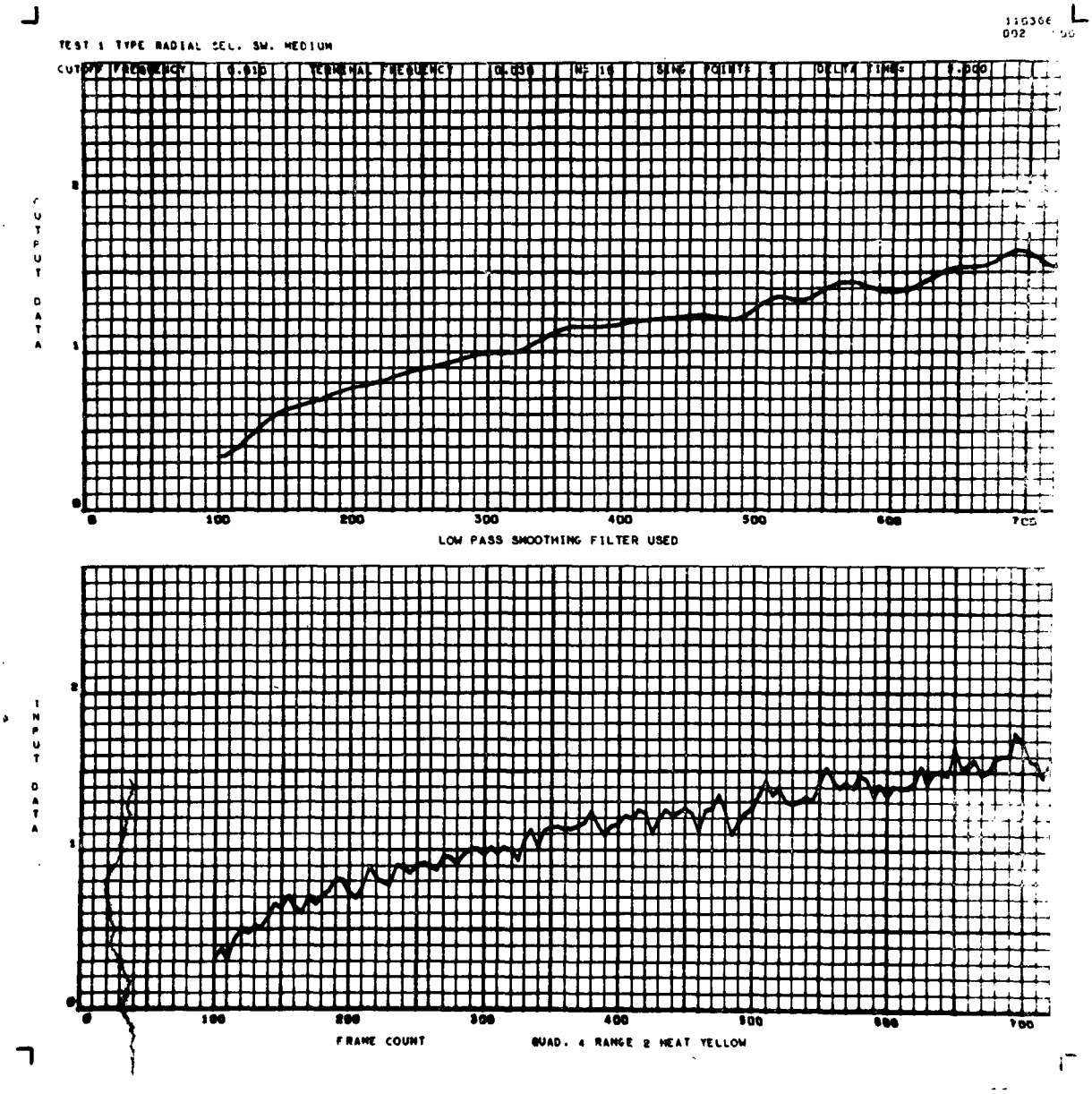

Figure A-11. Radial cell, run 1, quadrant 4, range 2, yellow, power on.

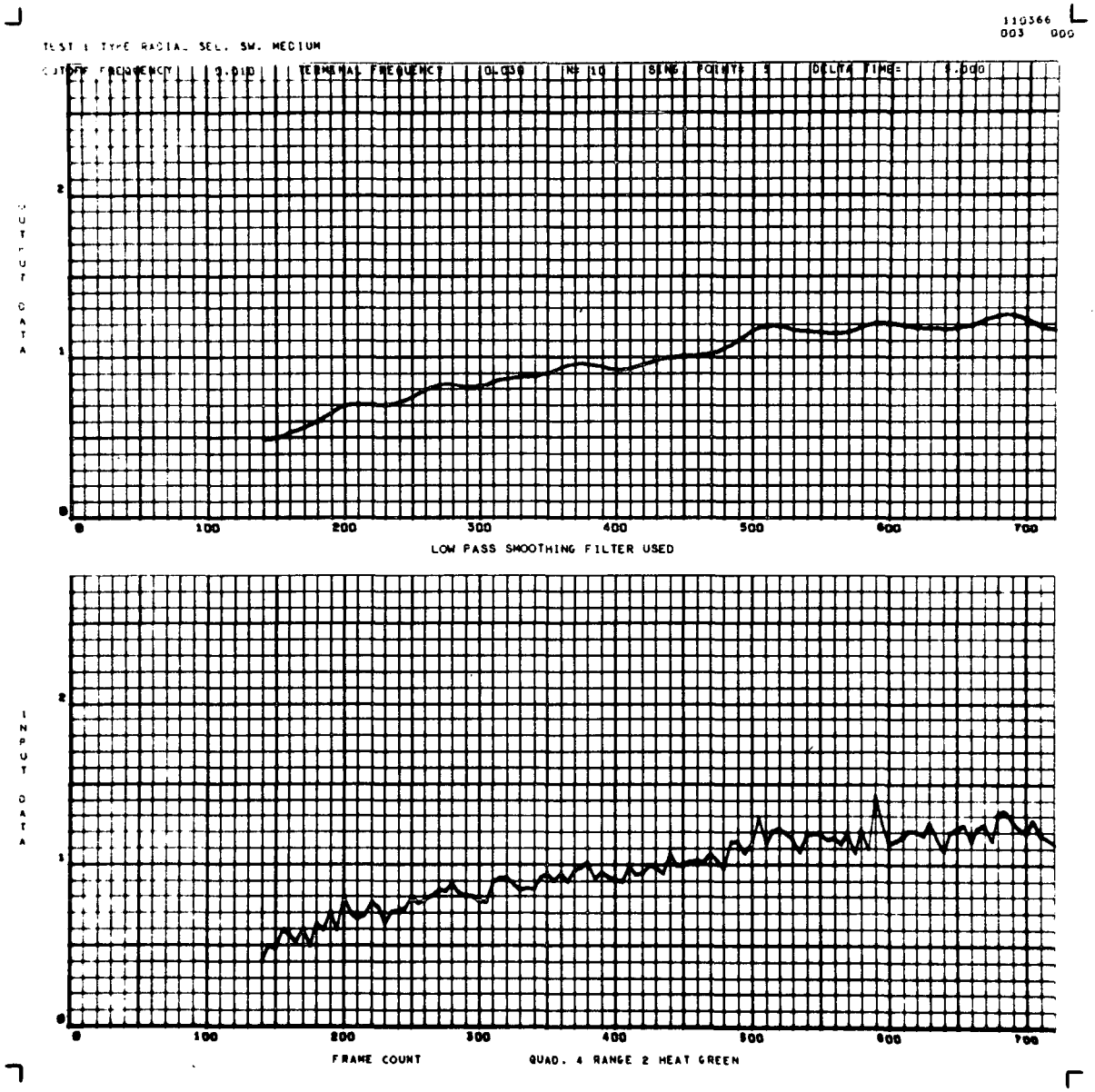

Figure A-12. Radial cell, run 1, quadrant 4, range 2, green, power on.

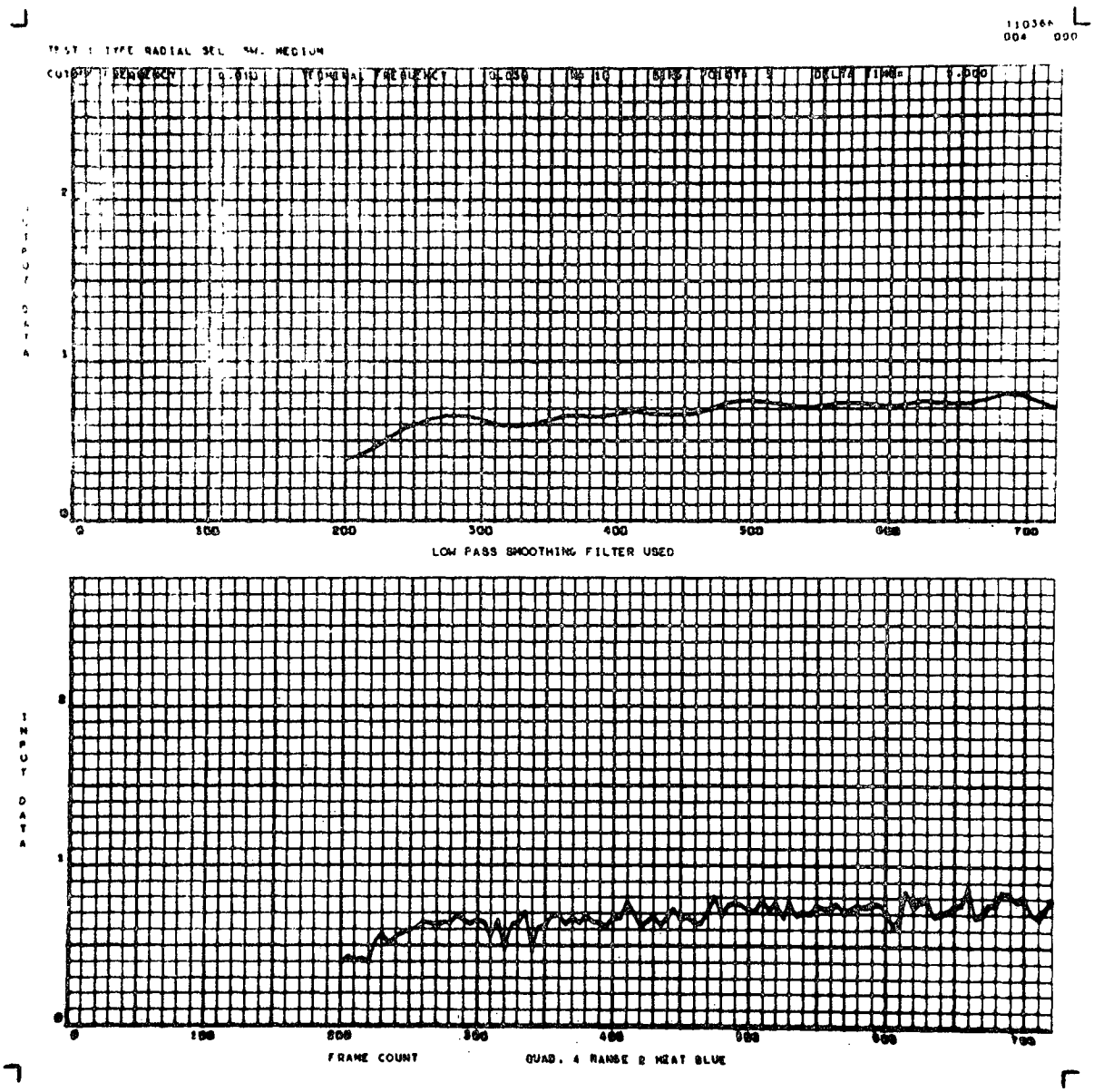

Figure A-13. Radial cell, run 1, quadrant 4, range 2, blue, power on.

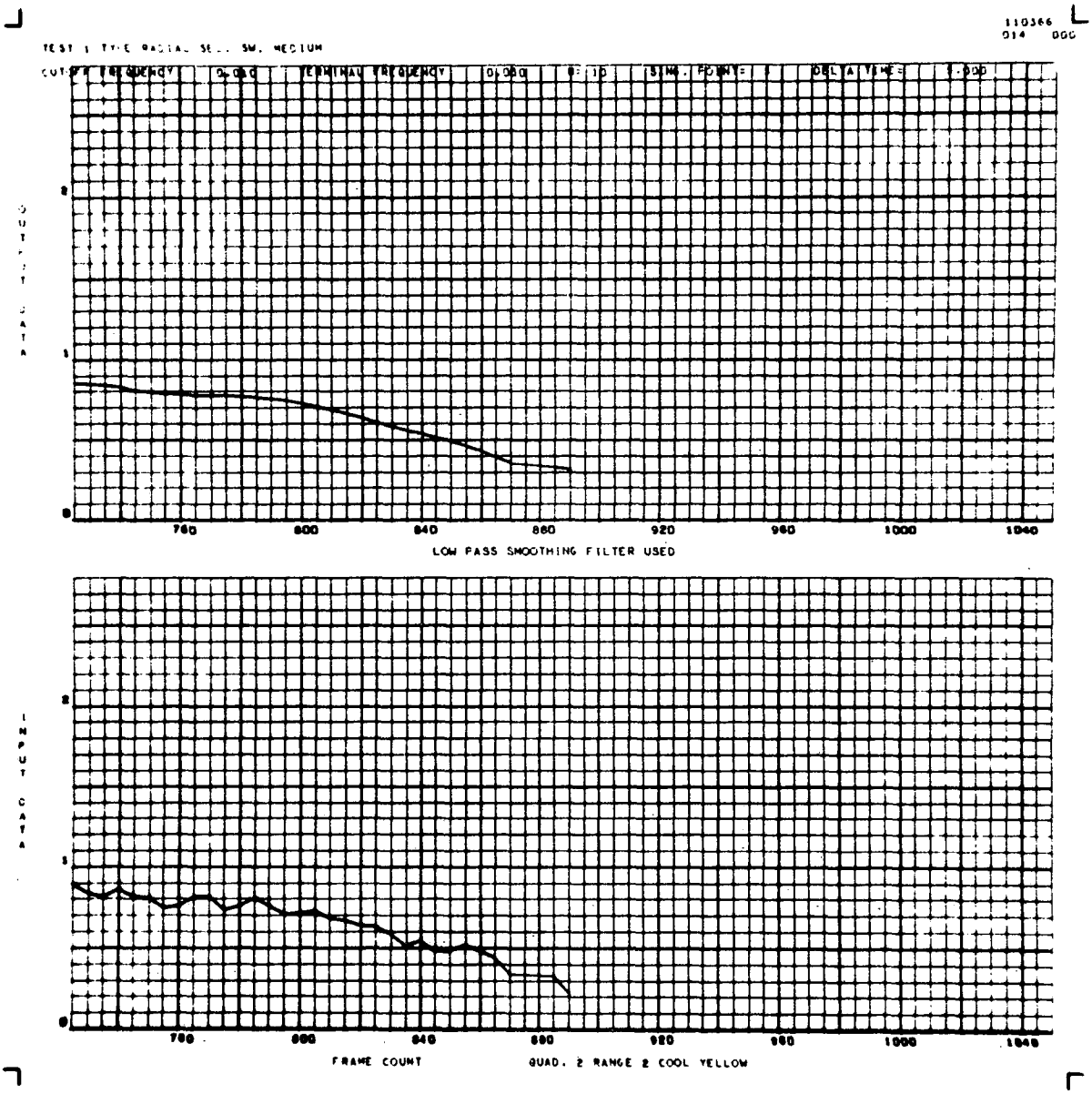

Figure A-14. Radial cell, run 1, quadrant 2, range 2, yellow, power off.

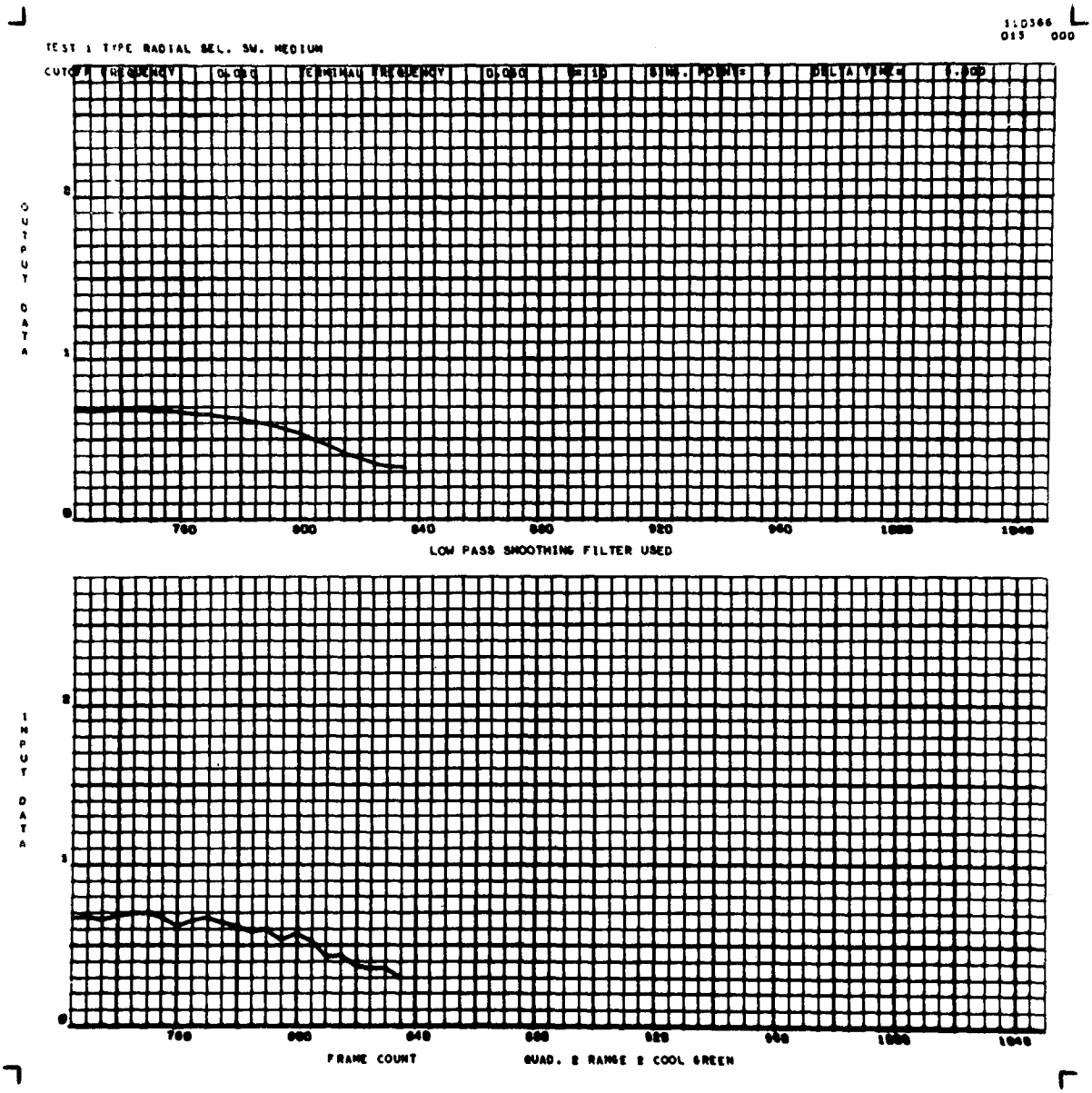

Figure A-15. Radial cell, run 1, quadrant 2, range 2, green, power off.

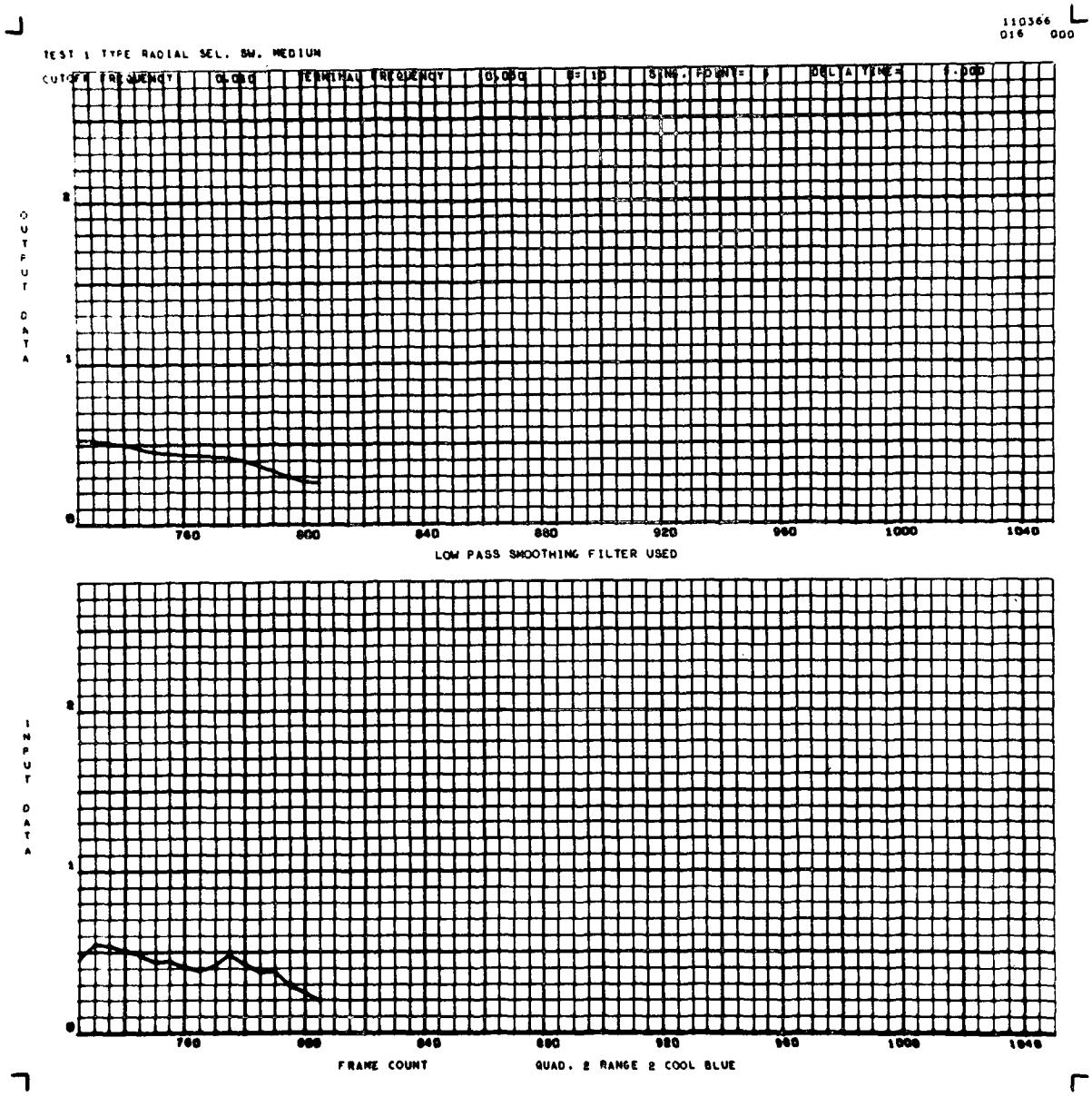

Figure A-16. Radial cell, run 1, quadrant 2, range 2, blue, power off.

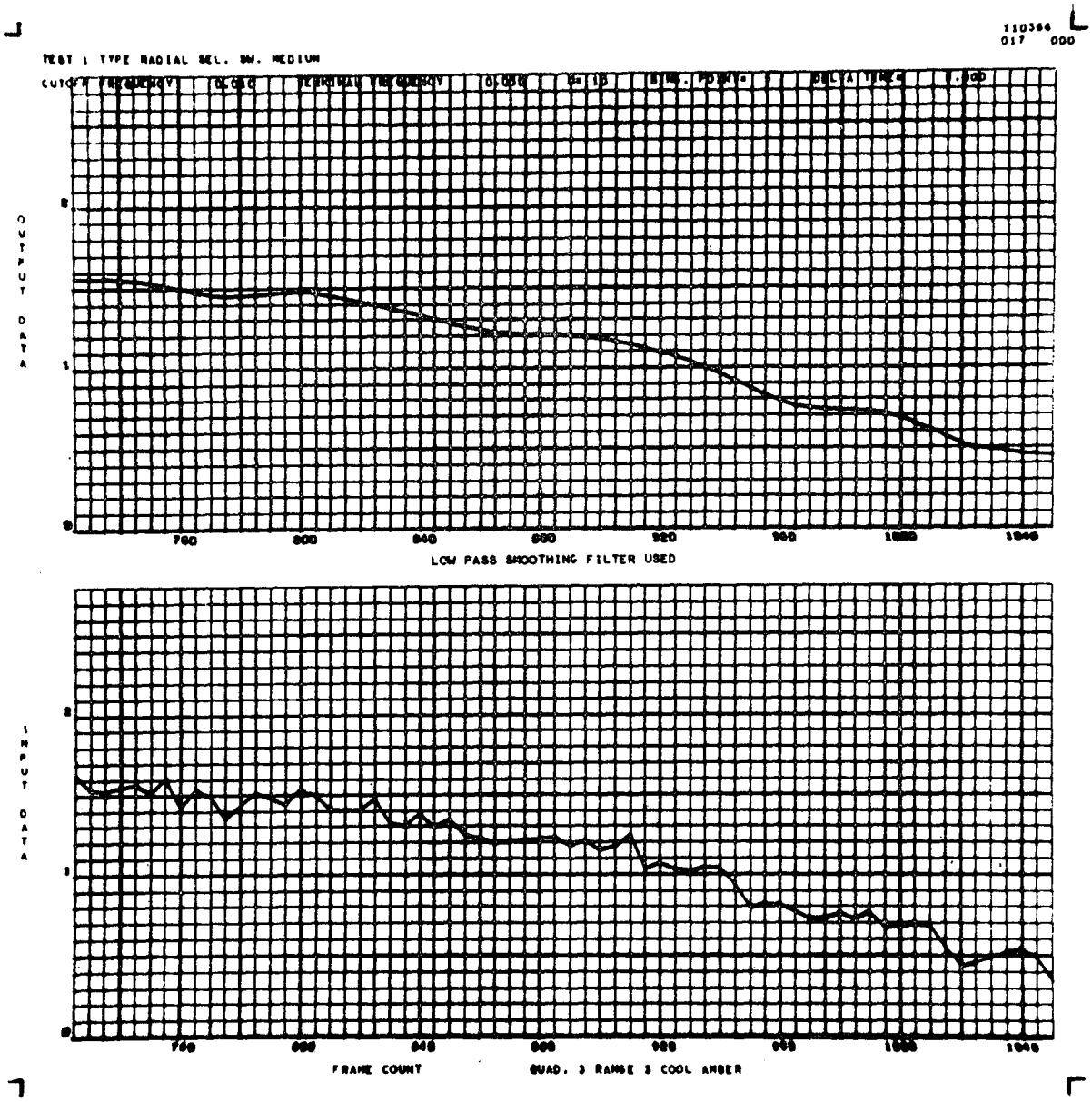

Figure A-17. Radial cell, run 1, quadrant 3, range 3, amber, power off.

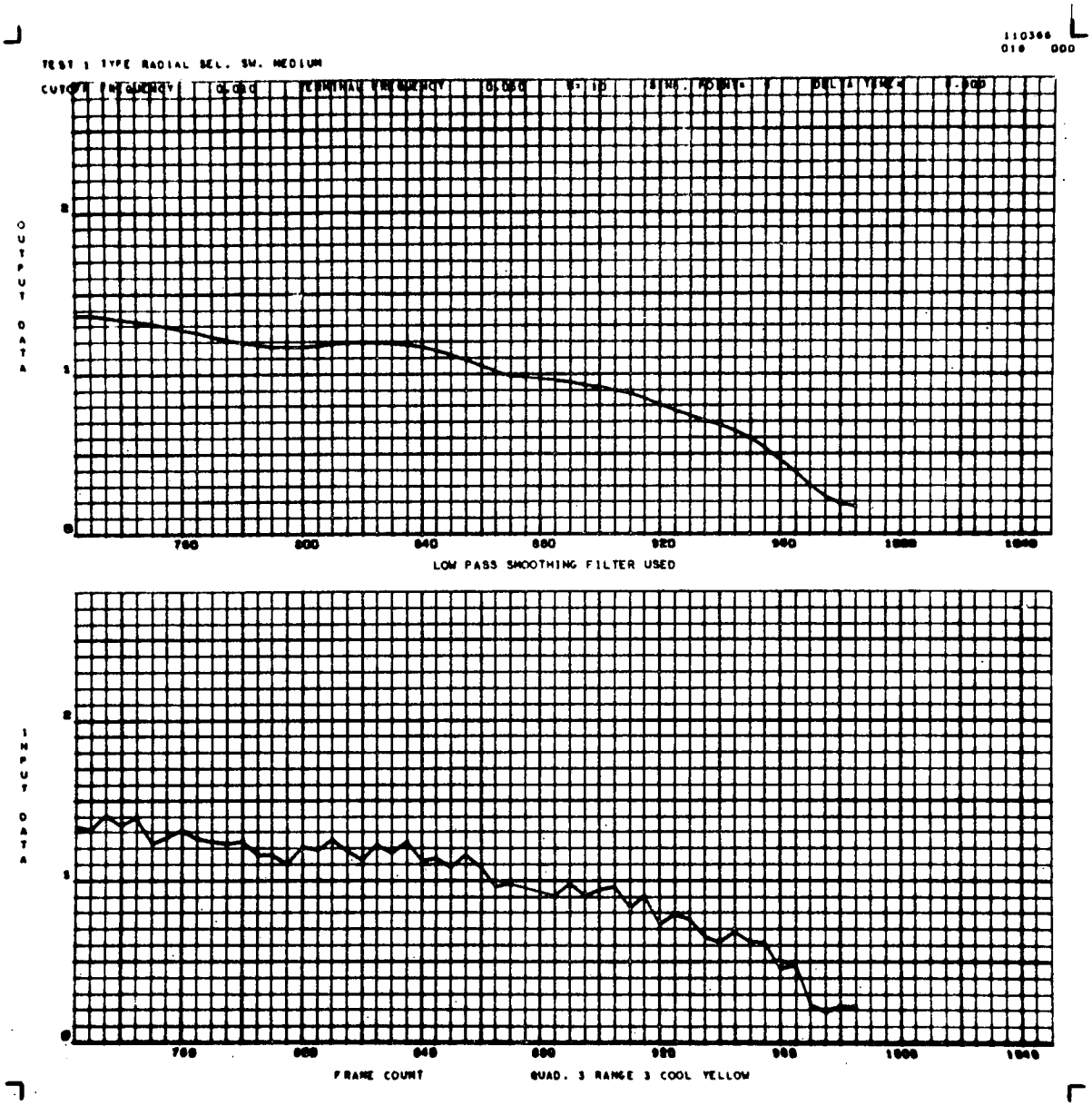

Figure A-18. Radial cell, run 1, quadrant 3, range 3, yellow, power off.

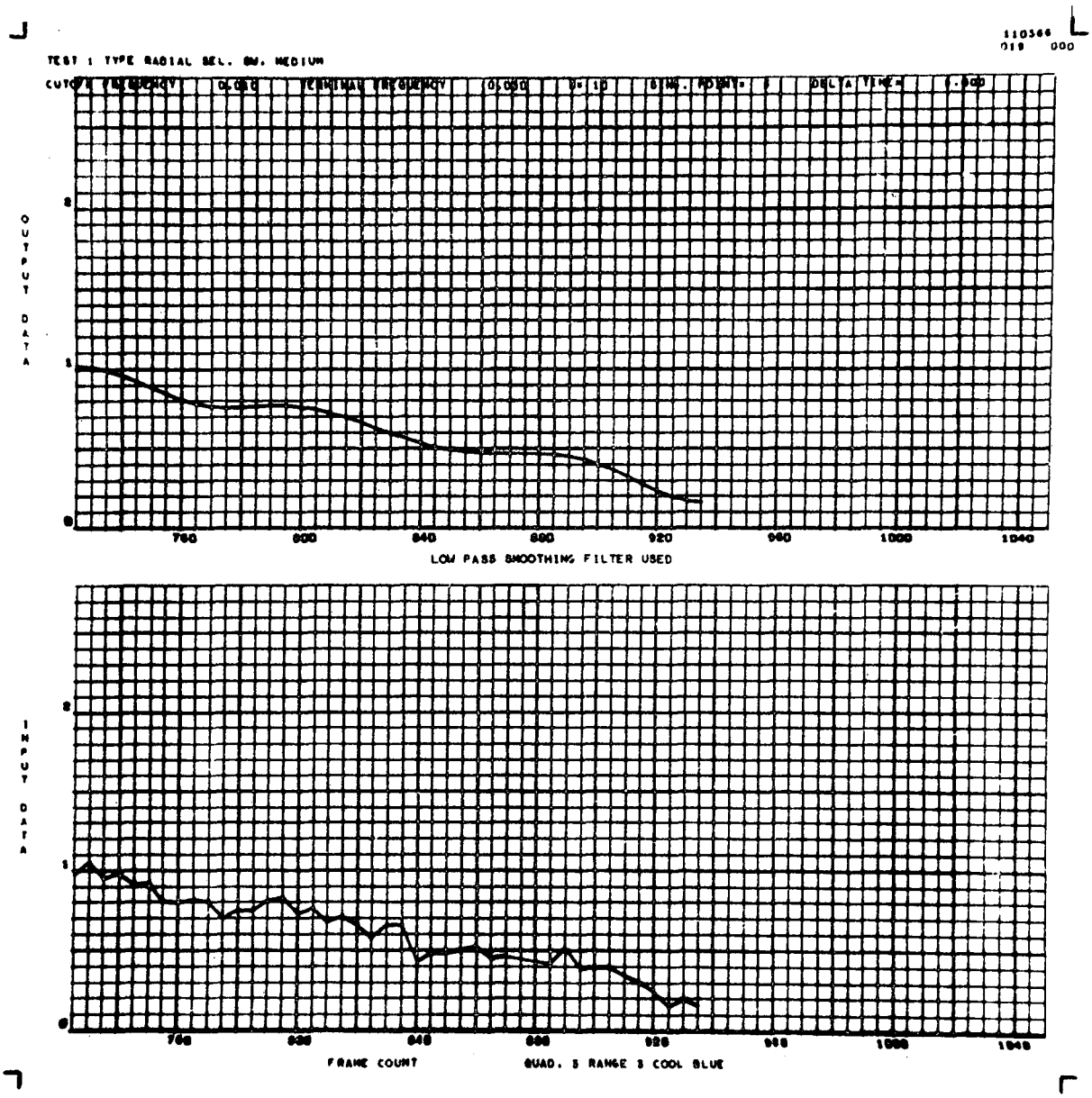

Figure A-19. Radial cell, run 1, quadrant 3, range 3, blue, power off.

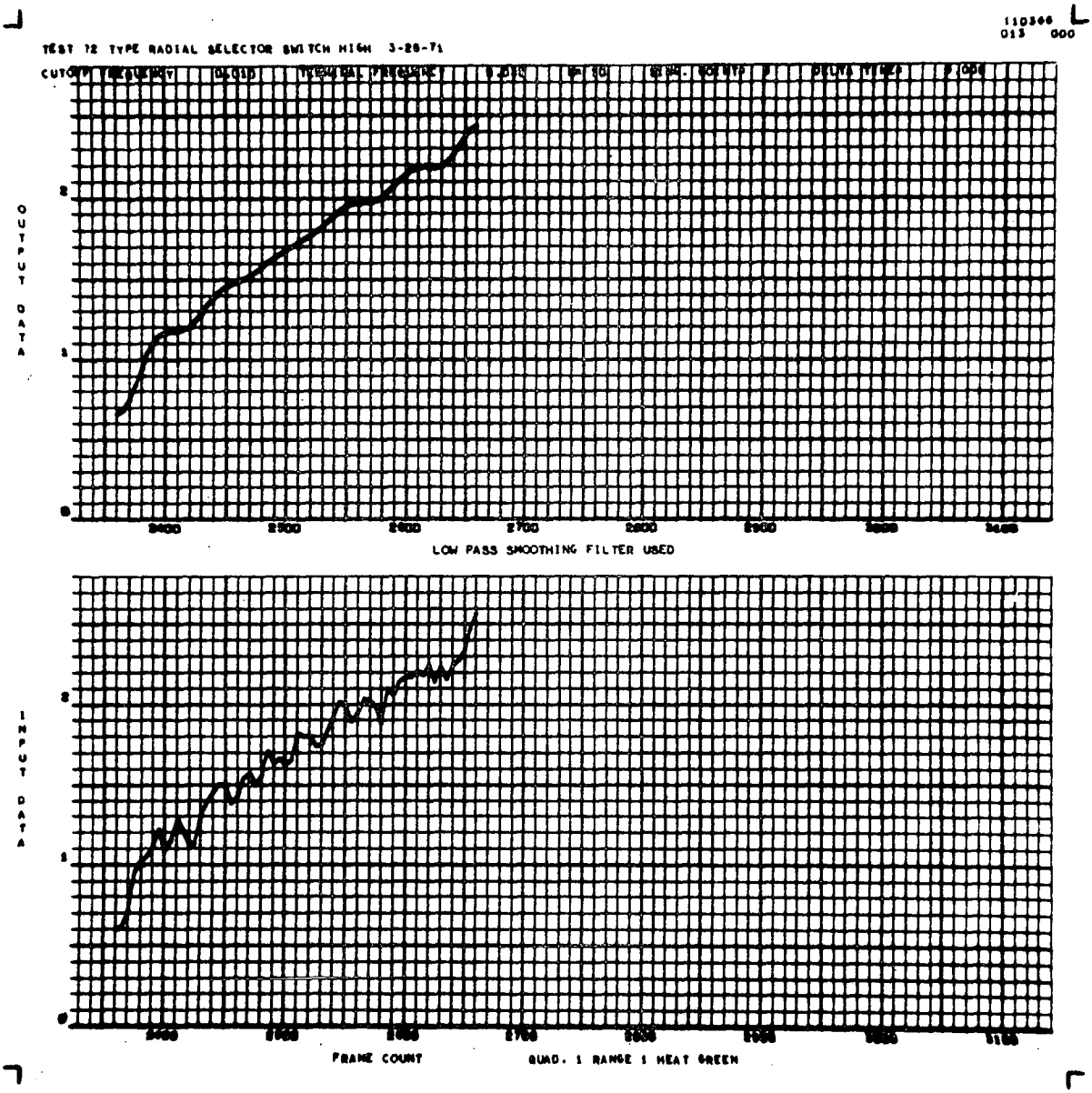

Figure A-20. Radial cell, run 2, quadrant 1, range 1, green, power on.

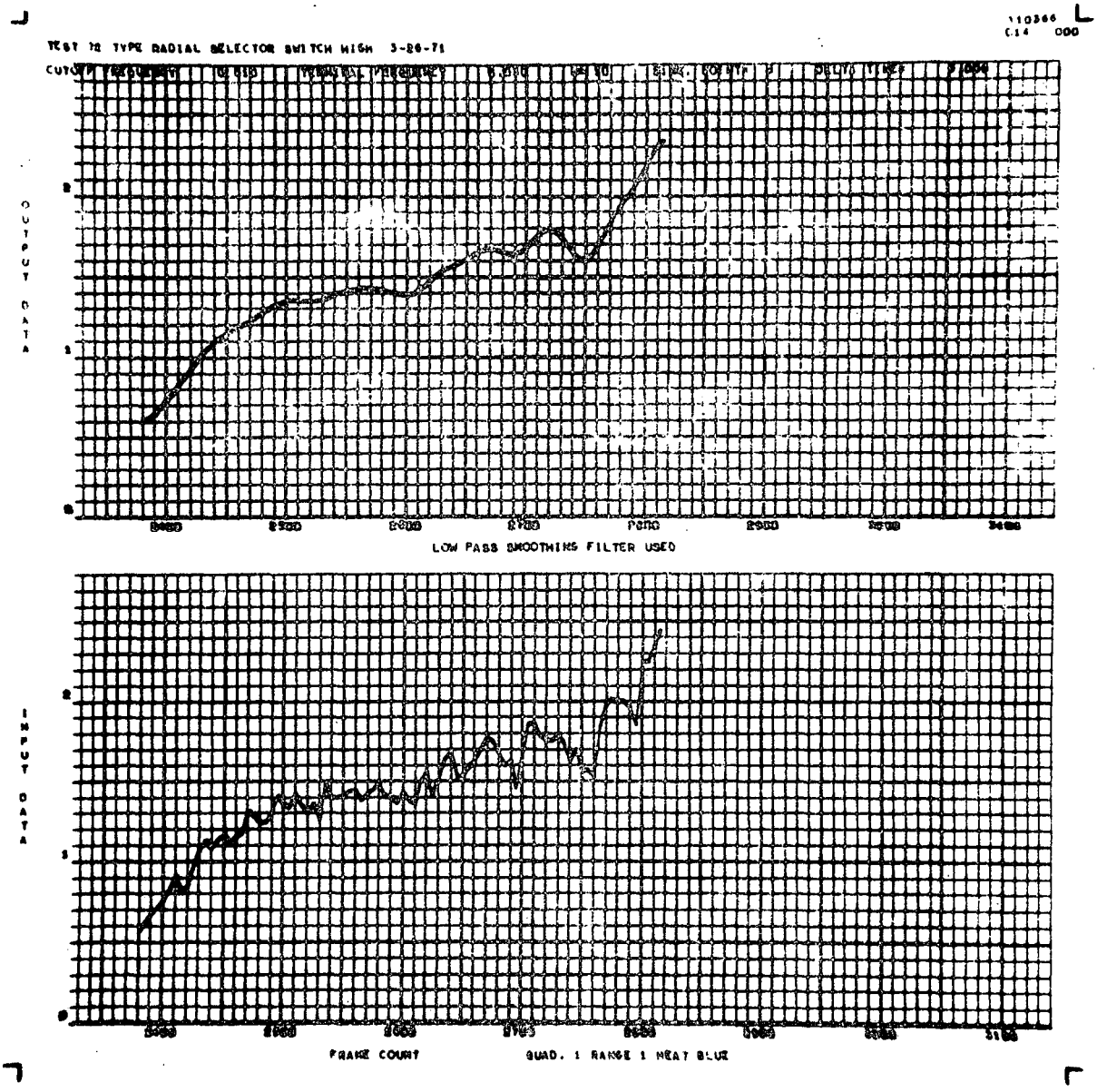

Figure A-21. Radial cell, run 2, quadrant 1, range 1, blue, power on.

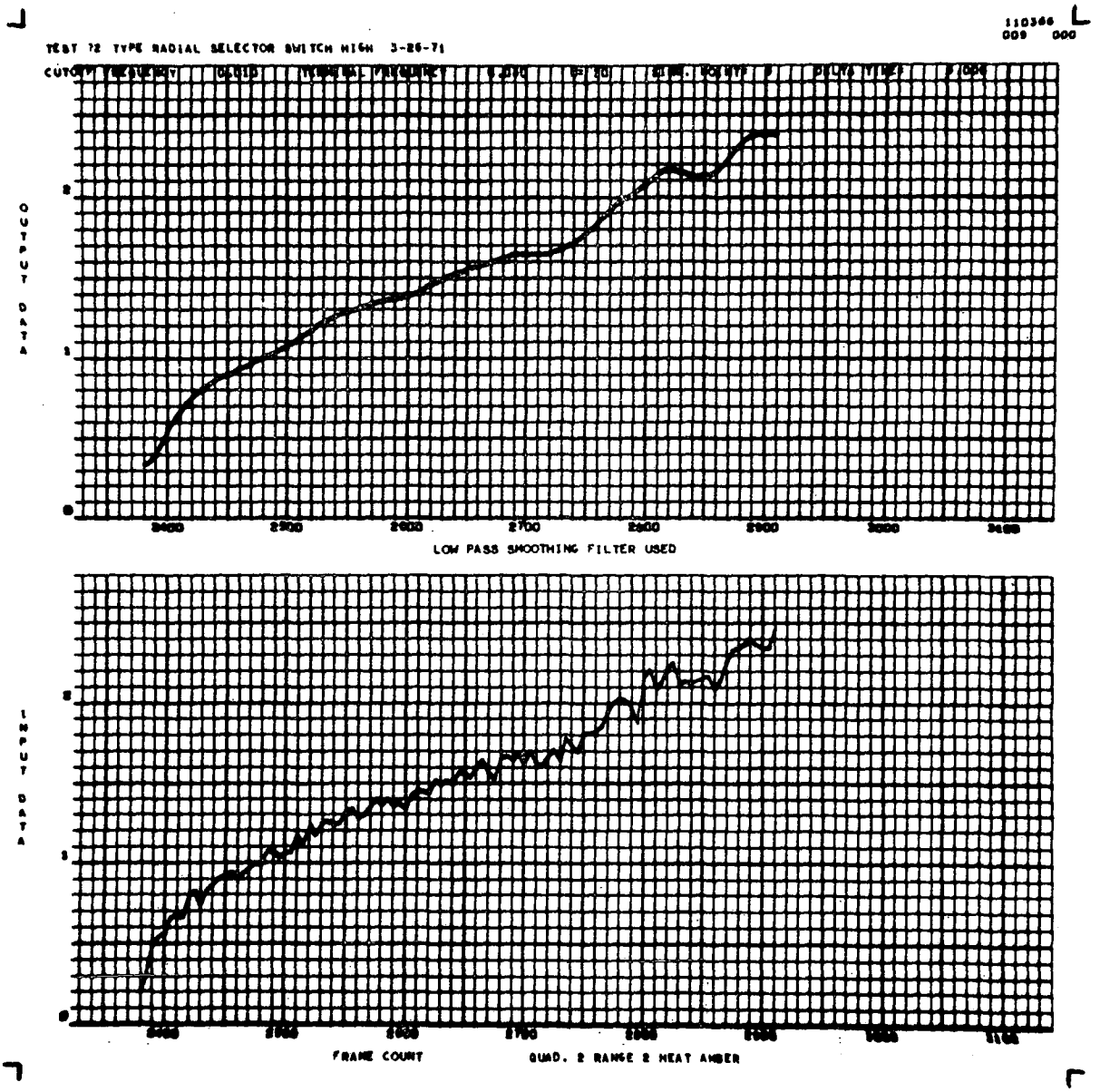

Figure A-22. Radial cell, run 2, quadrant 2, range 2, amber, power on.

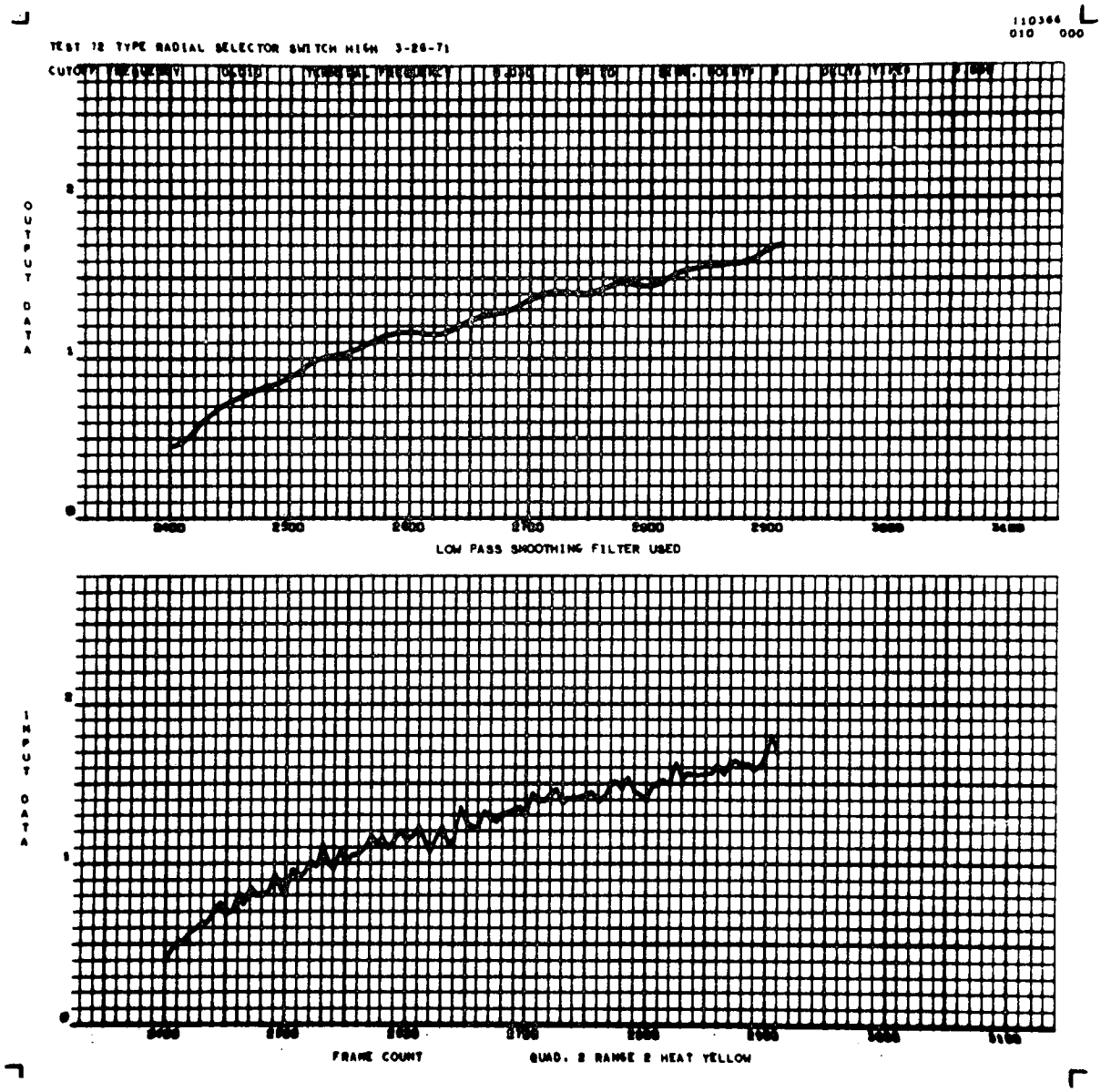

Figure A-23. Radial cell, run 2, quadrant 2, range 2, yellow, power on.

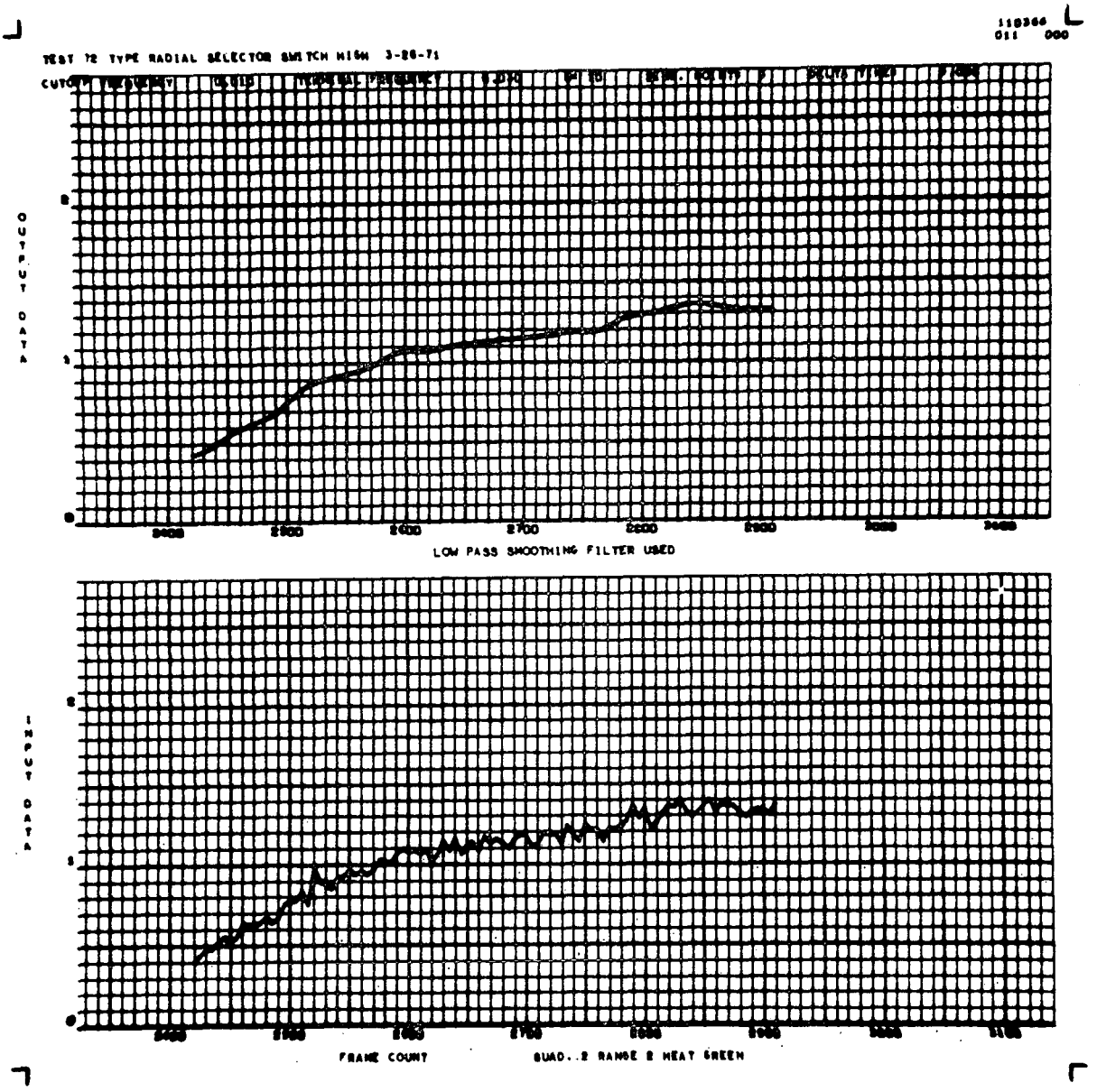

Figure A-24. Radial cell, run 2, quadrant 2, range 2, green, power on.

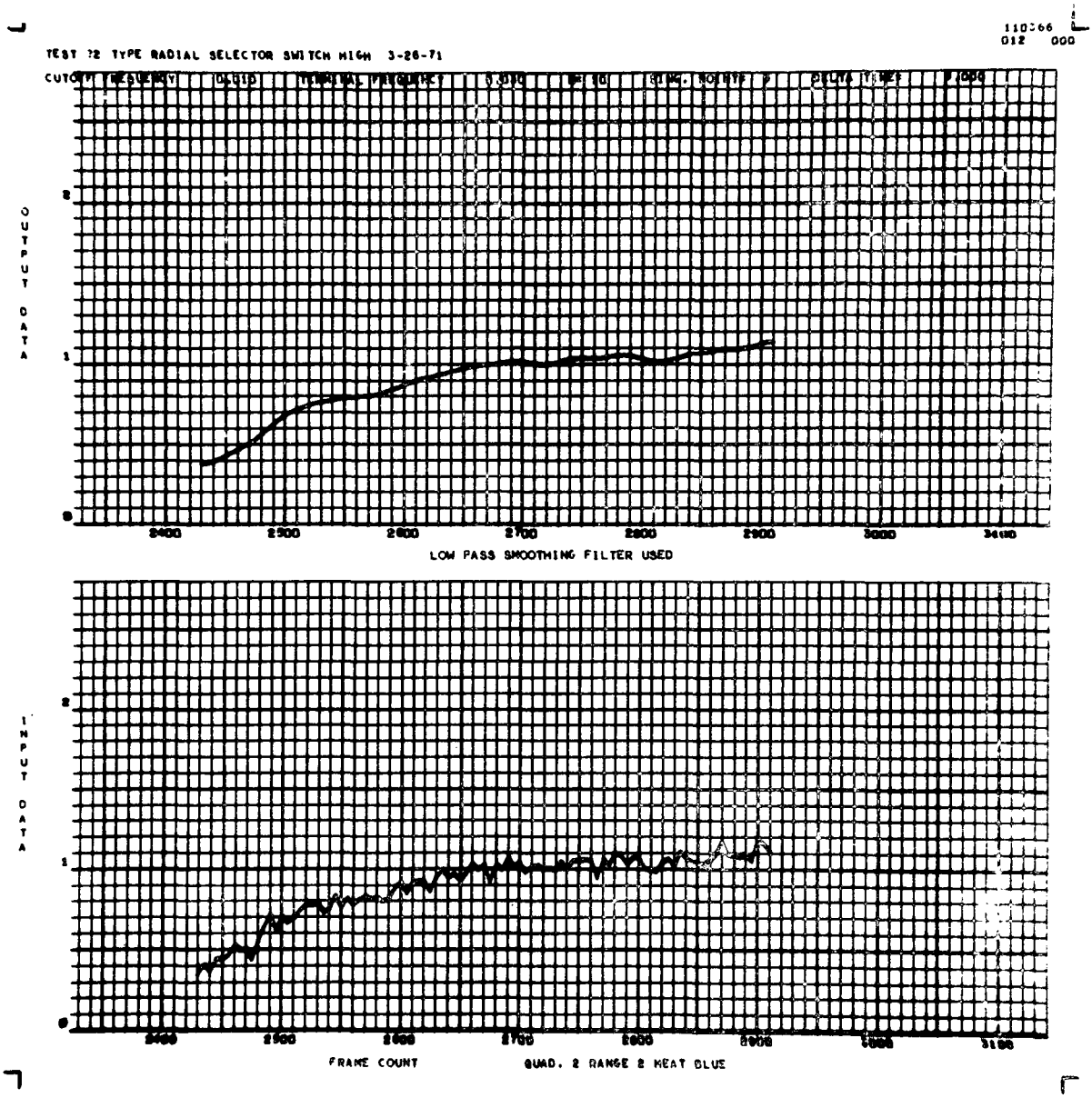

Figure A-25. Radial cell, run 2, quadrant 2, range 2, blue, power on.

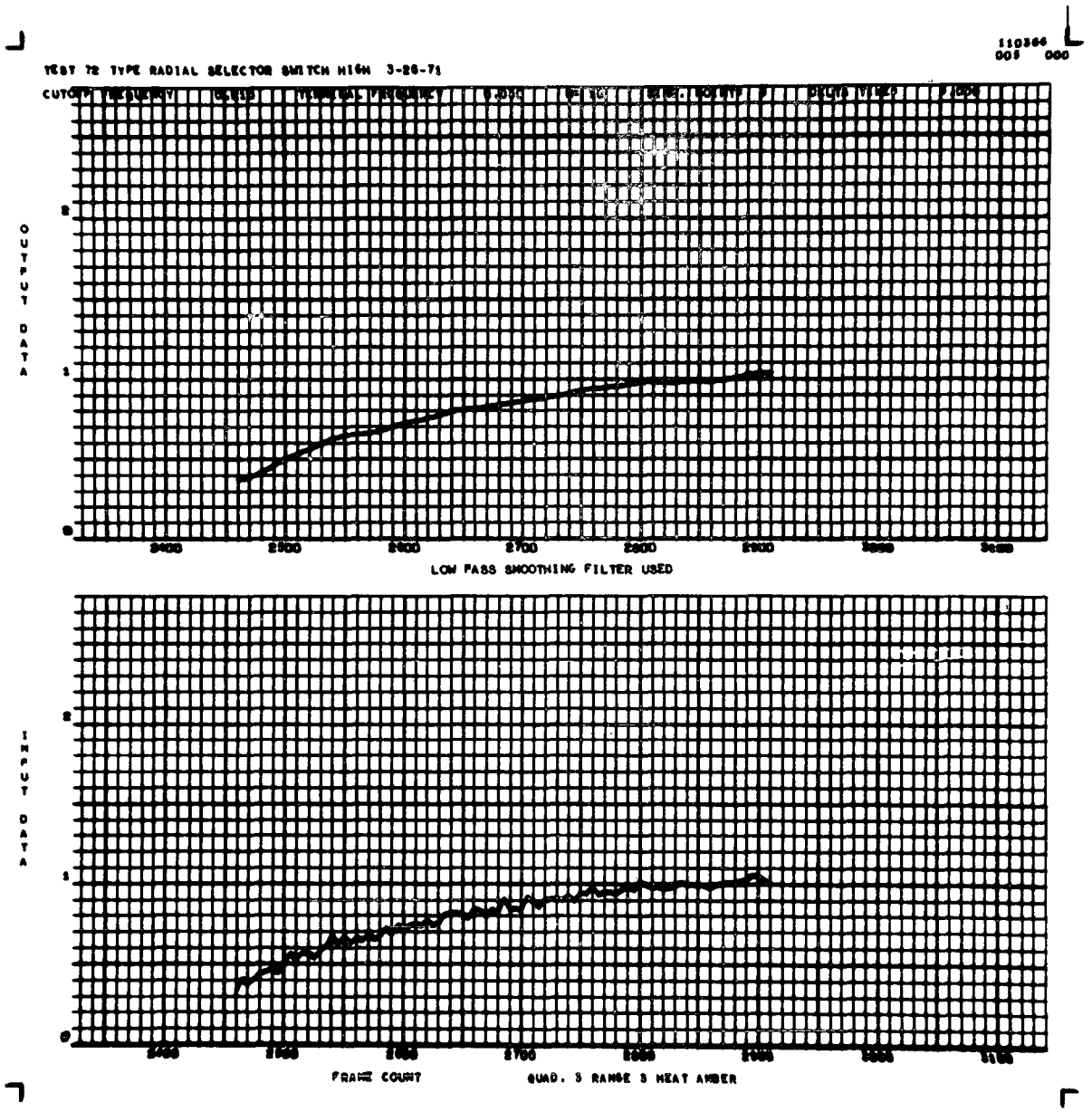

Figure A-26. Radial cell, run 2, quadrant 3, range 3, amber, power on.

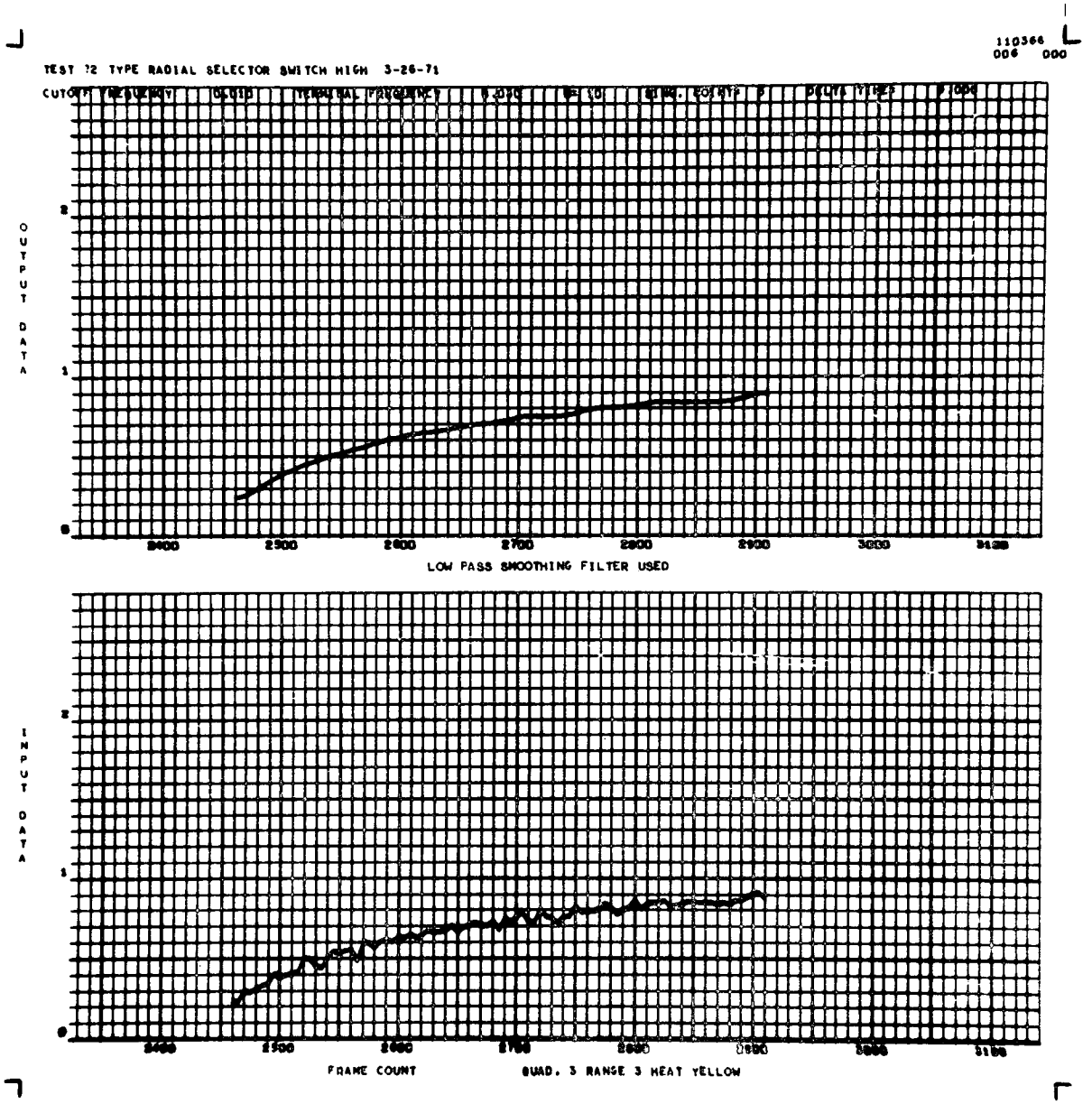

Figure A-27. Radial cell, run 2, quadrant 3, range 3, yellow, power on.

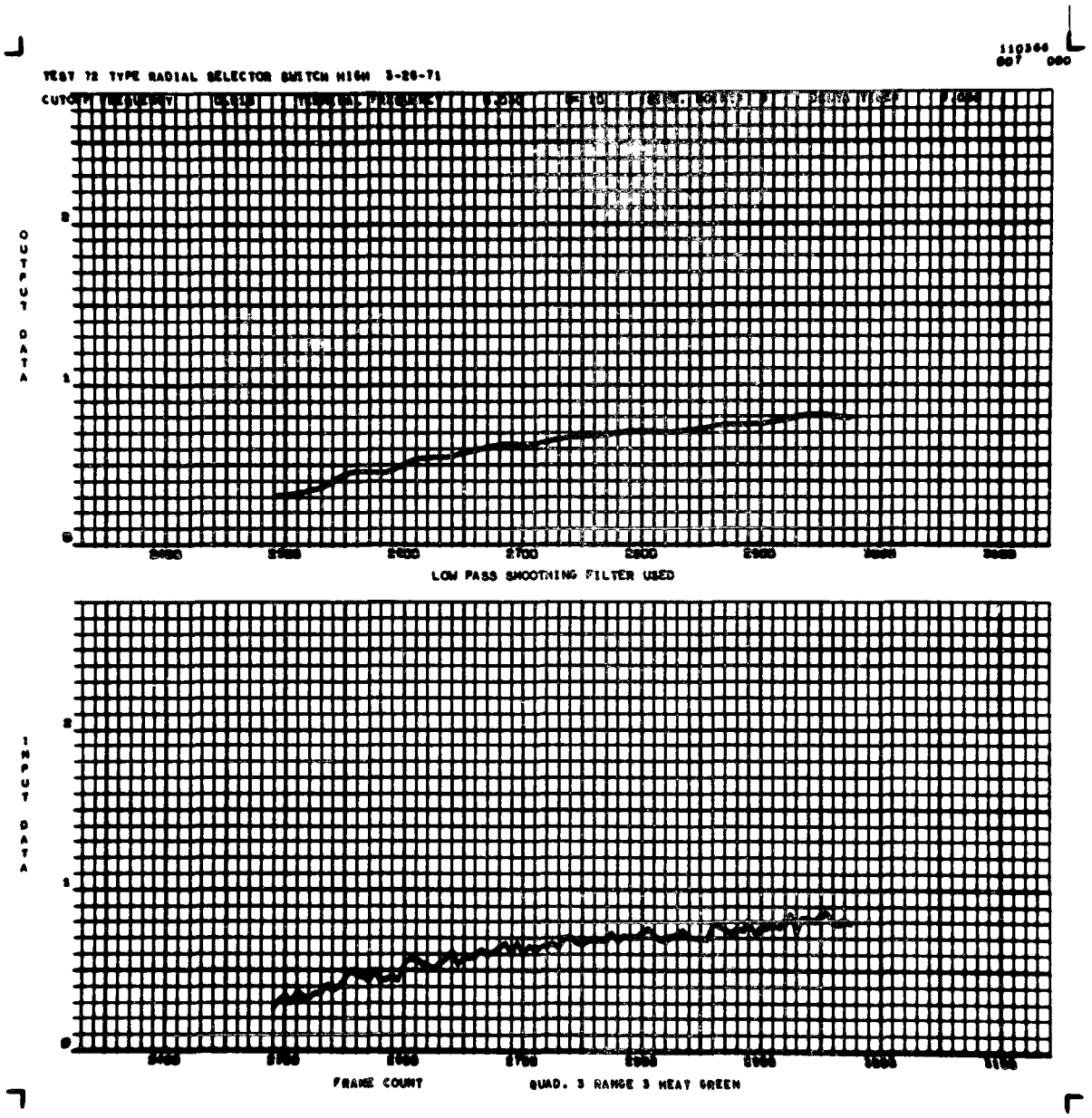

Figure A-28. Radial cell, run 2, quadrant 3, range 3, green, power on.

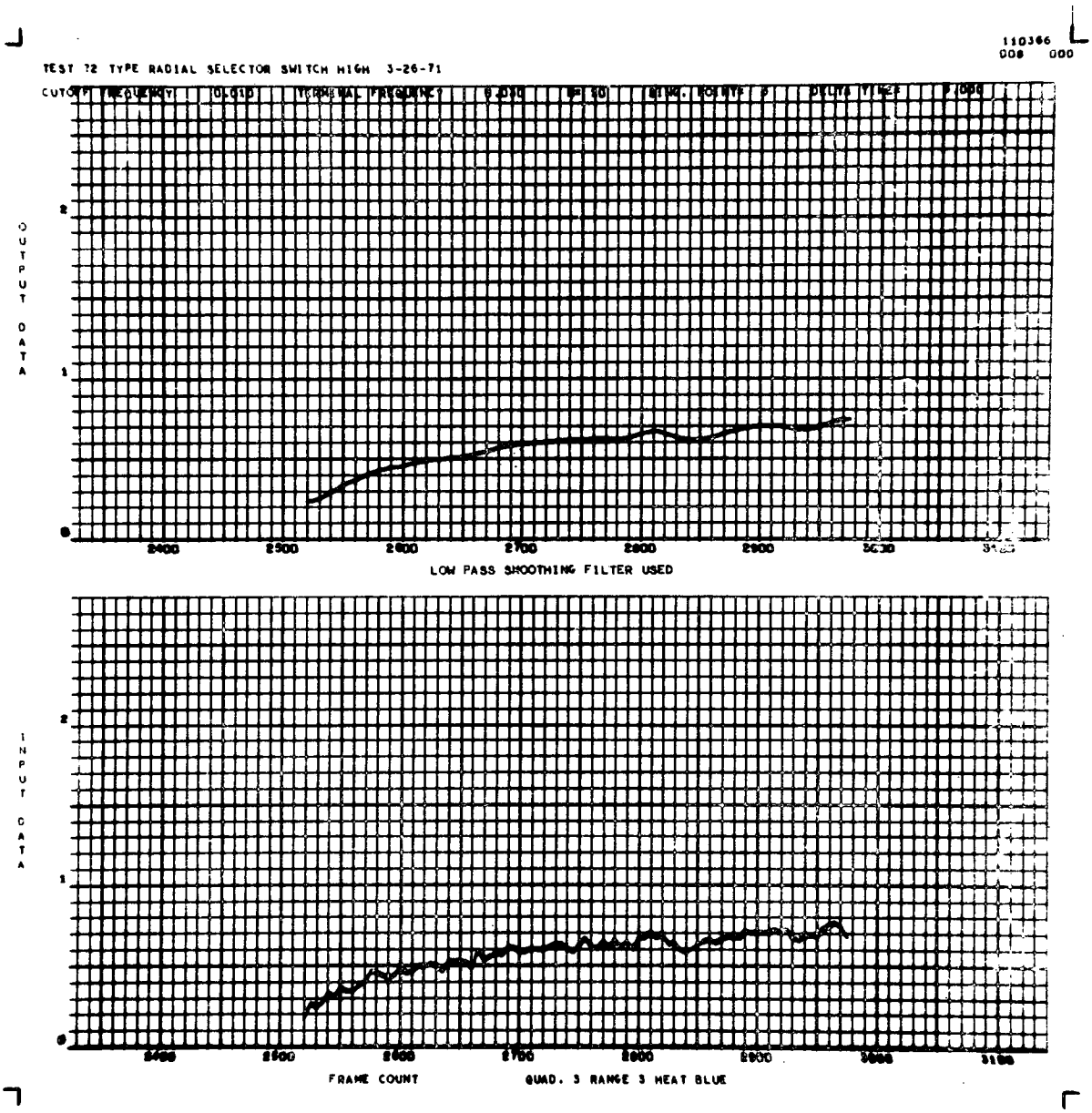

Figure A-29. Radial cell, run 2, quadrant 3, range 3, blue, power on.

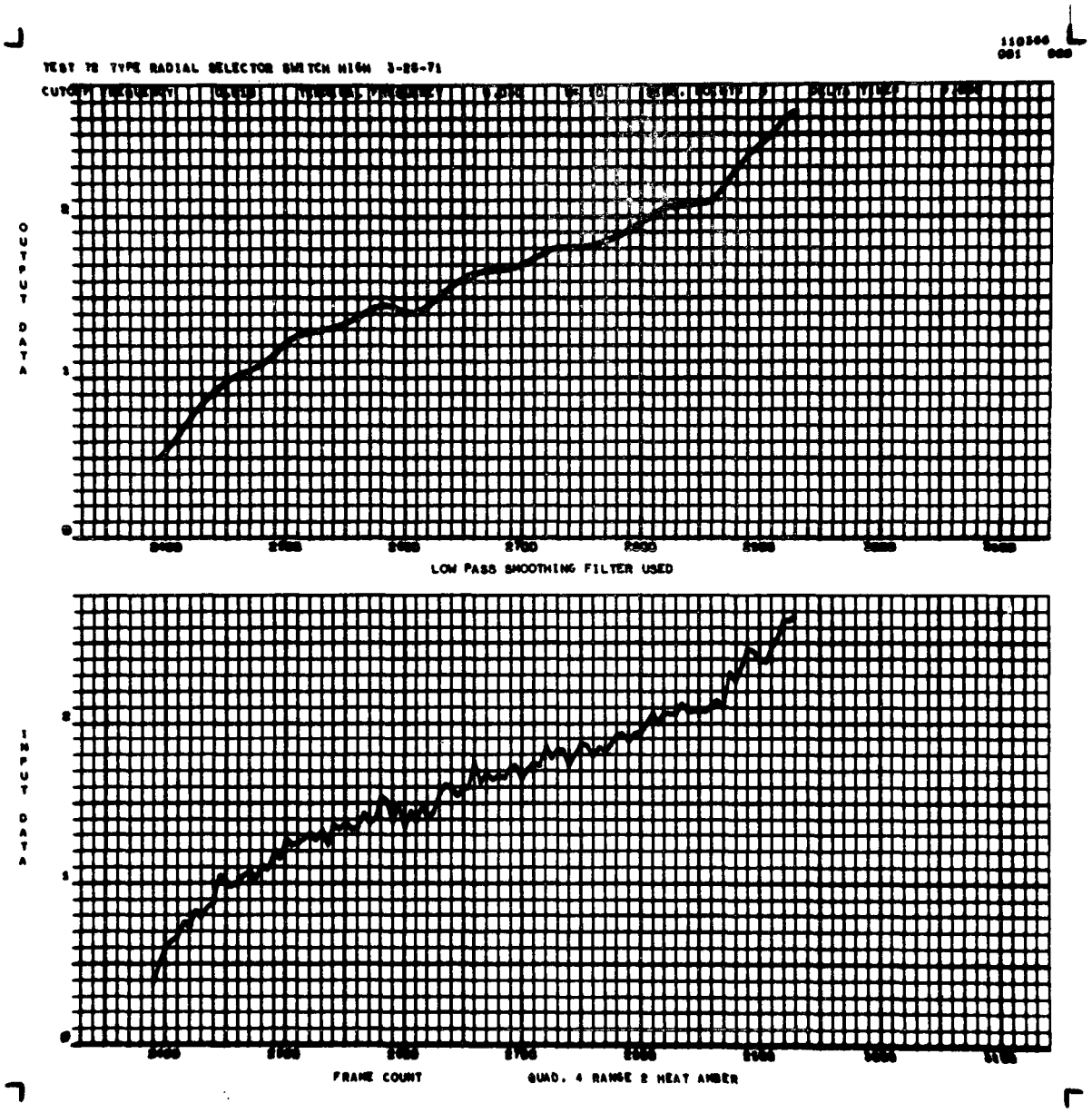

Figure A-30. Radial cell, run 2, quadrant 4, range 2, amber, power on.

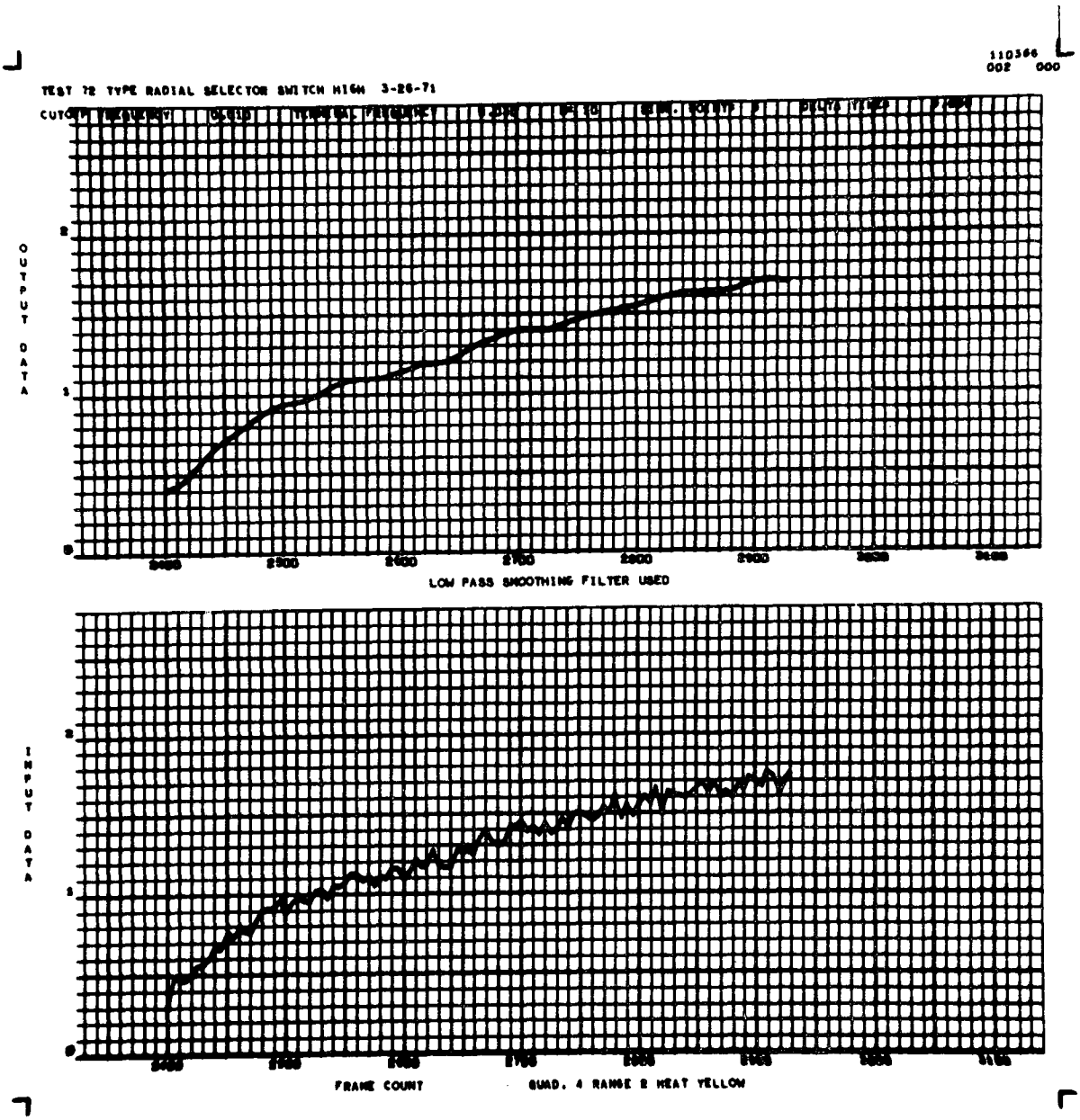

Figure A-31. Radial cell, run 2, quadrant 4, range 2, yellow, power on.

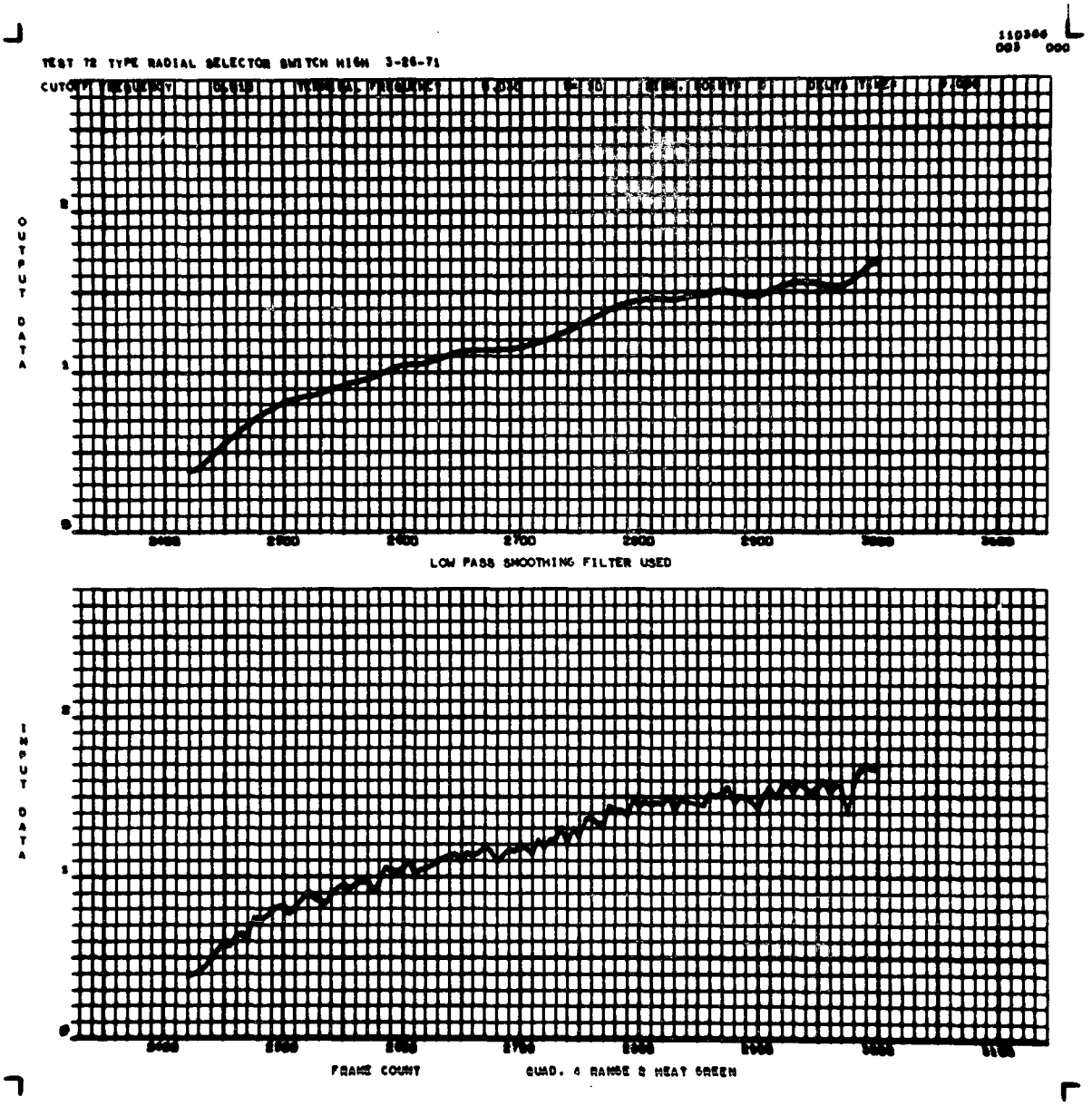

Figure A-32. Radial cell, run 2, quadrant 4, range 2, green, power on.

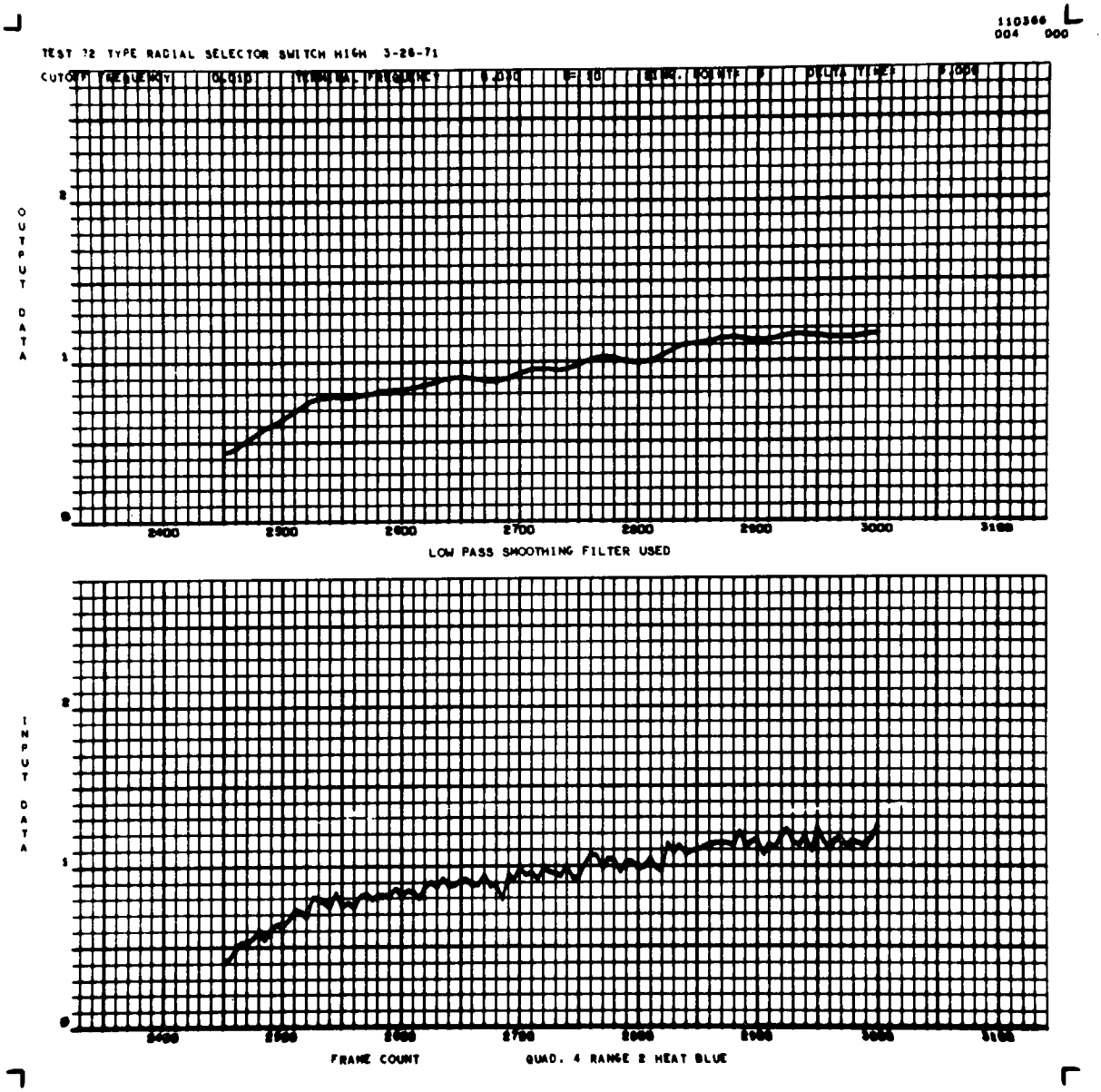

Figure A-33. Radial cell, run 2, quadrant 4, range 2, blue, power on.

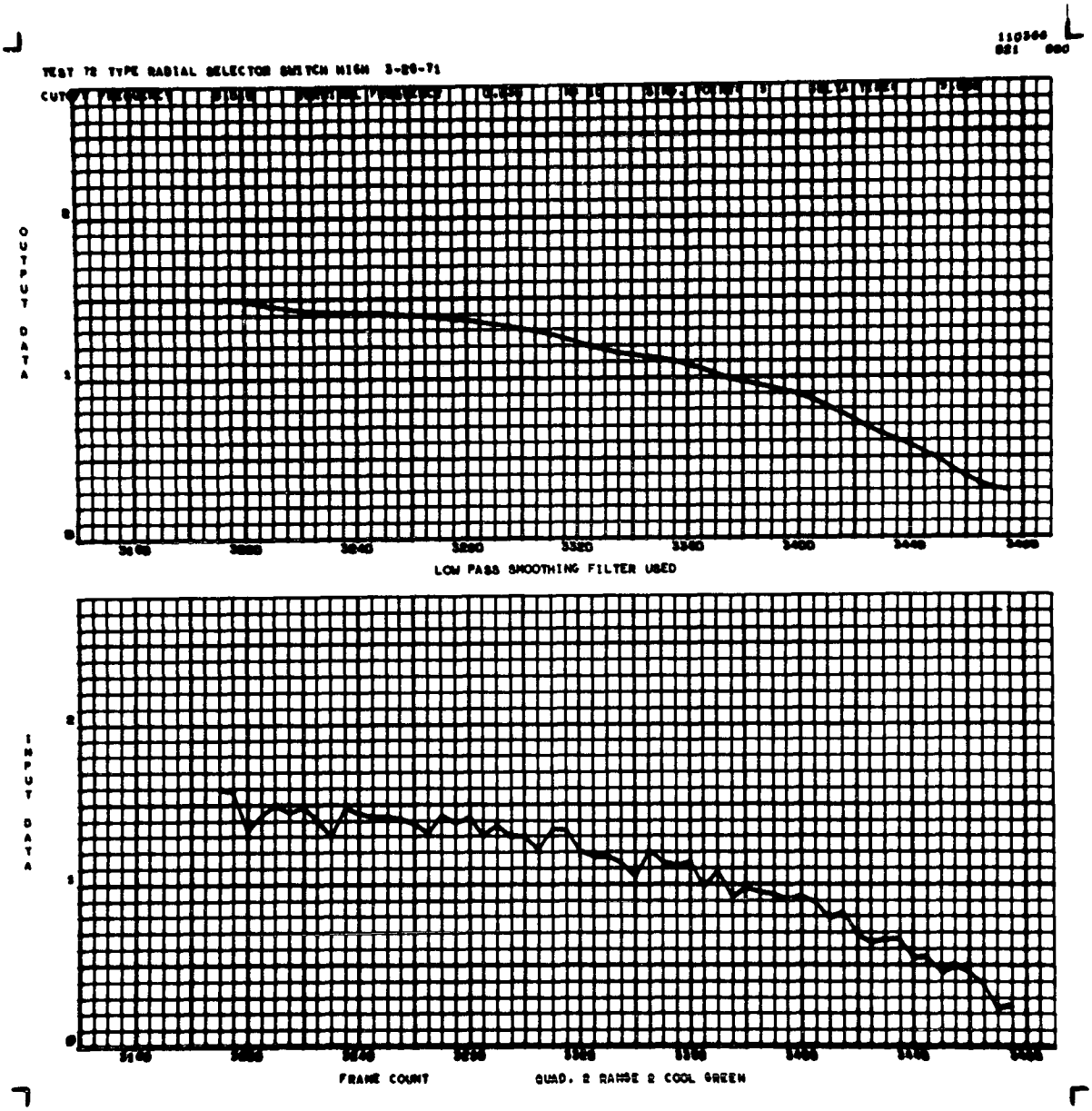

Figure A-34. Radial cell, run 2, quadrant 2, range 2, green, power off.

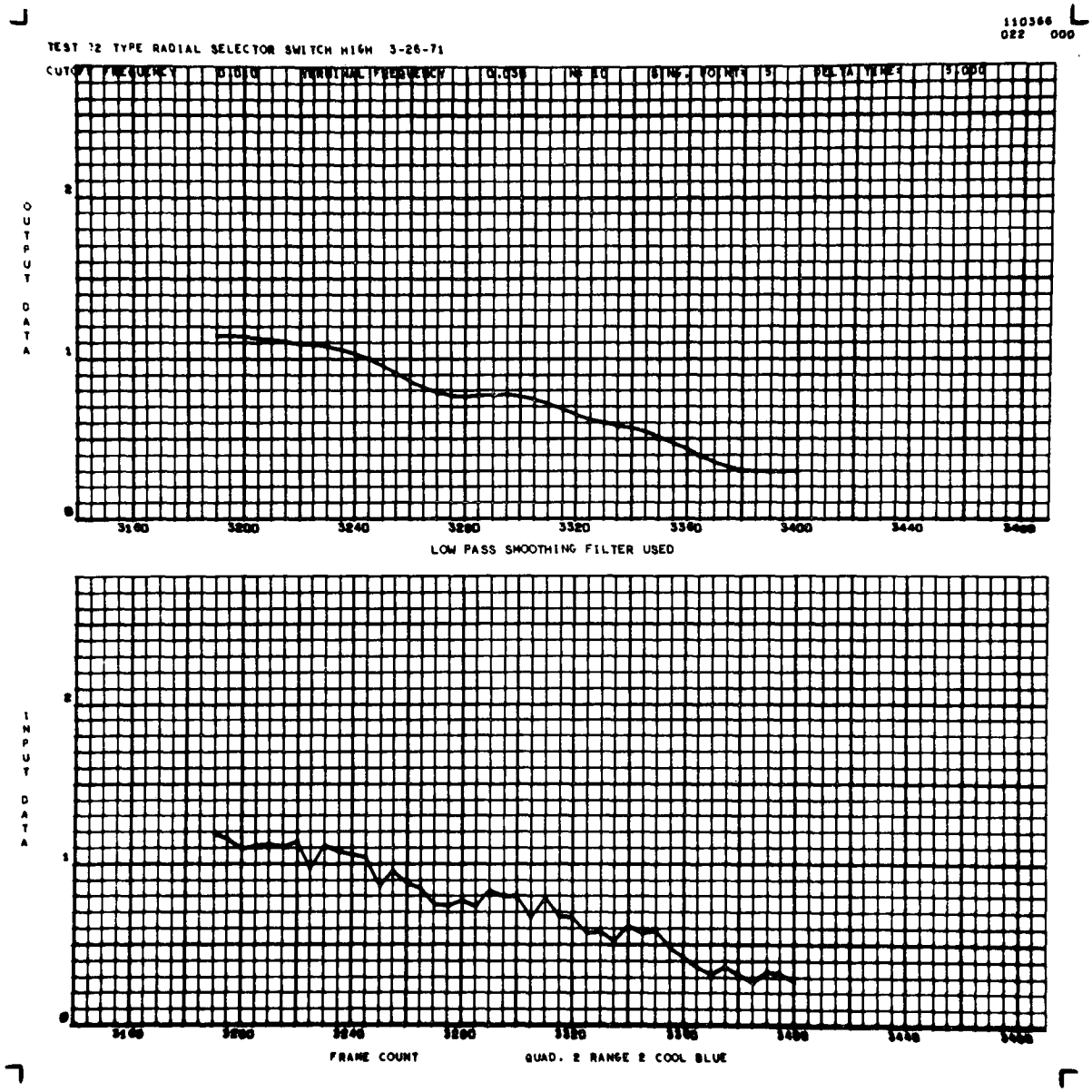

Figure A-35. Radial cell, run 2, quadrant 2, range 2, blue, power off.

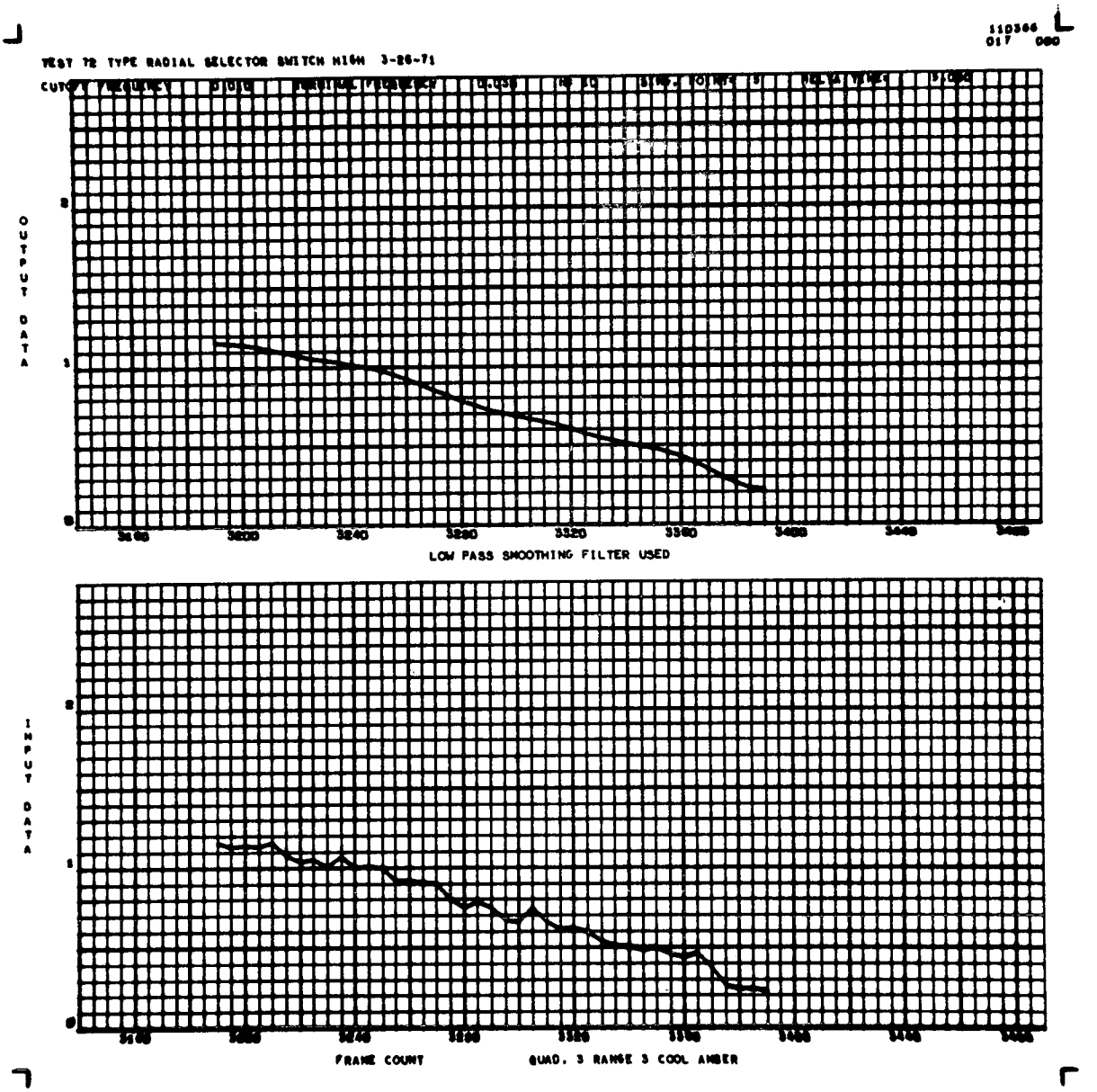

Figure A-36. Radial cell, run 2, quadrant 3, range 3, amber, power off.

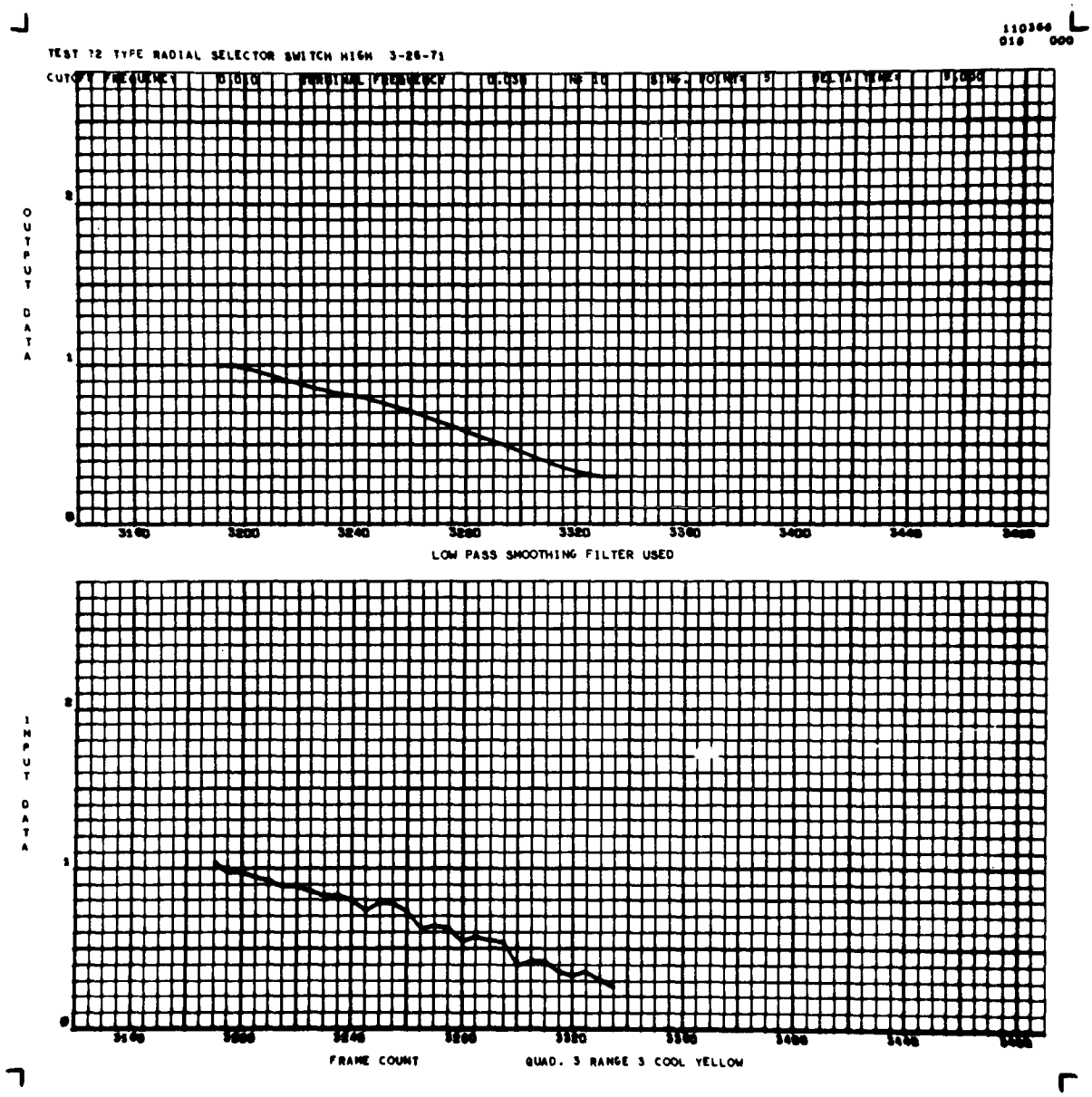

Figure A-37. Radial cell, run 2, quadrant 3, range 3, yellow, power off.

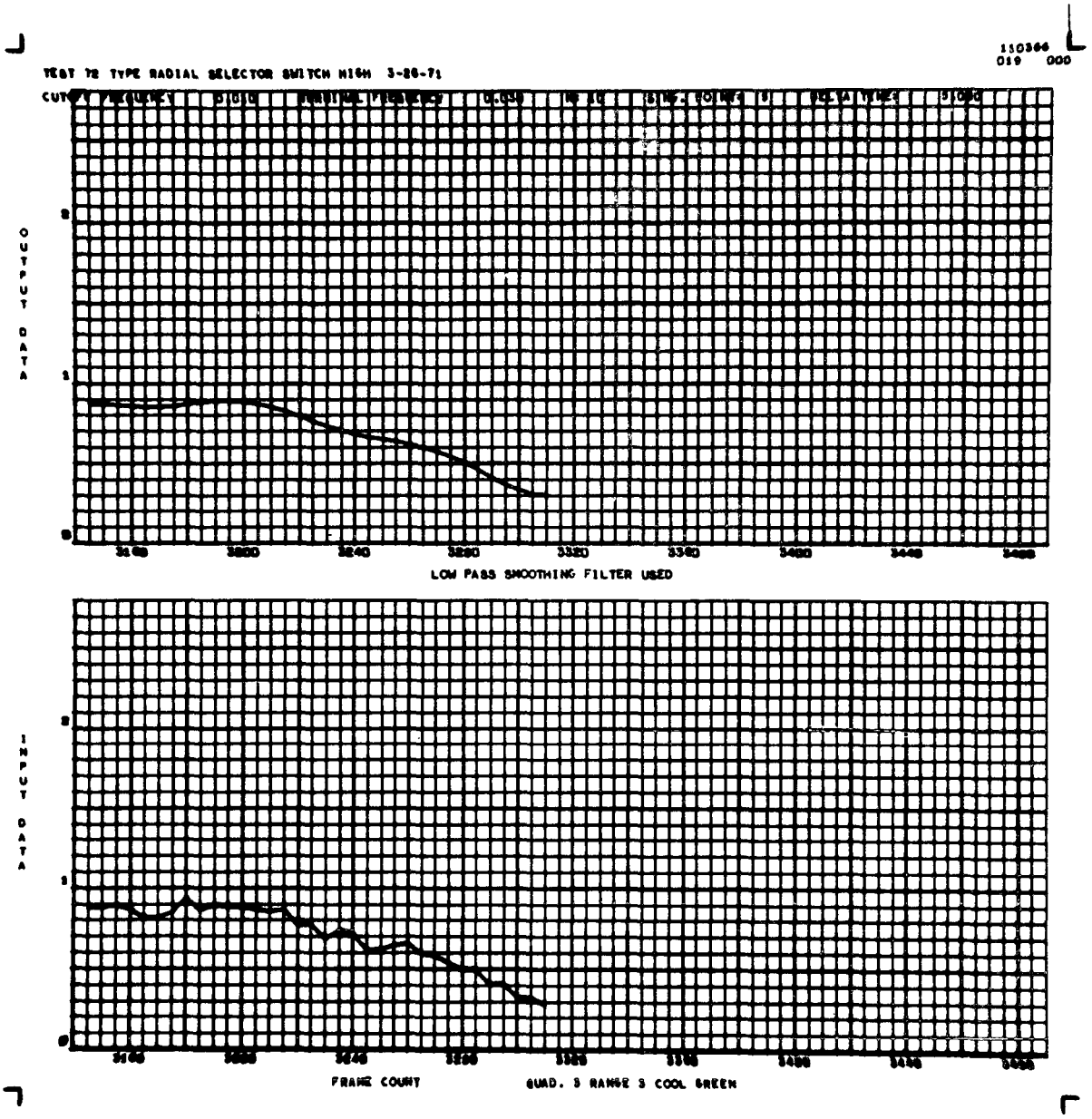

Figure A-38. Radial cell, run 2, quadrant 3, range 3, green, power off.

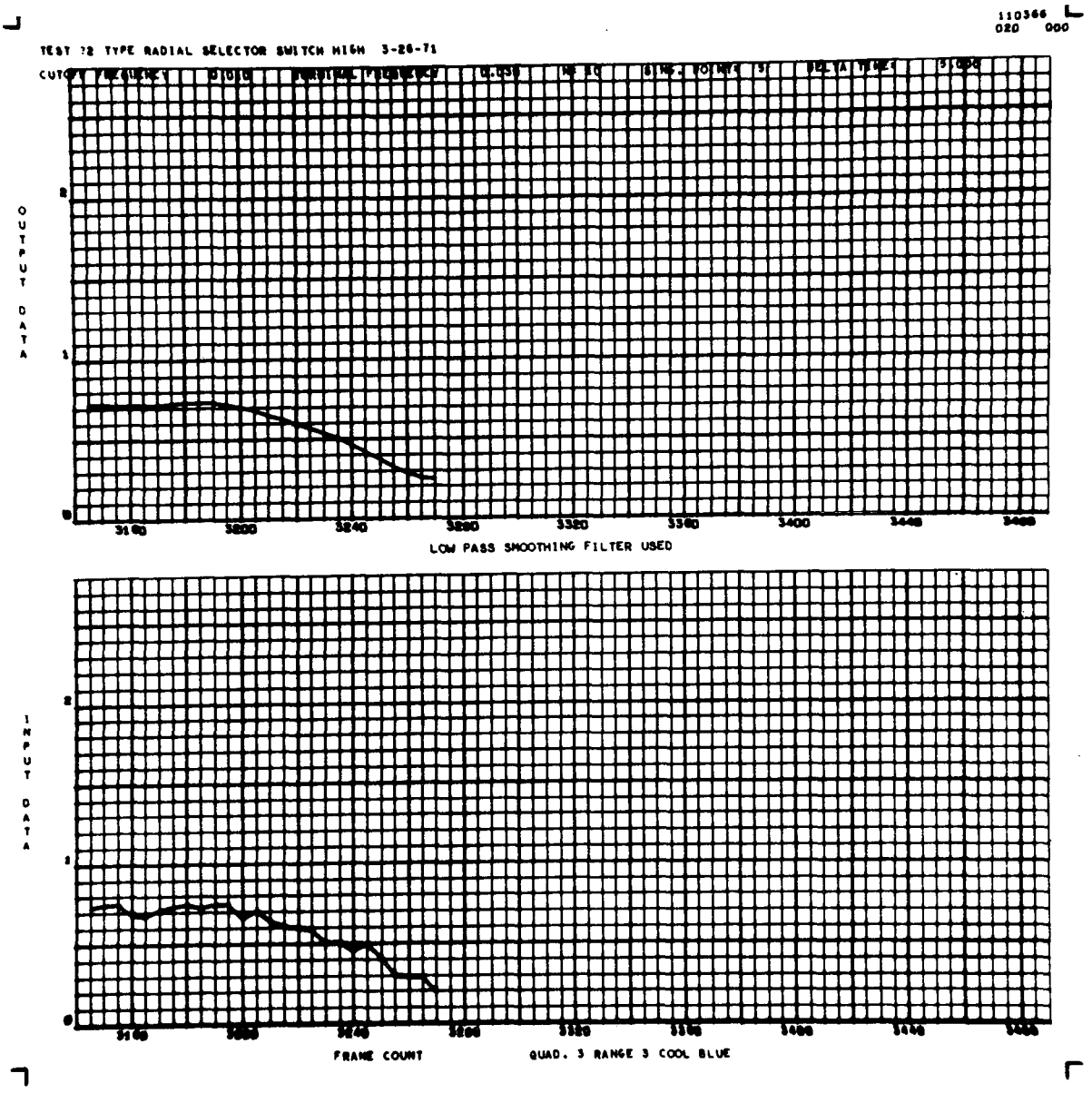

Figure A-39. Radial cell, run 2, quadrant 3, range 3, blue, power off.

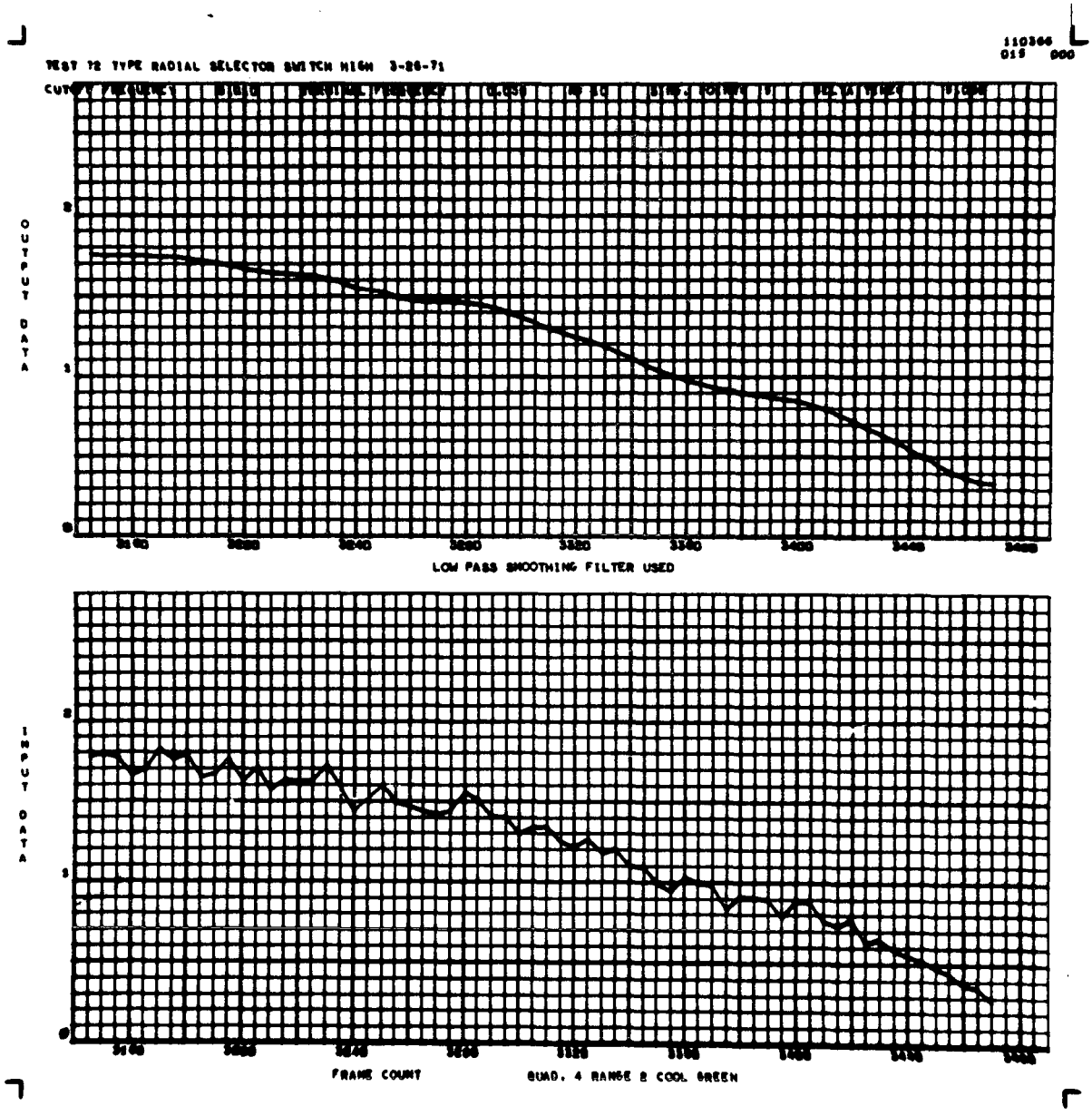

Figure A-40. Radial cell, run 2, quadrant 4, range 2, green, power off.

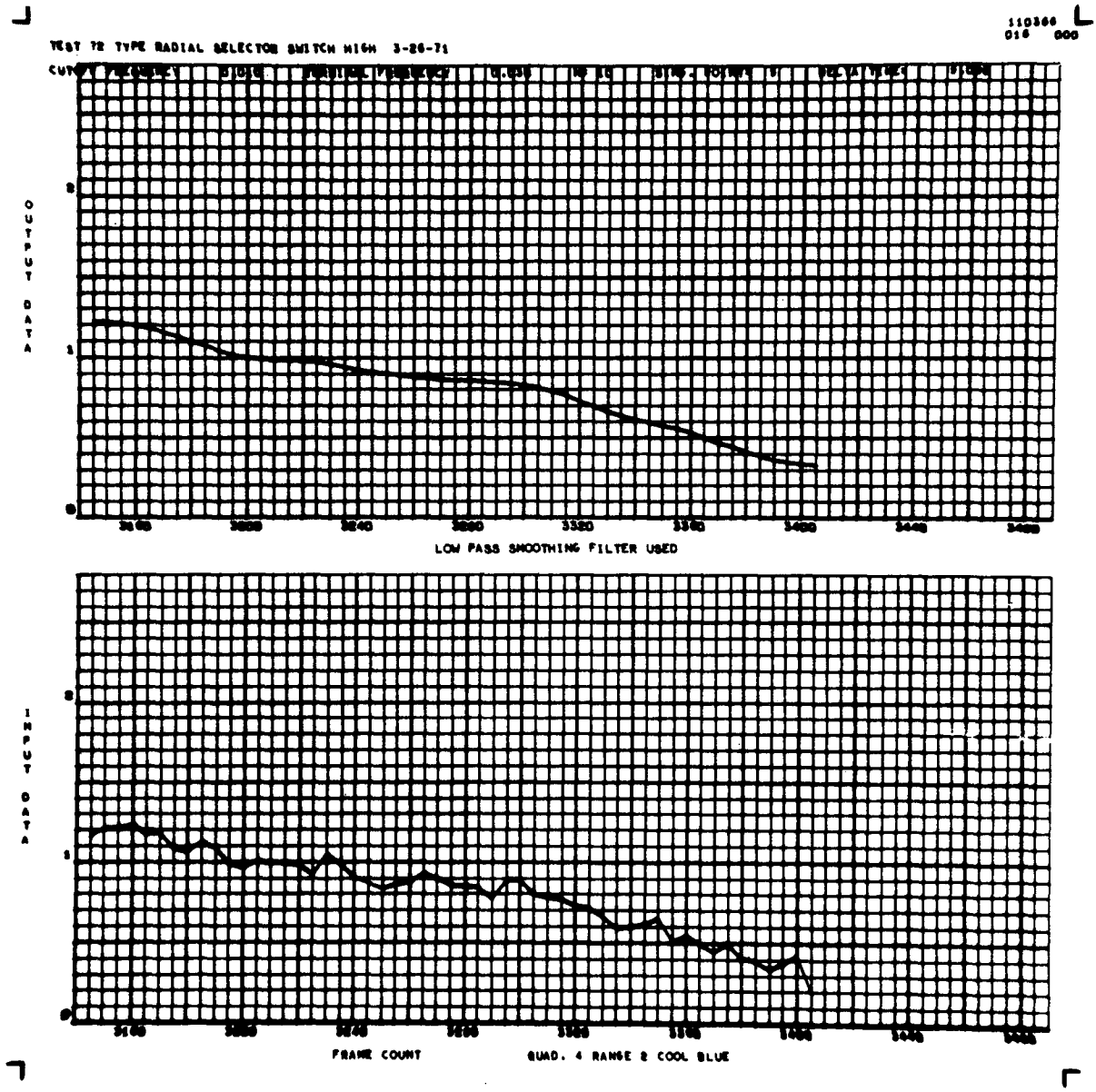

Figure A-41. Radial cell, run 2, quadrant 4, range 2, blue, power off.

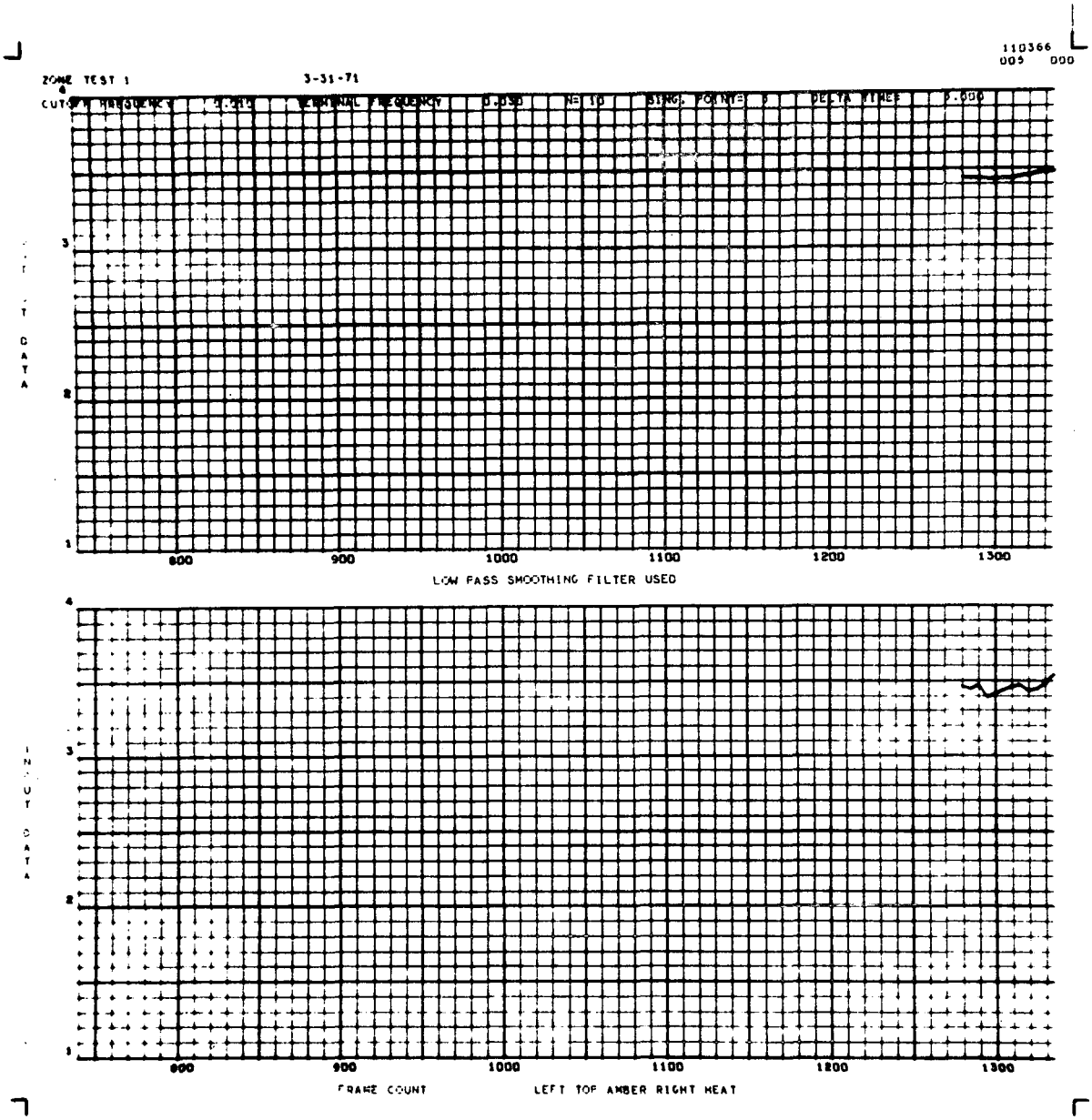

Figure A-42. Zone cell, run 1, left top, right, amber, power on.

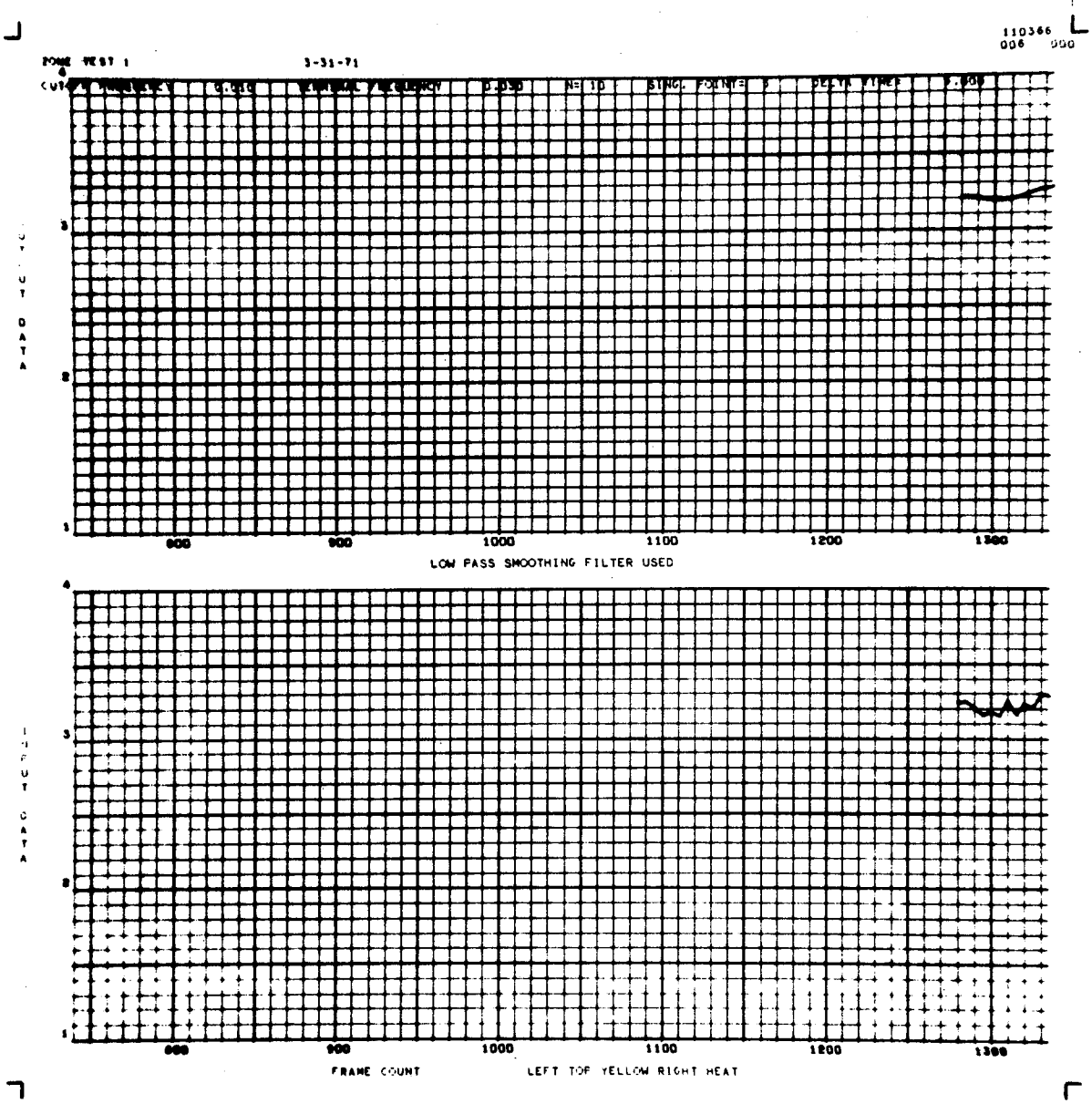

Figure A-43. Zone cell, run 1, left top, right, yellow, power on.

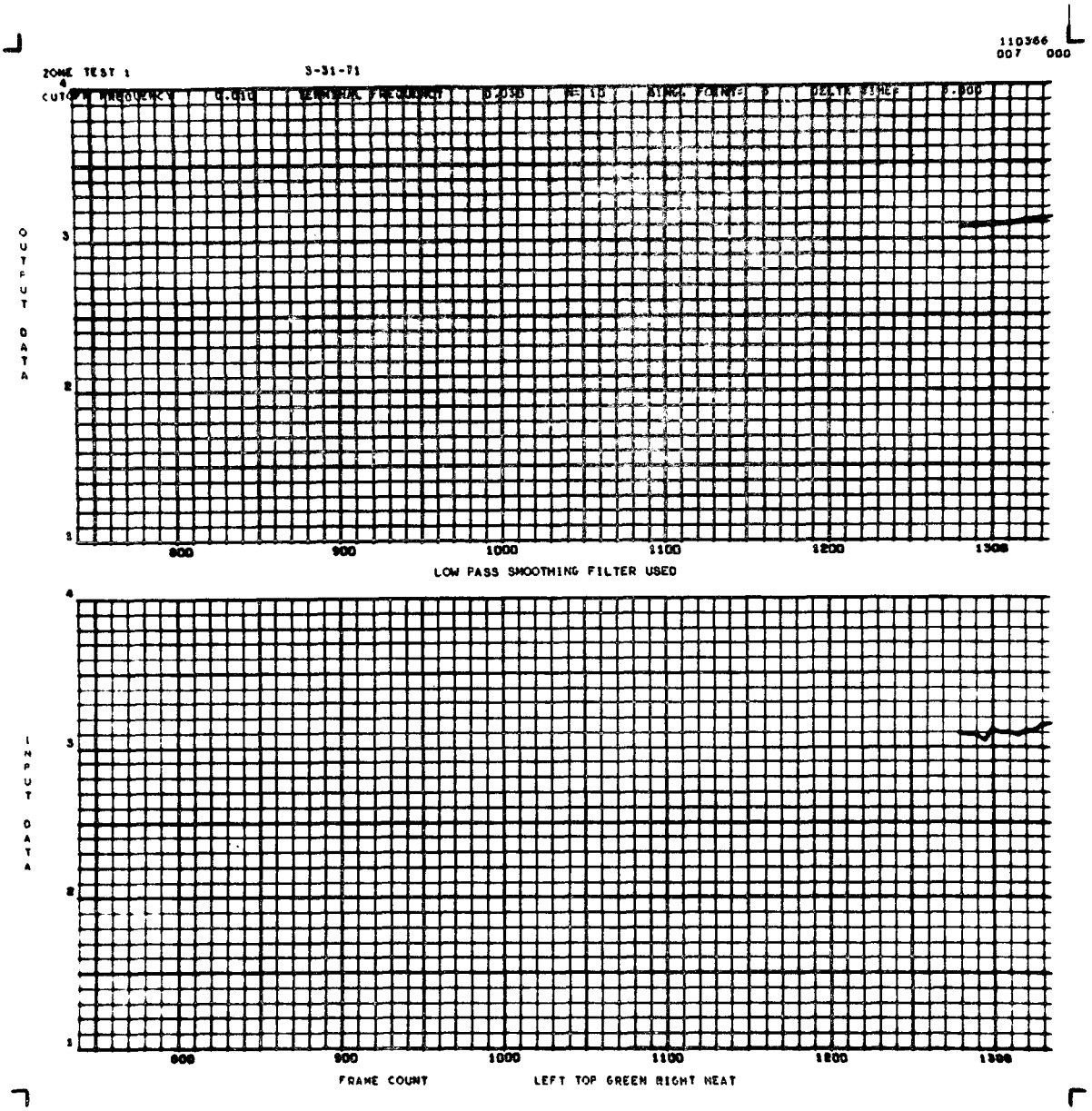

Figure A-44. Zone cell, run 1, left top, right, green, power on.

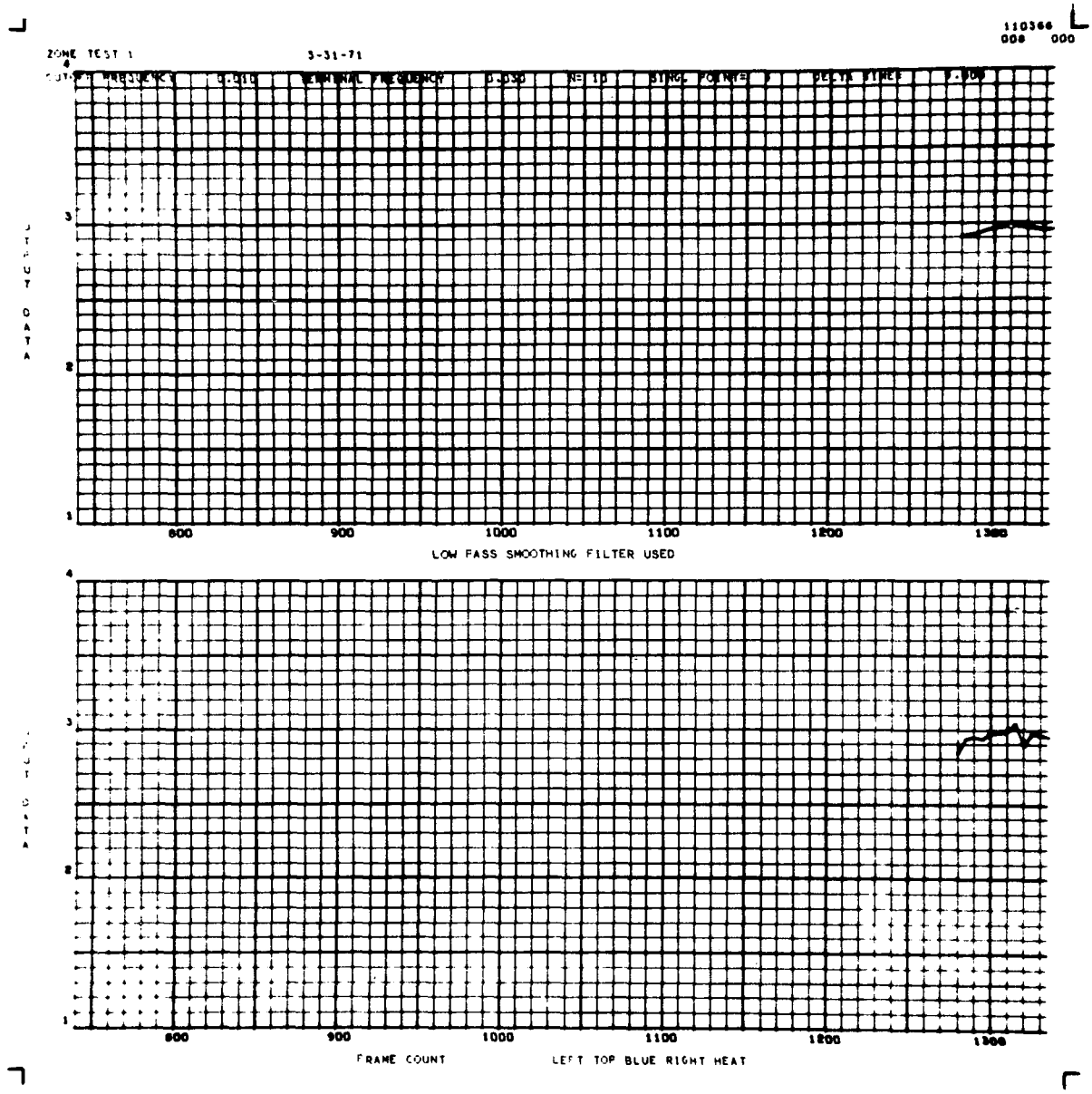

Figure A-45. Zone cell, run 1, left top, right, blue, power on.

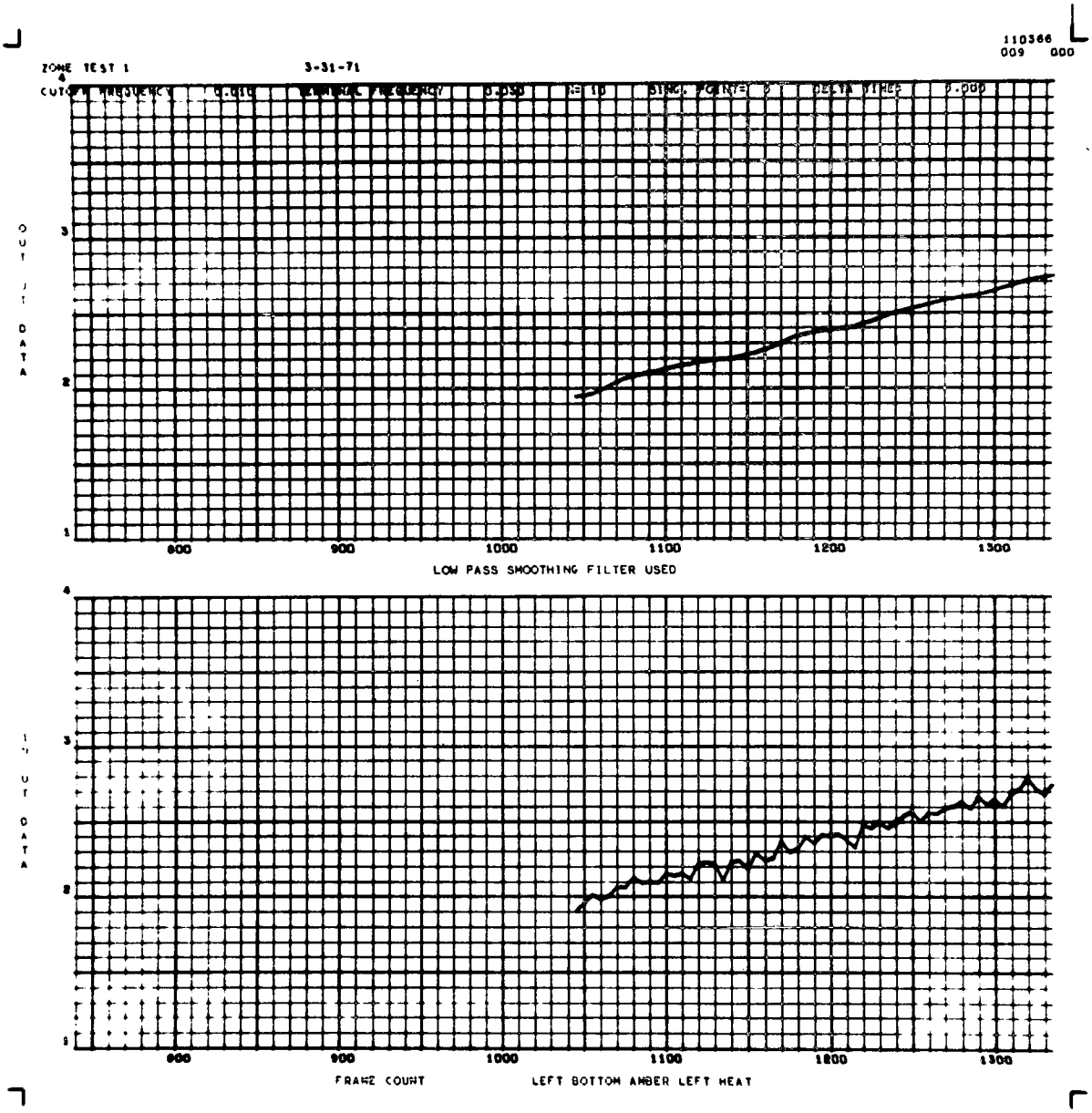

Figure A-46. Zone cell, run 1, left bottom, left, amber, power on.

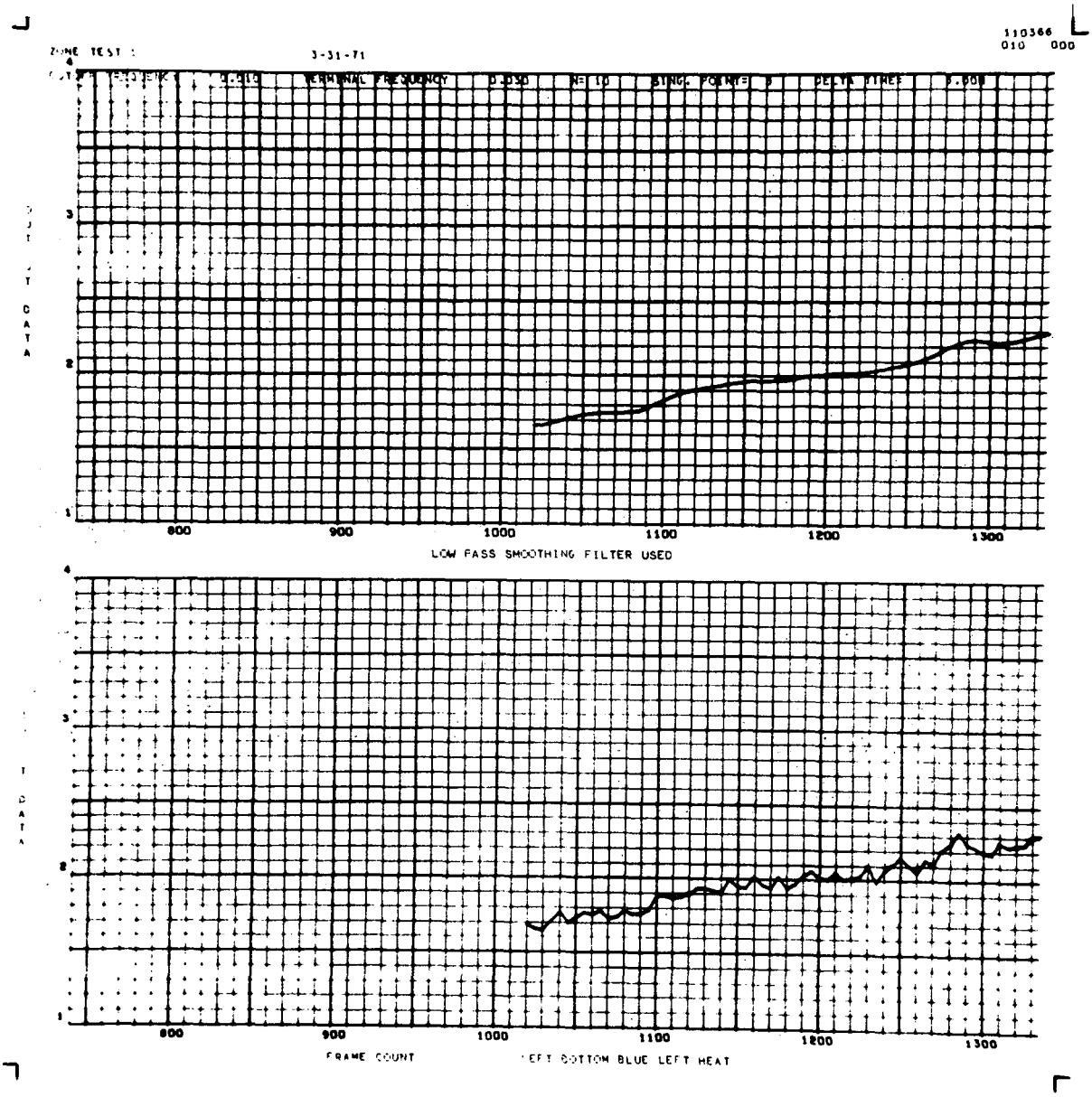

Figure A-47. Zone cell, run 1, left bottom, left, blue, power on.

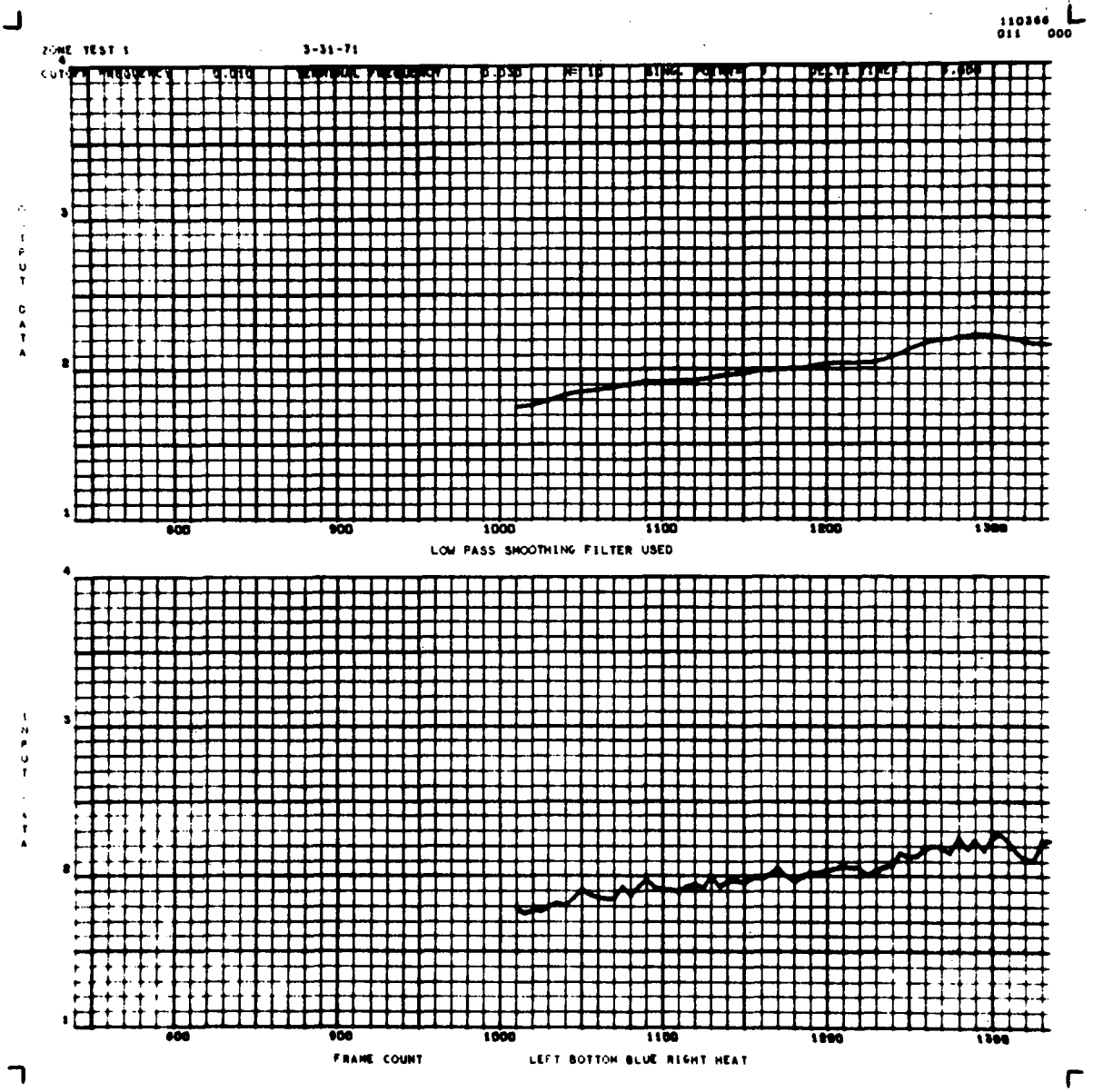

Figure A-48. Zone cell, run 1, left bottom, right, blue, power on.

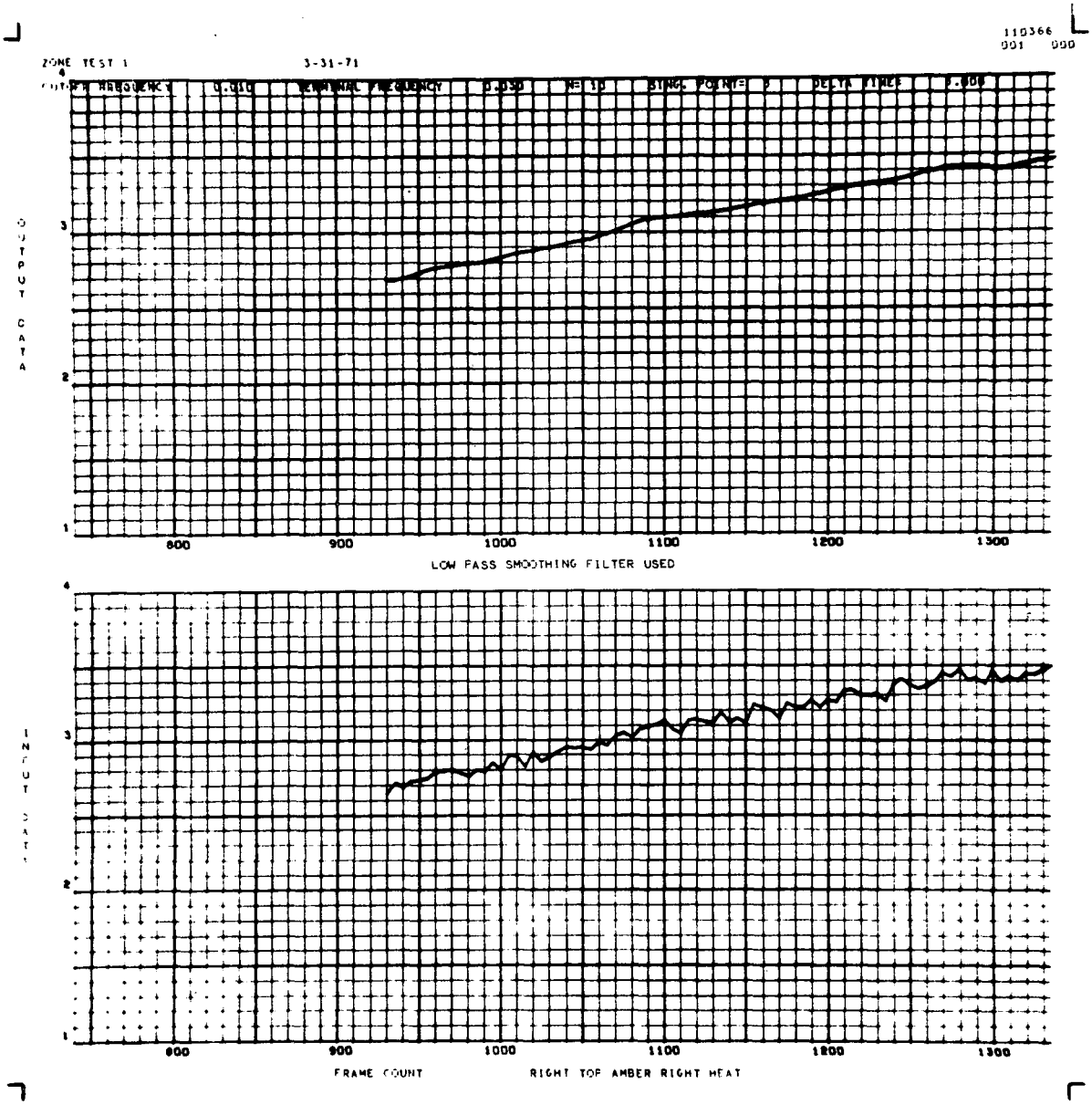

Figure A-49. Zone cell, run 1, right top, right, amber, power on.

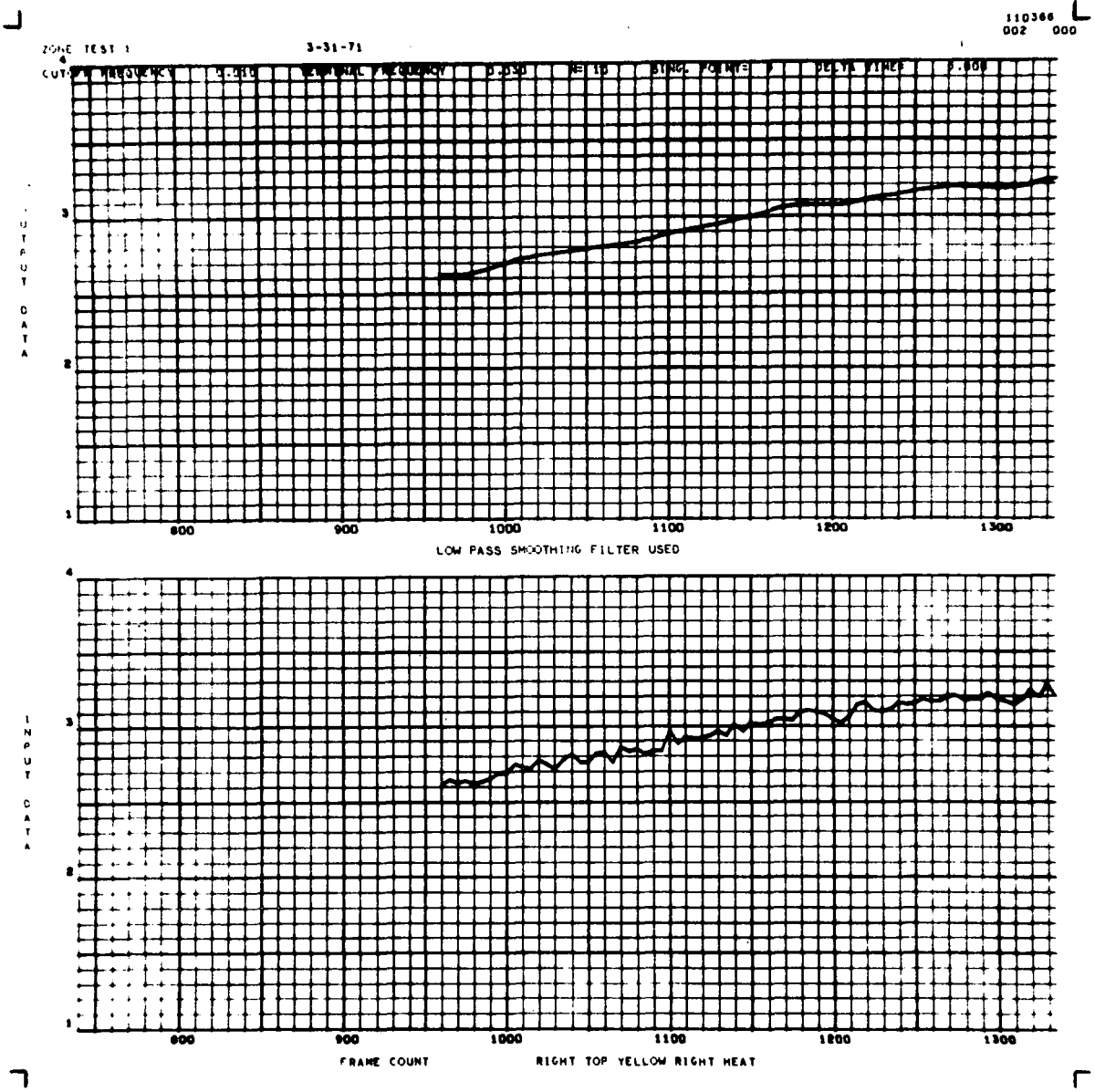

Figure A-50. Zone cell, run 1, right top, right, yellow, power on.

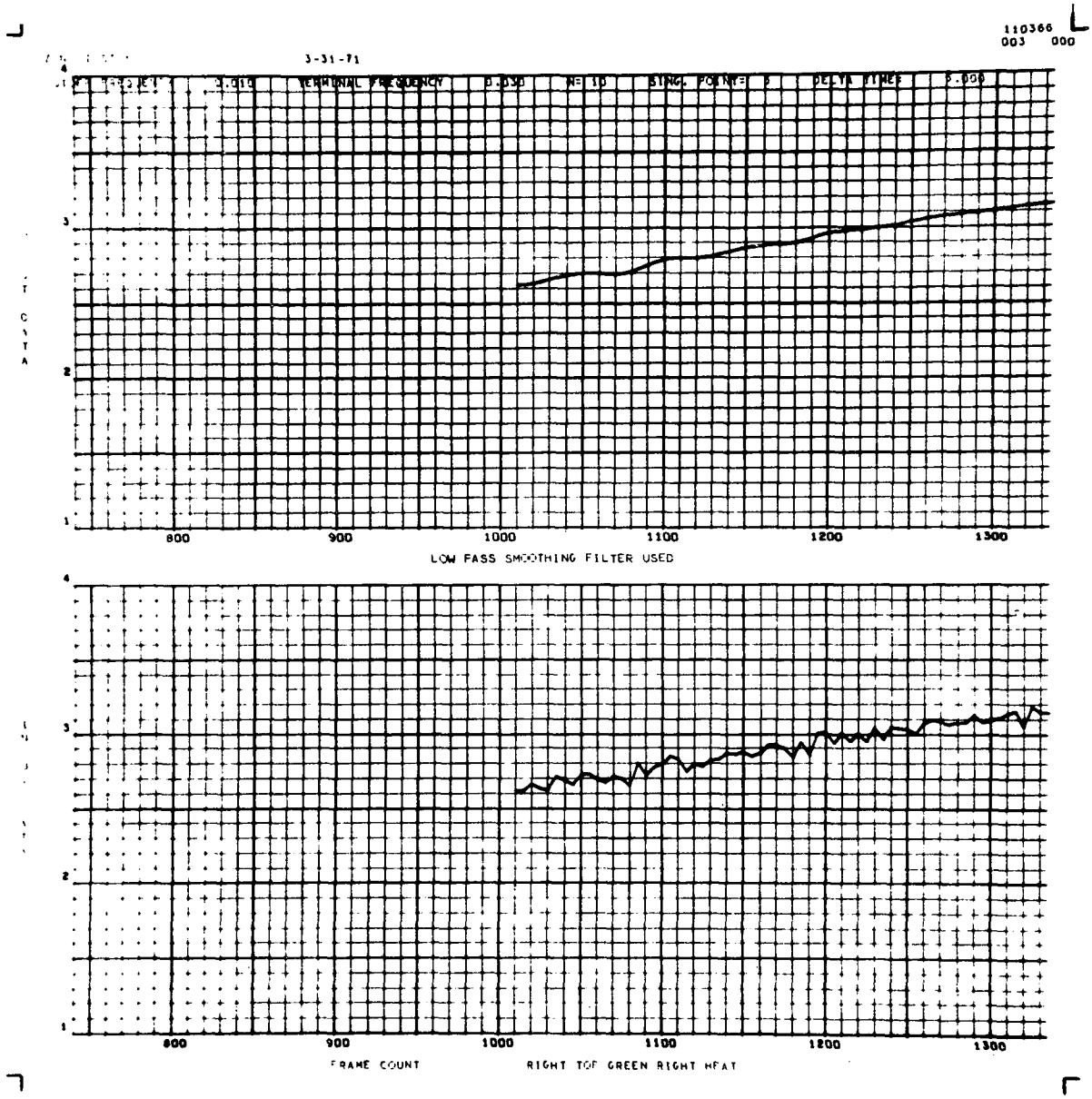

Figure A-51. Zone cell, run 1, right top, right, green, power on.

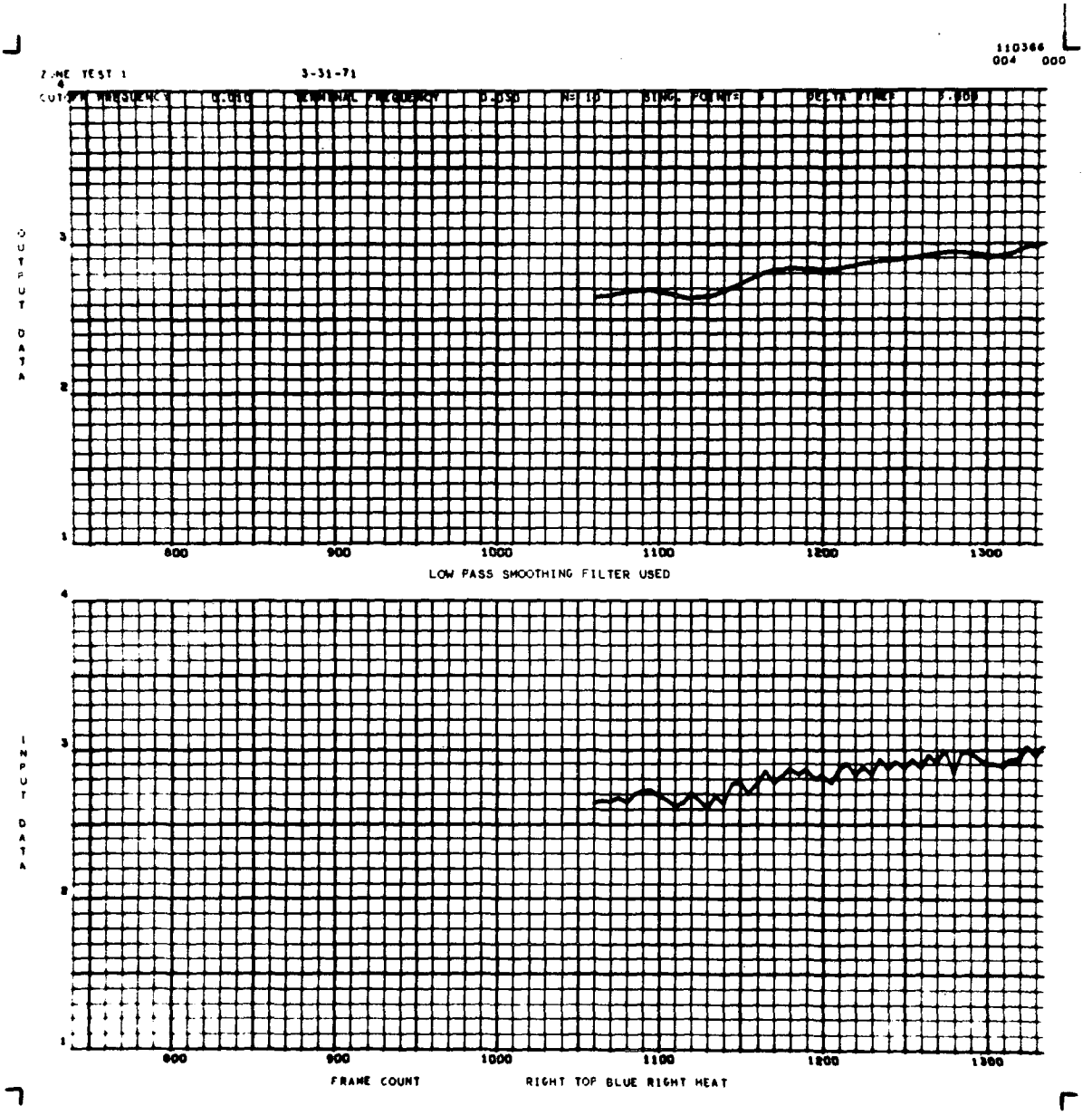

Figure A-52. Zone cell, run 1, right top, right, blue, power on.

C.2

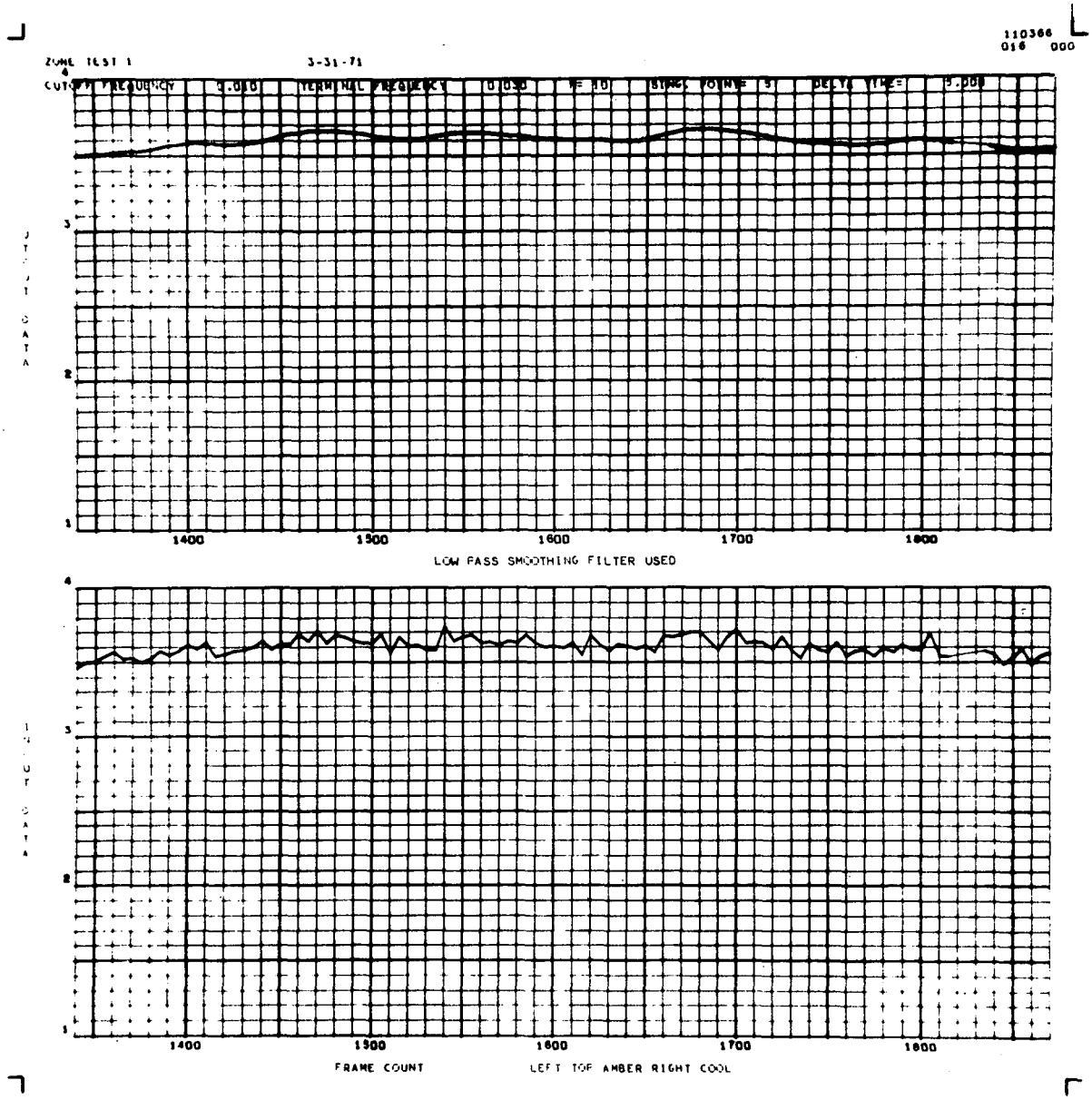

Figure A-53. Zone cell, run 1, left top, right, amber, power off.

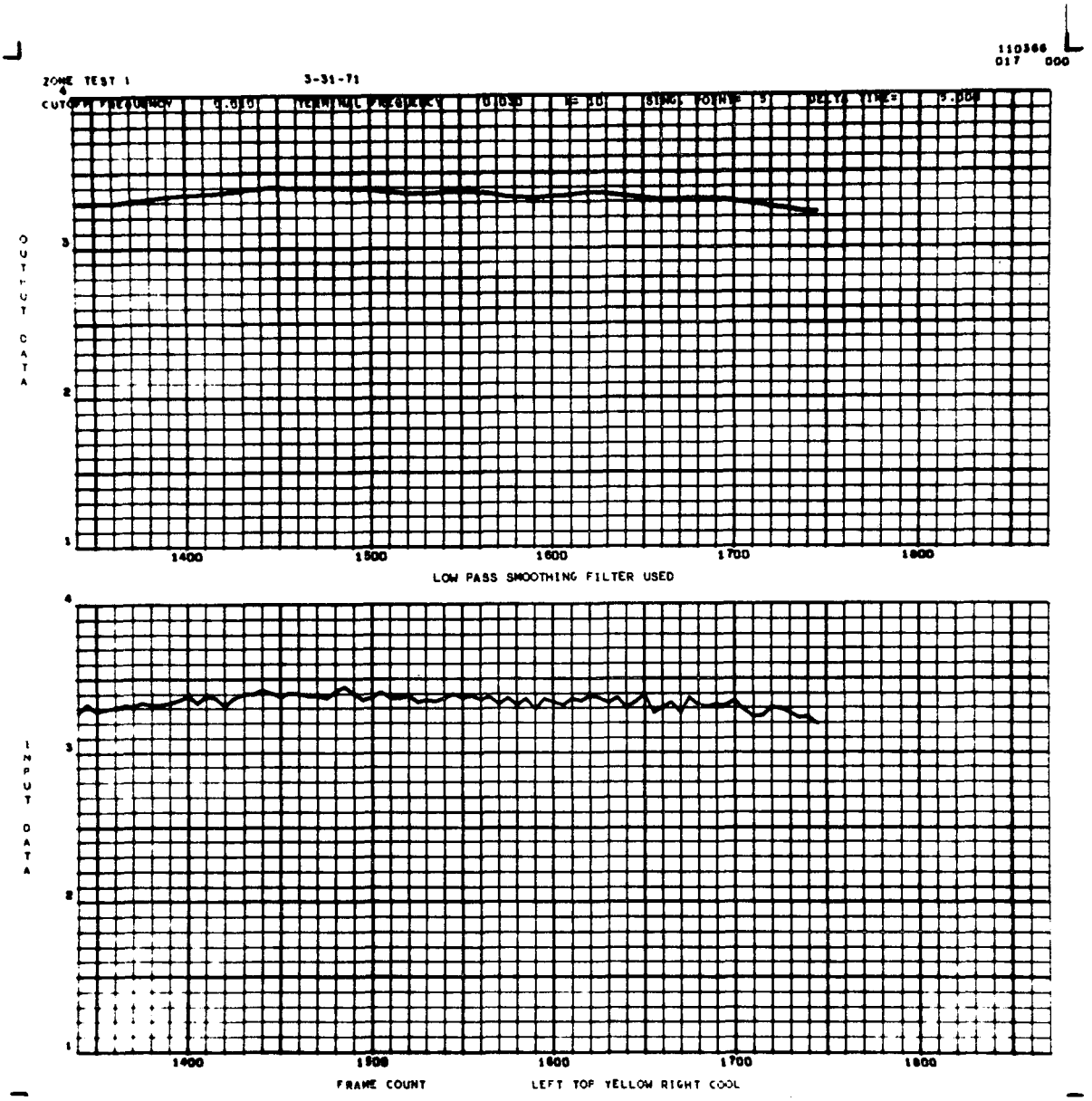

Figure A-54. Zone cell, run 1, left top, right, yellow, power off.

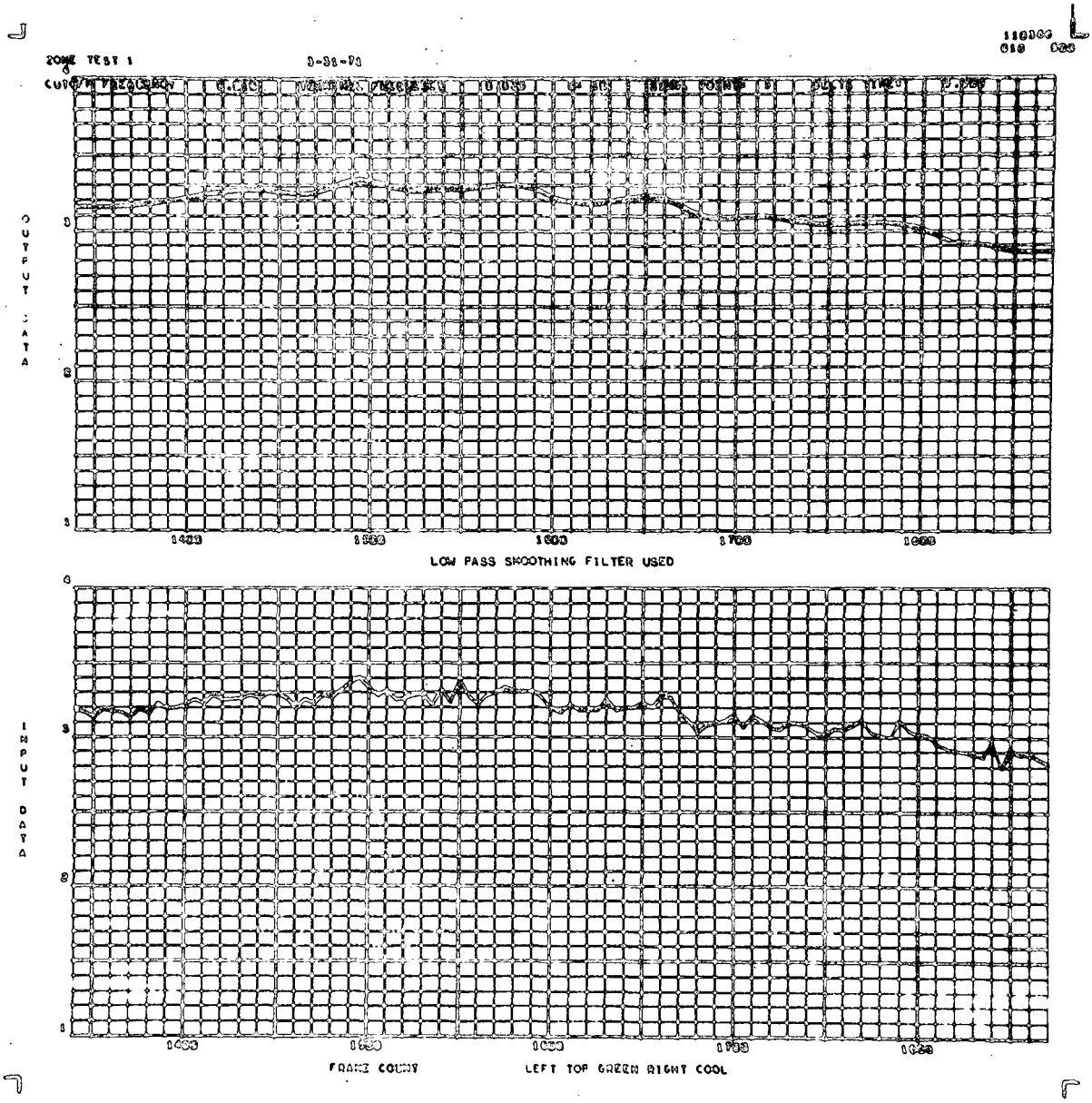

Figure A-55. Zone cell, run 1, left top, right, green, power off.

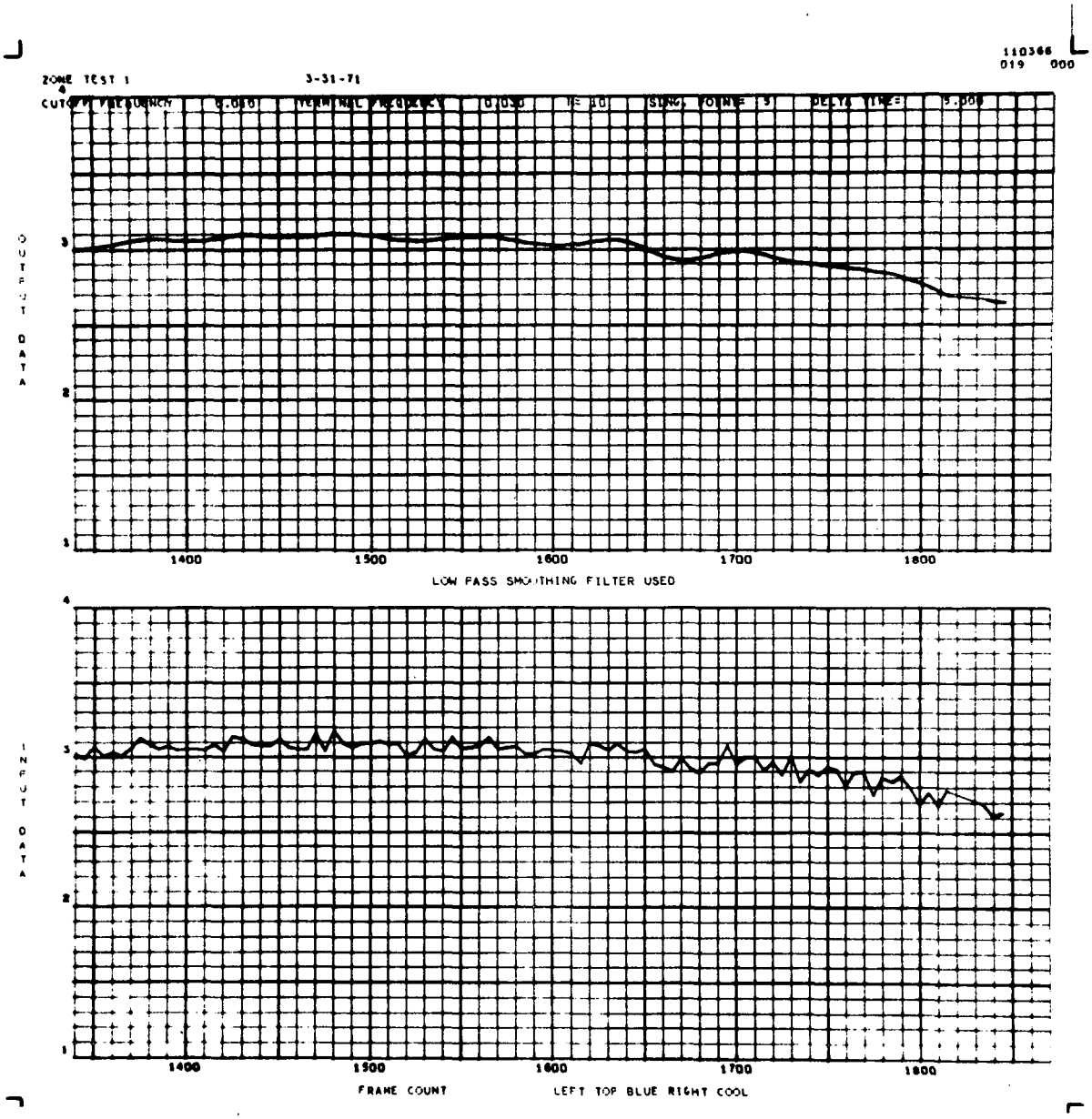

Figure A-56. Zone cell, run 1, left top, right, blue, power off.

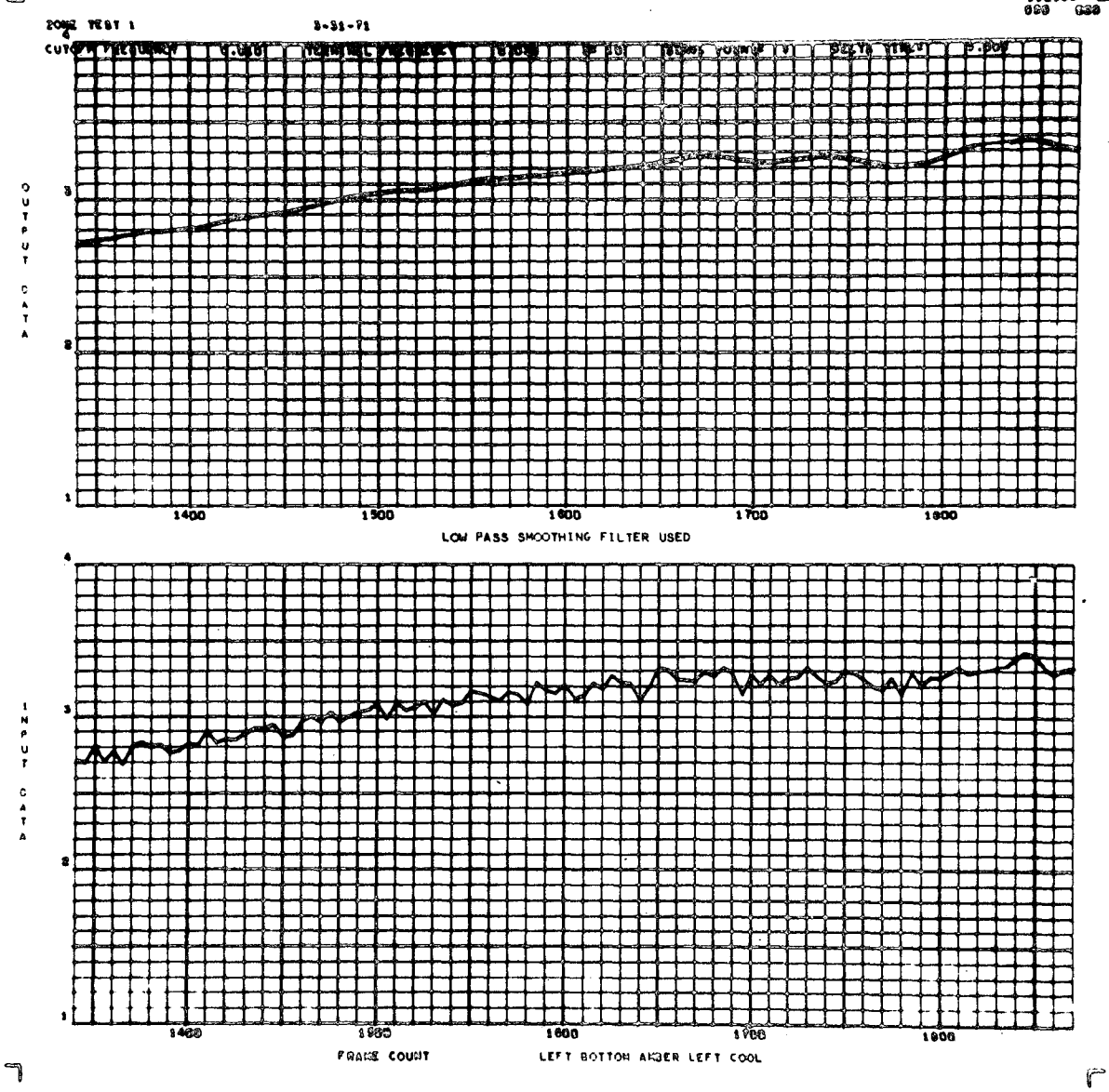

Figure A-57. Zone cell, run 1, left bottom, left, amber, power off.

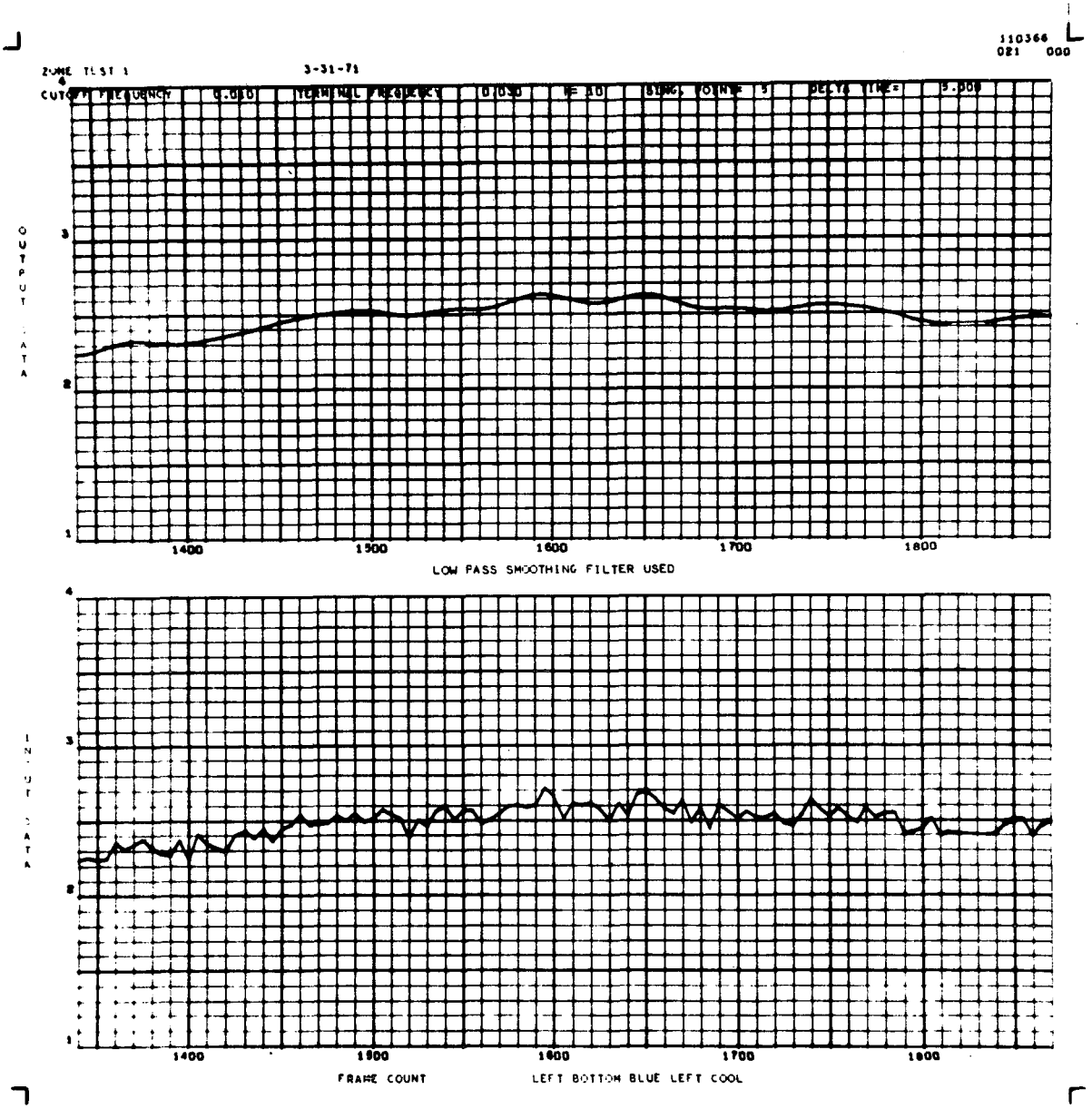

Figure A-58. Zone cell, run 1, left bottom, left, blue, power off.

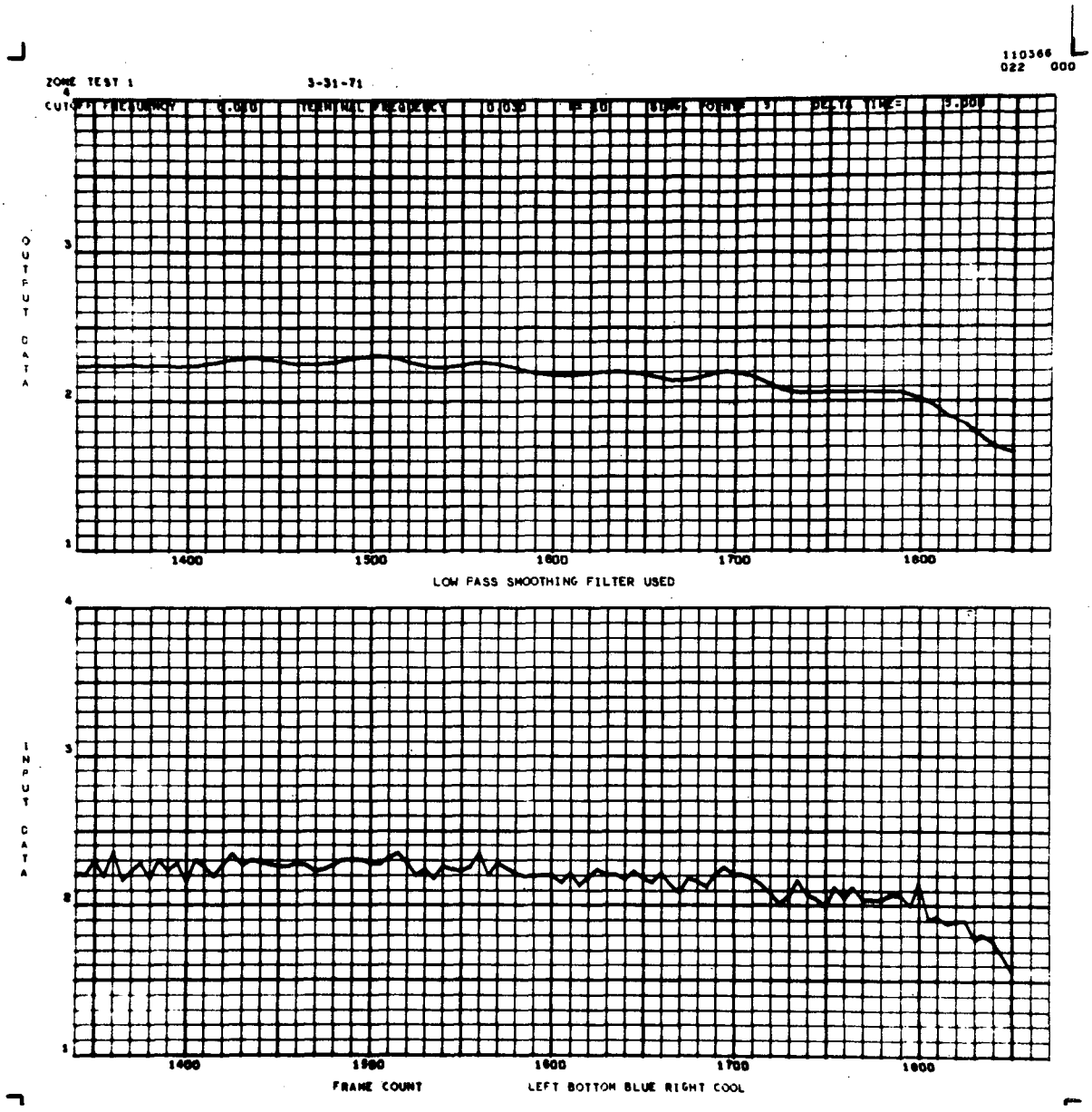

Figure A-59. Zone cell, run 1, left bottom, right, blue, power off.

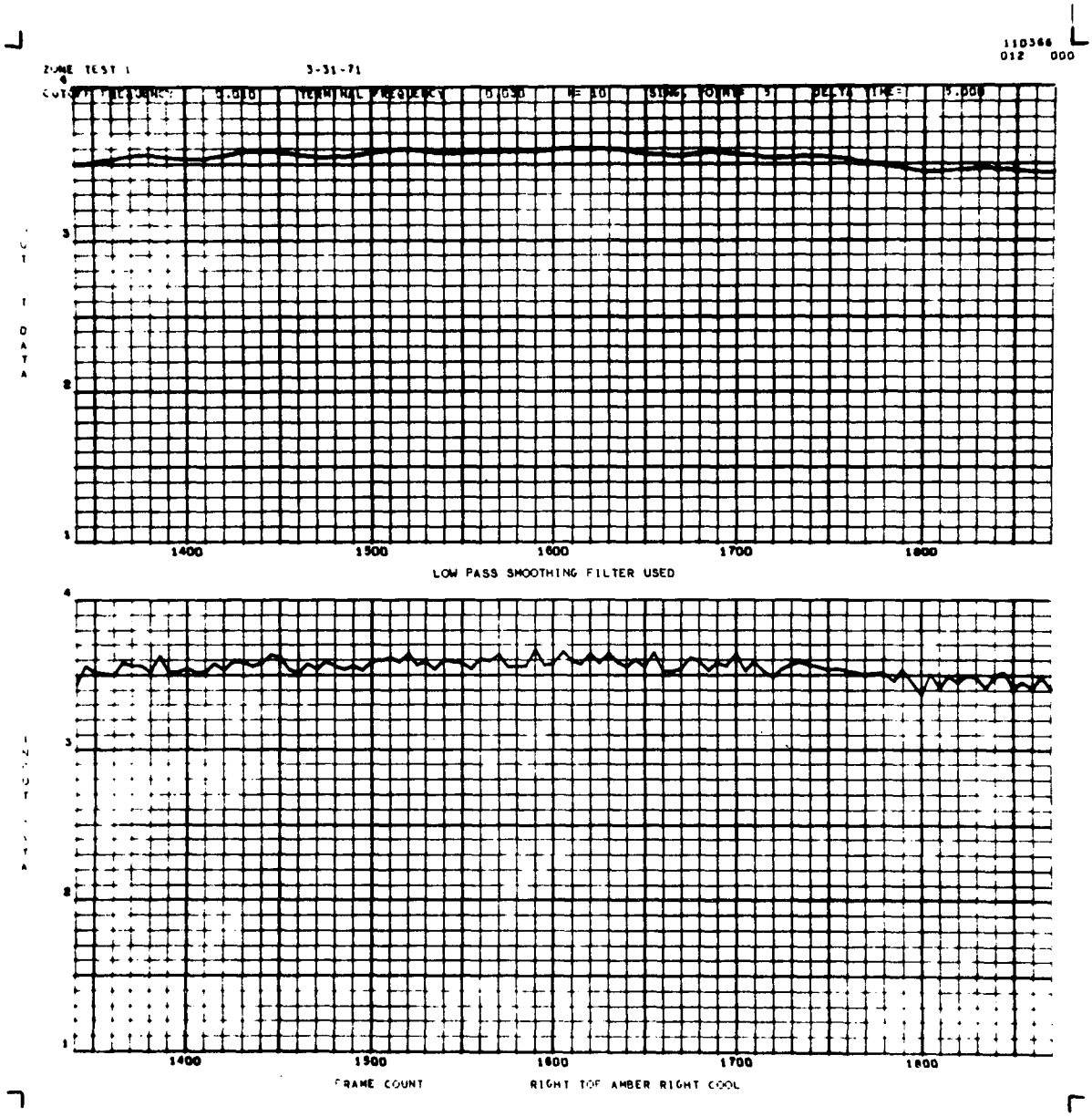

Figure A-60. Zone cell, run 1, right top, right, amber, power off.

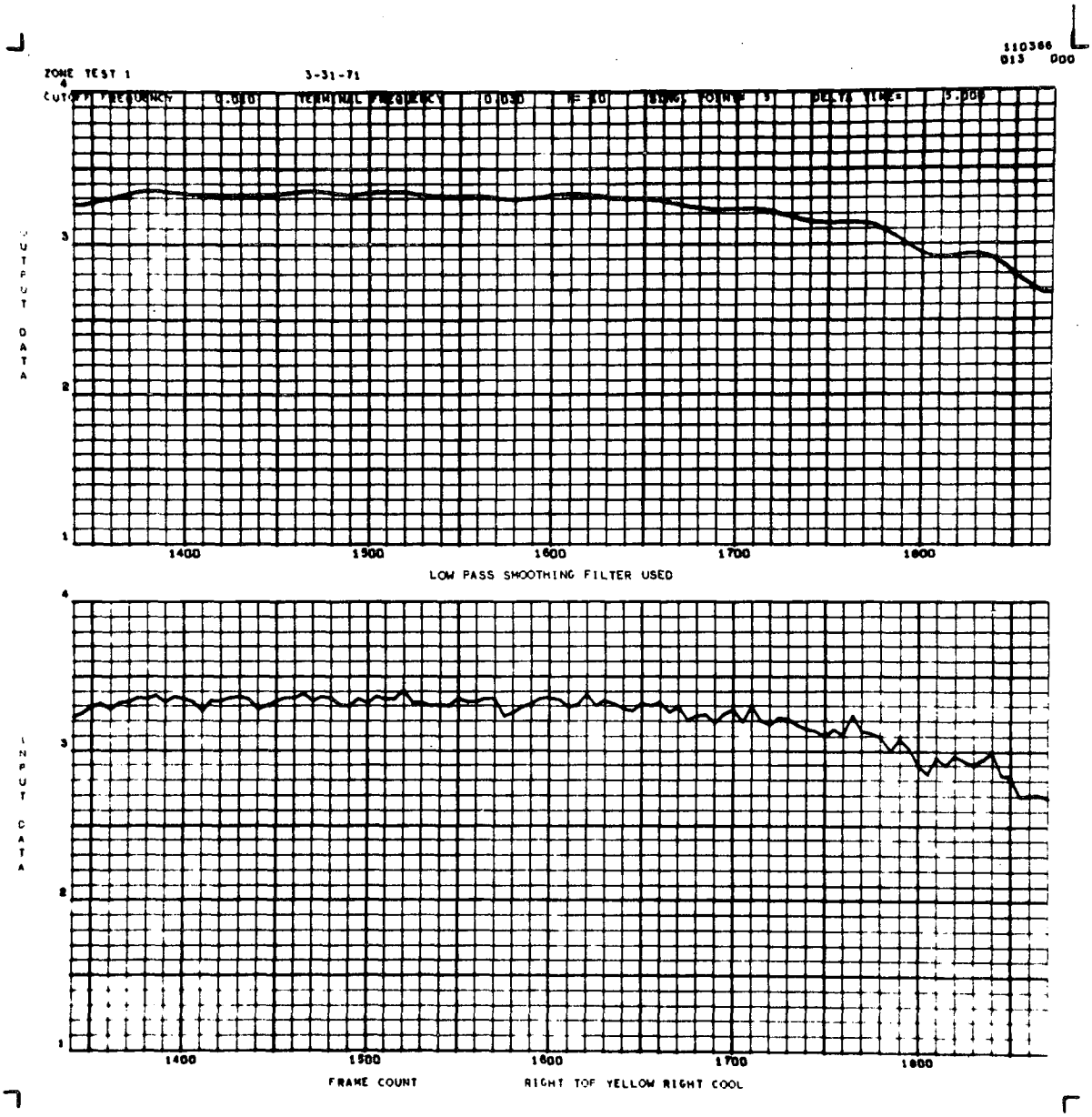

Figure A-61. Zone cell, run 1, right top, right, yellow, power off.

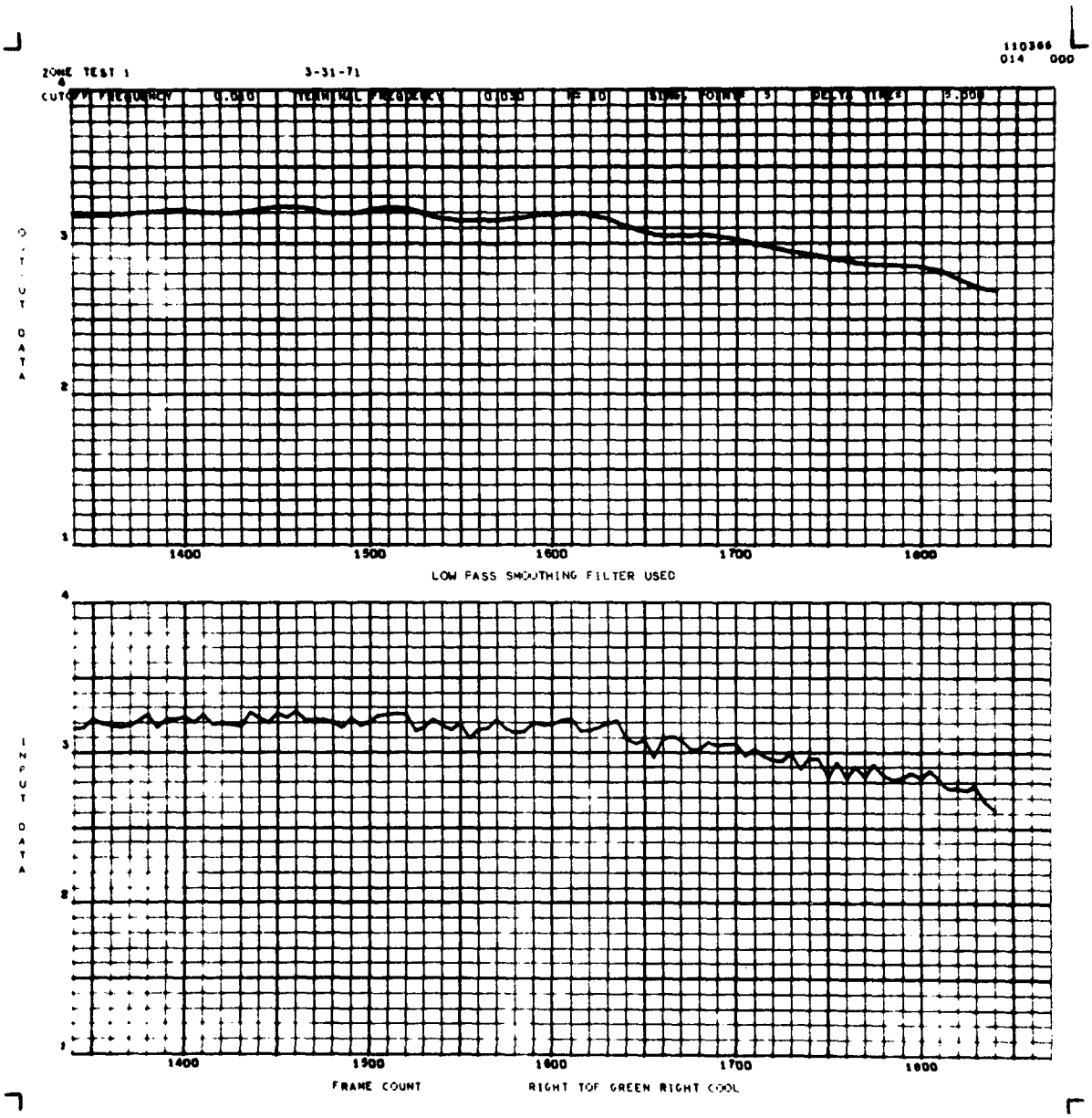

Figure A-62. Zone cell, run 1, right top, right, green, power off.

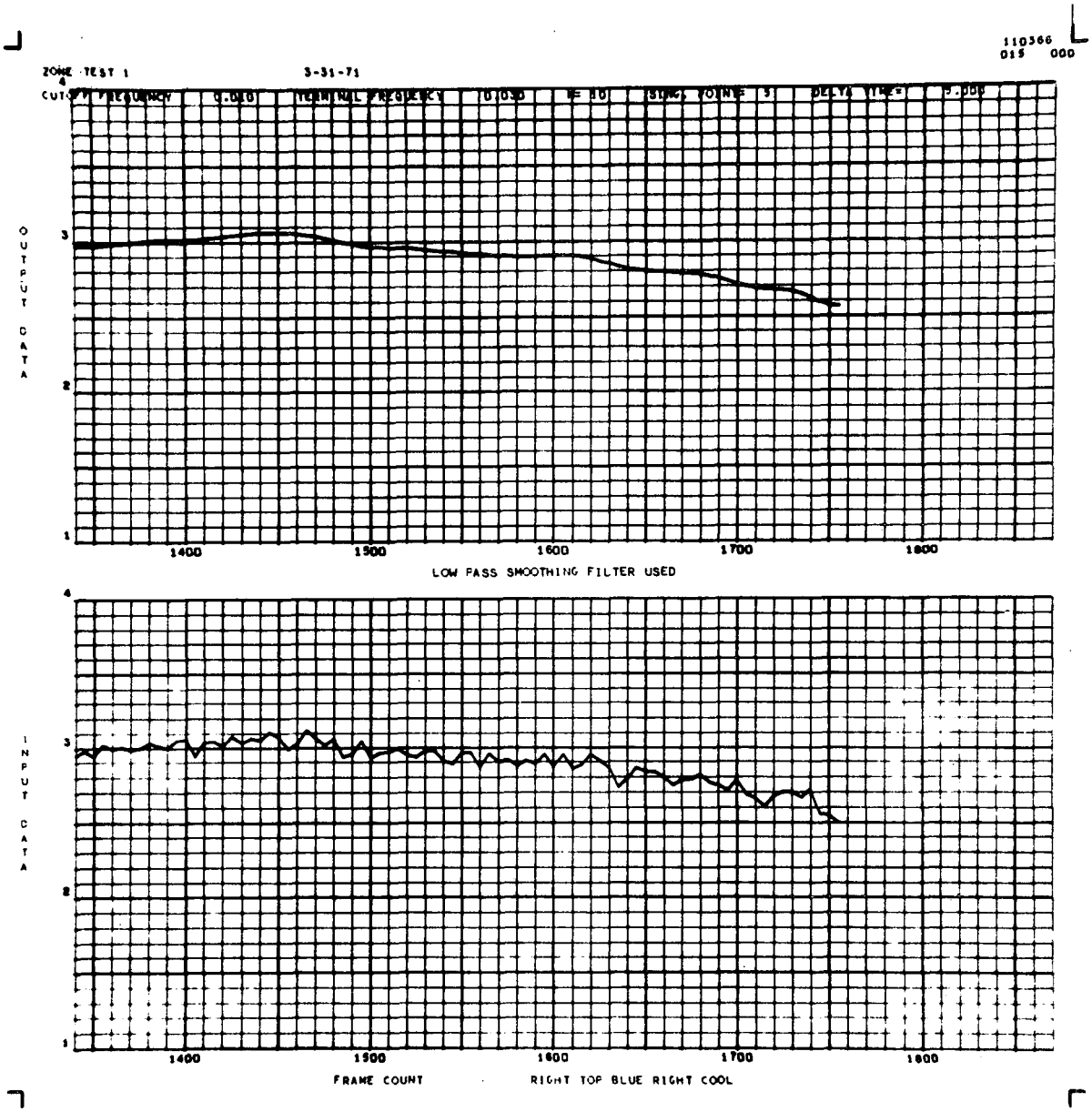

Figure A-63. Zone cell, run 1, right top, right, blue, power off.

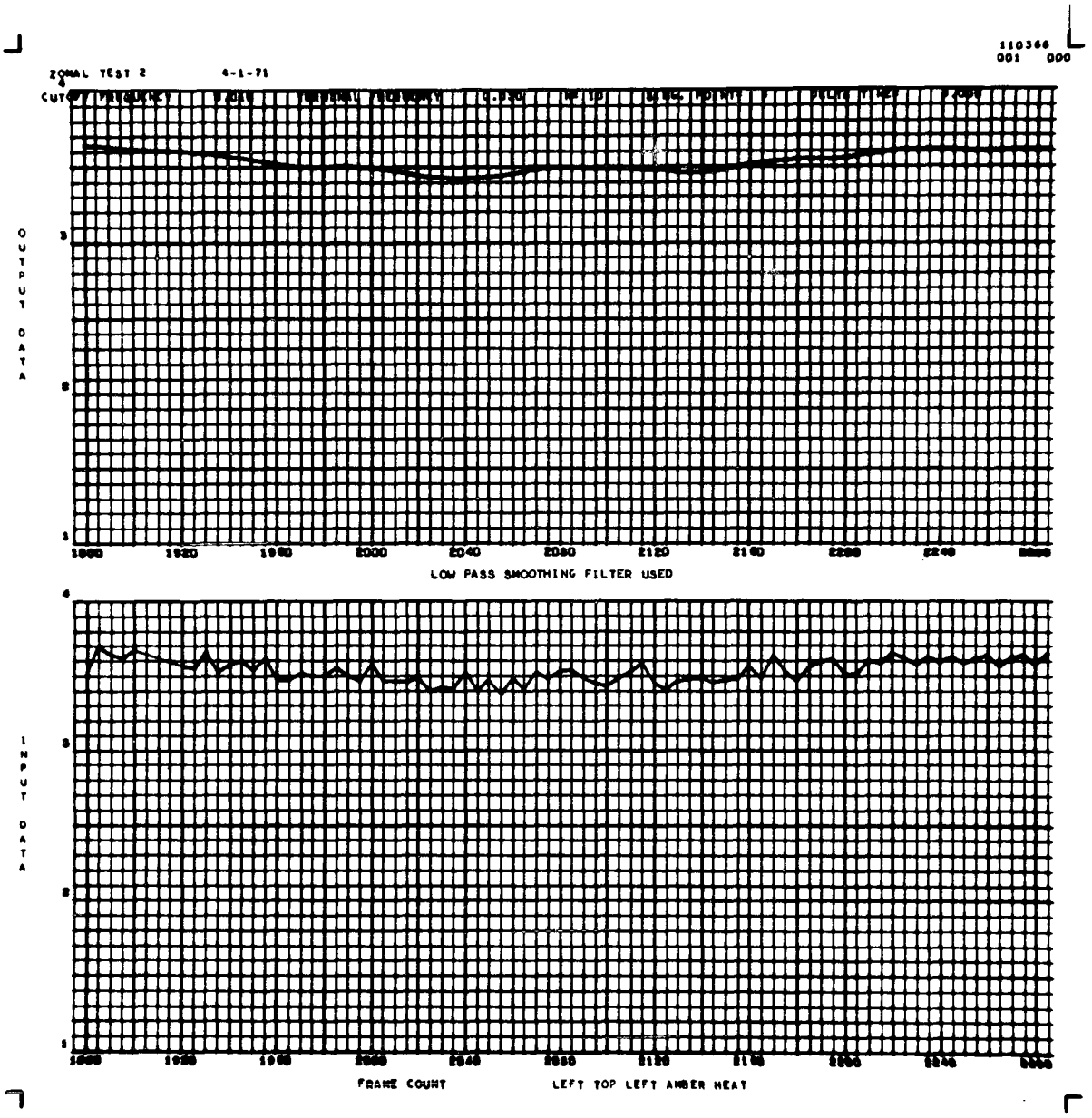

Figure A-64. Zone cell, run 2, left top, left, amber, power on.

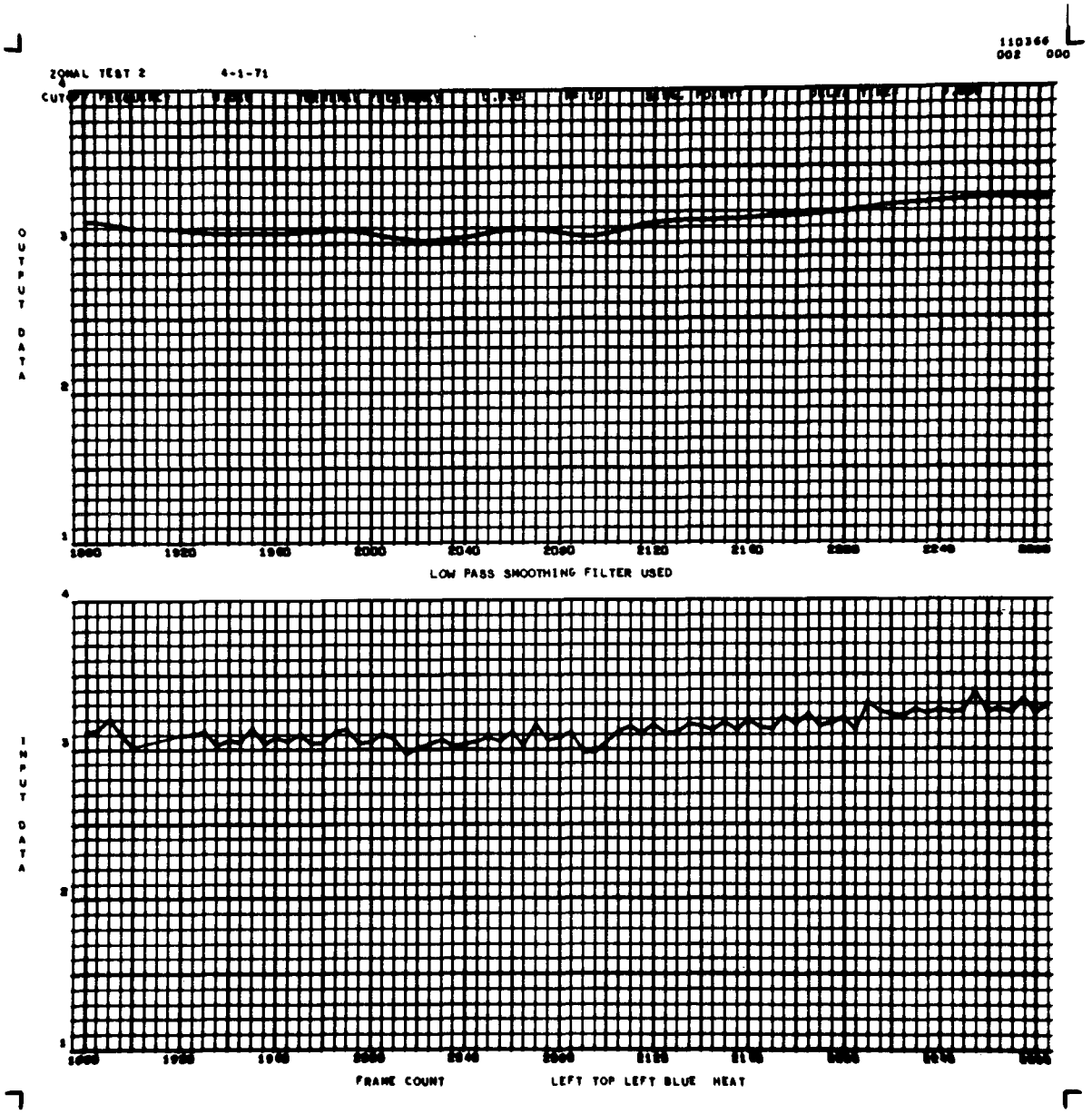

Figure A-65. Zone cell, run 2, left top, left, blue, power on.

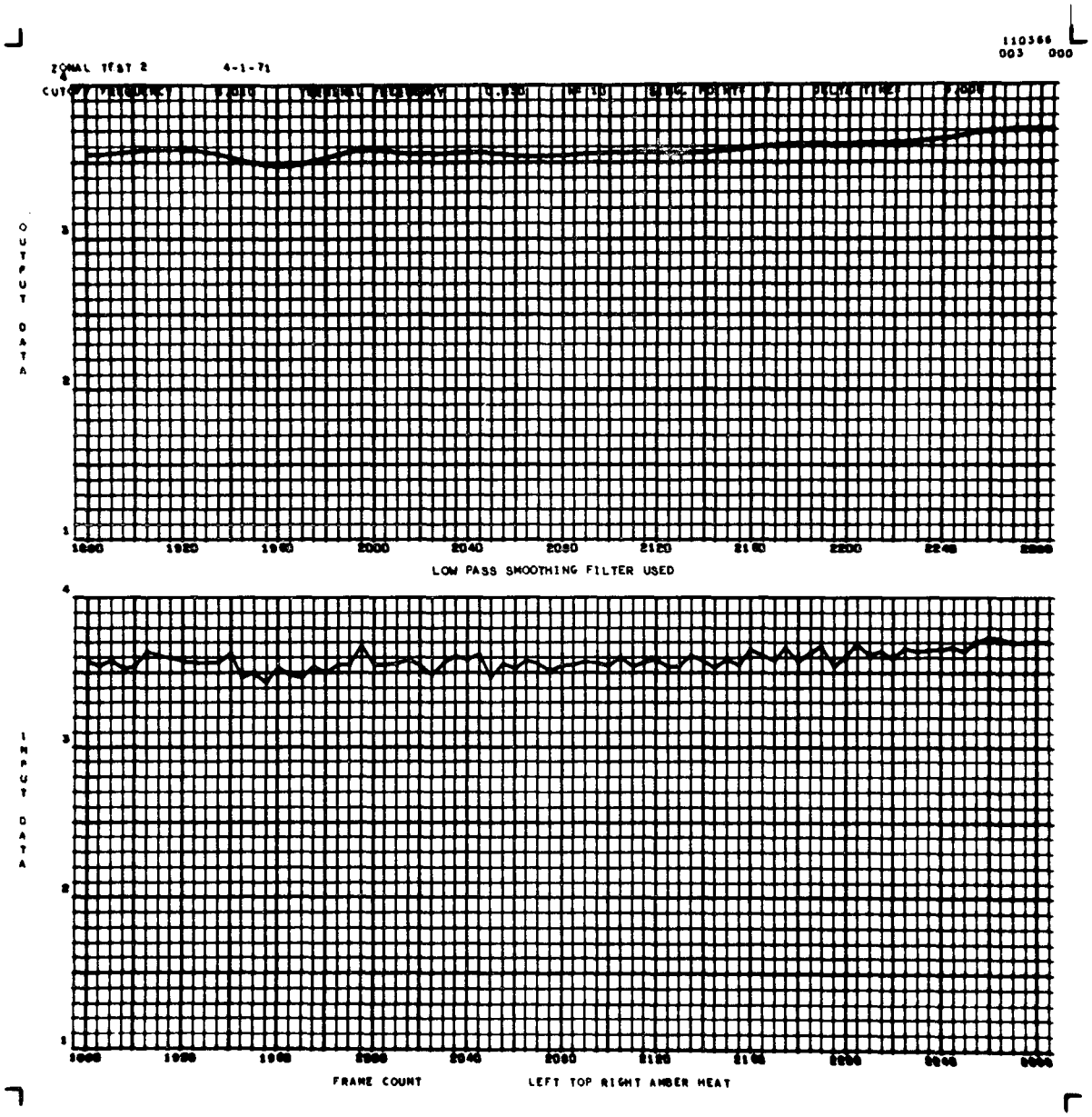

Figure A-66. Zone cell, run 2, left top, right, amber, power on.

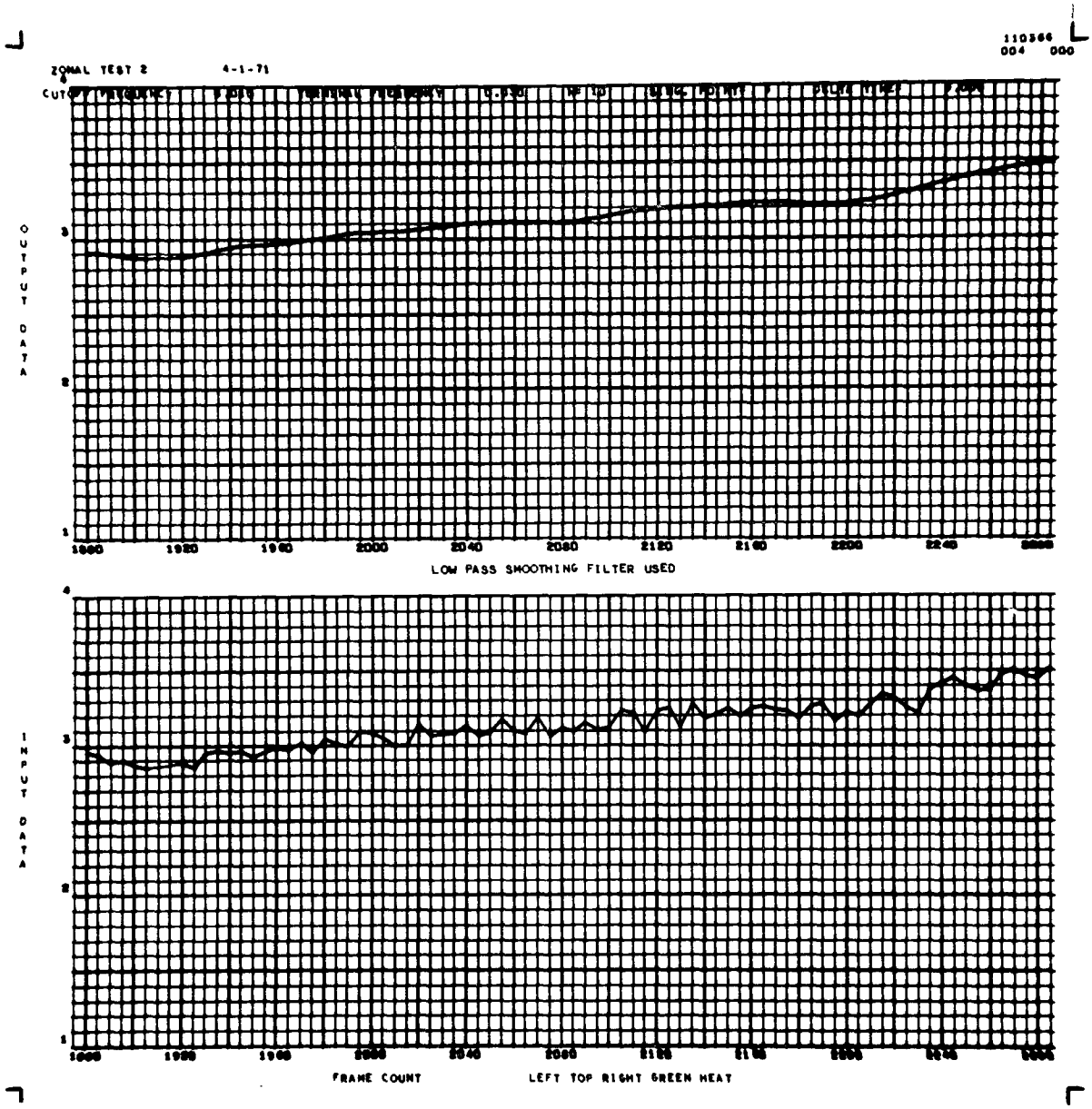

Figure A-67. Zone cell, run 2, left top, right, green, power on.

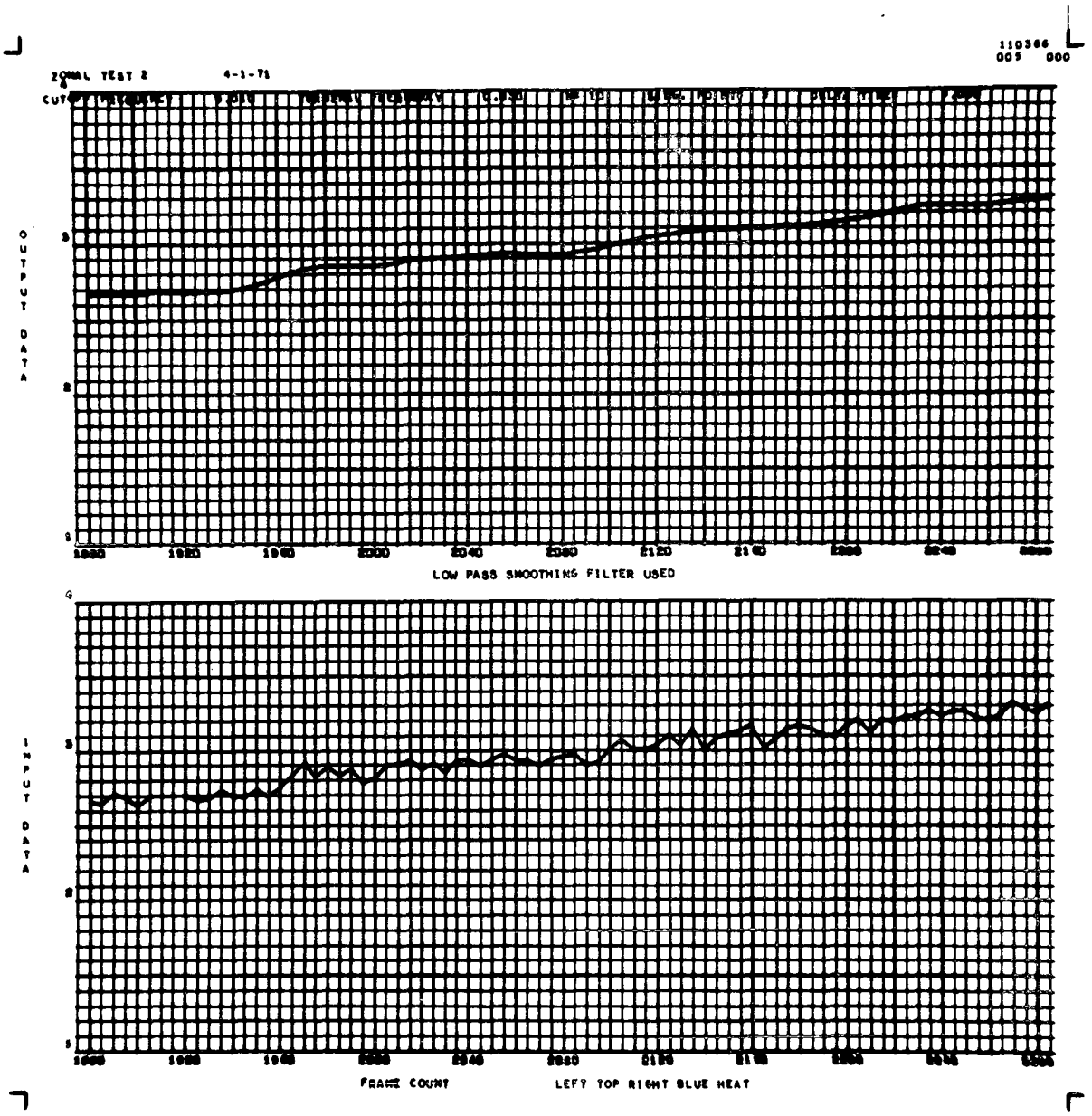

Figure A-68. Zone cell, run 2, left top, right, blue, power on.

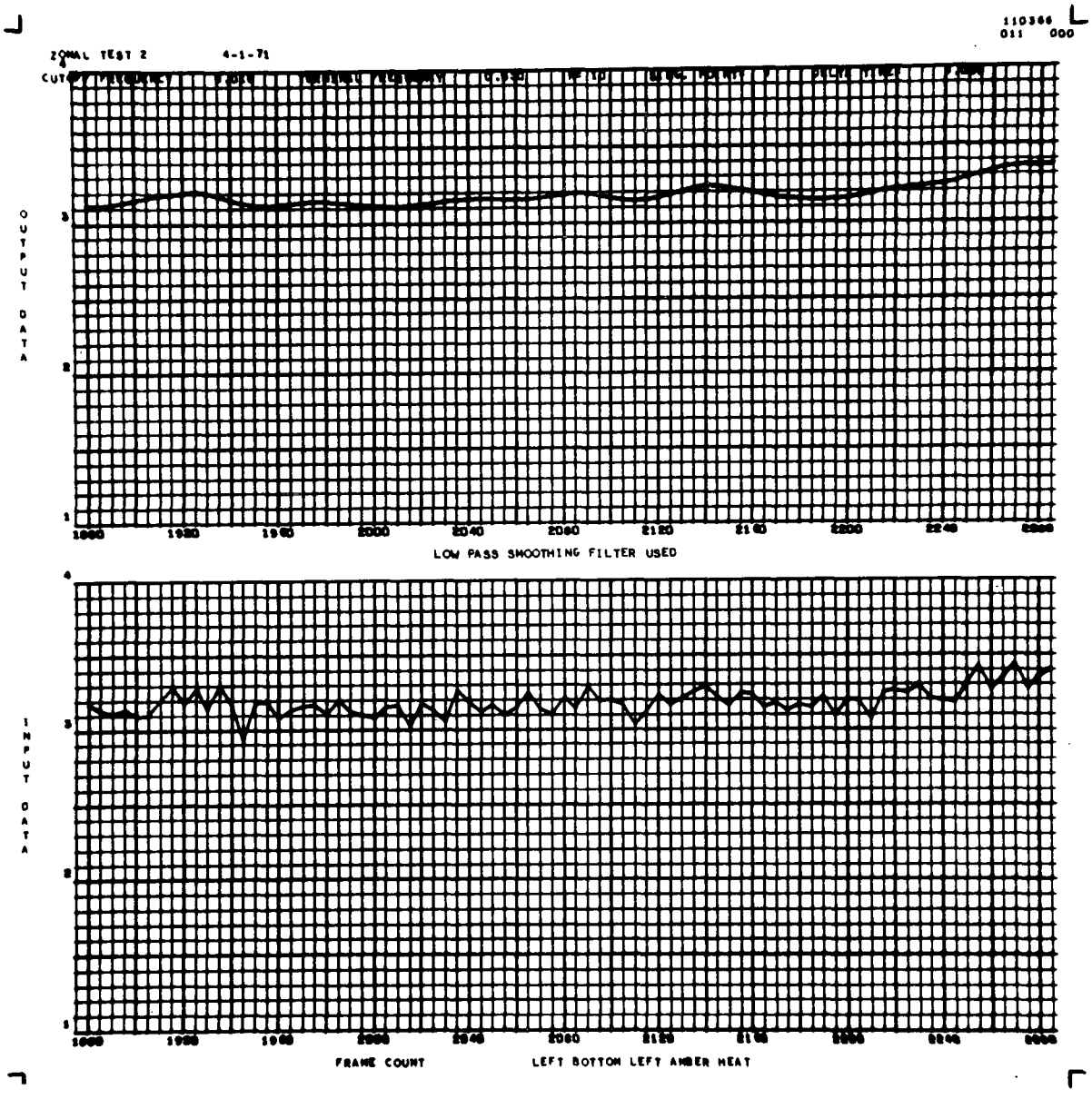

Figure A-69. Zone cell, run 2, left bottom, left, amber, power on.

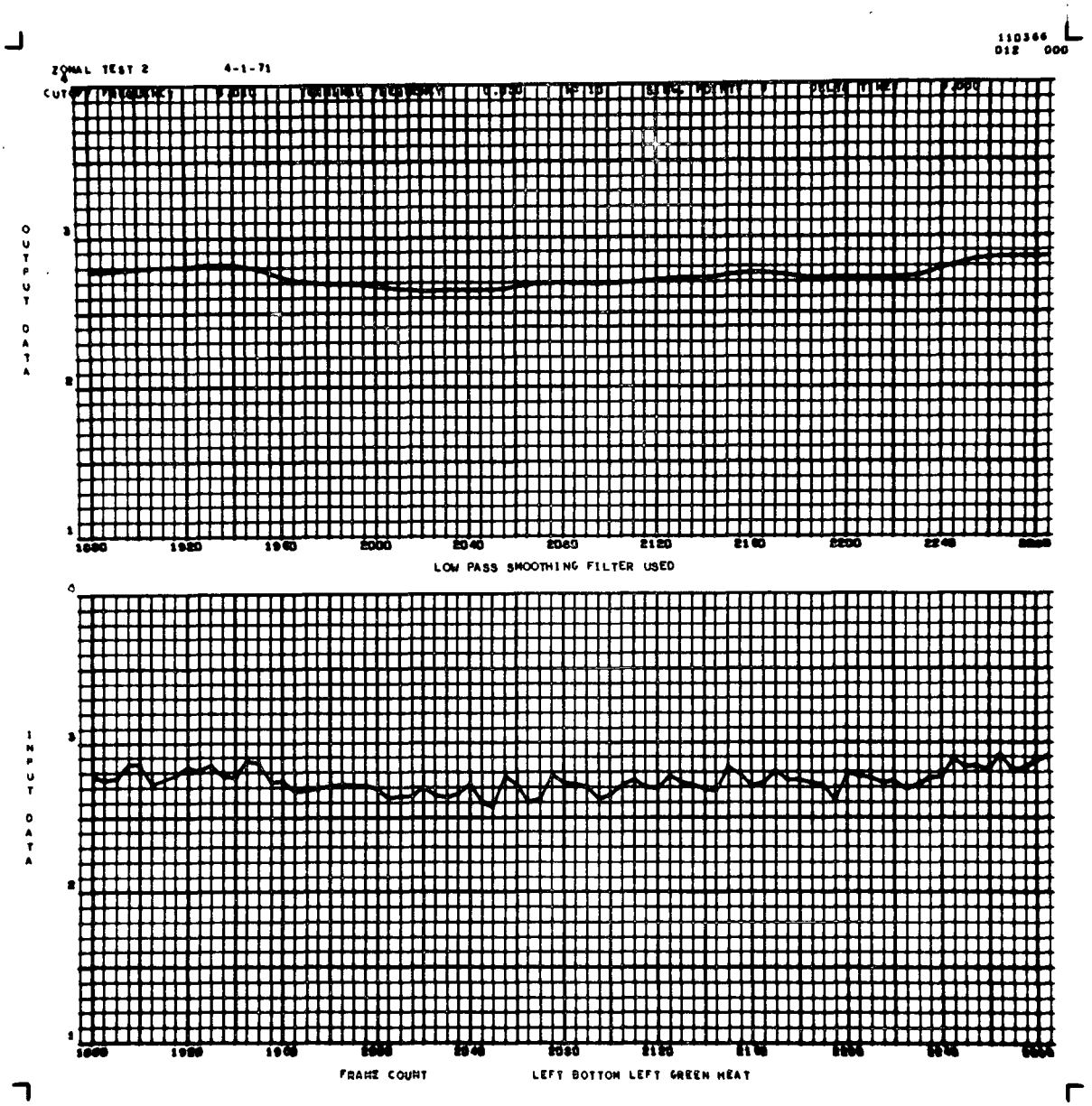

Figure A-70. Zone cell, run 2, left bottom, left, green, power on.

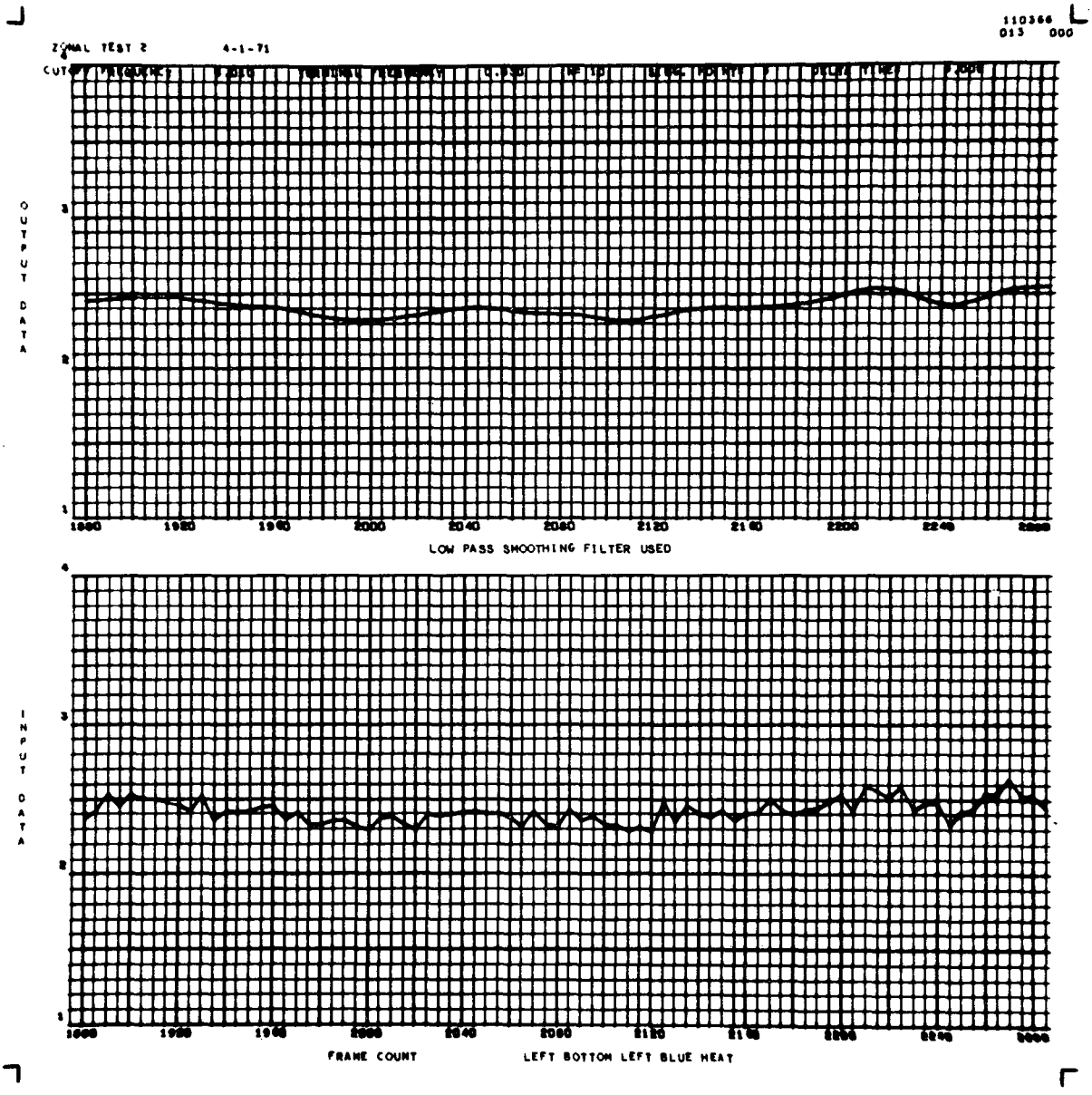

Figure A-71. Zone cell, run 2, left bottom, left, blue, power on.

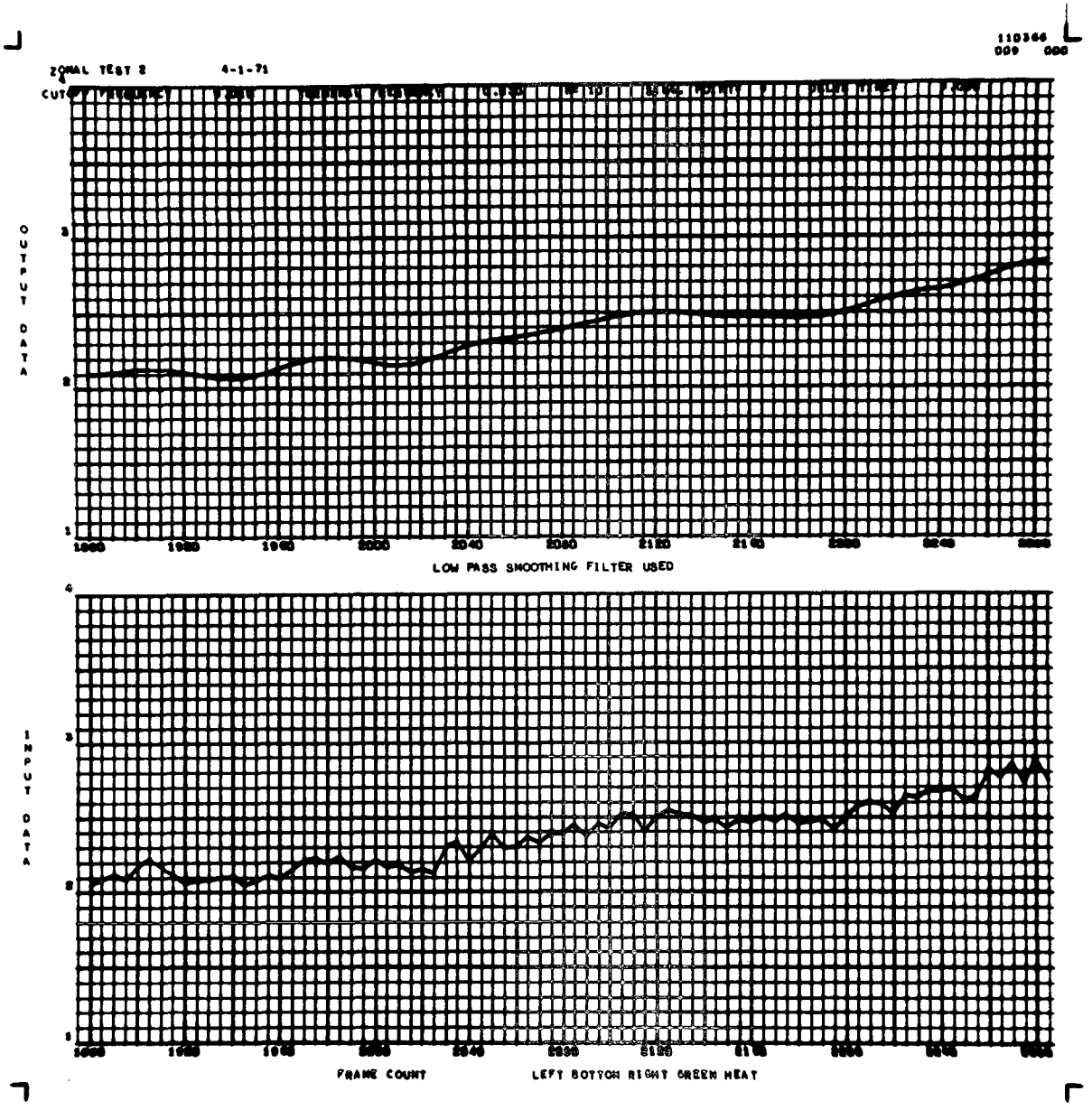

Figure A-72. Zone cell, run 2, left bottom, right, green, power on.

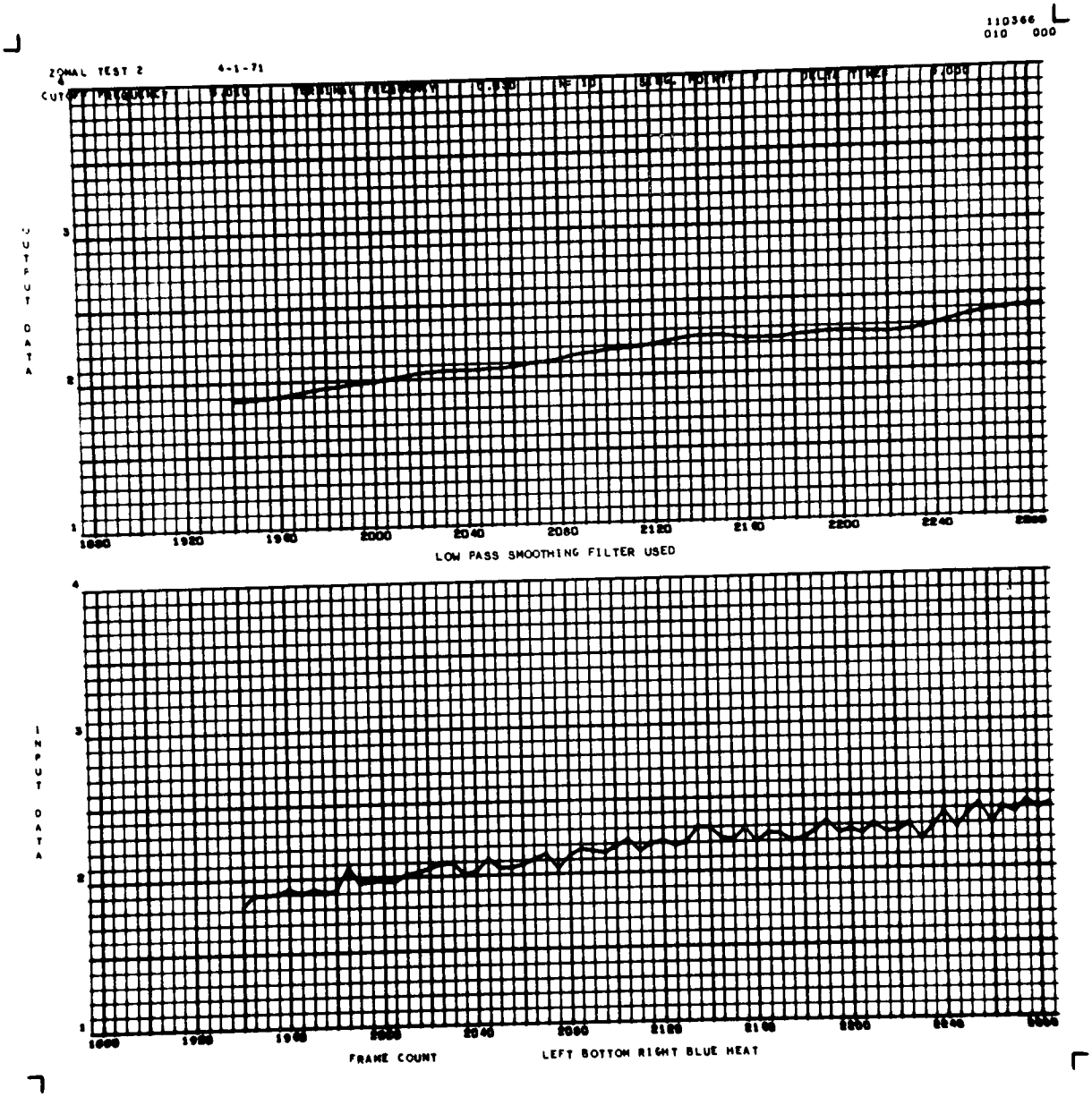

Figure A-73. Zone cell, run 2, left bottom, right, blue, power on.

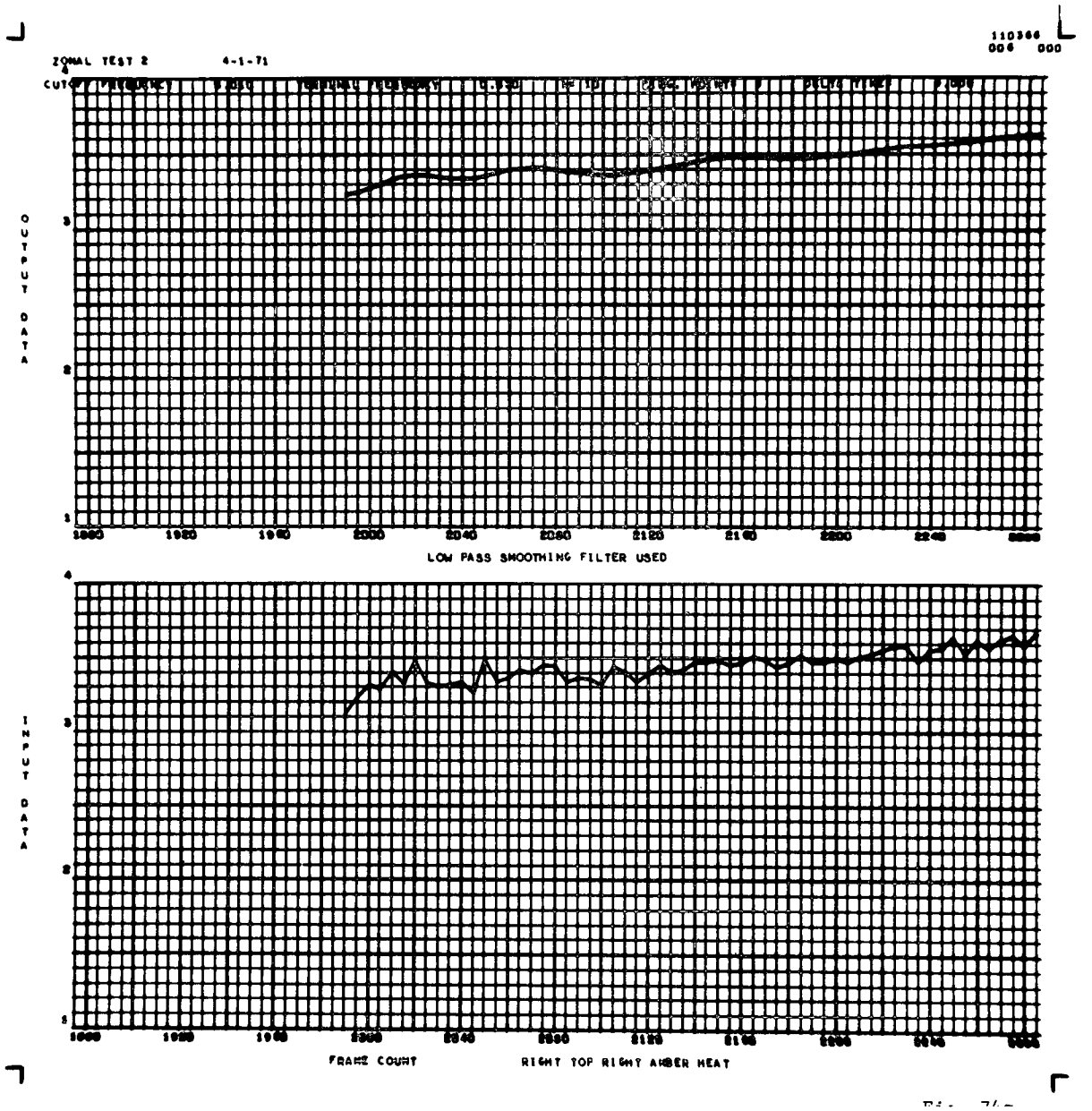

Figure A-74. Zone cell, run 2, right top, right, amber, power on.

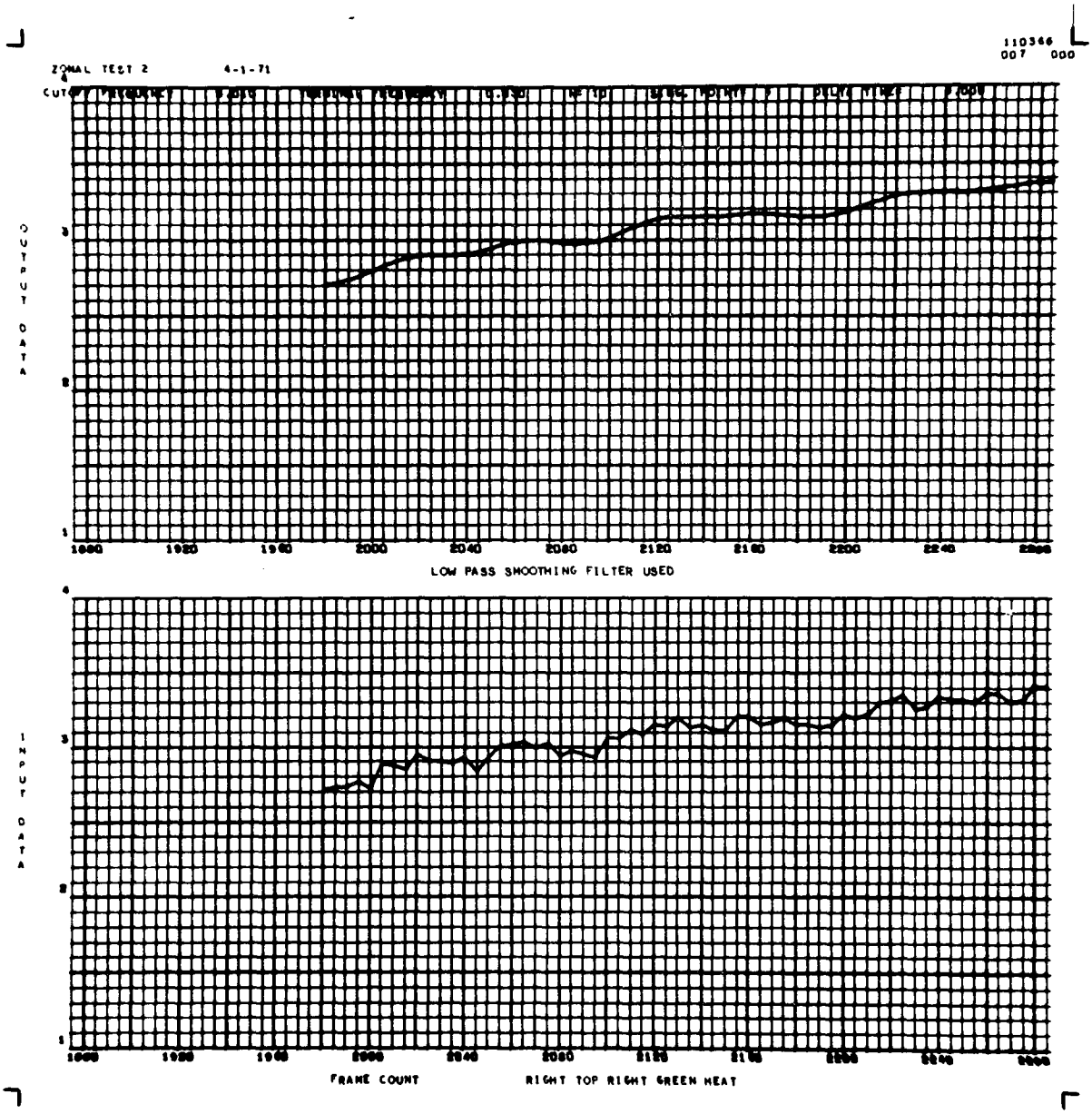

Figure A-75. Zone cell, run 2, right top, right, green, power on.

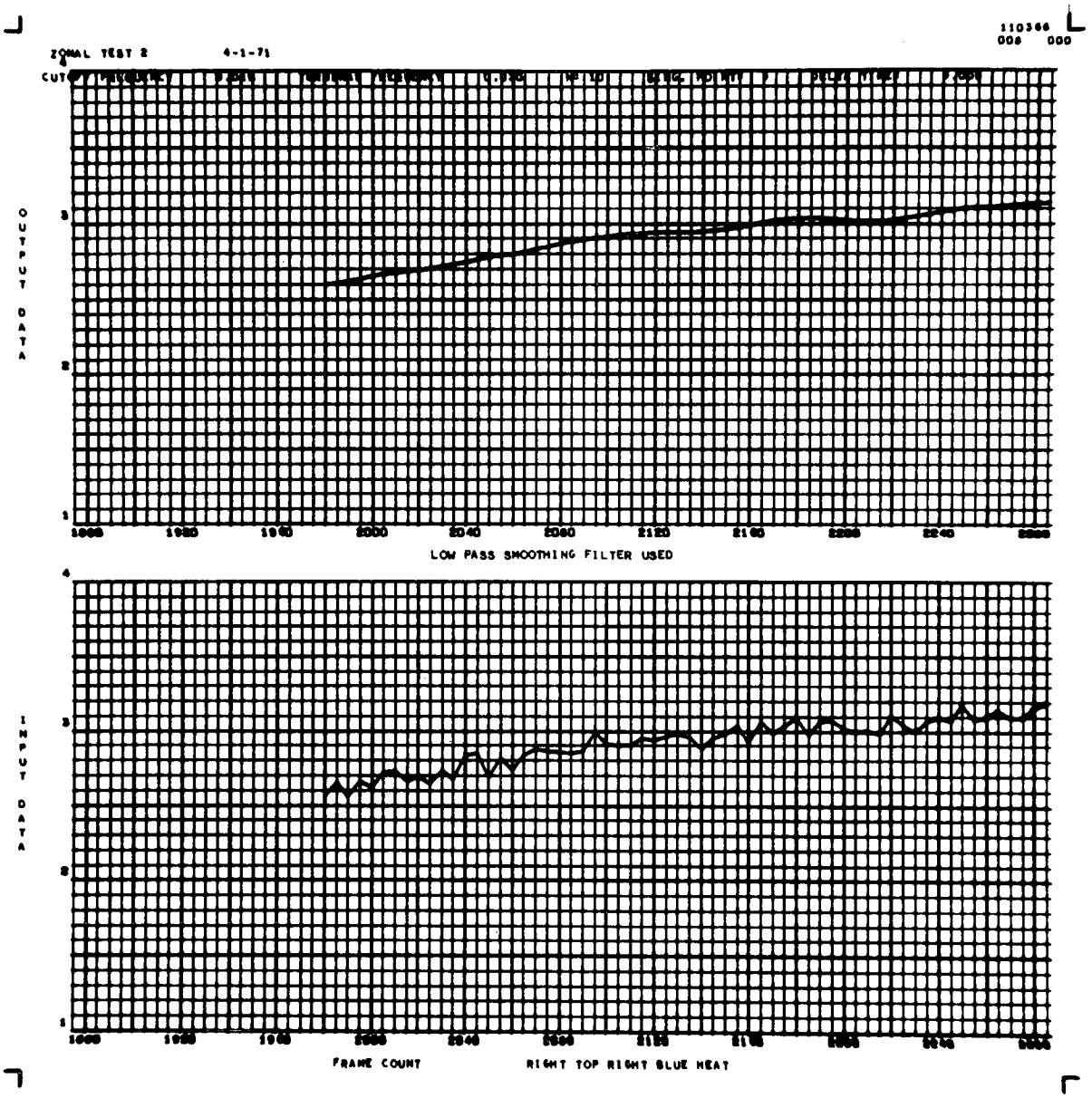

Figure A-76. Zone cell, run 2, right top, right, blue, power on.

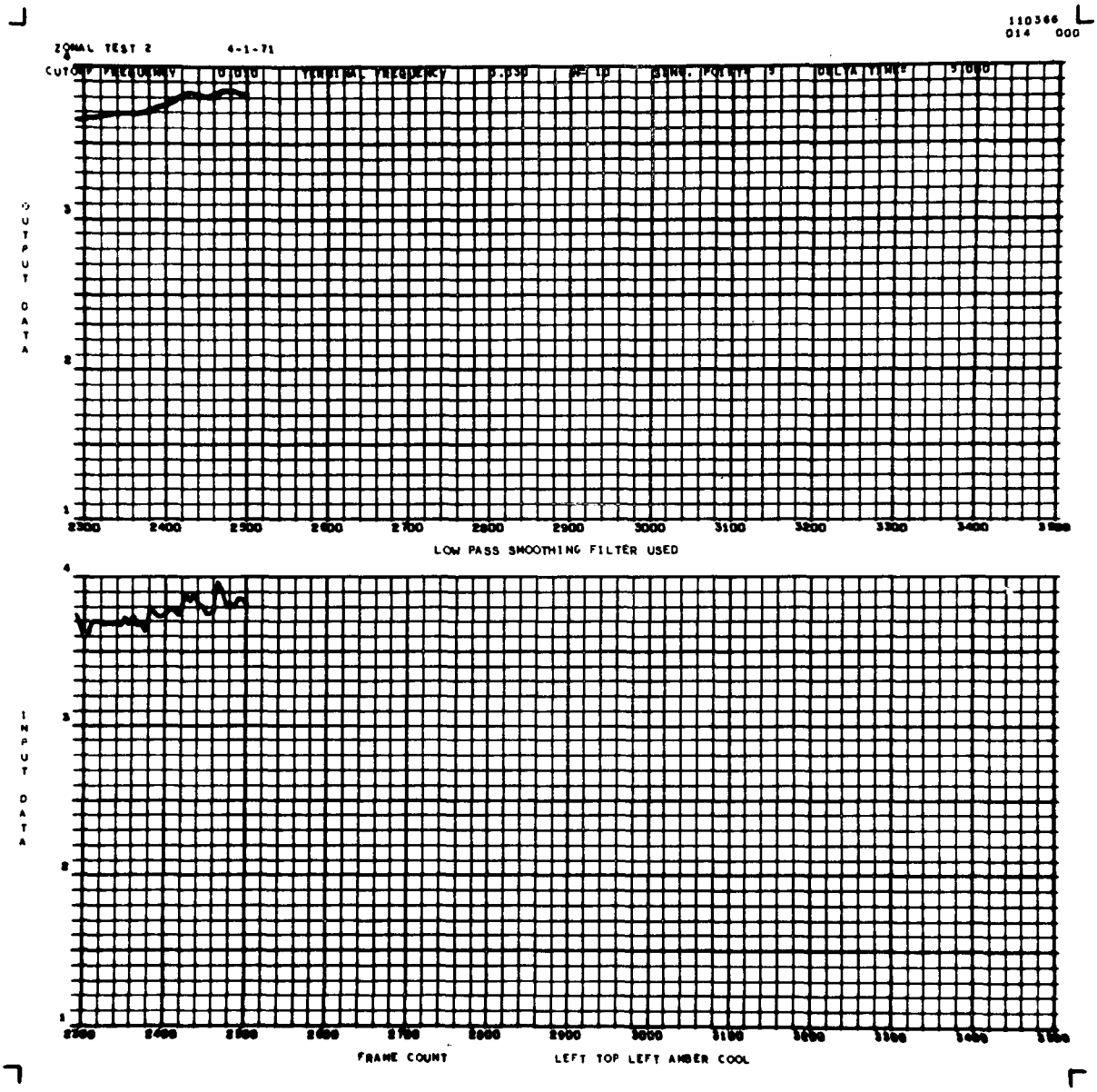

Figure A-77. Zone cell, run 2, left top, left, amber, power off.

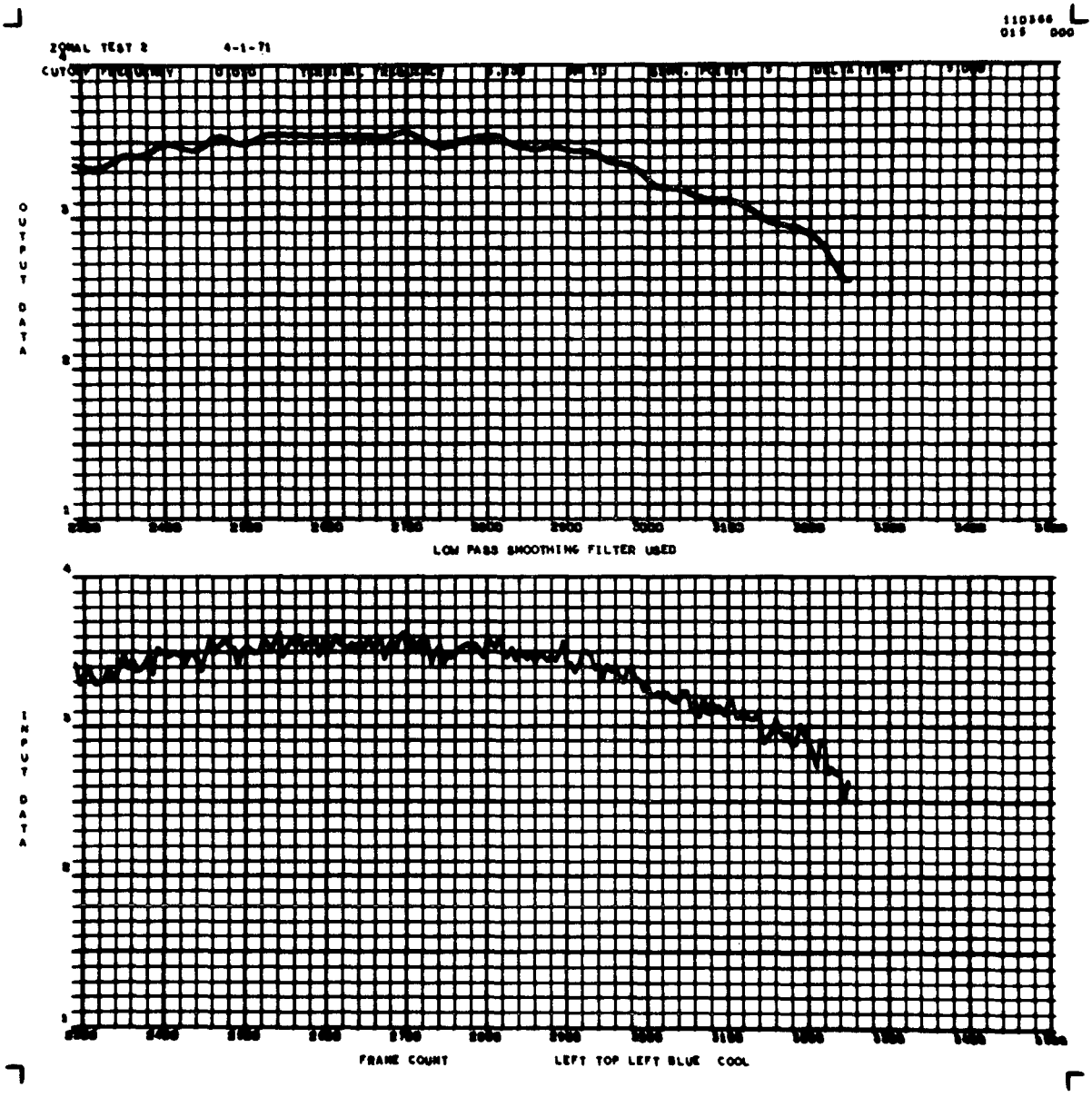

Figure A-78. Zone cell, run 2, left top, left, blue, power off.

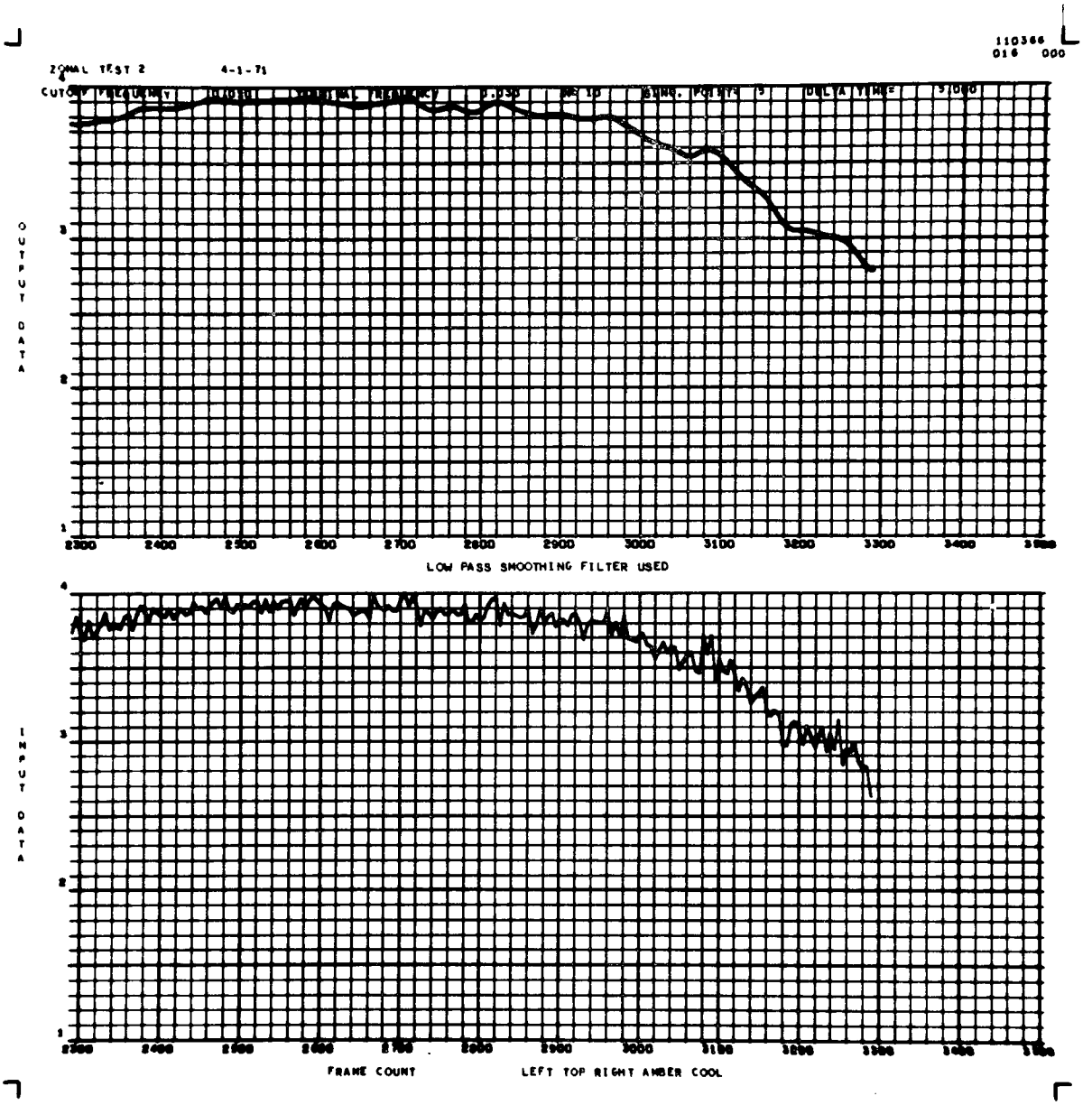

Figure A-79. Zone cell, run 2, left top, right, amber, power off.

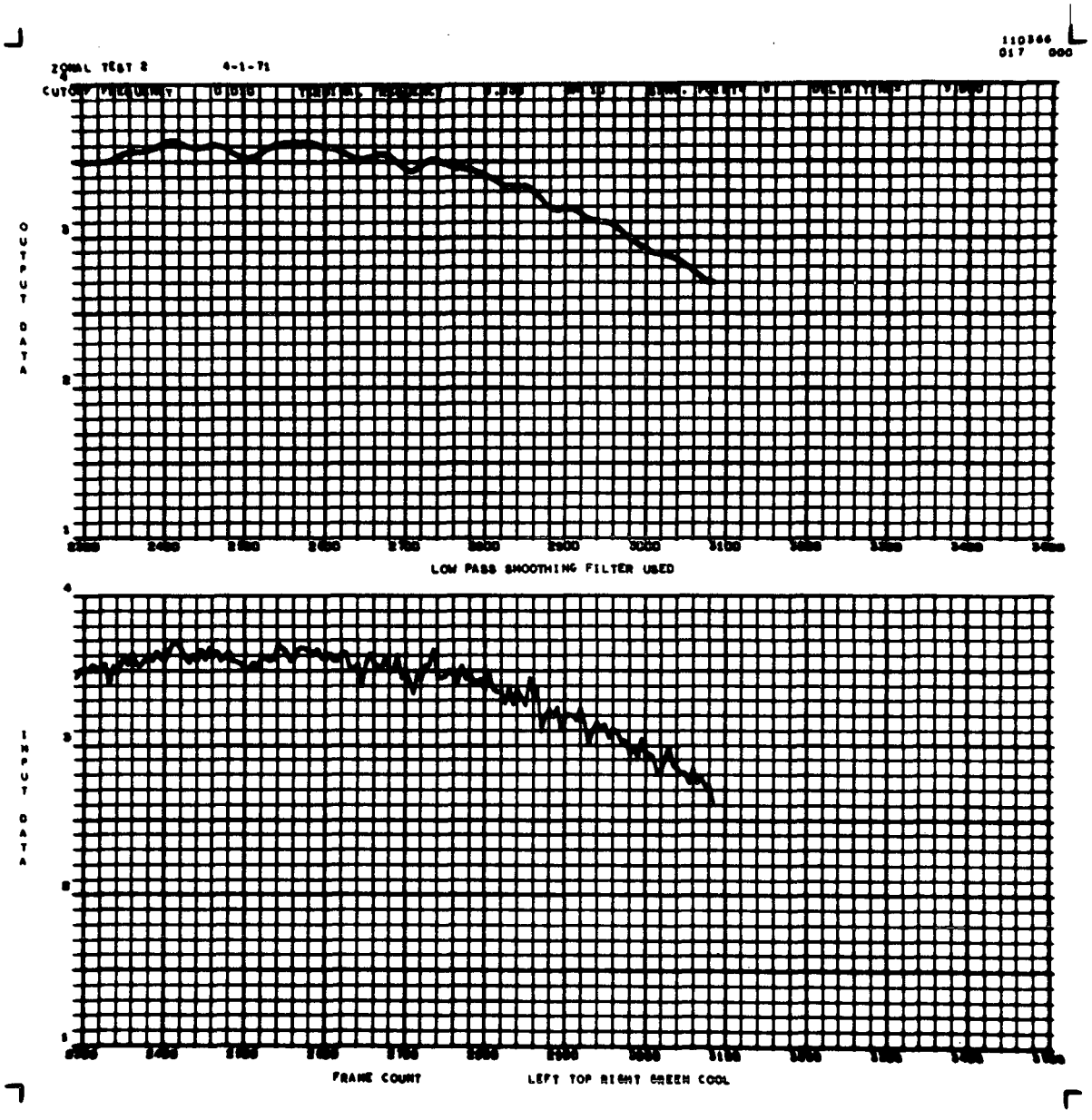

Figure A-80. Zone cell, run 2, left top, right, green, power off.

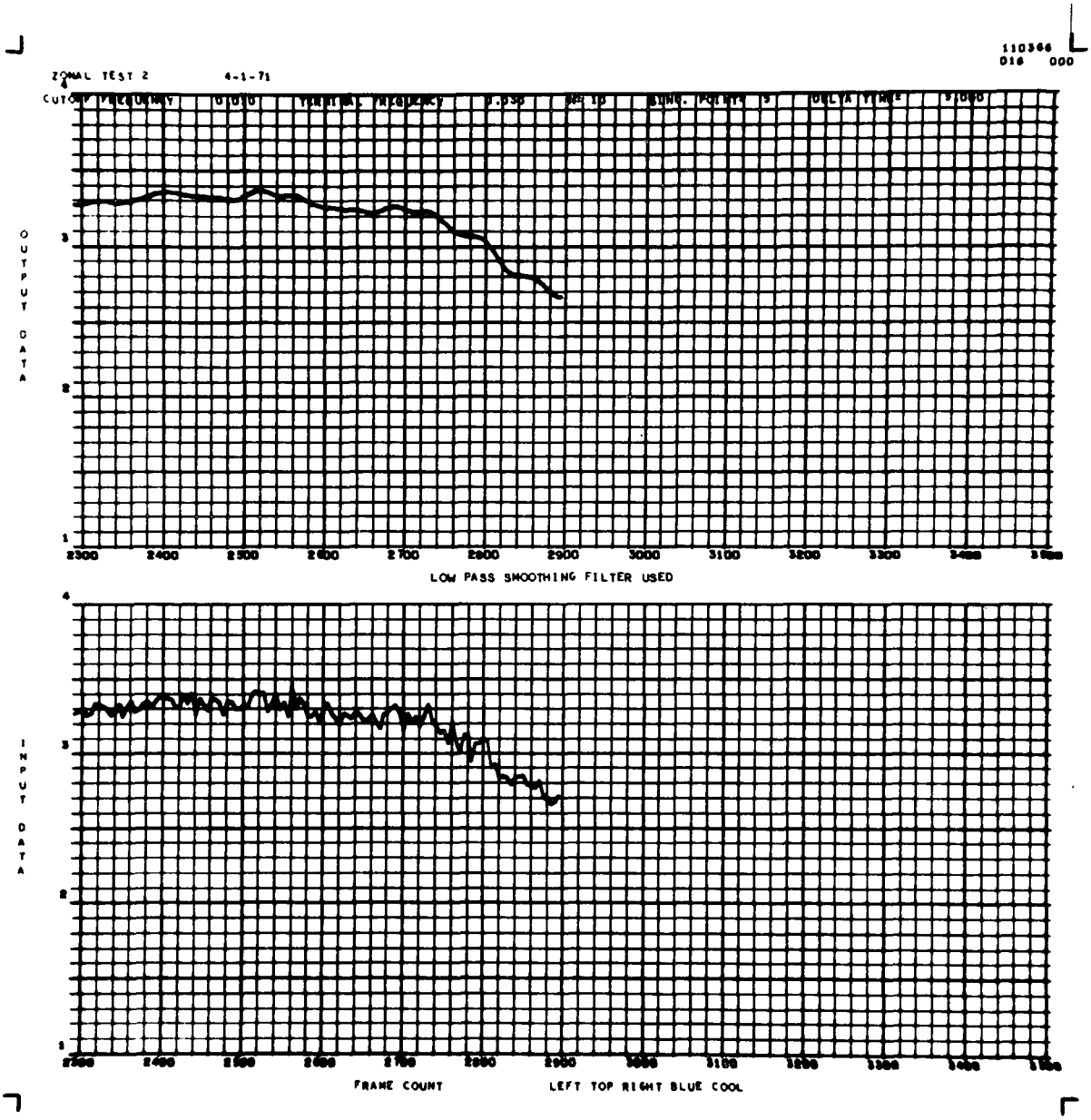

Figure A-81. Zone cell, run 2, left top, right, blue, power off.

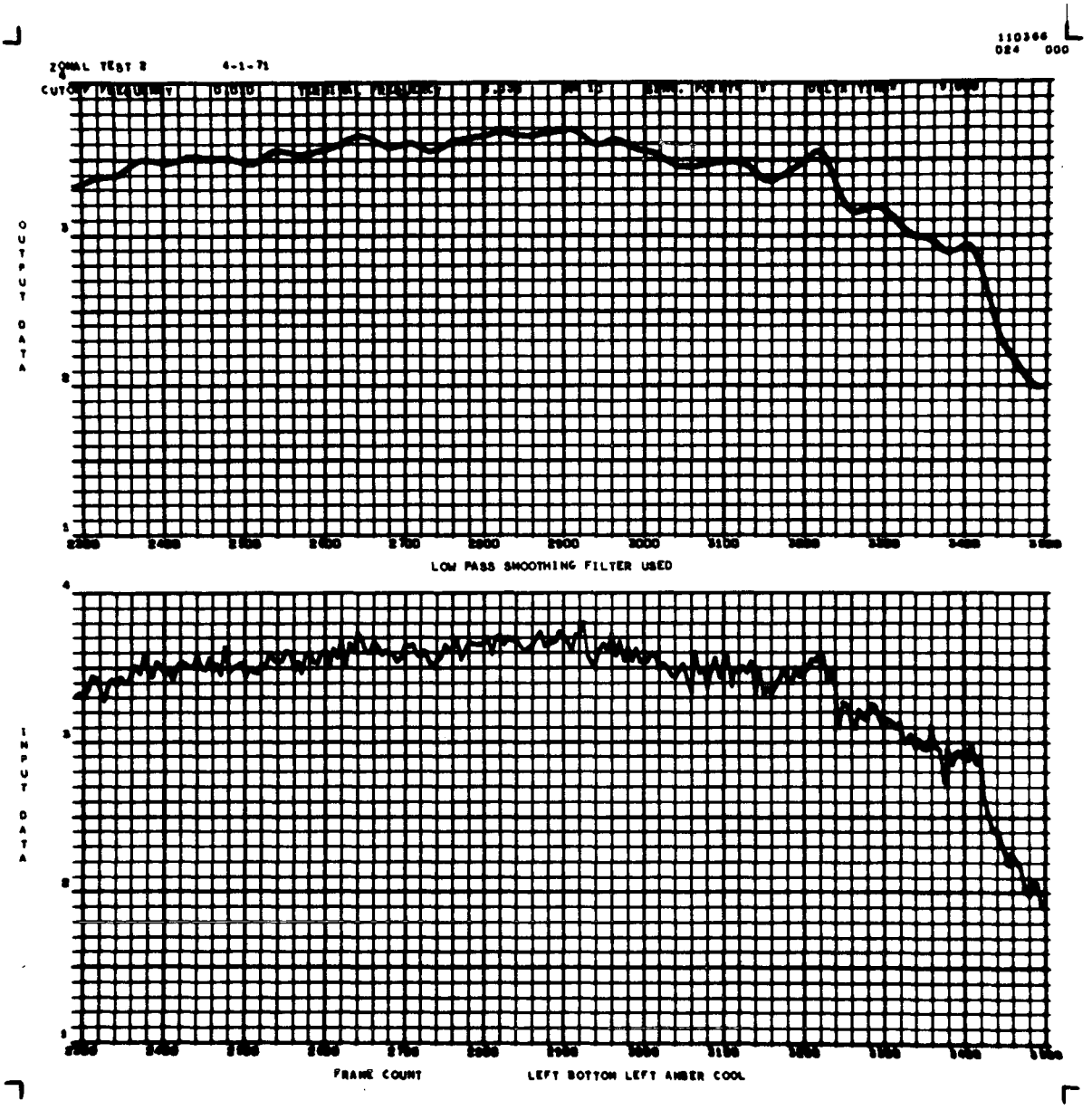

Figure A-82. Zone cell, run 2, left bottom, left, amber, power off.

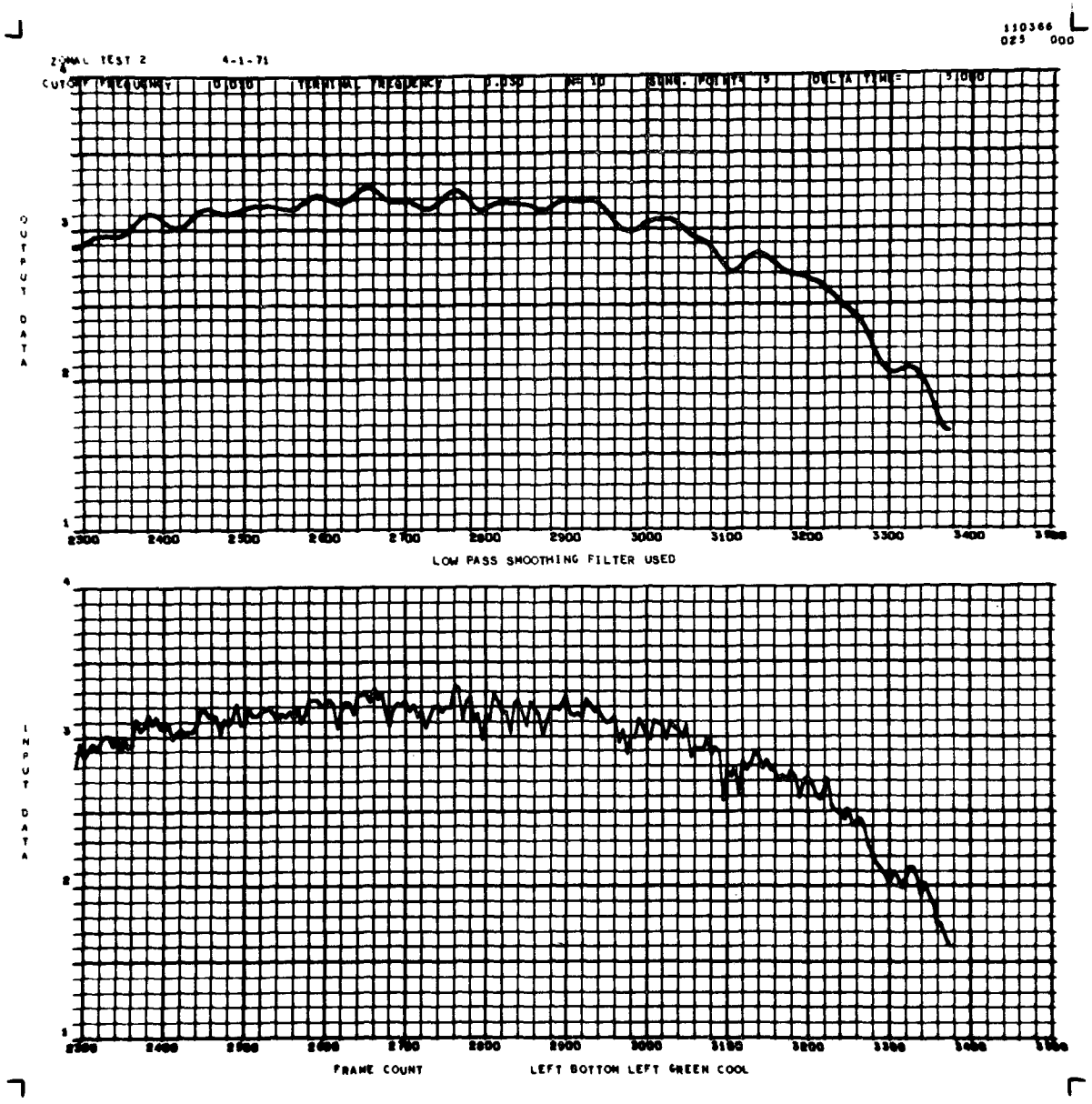

Figure A-83. Zone cell, run 2, left bottom, left, green, power off.

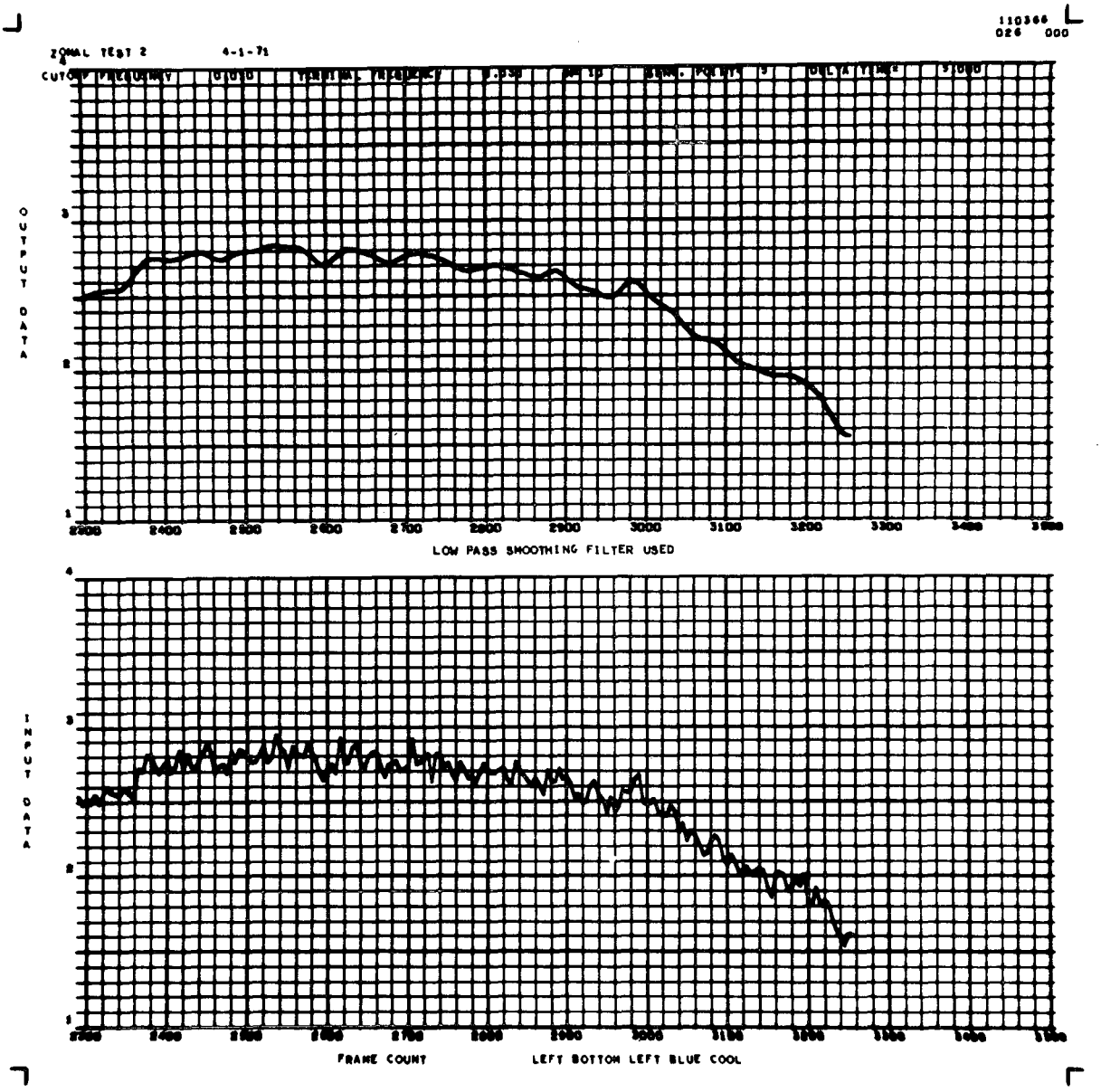

Figure A-84. Zone cell, run 2, left bottom, left, blue, power off.

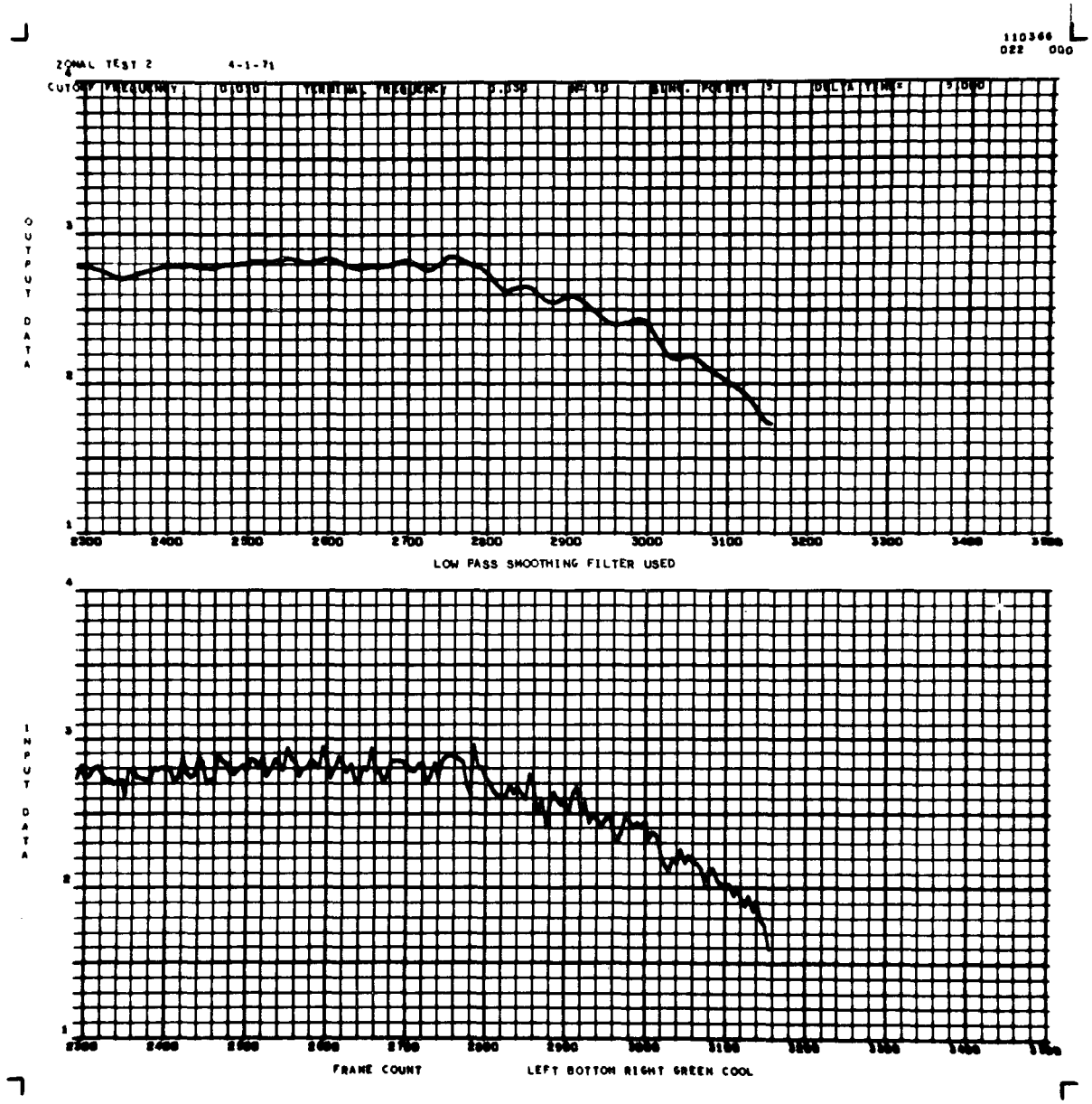

Figure A-85. Zone cell, run 2, left bottom, right, green, power off.

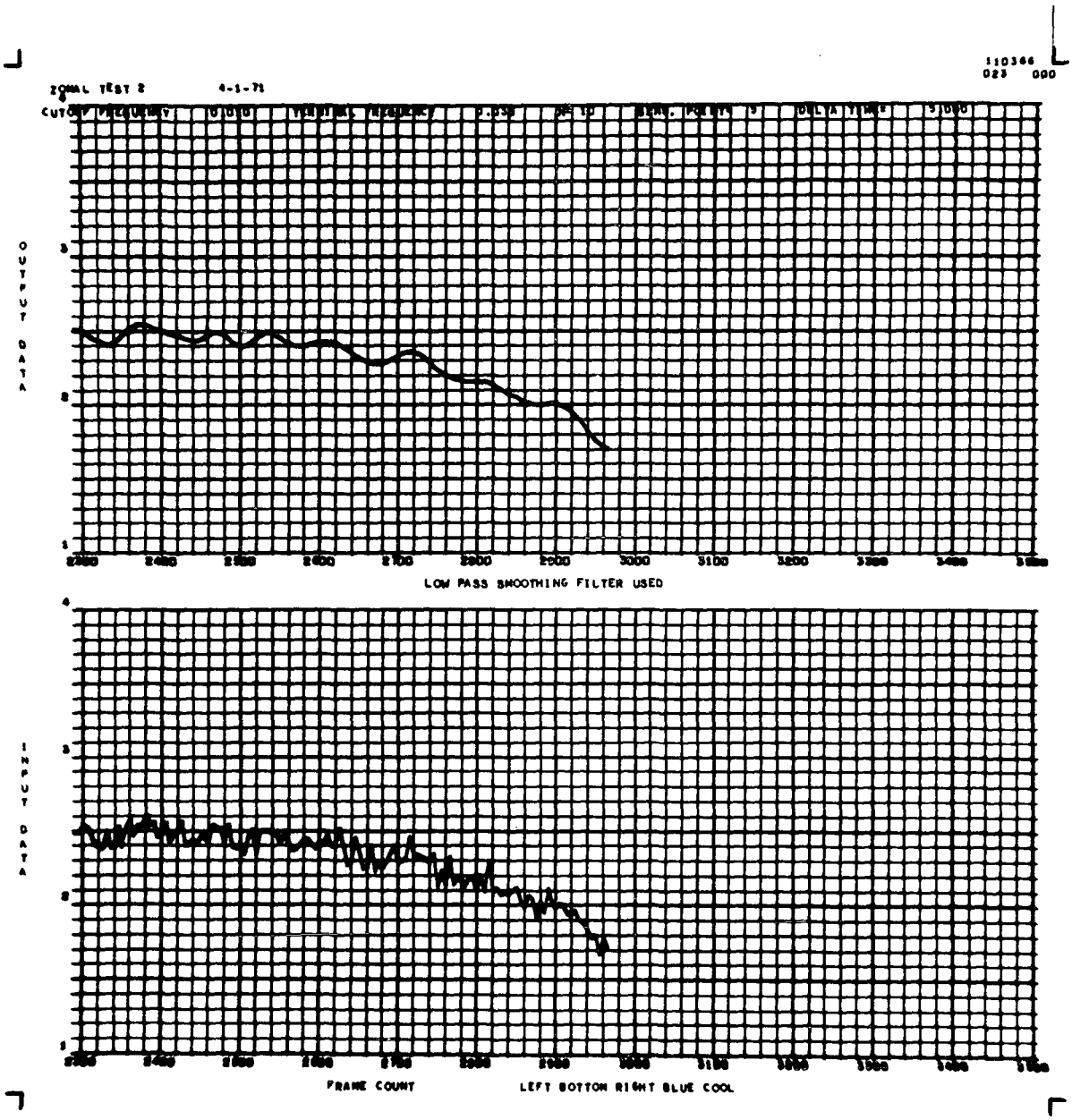

Figure A-86. Zone cell, run 2, left bottom, right, blue, power off.

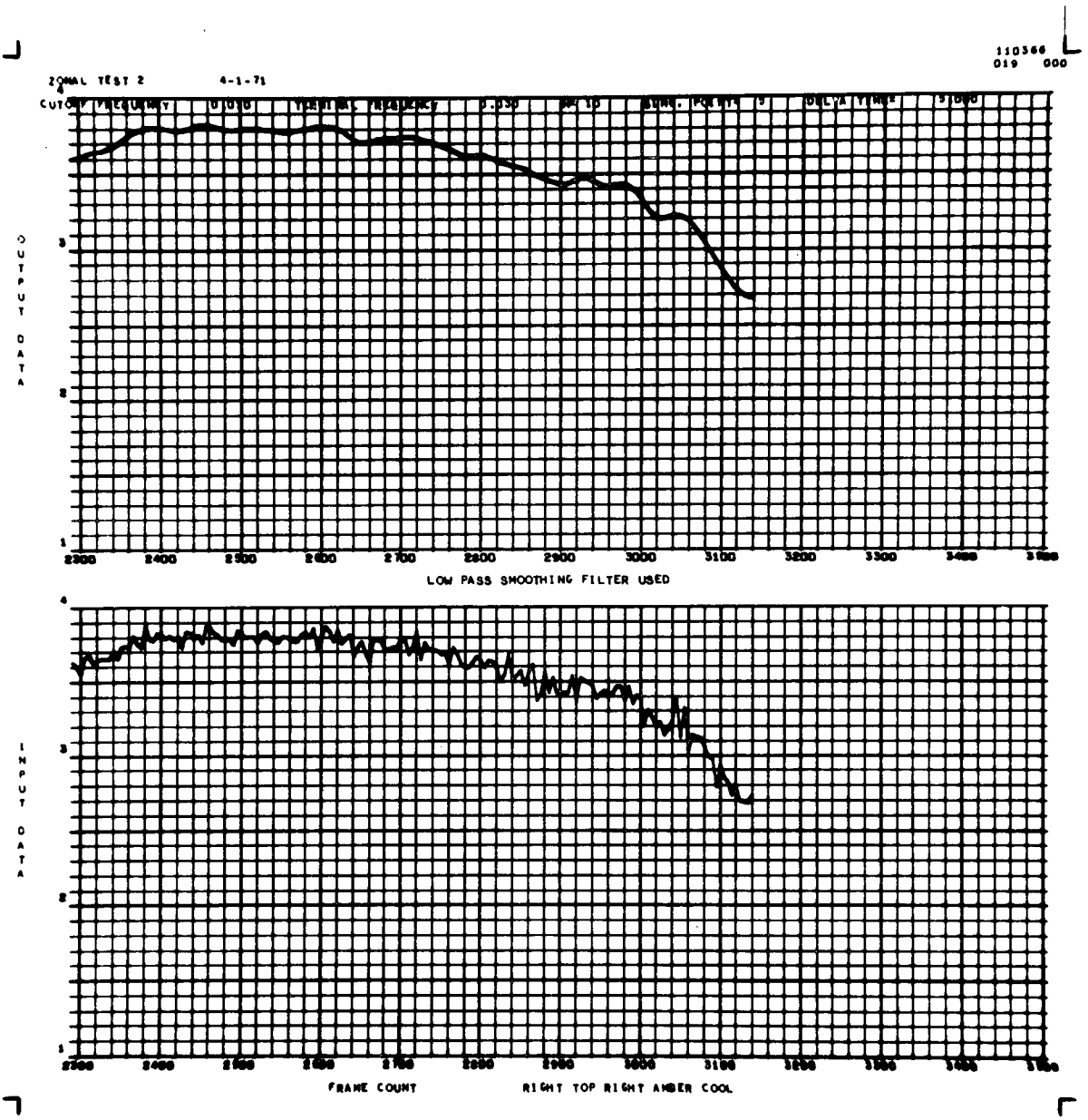

Figure A-87. Zone cell, run 2, right top, right, amber, power off.

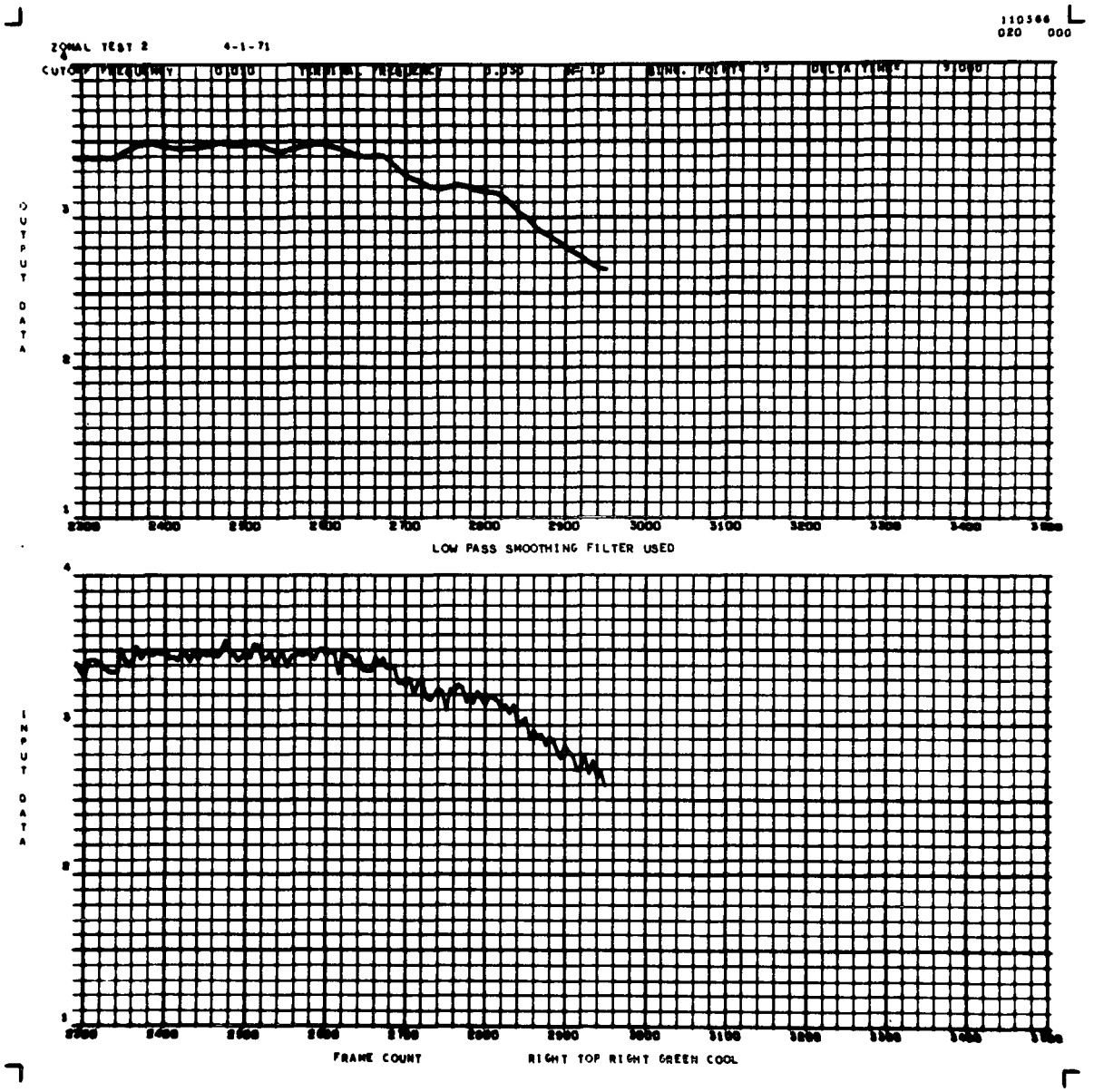

Figure A-88. Zone cell, run 2, right top, right, green, power off.

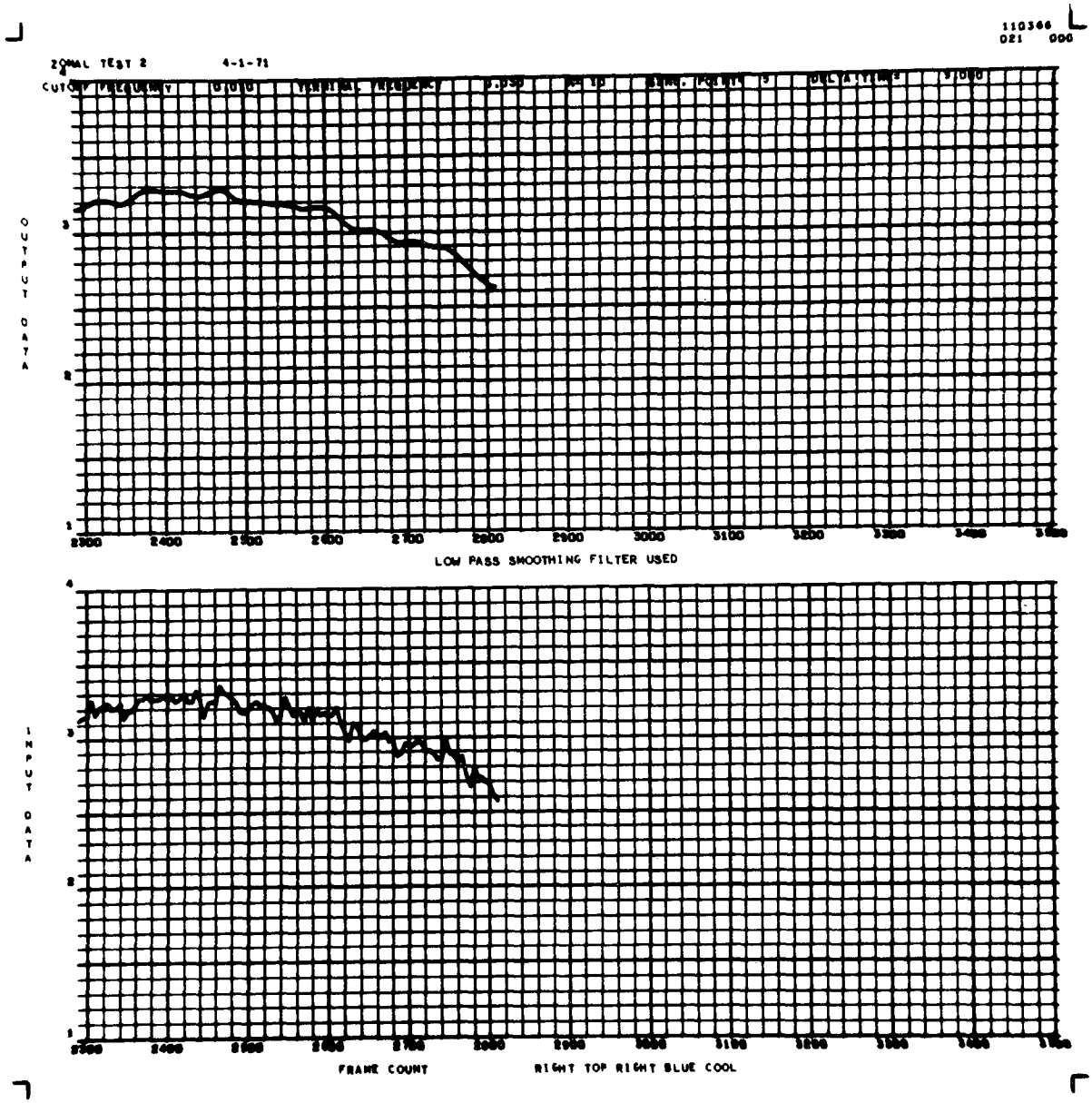

Figure A-89. Zone cell, run 2, right top, right, blue, power off.

REFERENCES

1. Gatewood, Eva; Morris, Marvin G.; and Holland, Robert L.: Acceleration Levels on the Heat Flow and Convection Demonstration — Apollo 14. NASA TM X-64644, Marshall Space Flight Center, Huntsville, Ala., Feb. 11, 1972.

2. Bénard, H.: Les tourbillions cellulaires dans une noppe liquids transportant de la chaleur pae convection eu regime permanent. Annales de chimie et physique, Vol. 23, 1901, p. 62.

3. Rayleigh, Lord: On the Convection Currents in a Horizontal Layer of Fluid when the Higher Temperature is on the Underside. Philosophical Magazine, Vol. 32, 1916, p. 529.

4. Block, M. J.: Surface Tension as the Cause of Bénard Cells and Surface Deformation in a Liquid Film. Nature, Vol. 178, 1956, p. 650.

5. Nield, D. A.: Surface Tension and Buoyancy Effects in Cellular Convection. Journal of Fluid Mechanics, Vol. 19, 1964, p. 341.

6. Pearson, J. R. A.: On Convection Cells Induced by Surface Tension. Journal of Fluid Mechanics, Vol. 4, 1958, p. 489.

7. Scriven, L. E.; and Sternling, C. V.: On Cellular Convection Driven by Surface Tension Gradients: Effects of Mean Surface Temperature and Surface Viscosity. Journal of Fluid Mechanics, Vol. 19, 1964, p. 321.

8. Davis, S. H.: Buoyancy Surface Tension Instability by the Method of Energy. Journal of Fluid Mechanics, Vol. 39, 1969, p. 347.

9. Debler, W. R.; and Wolf, L. W.: The Effects of Gravity and Surface Tension Gradients in Fluid Layers with Parabolic Temperatures Profiles. Journal of Heat Transfer, Vol. 92, No. 3, 1970, p. 351.

10. The Apollo 14 Heat Flow and Convection Demonstration Experiments — Final Results of Data Analysis. Report No. LMSC-HREC D225333, Contract NAS8-25577, Lockheed Missiles and Space Company, Huntsville, Ala., Sept. 1971.

REFERENCES (Concluded)

11. Eckert, E. R. G.; and Carlson, W. O.: Natural Convection in an Air Layer Enclosed Between Two Vertical Plates With Different Temperatures. International Journal of Heat Mass Transfer, Vol. 2, 1961, p. 106.

12. Lui, C. Y., et al.: Natural Convection Heat Transfer in Long Horizontal Cylindrical Annuli. Proceedings of the 1961 Heat Transfer Conference, University of Colorado, Boulder, Colo., Aug. 28 — Sept. 1, 1961, p. 976.

13. Larkin, B. L.: Heat Flow to a Confined Fluid in Zero Gravity. Progress in Astronautics and Aeronautics, Vol. 20, 1967, p. 819.

14. Manufacturing Technology Unique to Zero Gravity Environment. Report on NASA — Marshall Space Flight Center meeting, Process Engineering Laboratory, Huntsville, Ala., Nov. 1, 1968.

15. Space Processing and Manufacturing. Report No. ME-69-1, Process Engineering Laboratory, NASA — Marshall Space Flight Center, Huntsville, Ala., Oct. 21, 1969.

APPROVAL

HEAT FLOW AND CONVECTION DEMONSTRATION (APOLLO 14)

By Tommy C. Bannister

The information in this report has been reviewed for security classification. Review of any information concerning Department of Defense or Atomic Energy Commission programs has been made by the MSFC Security Classification Officer. This report, in its entirety, has been determined to be unclassified.

This document has also been reviewed and approved for technical accuracy.

William C. Snoddy

WILLIAM C. SNODDY
Chief, Electromagnetic and Solid State Physics Division

Ray V. Hembree, for

W. HAEUSSERMANN
Acting Director, Space Sciences Laboratory